NOVEL EDIBLE MICROCARRIERS FOR THE SCALABLE PRODUCTION OF CULTIVATED MEAT

BENJAMIN DAGÈS

Doctor of Philosophy

ASTON UNIVERSITY

December 2024

Abstract

Cultivated meat, grown from stem cells *in vitro*, has the potential to supply ever-growing demand for meat products while alleviating negative impacts of intensive animal farming on the environment, food security and animal welfare. Despite recent advances, several challenges concerning scalability of production and affordability have impeded access to cultivated meat, even in countries where it has received official approval.

This study uses silk fibroin, degummed from *Bombyx mori* cocoons, to design edible irregular microcarriers that mimic the extracellular matrix of skeletal muscle. Using both laboratory needle and industrial-scale needleless electrospinners, a 12% (w/w) silk fibroin in formic acid polymer solution was formed into non-woven nanofibrous mats (diameter: 98-166 nm) that were subsequently stabilised by immersion in monohydric alcohols to induce β-sheet crystallinity and prevent dissolution in aqueous solutions. Upon contact with bovine mesenchymal stem cells (bMSCs), the supports demonstrated excellent cytocompatibility, and good attachment and proliferation. Blending silk fibroin with 6.25% (w/w) zein enhanced the performance of the supports in static cell cultures without compromising their physical characteristics.

To improve the surface-to-volume ratio and enable use in stirred tank reactors, non-spheroid fibrous microcarriers were formed by hand-slicing or cryomilling the electrospun mats. These promoted bMSC expansion, with cell yields comparable to those of commercial microcarriers. The blended silk fibroin/zein microcarriers outperformed all others in static conditions.

In parallel, supermarket beef and plant-based burgers were tested to quantify their mechanical and textural properties. Seven burgers, with varying compositions of beef, fat and secondary ingredient contents, and social markers (*e.g.* price, brand), were tested. The results provided a range of sensory properties of traditional meat, which can inform the upstream production of cultivated meat products.

Keywords: Scale-up; Cultivated meat; Silk Fibroin; Electrospinning; Tissue Engineering; Microcarriers; Edible biomaterials; Texture.

Acknowledgements

As I conclude the long and eventful journey that has been my PhD, I would like to thank those who played an active and supporting role in helping me get through it.

Firstly, I want to thank the five most important people, without whom there would be no thesis at all – my supervisors Eirini Theodosiou, Jean-Baptiste Souppez, Petra Hanga, Paul Topham and my close colleague and friend Joe Homer.

Eirini, you have been the best supervisor I could have ever asked for; I am especially thankful to you for guiding me through this journey, always making time for me for professional and personal reasons and nudging me out of my French pessimism.

JB, it's such an amazing coincidence that we both ended up at Aston at the same time, and even more so that you became my second supervisor! From our schooldays at Charlemagne to the completion of my PhD, you have always looked out for me and gone out of your way to help me – for that I am eternally grateful.

Petra, I did this PhD because I was inspired by you, and although you left quite early on, I am so grateful for your continued involvement and support until the very end.

Paul, I am really grateful for the wisdom, support, time, equipment access and many beers offered at the Sack of Potatoes throughout the years.

Joe, you were my mentor during this entire process. You taught me almost everything I needed to accomplish this PhD and have always been there to help me out when I was stuck with experiments, needed assistance to interpret my results or just got acid all over myself… again.

To the MB111 gang, colleagues and friends. I thank you for the nerf gun battles, the general knowledge quizzes, the riddles, the card games, the countless chess games, the badminton and the philosophical debates. I doubt other PhD students have that much fun at the office! On a more serious note, I want to thank Bridget, Anisha, Georgia and Bawan (my chess rival). I really value all the help you have given me in understanding basic chemistry and physics concepts, and I feel lucky that we all got to share most of our journeys together. I'd also like to thank Alice and Louis, my replacements, for helping me set up the Aston Alternative Protein Project and helping me prepare some experiments in the last few months of my PhD. I wish you had both started sooner, I have no doubt we would have achieved a lot together.

To my brothers Tom and Matthew, I want to thank you for helping me time and time again by explaining complex mathematical and statistical concepts. I also want to thank my parents for always

believing in me; whose financial and of course, emotional support, have enabled me to pursue this career.

To Amy, who started this journey as my girlfriend, then my fiancée and now my wife, thank you for putting up with me. I know how hard this was for you too, and the sacrifices you had to make for us to be together. I love you. I also thank you for bearing Birmingham and for being my alarm clock most mornings, it's all over now!

To Vincent, my best friend and best man, both of us still students in our thirties… I thank you for your ever-lasting friendship and support. You may have narrowly beaten me in the race to becoming a doctor, but at least I'll be the first out of education! I'll let you know what it's like paying full-price cinema tickets…

And finally, I want to thank two extremely special individuals who have shown me unwavering emotional support, comforted me and cheered me up at my lowest points, and even stayed up all night with me when I was writing up. You may not be traditionally educated or academically minded, but this PhD is as much mine as it is yours, and for that, Truffle the Pug and Mochi the cat, I dedicate my thesis to you.

Collaborator Acknowledgements

Supervision of final year MEng Projects

Parts of the work presented in Chapters III, IV and V were aided by four MEng in Chemical Engineering students, working on separate research projects, whom I supervised directly. They remained actively involved in the planning, design, experimental work and analysis through every stage of this work.

Jaskaran Chodda worked on characterising the mechanical properties (tensile, flexural, compressive and cutting) of raw and cooked beef burgers, and providing the groundwork for the larger study presented in Chapter V. Jack Fabian explored ways to improve the degumming of silk fibroin fibres and played an active role in the characterisation of needle-electrospun regenerated silk fibroin mats presented in Chapter III. In addition, Jack processed the mechanical and textural data for the characterisation of beef and plant-based burgers presented in Chapter V. Nikita Puri and Michael Malhi worked on psyllium husk and zein blends, respectively, identifying optimal blending concentrations and characterising the resulting needle-electrospun blended mats. These results were presented in Chapter IV.

Collaboration with the Technical University of Liberec (TUL), Czech Republic

All needleless electrospinning work was carried out at TUL, under the supervision of Mirka Rysova for DC electrospinning (benchtop and Nanospider™) and under Jan Valtera for AC electrospinning, during a 3-week visit. Mirka Rysova also produced additional Nanospider™ electrospun mat on request.

Collaboration for the characterisation of beef and plant-based burgers

Much of the work presented in Chapter V was carried out as a collaboration between my PhD research and the Aston Engineering department led by Jean-Baptiste Souppez. As such, a lot of the experimental work was undertaken by students Mariya Khan and Munthaha Rhiya, whom I did not supervise but whose work I helped plan and discuss.

List of publications

Dagès, B. A. S., Fabian, J., Polakova, D., Rysova, M., Topham, P. D., Souppez, J. -B., Hanga, M. P., & Theodosiou, E. (2025). Edible electrospun materials for scalable cultivated beef production. *Food and Bioproducts Processing*, 149, 118-129. https://doi.org/10.1016/j.fbp.2024.11.012

Souppez, J. -B. R. G., **Dagès, B. A. S.**, Pavar, G. S., Fabian, J., Thomas, J. M., & Theodosiou, E. (2025). Mechanical properties and texture profile analysis of beef burgers and plant-based analogues. *Journal of Food Engineering*, *385*, 112259. https://doi.org/10.1016/j.jfoodeng.2024.112259

Moutsatsou, P., Cameron, P., **Dagès, B.**, Nienow, A. W., Lye, G., Theodosiou, E., & Hanga, M. P. (2023). Scaling cell production sustainably in cultured meat product development. In M. Post, C. Connon & C. Bryant (Eds.), *Advances in cultured meat technology* (1st ed., pp261-296). Burleigh Dodds Science Publishing. https://doi.org/10.19103/AS.2023.0130.11

List of conference presentations

Johnson, A., **Dagès, B. A. S.,** Savers, A., Rysova, M., Topham, P. D., Hanga, M. P., Souppez, J. -B., & Theodosiou, E. (2024, November 17-19). *Optimising microcarriers for scalable cultivated meat production* [Poster Presentation – delivered by Johnson, A.]. 10th International Scientific Conference on Cultured Meat ISCCM10, Maastricht, Netherlands.

Souppez, J. -B., **Dagès, B. A. S.**, Pavar, G., Fabian, J., Thomas, J. M., & Theodosiou, E. (2024, June 12). *What makes a good burger? Quantifying meat texture to inform cultivated meat production* [Oral Presentation – delivered by Dages B. A. S.]. Cultivate 2024, Sheffield, UK.

Dagès, B. A. S., Johnson, A., Rysova, M., Topham, P. D., Souppez, J-. B., Thomas, J. M., Hanga, M. P., & Theodosiou, E. (2024, June 12) *Towards making cultivated meat burgers – microcarrier design and optimisation* [Oral Presentation – delivered by Theodosiou, E.]. Cultivate 2024, Sheffield, UK

Dagès, B. A. S., Fabian, J., Thomas, J. M., Rysova, M., Souppez, J. -B., Hanga, M. P., & Theodosiou, E. (2024, April 16) *Intensifying production of cultivated meat using microcarriers* [Invited Oral Presentation – delivered by Theodosiou, E.]. IChemE BESIG Meeting – Cultured meat: A new era in food bioprocessing 2, London, UK.

Dagès, B. A. S., Chodda, J., Souppez, J. -B., Wall, I., Hanga, M. P., & Theodosiou, E. (2023, June 20). *Scaling cultivated meat production with edible non-woven supports* [Oral and Poster Presentation – delivered by Dages, B. A. S.]. Cultivate 2023, Bath, UK.

Dagès, B. A. S., Fabian, J., Rysova, M., Topham, P. D., Souppez, J. -B., Hanga, M. P., & Theodosiou, E. (2023, January 11-12). *Novel microcarriers for the scalable production of cultivated meats* [Oral and Poster Presentation – delivered by Dages, B. A. S.]. ESACT-UK 33rd Annual Meeting, Nottingham, UK.

Dagès, B. A. S., Chodda, J., Souppez, J. -B., Wall, I., Hanga, M. P., & Theodosiou, E. (2022, May 12). *Novel microcarriers for the scalable production of cultivated meats* [Poster Presentation – delivered by Dages, B. A. S.]. Cultivate 2022, Birmingham, UK.

Other related research outputs

I published a fictional abstract in the Journal of Imaginary Research Volume Nine (2024):

Dagès, B. (2024). Establishing *in vitro* cultures of human autologous stem cells for consensual meat production. *Journal of Imaginary Research*, *9*, 33-34. https://journalofimaginaryresearch.home.blog/2024/01/24/journal-of-imaginary-research-volume-nine-2024/

I presented a story board summarising my PhD (see below) for the 2023 BESIG iChemE Seasonal Competition. I won first prize (£500).

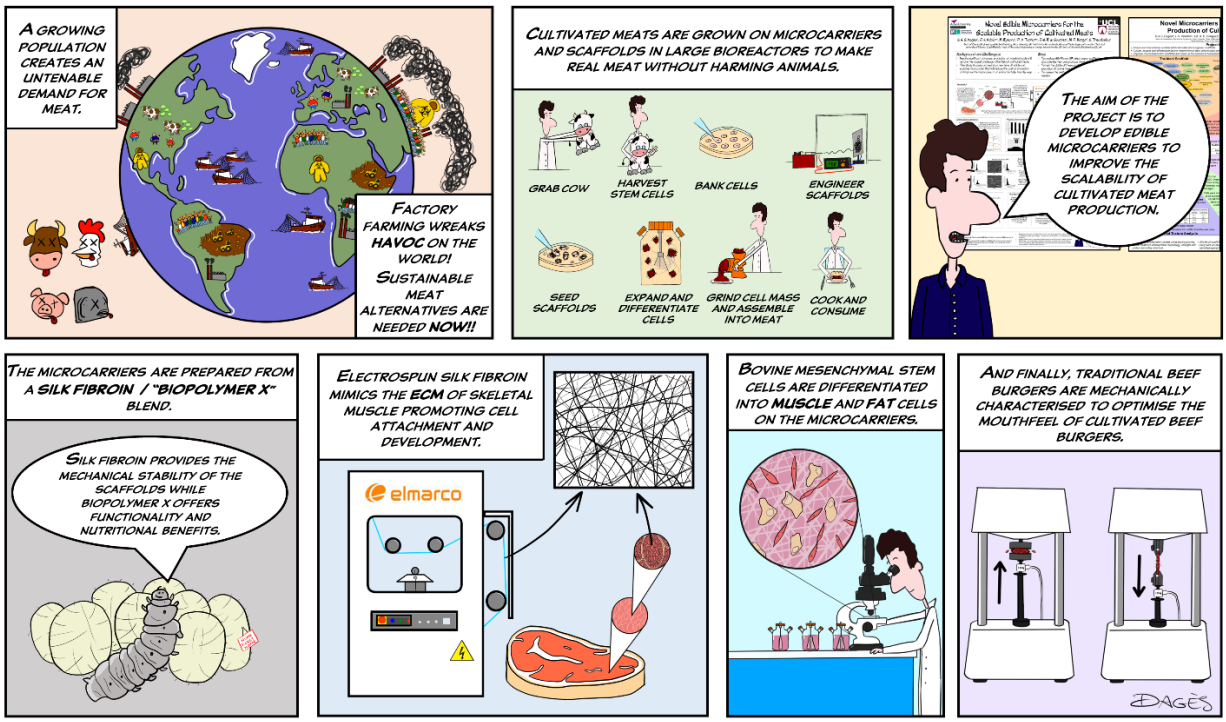

I founded and presided over the Aston Agricell Society, a student society aimed at helping students discover cultivated meats and alternative protein, encouraging them to undertake academic research

projects in the field, and visiting cultivated meat start-ups. I then led the transition towards the Aston Alternative Protein Project, a collaboration of student societies across the globe aimed at promoting and educating on alternative protein, coordinated by the Good Food Institute (GFI).

List of Contents

Contents

List of abbreviations

AC	Alternative current
AMR	Antimicrobial resistance
B1-B7	Burgers (1-7)
BFGF	Basic fibroblast growth factor
bMSC	Bovine mesenchymal stem cell
C3	Cytodex-3
CO_2eq/kg	Carbon dioxide equivalent per kilo of product
DC	Direct current
DGEA	Asp-Gly-Glu-Ala peptide motif
DMSO	Dimethylsulfoxide
DPBS	Dubelcco's phosphate-buffered saline
DSF	Degummed silk fibroin
EC	European Commission
ECM	Extracellular matrix
EDTA	Ethylenediaminetetraacetic acid
EFSA	European Food Standards Authority
ESC	Embryonic stem cell
EtOH	Ethanol
FA	Formic acid
FAO	Food and Agriculture Organization
FBS	Foetal bovine serum
FDA	Food and Drug Administration
FTIR	Fourier Transform Infrared spectroscopy
GDP	Gross domestic product
GFI	Good Food Institute
GHG	Greenhouse gas
GMO	Genetically Modified Organism
GRAS	Generally Regarded As Safe
GWP	Global Warming Potential
HSD	Honestly Significant Difference test
HX	Hybrid X
IKVAV	Ile-Lys-Val-Ala-Val peptide motif

iPSC	Induced pluripotent stem cell
iRJS	Immersed rotary jet spinning
ISO	International Organization for Standardization
iβS	Intermolecular β-sheet
Iβ S	Intramolecular β-sheet
LC1, LC2	Load cell 1, Load cell 2
LCA	Life cycle analysis
MeOH	Methanol
MSC	Mesenchymal stem cell
MYF	Myogenic factor
MYOD	Myoblast determination protein
MYOG	Myogenin transcription factor
NASA	US National Aeronautics and Space Administration
NLSF	Needleless (benchtop) electrospun silk fibroin (-U untreated, -E Ethanol-treated)
NSF	Needleless (NanospiderAdd logo) electrospun silk fibroin (-U untreated, -E Ethanol-treated)
PAFF	Standing Committee on Plants, Animals, Food and Feed
PBA	Plant-based analogue
PCL	Polycaprolactone
PDA	Polydopamine
PEG	Polyethylene glycol
PEO	Polyethylene oxide
PH_{χ}	Electrospun psyllium husk (prepared at χ % (w/w) in formic acid; -U untreated, -E Ethanol treated)
PLGA	Poly lactic-co-glycolic acid
PLLA	Poly-L-lactic acid
PMMA	Polymethyl methacrylate
RC	Random coil
RGD	Arginylglycylaspartic acid (Arg-Gly-Asp peptide motif)
RSF	Regenerated silk fibroin
SC	Satellite cell
SFA	Singapore Food Agency
SFPH	Silk fibroin and psyllium husk blends

SFUV$_{\omega}$'	Silk fibroin (prepared at ϕ % ADD to SFUV or take out. Think you should put SF first (w/w) in formic acid; -U untreated, -E ethanol-treated, -U-->E untreated followed by UV followed by Ethanol treatment)
SFZ	Silk fibroin and zein blends (-U untreated, -E Ethanol-treated)
SF$_{\phi}$	Electrospun silk fibroin (prepared at ϕ % (w/w) in formic acid; -U untreated, -E Ethanol-treated, -M Methanol-treated)
SGD	Singapore Dollar (currency)
SP	Solohill Plastic
STR	Stirred Tank Reactor
TUL	Technical University of Liberec
TPA	Texture profile analysis
UNDP	United Nations Development Programme
UNEP	United Nations Environment Programme
USDA	United States Department of Agriculture
WBSF	Warner-Bratzler Shear Force
Z$_{\psi}$	Electrospun zein (prepared at ψ % (w/w) in formic acid; -U untreated, -E Ethanol-treated)
αH	α-helix
αMEM	Alpha Minimum Essential Medium
βS	B-sheet
βt	β-turn

Nomenclature

$\boldsymbol{A}$	Absorbance	-
$\boldsymbol{a_f}$	Fibrous area	(cm2)
$\boldsymbol{A_h}$	Adhesiveness	(N.s)
$\boldsymbol{B}$	Bias	(N or mm)
$\boldsymbol{C_h}$	Chewiness	(N)
$\boldsymbol{C_o}$	Cohesiveness	-
$\boldsymbol{c_{live\ cells}}$	Concentration of live cells	(cells/mL)
$\boldsymbol{DF}$	Dilution factor	-
$\boldsymbol{df}$	Degrees of freedom	-

$\boldsymbol{Dr}$	Degumming ratio	(%)
$\boldsymbol{DT}$	Doubling time	(h)
$\boldsymbol{E}$	Young's modulus	(MPa)
$\boldsymbol{E_S}$	Seeding efficiency	(%)
$\boldsymbol{f_a}$	Density of the amide I spectrum (1600-1708 cm^{-1})	-
$\boldsymbol{f_a''}$	Second derivative of the amide I spectrum	-
$\boldsymbol{f_{X_i}}$	Density of Gaussian distributions	-
$\boldsymbol{F}$	Force	(N)
$\boldsymbol{FI}$	Fold increase	-
$\boldsymbol{k}$	Sub-populations	-
$\boldsymbol{GR}$	Growth rate	(h^{-1})
$\boldsymbol{H}$	Hardness	(N)
$\boldsymbol{h}$	Height	(cm or mm)
$\boldsymbol{I}$	Intensity ratio	-
$\boldsymbol{k}$	Categories	-
$\boldsymbol{L}$	Length	(cm or mm)
$\boldsymbol{l}$	Width	(cm or mm)
$\boldsymbol{M_{cooked}, M_{raw}}$	Cooked mass, raw mass	(g)
$\boldsymbol{MSE}$	Mean Square Error	-
$\boldsymbol{n}$	Observations or number	-
$\boldsymbol{N_0}$	Seeding density	(cells/cm2)
$\boldsymbol{N_{live\ cells}}$	Density of live cells	(cells/square)
$\boldsymbol{N_s, N_f}$	Density of cells at start or end of exponential growth stage	(cells/cm2)
$\boldsymbol{\emptyset}$	Fibre diameter	(nm)
$\boldsymbol{P}$	Precision	-
$\boldsymbol{p}$	p-value	-
$\boldsymbol{P_{cocoon}}$	Price of cocoons, regenerated silk fibroin, or commercial silk fibroin	(GBP/g)
$\boldsymbol{P_{com}}$	Price of commercial silk fibroin	GBP/g)
$\boldsymbol{P_{RSF}}$	Price of RSF or cocoons	(GBP/g)
$\boldsymbol{q}$	Studentised range distribution	(cm)
$\boldsymbol{R}$	Resilience	-
$\boldsymbol{r}$	Radius	(cm)
$\boldsymbol{RA_i}$	Relative area of Gaussian distributions	-

$\%\boldsymbol{RH}$	Relative humidity	(%)
$\boldsymbol{Rr}$	Regeneration ratio	(%)
$\boldsymbol{S}$	Springiness	-
$\boldsymbol{s}$	Span	(mm)
$\boldsymbol{SA}$	Surface area	(cm^2)
$\boldsymbol{SD}$	Standard deviation	-
$\boldsymbol{SSA}$	Specific surface area	(cm2/g)
$\boldsymbol{T}$	Tukey's criterion	-
$\boldsymbol{T}(\%)$	Transmittance	(%)
$\boldsymbol{T_m}$	Melting temperature	(°C)
$\boldsymbol{T_s}$	Sampling time	(s)
$\boldsymbol{U}$	Uncertainty	-
$\boldsymbol{V_s}$	Volume of haemocytometer square	(mL)
$\boldsymbol{W}$	Weight	(mg)
$\boldsymbol{w}$	Wavenumber	(cm^{-1})
$\boldsymbol{X_i}$	Gaussian distribution	
$\boldsymbol{Y_f}(\%)$	Final regeneration yield	(%)
$\boldsymbol{Y_M}, \boldsymbol{Y_V}$	Yield by volume, Yield by mass	-
$\boldsymbol{\varepsilon}$	Strain	(%)
$\boldsymbol{\varepsilon_y}$	Yield strain	(%)
$\boldsymbol{\lambda}$	Wavelength	(nm)
$\boldsymbol{\mu}$	Shear modulus	(MPa)
$\boldsymbol{\mu_i}$	Summit of Gaussian distribution i	(cm^{-1})
$\boldsymbol{\nu}$	Poisson ratio	-
$\boldsymbol{\rho}$	Density	(g/cm3)
$\boldsymbol{\sigma}, \boldsymbol{\sigma_f}$	Stress, Flexural stress	(MPa)
$\boldsymbol{\sigma_{max}}$	Ultimate tensile strength	(MPa)
$\boldsymbol{\sigma_i}$	Standard deviation of Gaussian distribution i	-
$\boldsymbol{\varphi}$	Porosity	(%)
$\boldsymbol{\omega}$	Deflection	(mm)

List of Figures

List of Tables

CHAPTER I

INTRODUCTION AND LITERATURE REVIEW

1.1 Background

How can we continue to feed an ever-growing population? At 8.2 billion in 2024, the global population is predicted to reach 9.7 billion by 2050 (UN, 2024) driving up the demand for meat, despite its production being strongly associated with environmental degradation, climate change, animal welfare and public health issues (Tilman, 1999). While a growing collective awareness of these problems in developed countries, has led to an increasing number of individuals reducing their meat consumption (flexitarianism) or shifting entirely to vegetarian or vegan diets (Salehi *et al*., 2023; Strässner *et al*., 2024), there has also been strong reluctance globally, especially in emerging countries, to cut down on meat consumption (Chikri and Hocquette, 2020; Mensah *et al*., 2022). In fact, it has been shown that in emerging countries meat consumption increases with rising income, mainly due to urbanisation and the expansion of the middle class (Delgado., 2003; Mensah *et al*., 2022), and only peaks at high levels of GDP per capita (Whitton *et al*., 2021). At the global scale, increases in both population and per capita meat intake in low- to middle-income countries, particularly in Sub-Saharan Africa and the Indian subcontinent, will be likely to dwarf the impacts of flexitarianism in high-income countries (Mensah *et al*., 2022, OECD/FAO,2024).

To maximise food production and keep costs as low as possible, most farms operate as factories or intensive farming systems which are known to be more destructive than traditional farming models. Consequently, animal farming is considered to be the most polluting and damaging industry to the environment (**Figure 1**), being responsible for 14.5% of all greenhouse gas (GHG) emissions (7.1 Gt/year), including 37% of all methane (CH_4; FAO, 2011), released as part of the natural digestive process of ruminants (*e.g.* cattle, sheep, buffalo). The industry also uses up to 30% of terrestrial land and 8% of global freshwater (FAO, 2011), mostly to grow livestock feed, of which 97% of ingested calories, throughout an animal's life, will end up being used for the maintenance of its vital systems and non-edible parts (Ben-Arye and Levenberg, 2019). With more farms being built to sustain meat demand, more arable land is needed, leading to the clearing of large forest areas and in turn resulting in ecocide (Vale *et al.*, 2019). It was recently reported that the Amazon Rainforest, once the largest carbon dioxide (CO_2) sink in the world, had become a neutral or net contributor of CO_2 (especially parts

of the Brazilian Amazon), partly due to deforestation for cattle farms (Brienen *et al.*, 2015; Kruid *et al.*, 2021). Another environmental concern is the heavy use of pesticides employed in the production of animal feed which has been shown to contribute to the disappearance of pollinating insects that are essential for the reproduction of plants (Brühl *et al.*, 2021). Moreover, uncontrolled intensive farming can cause loss of organic matter in soil, as well as soil contamination, thereby further reducing agricultural yield, and threatening food safety and sanitation (Kopittke *et al.*, 2019).

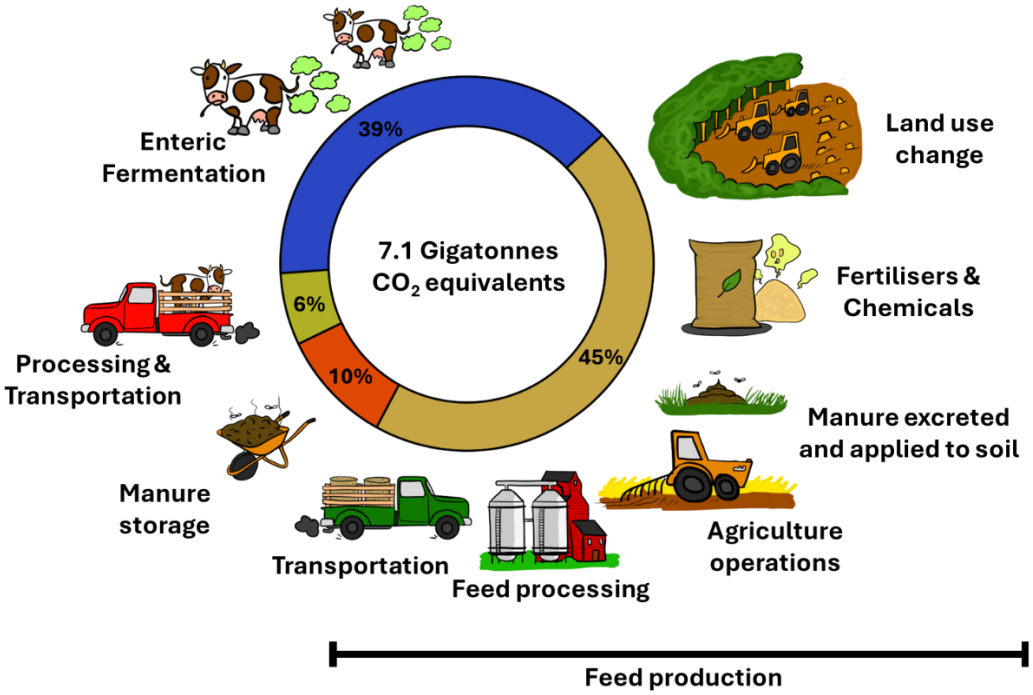

Figure 1: Source of livestock GHG emissions (Reproduced from Grossi et al., 2019).

Raising animals is very costly, and even more so when done in a humane manner (Fernandes *et al*., 2021). It can therefore be difficult to incentivise lower-income farmers to invest in animal welfare (Nollkaemper, 2023). As a result, animals are often raised under minimum legal standards, with many reports of abuse and poor legal enforcement (Anomaly, 2015). To maximise output, animals can be raised in tight spaces sometimes preventing free movement, and with high population densities, low ventilation and rudimentary diets, livestock animals are prone to disease (FAWC, 2012). To avoid outbreaks, farm animals are fed large quantities of antibiotics and vaccines that have been shown to positively correlate with the rise of antimicrobial resistance (AMR) in developed countries (Martin *et al*., 2015; Yang *et al*., 2018). By the year 2050, it has been predicted that AMR will be a leading cause of mortality in humans, ahead of cancer, creating a significant financial burden as well as a negative impact on health (WHO, 2012; O'Neill, 2014; WHO, 2014). In addition, prolonged human contact with diseased animals can lead to zoonotic infections. Antigenic shifts in viruses can create new viral subtypes, capable of animal-to-human transmission, which can mutate further to acquire human-to-

human transmission as was the case in the H5N1 swine and H1N1 bird influenza epidemics (Schmidt, 2009; Wibawa, *et al.*, 2011). According to the UK's National Risk Register of Civil Emergencies, pandemic flu scores highest in likeliness and severity amongst the emergencies likely to happen within five years (Nokes, 2017).

Given the increasing global demand for meat and the associated environmental damage, global warming, public health risks and animal welfare issues, it is clear that current animal protein production systems are no longer sustainable. As a result, there is a critical need for alternative sources of protein.

1.2 Sustainable Alternative Protein

To be successful, new foods must be sustainable, appealing to consumers and capable of competing in the current food market, without compromising dietary habits and cultural models (Bryant, 2020). Given the popularity of meat, alternative protein products should aim to replicate its organoleptic properties at a competitive price while addressing environmental, health and animal welfare issues (Post *et al*., 2020). Currently, the following four groups of meat alternatives have been developed and commercialised: plant-based analogues (PBAs), insect-based meats, mycoprotein and cultivated meats. PBAs (**Figure 2A**) are readily available, and are popular meat substitutes that appeal to vegans, vegetarians and flexitarians. The first PBA products were developed in the late 1960s and popularised by the hippie movement that promoted vegetarianism and healthy lifestyles. One of the first commercial products, often attributed as the 1982 "VegeBurger", was assembled from dry textured vegetable protein, a hallmark of the first generation of PBAs that was only popular with vegetarians (Smith, 2014; Penna Franca *et al*., 2022). In recent years, however, a lot of research and development has gone into developing a new generation of PBAs, designed for flexitarians, that accurately mimic the look, feel, smell and taste of traditional meat products (Rubio, *et al.*, 2020; Penna Franca *et al*., 2022; Benković *et al*., 2023). Insect-based meats (**Figure 2B**) are generally composed of crushed insects extruded into meat-like products. Unlike PBA, these products are virtually non-existent in many Western countries as insects are viewed as unappetising or even disgusting (de Koening *et al.*, 2020). Moreover, the products are not vegetarian, and insects must be reared and slaughtered, which poses ethical issues. Despite this, insect-based meats represent an excellent source of animal protein with a relatively low carbon impact (van Huis and Oonincx, 2017). Mycoprotein products (**Figure 2C**) such as Quorn, have been developed since the 1960s by using mycelia to convert agro-industrial waste-products into mycoprotein biomass through microbial fermentation processes (Majunder *et al*., 2024). These products are created in large-scale solid-state or submerged fermenters. Similarly to PBAs,

mycoprotein products are vegan and are popular with flexitarians due to the unique texture and flavour of mycoproteins that closely resembles meat (Souza Filho *et al*., 2019).

Figure 2: Alternative protein burgers. A) Plant-based (Beyond meat, n. d.), B) Insect-based (Space10, 2019), (C) Mycoprotein (Quorn, n. d.), (D) Cultivated meat (Parry, 2013)

Finally, cultivated meats (**Figure 2D**) are the latest development in alternative protein. Despite having been developed since the start of the 21st century, less than a handful of products have been approved for commercialisation anywhere in the world, making these cultivated products virtually inaccessible at this time (Benjaminson *et al*., 2002; Reynolds, 2024). Unlike other alternative proteins that aim to replicate the sensory properties of meat, cultivated meat is meat that has been grown and assembled in a laboratory, *in vitro*, using tissue engineering techniques instead of being grown in an animal, *in vivo*, as is traditional meat. As such, cultivated meat can be considered slaughter- and cruelty-free (Bryant, 2020). The principle of cultivated meat relies on the *in vitro* proliferation and differentiation of stem cells into the tissues that constitute meat (*i.e.* skeletal muscle or specific organs).

The main steps of cultivated meat production are schematised in **Figure 3**. First, stem cells are isolated from a live animal by means of a non-invasive biopsy. The stem cells are then cryopreserved, and if necessary immortalised, to create a cell bank, entirely removing the need for animals from this point on. The cells are then proliferated on engineered scaffolds or microcarriers in stir tank bioreactors to produce a cell biomass. The expanded stem cells are then differentiated into myocytes and adipocytes and the tissues are matured to form microtissues that can be assembled into unstructured products

(*e.g.* sausages, nuggets and burgers) or structured products (*e.g.* steaks, ribs and fillets). Meanwhile, the animal that the cells were harvested from continues to live on.

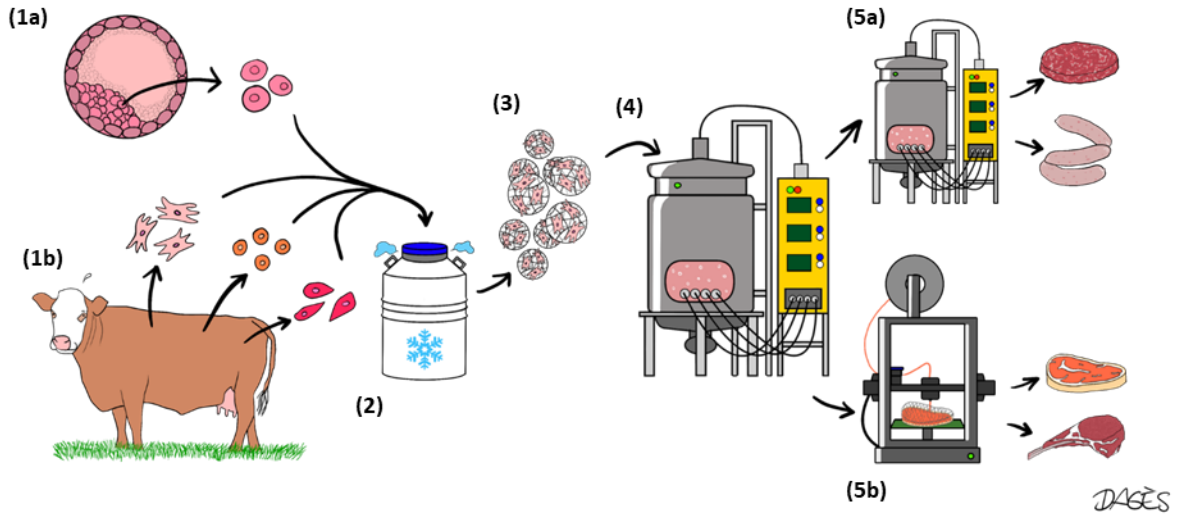

*Figure 3: Schematic representation of the production of cultivated beef. Starting cells which can be either **(1a)** embryonic stem cells derived harvested from embryos; or **(1b)** mesenchymal stem cells, induced pluripotent stem cells and precursor cells, such as satellite cells, harvested from the tissue of an animal. **(2)** The cells are cryopreserved for future use. **(3)** The cells are seeded on 3D supports such as microcarriers. **(4)** The cells are expanded on their supports in stirred tank bioreactors. **(5a)** The cells are differentiated in the bioreactor and the final cell mass is assembled into unstructured meat products, such as burgers and sausages. **(5b)** The cells are differentiated on 3D scaffold, enabling the creation of structured cuts.*

1.3 Advantages and Disadvantages of Cultivated Meat

Although stakeholders and most scientists claim that cultivated meats would positively impact the environment, public health systems and animal welfare issues, there is no consensus in the scientific community on the nature and extent of these impacts. Both advocates and critics of cultivated meats often repeat unsubstantiated claims, share biased views and ignore the bigger picture. In this section, the advantages and disadvantages of cultivated meats will be explored by sharing and critiquing both sides of the argument.

1.3.1 Environmental impact

Carbon dioxide (CO_2), methane (CH_4) and nitrous oxide (N_2O) are considered the three most common greenhouse gas (GHG) emissions, which are all emitted in large quantities by the animal farming industry (Liu *et al.*, 2018; Grossi *et al.*, 2019; Tian *et al.*, 2020; Lamb *et al.*, 2021). In addition to the CH_4 released by livestock, it is important to note that large quantities of N_2O and CO_2 are produced from fertilisers for livestock feed, animal transport and meat processing (Grossi, *et al.*, 2019). Cultivated meat proponents generally argue that large-scale cultivated meat production would have a lower global warming potential due to the absence of reared animals producing CH_4 and animal feed agriculture producing N_2O (Tuomisto and de Mattos, 2011; Mattick *et al.*, 2015). However, critics often

point out that the energy required to produce ingredients for culture media, warm incubators and bioreactors would produce enormous amounts of CO_2, exceeding the environmental impacts of livestock farming (Lynch and Pierrehimbert, 2019; Chriki and Hocquette, 2020). It could be argued that neither advocates nor critics are entirely correct in their assessments as all life cycle assessments (LCAs) are based on modelling and assumptions which may not hold true (Tuomisto *et al*., 2022). Smetana *et al*. (2015) showed that while the environmental impacts of production are currently higher for cultivated meat than for other alternative proteins there is a lot of room for improvement as cultivated meat research and development is still in its infancy (Smetana *et al*., 2015). Lynch and Pierrehimbert (2019) argued that cultivated meat production has no long-term benefits on the environment due to the high amounts of energy consumed in production, resulting in high emissions of CO_2, which remain in the atmosphere for much longer (>100 y) than CH_4 (12 y) (Hocquette *et al*., 2024; Lynch and Pierrehimbert, 2019). However, this argument overlooks the fact that the global warming effect of CH_4 is 28 times higher than that of CO_2 meaning that CH_4 emissions have a much larger immediate impact on global warming. It also assumed that methods of cultivated meat production would never change, ignoring the potential for improvements *e.g.* optimization of bioreactors, development of alternative culture media not derived from animals, and a reduction in the amount of energy and the use of fossil fuels. Tuomisto *et al*. (2022) showed that switching energy types from fossil fuels to wind power, using media free of foetal bovine serum, and increasing cell biomass during differentiation could reduce the environmental impact of cultivated meat by 73-82% (Tuomisto et al., 2022). In addition, they argued that, given these modifications, the production of cultivated beef would have a lower impact on energy consumption, global warming, land use, ozone formation, terrestrial acidification and water consumption than traditionally farmed beef. They did, however, confirm that the environmental impact of cultivated poultry would be higher than, or equal to, the environmental impact of traditionally farmed poultry (Tuomisto *et al*., 2024). In response, Hocquette *et al*. (2024) suggested the study ignored GHG emissions related to cell harvesting, medium and biomaterial recycling, and water treatment (Hocquette *et al*., 2024). Lastly, critics often insist that traditional farming could be made more sustainable. For example, there has been a lot of research into breeding genetically modified animals to produce less CH_4, with the Enviropig being a notable example (Petersen, 2018). That said, GMO products also suffer from neophobia and are widely rejected by the public (Siegriest and Hartmann, 2020).

Other arguments concern the use of land. While it is evident that cultivated meat production will occupy a much smaller space than the 40% of terrestrial land used for animal feed and grazing land (Herrero *et al.*, 2013), it should be noted that 50% of the land used by animals is considered non-arable (Hocquette *et al*., 2024). Still, Alexander *et al*. (2017b) showed that if 50% of traditional meat

was replaced with cultivated meat, there would be an increase of 29% in arable land that could be used for other purposes (Alexander *et al.*, 2017b). In response, critics argue that animals play a significant role in landscaping, maintaining soil carbon content and soil fertility (Teague, *et al.*, 2016). Animal dung being rich in organic matter, nitrogen and phosphorous, is used as manure providing essential nutrients to plants that eventually feed humans (Loyon, 2017). Animal grazing is also an important factor in landscaping and promotes biodiversity in plant and insect life (Chriki and Hocquette, 2020).

Another area of debate is the effect cultivated meat would have on employment. In the year 2000, 1.3 billion people worldwide were involved in agriculture (Herrero, *et al.*, 2013). If a significant shift from traditional to cultivated meat were to occur, the livelihoods of hundreds of millions of people would be at risk. Cultivated meat proponents would, however, assert that many jobs could transition towards the cultivated meat industry, ignoring the fact that many of these jobs would require a different skillset or level of education (Bryant, 2020). Nevertheless, it could be argued that the traditional farming model is already obsolete as it is very heavily subsidised and should be replaced with a sustainable and efficient alternative protein production system. A recent joint report from the Food and Agriculture Organization (FAO), United Nations Development Programme (UNDP) and United Nations Environment Programme (UNEP) outlined that 87% of world agricultural subsidies (representing USD540 B annually) were misspent, leading to distorted food prices, environmental degradation, inequality, and human health problems (FAO, 2021).

1.3.2 Public health

Cultivated meat suffers like many novel foods from neophobia (Hamlin *et al*., 2022). Despite the lengthy procedures required to prove food safety for regulatory approval, little is known about the long-term effects of frequent consumption of cultivated meats. In most countries, as for other foods, food safety regulations ensure that all ingredients have GRAS (generally regarded as safe) or equivalent status and have not caused any known side-effects in at least 10 years of commercialisation (Lanzoni *et al.,* 2024). However, food safety concerns extend beyond the list of ingredients to other considerations such as their quality and source. There is concern, for example, that genetic instability in cell lines could lead to cancer-like properties with phenotypic and metabolic changes to the cells (Hocquette *et al*., 2024). Moreover, the mid- to long-term effects of consuming the growth hormones used to stimulate cell proliferation are unknown (Chriki and Hocquette, 2020), and some regulatory bodies such as the European Commission have already banned the use of these substances in foods (Directive 81/602/EEC; European Commission, 1981).

On the other hand, cultivated meat has several known advantages for public health. Since it is grown *in vitro* in controlled and sterile environments (Ben-Arye and Levenberg, 2019), the whole process is far less susceptible to contamination than traditional meat production. In addition, the use of antibiotics in culture media is not necessary and the consequent reduction in their use would limit the emergence of AMR (McNamara and Bomkamp, 2022). Sterile *in vitro* cultures also eliminate the risk of personnel contracting zoonotic infections. Furthermore, in the case of sample contamination, batches are easily identified and removed from production (Djisalov *et al.*, 2021), removing the need to precautionarily cull entire populations of farm animals (Miguel *et al.*, 2020). Finally, the nutritional and biological profiles of cultivated meats could be engineered to reduce the risk of numerous health conditions, such as obesity, high cholesterol, type-2 diabetes and colorectal cancer, which have been linked with the consumption of meat, particularly red meat (Du *et al.*, 2020; Domingo and Nadal, 2017; Treich, *et al.*, 2021; Wolk, 2016).

1.3.3 Animal welfare and other ethical issues

Advocates for cultivated meats often insist that the removal of animals from the meat cultivation process would result in the elimination of many animal welfare issues (Bhat *et al.*, 2015). It should be noted, however, that even if all meat was cultivated, there would always be a need for a small number of reared animals for the harvesting of stem cells. In addition, critics often accuse proponents of hypocrisy because foetal bovine serum (FBS), which has been used in large quantities to supplement culture medium in cultivated meat research, requires the killing of foetal calves and the draining of their blood. Fortunately, extensive research in medium optimisation has led to the development of several serum-free alternatives, such as Beefy-9™, specifically designed for cultivated beef production (Stout *et al*., 2022) and xeno-free media like Essential8™ or TeSR™ that can be supplemented with a cocktail of plant and fungal derivatives (Kolkmann *et al*., 2019; Mitić *et al*., 2022; Yamanaka *et al*., 2023). In addition, most cultivated meat start-ups that have entered the production stage have developed in-house serum-free media (Mosa Meat, 2019; UPSIDE Foods, 2021).

Another ethical dilemma arises where animals must be ritually slaughtered for their meat to be permitted as food, according to religious laws or cultural practices. This makes the process of cell isolation from live animals, and subsequent culturing of meat, problematic. Jewish and Muslim authorities have long debated whether cultivated meat could ever be considered kosher (permitted by Jewish law) or halal (permitted by Muslim law) (GFI, 2018). Although there is no consensus in either religion, some religious scholars have stated that for cultivated meat to be permitted, stem cells should be isolated from the carcass of a ritually slaughtered animal that is permitted as food (Hamdan *et al*., 2024). Another view which the Israeli Chief Rabbi recently stated, is that cultivated meat is not subject to the religious laws concerning meat as he does not consider it to be meat at all (Klein, 2023).

1.3.4 Food Insecurity

Food insecurity caused by over-reliance on traditional agriculture is a matter that is often neglected by both proponents and critics of cultivated meat. The coronavirus disease 2019 (COVID-19) and the ongoing war in Ukraine have put significant strain on global food security and highlighted major flaws in traditional agricultural food systems and the fragility of the global food supply chain. During the pandemic, abattoirs became hotspots for COVID-19 transmission due to the proximity of workers for long hours in cold temperatures which facilitated cross-contamination (Choi *et al*., 2023; Higuita *et al*., 2023), forcing many abattoirs to shut down or run at partial capacity (Grandin, 2021). In fact, disruptions in markets caused by the COVID-19 pandemic led to a 28% increase in the FAO global food price index in 2021 (de La Hamaide, 2023). In addition, the ongoing wars in Ukraine and the Middle East, which have the potential to spill-out to neighbouring regions, further demonstrate the fragility of global food supply. The war in Ukraine has driven up energy prices and caused a sharp decline in cereal exports, contributing to a 14.3% increase in the FAO global food price index in 2022 (de La Hamaide, 2023). It is to be noted that Ukraine is the largest producer of wheat and cereals for both human and livestock consumption, exporting to many countries, some of which had populations already living in a state of food insecurity prior to the war (Filho *et al*., 2023; Laber *et al*., 2023). Livestock epidemics, such as H1N1 avian influenza, have also contributed to supply shortages, trade flow disruptions and loss of consumer confidence (Rzymski *et al*., 2021).

All these recent events should serve as a wake-up call to start producing food in a more controllable and secure way, and transition to renewable energy systems (Rzymski *et al*., 2021). Cultivated meats could help to ensure food security even in the worst eventualities such as global pandemics, wars, nuclear accidents or famines (Xia *et al*., 2022).

1.4 History of the development of cultivated meat

The development of cultivated meat was hailed by a series of predictions, the popularisation of science fiction, and major scientific breakthroughs within the last 100 years or so. One of the first recorded mentions of artificial meat as a concept was described in 1894 by French chemist Pierre Eugene Marcellin Berthelot who predicted that, by the year 2000, eggs, milk and meat would be synthesised in factories (Kirsch *et al*., 2023), although he did not explain how these might be produced. In 1930, British politician Frederick Edwin Smith, 1st Earl of Birkenhead, envisioned a near future where steaks could be grown in suitable media in a laboratory, substantially cutting down the time needed to rear animals to produce meat (Smith, 1930). In 1931, Winston Churchill famously published *Fifty Years Hence* in which he wrote ‘We shall escape the absurdity of growing a whole chicken in order to eat

the breast or wing, by growing these parts separately under a suitable medium...The new foods will from the outset be practically indistinguishable from the natural products, and any changes will be so gradual as to escape observation.' He stated that this would be possible as further understanding of growth hormones would allow the control of growth *in vitro* (Churchill, 1931). These predictions came at a time of major and exciting breakthroughs in cell culture and the newly forming field of tissue culture led by scientists such as Carrell, Burrows and Harrison (Jedrzejczak-Silicka, 2017). In 1912, Alexis Carrell, for the first time successfully expanded and immortalised a culture of embryonic chicken heart fibroblasts. By culturing the tissue under aseptic conditions and supplementing the media with chicken embryo extracts, he demonstrated that nutrients present in media participated in the formation of protoplasm, thus contributing to cell growth and division, and that cells could, in theory, divide indefinitely outside the body (Carrell, 1912). Ten years, and 1860 cell passages, later, Albert Ebeling described Carrell's cell line as still displaying a similar appearance, functionality and growth rate as the original culture. He also pointed out that from the original 1 mm^3 of biopsied heart tissue, cultured over 10 years, 30,000 cultures had been established, and that if the cells had been dividing continuously in that period, their total mass would have exceeded the mass of the Sun (Ebeling, 1922). Carrell's immortal chick cell line was terminated in 1946, far exceeding the life expectancy of a chicken (Witkowski, 1980).

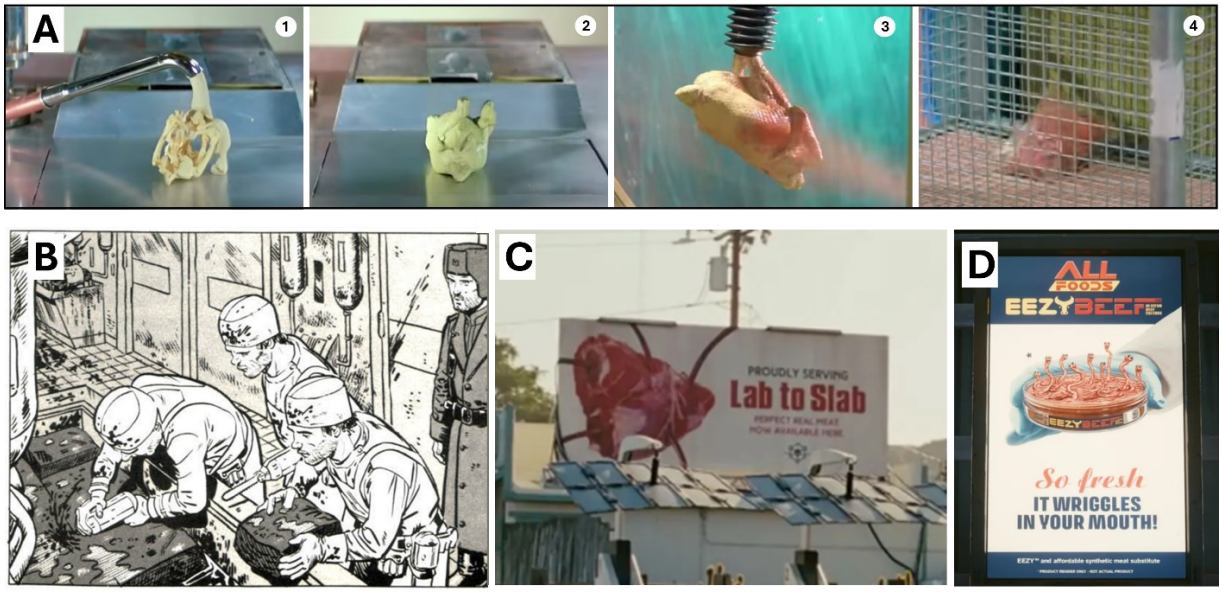

Figure 4: Cultivated meat in pop culture. (A) Lab grown chicken from film The Wing or the Thigh (Zidi, 1976), (1) An artificial meat paste is cast on a synthetic skeleton scaffold and shaped to resemble a raw chicken (2), (3) the chicken is then spray-painted to mimic colour of real meat, (4) the product is immediately packaged and ready for sale. (B) A semi-living and constantly regenerating slab of meat referred to as the Mother in the Snowpiercer comic book (Lob and Rochette, 1982), (C) a billboard advertising lab grown meat as "perfect real meat" in the third season of the Westworld television series (Nolan and Joy, 2016-2022), (D) An advert for EEZY Beef, a frequent reference to cultivated meat in the video game Cyberpunk 2077 (CD Projekt, 2022).

These achievements continued to inspire the public, and from the 1940s, references to artificial or synthesised meat multiplied in science fiction literature (**Figure 4**) with notable examples including *Ashes, Ashes* (Barjavel, 1943), *The Space Merchants* (Pohl and Kornbluth, 1952), *The Four Day Planet* (Beam Piper, 1961/2006) and *Snowpiercer* (Lob and Rochette, 1982). Artificial meat was also depicted on screen notably in *Star Trek* where the crew were often seen using food synthesisers and protein resequencers in the various series (Castle, 2022). In most science-fiction references, synthetic meat is depicted negatively, often grown as an *ersatz* product (an inferior-quality replacement product) in dystopian universes or in outer-space where traditional food is unavailable. In the French comedy film *The Wing or the Thigh* (Zidi, 1976), the protagonists break into a factory synthesising whole chickens and fish products, shown in a way that disgust the viewer and vilifies the artificial meat as a threat to French gastronomy and *haute cuisine*. Science-fiction writers were not the only people who were inspired by advances in tissue engineering. After experiencing near-starvation as a prisoner of war and witnessing the very cruel treatment of animals by his Japanese captors, Dutch physician Willem Van Eelen felt a moral responsibility to eliminate animal suffering (Wurgaft, 2015). In 1953, excited by large-scale tissue engineering experiments happening at the time, Van Eelen imagined employing these methods to produce meat, at which point he started his life journey dedicated to researching, promoting and acquiring funds for the development of cultivated meat (Balasubramanian *et al*., 2021). In 1981, Evans and Kaufman successfully isolated embryonic stem cells, describing these as self-renewing pluripotent cells (Evans and Kaufman, 1981). The potential of these cellular properties was immediately recognised by Van Eelen for the production of cultivated meat, which had, until then, been only theoretically possible. In 1999, Van Eelen filed the first patent for industrial production of meat using cell culture methods (Van Eelen, 1999). Van Eelen is now considered by many as the Godfather of *in vitro* meat. It was around this time that the first experiments designed to produce lab-grown meat for human consumption started gaining traction. Seemingly straight out of science fiction, the first studies aiming to culture meat were piloted by the United States (US) National Aeronautics and Space Administration (NASA) with the objective of growing animal protein for long-term space travel (Benjaminson *et al*, 2002). In the first experiment, Benjaminson *et al*. cultured goldfish steaks to increase their size. Although the product was not tasted, an inspection revealed that the tissue looked and smelled like fish making it 'acceptable as food' (Benjaminson *et al*., 2002). Following this success, the team also cultured chicken steaks (Wolfson *et al*., 2002), but all subsequent projects were shelved by NASA when space travel was no longer considered a priority (Stephens *et al*., 2019). Around the same time, Oron Catts and Ionat Zurr used tissue engineering techniques for artistic expression and started developing *semi-living* tissues *in vitro*. As part of the exhibition *L'Art Biotech* in France (2003), Catts and Zurr designed *Disembodied Cuisine*, exploring the idea of growing victimless meat.

This art installation was constructed in two parts with healthy frogs living their best life on one side, and steaks from these same frogs being cultured *in vitro* on polymeric scaffolds on the other side. On the exhibition's last day, the cultivated steaks were consumed in front of the healthy frogs (Stephens *et al*., 2019), marking the first time that humans ate cultivated meat (Treich *et al*., 2021). In 2004, New Harvest was founded with the goal of promoting cultivated meats and funding academic research via philanthropic donations (Kirsch *et al*., 2023). New Harvest also played a significant role in steering the first wave of researchers in this field (Stephen *et al*., 2019). In 2011, Mark Post from the University of Maastricht claimed in *The New Yorker* that growing beef burgers was already possible with current technology, but significant financial support would be needed to make it a reality. Two years later and following the hefty financial donation from Google co-founder Sergei Brin, Mark Post revealed the first ever cultivated beef burger to the world (Post, 2014). Despite a production cost of €250,000, this event placed cultivated meat firmly into reality, driving financial investments into high-tech ventures. This led to the advent of the start-ups and a second wave of research (Stephens *et al*., 2019). By 2016, several start-ups including Mosa Meat (founded by Mark Post), Memphis Meats and Modern Meadows were founded, and new and cheaper products were developed, with Memphis Meats producing a cultivated meatball for around US$1,200, a fraction of the cost of Post's burger made three years prior (Fernandes *et al*., 2022). That same year the Good Food Institute (GFI) was founded with the mission of raising awareness of cultivated meats and funding start-ups. Both the GFI and New Harvest would go on to play a significant role in the research outputs and technological breakthroughs in the following years.

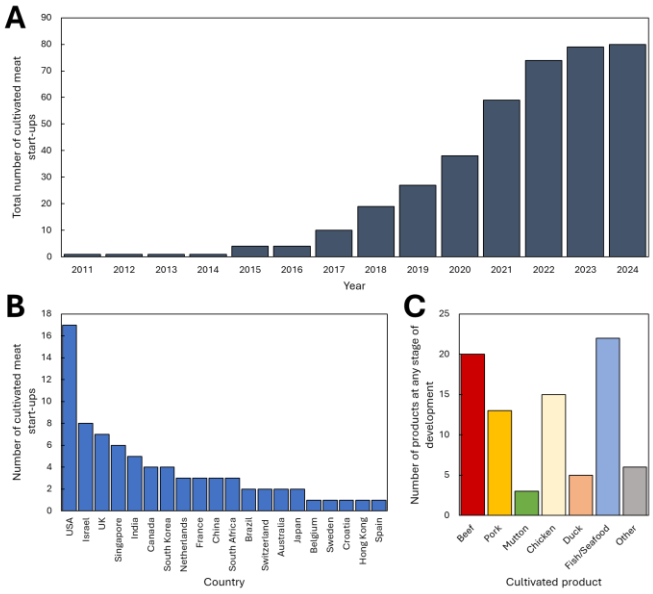

Figure 5: Rise of the start-ups. (A) growth of start-ups dedicated to cultivated meat end-product development and manufacturing, (B) number of cultivated meat start-ups by country, (C) number of products in development (GFI, 2024).

With an increasing number of start-ups dedicated to the development and production of cultivated meat end-products (**Figure 5**), and with the support of a plethora of industries transitioning to facilitate cultivated meat production, scientific breakthroughs have occurred very rapidly. In 2018, after three years of development, Aleph Farms produced the first cultivated beef steak, consisting of aligned myocytes that mimicked the mouthfeel of traditional steaks. It was the first ever structured product to be unveiled to the public and it had an estimated cost of US$50. This relatively low cost was attributed to the use of serum-free media (GFI, 2018). However, its thickness was only 5 mm due to issues regarding tissue perfusion (Carrington, 2018). It took another three years before Aleph Farms produced thick marbled steaks, assembled using 3D bioprinting technology (Badoim, 2021; GFI, 2021b). Like its predecessor it had a cost of US$50, but its size was larger than the 2018 prototype. In 2023, Australian start-up Vow shocked the world by presenting the Mammoth Meatball which used the DNA of the extinct woolly mammoth to engineer the gargantuan meat product (Carrington, 2023). This breakthrough opened up new possibilities for designing new flavours for meat of extinct, hybrid or genetically modified creatures.

A drive to deliver products to market and gain a competitive edge, led many start-ups to enter the production phase even before starting the regulatory approval processes in their countries (Nurul Alam *et al*., 2024). Regulation was, and remains a challenge for authorities worldwide, given the range of cultivated products that could potentially enter the market. The European Union (EU) already had a system for regulating novel foods in place, and in 2019 updated the policy on novel foods *Regulation EU 2015/2283* to include cultivated meat products (Lanzoni *et al*., 2024). To apply for approval, a scientific dossier including food safety studies must first be submitted to the EU Commission for examination. If the novel food is liable to have an effect on human health the Commission requests the European Food Safety Authority (EFSA) to carry out a risk assessment. The EFSA must then draft a decision on whether to accept or deny the authorisation which becomes final after the approval of the Plants, Animals, Food and Feed (PAFF) standing committee, which includes a representative of each EU member state. If a product is authorised, it is added to the Union List of Novel Foods with a generic effect which allows any company to market the novel food without submitting a new application (Lanzoni *et al*., 2024). Regulatory approval therefore relies on back-and-forth bureaucratic interactions that can take years and be financially draining. To make things worse, there are no global standards on how to treat, define or legalise novel foods.

In the USA, in the absence of specific legislation on the approval of novel foods, a joint effort was made in 2019 by the Food and Drug Administration (FDA) and the United States Department of Agriculture (USDA) to outline a path to bringing cultivated products to market. Now the FDA is responsible for guiding applicants through the regulatory process and assessing the initial stages of

production regarding safety guidelines. The USDA then takes over and is responsible for the oversight of marketing, labelling and packaging (Lanzoni *et al*., 2024). In December 2020, the Singapore Food Agency (SFA) approved the marketing of Eat Just's cultivated chicken nuggets, making Singapore the first country in the world to approve a cultivated meat product (BBC, 2020). In June 2023, the USA became the second country to legalise cultivated chicken products from both UPSIDE Foods (formerly Memphis Meats) and GOOD Meat (a subsidiary of Eat Just, Inc) (Milman, 2023). Later that year, Israel became the first country to approve a cultivated beef product, a 3D printed steak, manufactured by Aleph Farms (Southney, 2024). Finally, in June 2024, the United Kingdom (UK) became the first European country to approve the sale of cultivated chicken, albeit as pet food, manufactured by Meatly (Jones, 2024). In July 2024, French start-up Gourmey submitted the first application for regulatory approval in the EU to authorise sale of cultivated duck foie gras (Bambridge-Sutton, 2024). The approval process, expected to take 18 months, could lead Gourmey to compete with Aleph Farms to be the first company to market cultivated meats in the European continent, following Aleph Farm's filing for approval in Switzerland and the UK in 2022 (GFI, 2023). Despite the approval of several cultivated products, they have not been widely available anywhere, as they have only been produced in tiny quantities. In Singapore, in 2024, GOOD Meat announced the sale of its frozen cultivated chicken nugget, available only from Huber's Butchery for S$7.20 (approximately US$5.50 for 120 g). Previously its cultivated chicken had been available exclusively at the restaurant of the 1880 club (GOOD Meat, 2024). In the USA, GOOD Meat and UPSIDE Foods products were sold exclusively at restaurants China Chilcano and Bar Crenn, respectively. However, it has been reported that all sales in the US and Singapore have now ceased entirely, making cultivated meat completely inaccessible (Reynolds, 2024). Nonetheless, while Aleph Farms has yet to publicly release its product, its sale is expected soon in one of the restaurants of Michelin-starred chef Eyal Shani (Mridul, 2024).

Despite a global rise in attitudes favouring the development of cultivated meat products, recent pushbacks may curb progress. In 2024, Italy, France and Austria wrote to the EU Commission calling for a ban on cultivated meat in the EU in favour of primary farm-based food production (5469/1/24 REV 1, 2024). The letter which was supported by the Czech Republic, Cyprus, Greece, Hungary, Luxemburg, Malta, Romania and Slovakia also called for more transparency regarding the cultivated products which should 'never be called meat'. They also asked the EU commission to conduct a science-based and comprehensive assessment of the development of cultivated meat production which it deemed a non-sustainable alternative to farm-based production. To justify this statement, the authors cherrypicked references by only citing the notoriously biased Lynch and Pierrehumbert paper (2019) as well as a non-peer reviewed article claiming cultivated meat production to be 25 times worse for the environment than traditional farming. The countries then immediately called on the

commission to ‘ensure accurate and independent science-based information-sharing and counter any green-washing campaigns’, which (as comical as it sounds to any scientist) exemplifies a complete rejection of cultivated meat by many European countries, regardless of what the science actually says. To protect their culinary heritage, Italy passed a bill in parliament banning the production, import and commercialisation of *synthetic* meats, and together with France decreed that plant-based and cultivated products could no longer use any descriptors of meat (such as salami, sausage, steak or burger; Sabelli, 2023). Although, both bills were unconstitutional and violated EU legal procedures, the growing reticence of these countries could influence or even block outright the ruling of the PAFF in the final stage of novel food regulatory approval. Similarly, despite the USA leading the industrial and academic output in the field and having already approved the sale of two cultivated meat products, Florida and Alabama passed bans on cultivated meat to ’fight back against the global elite’s plan to force the world to eat meat grown in a petri dish or bugs’ as stated by Florida Governor Rob De Santis (Honderich, 2024). In addition, Arizona, Tennessee, Iowa, Nebraska and Illinois have also proposed bans concerning the sale or labelling of cultivated meat (Nowell, 2024). In both Europe and the US, objectors to cultivated meat defined the foods as *fake*, *artificially lab-grown* or *synthetic*, rather than *cultivated* or *cultured* as they are overwhelmingly defined by everyone else (Hocquette *et al*., 2024). Interestingly, several studies have shown that nomenclature plays a significant role in consumer acceptance and in providing descriptive information about products (Siegriest *et al*., 2018; Stephens *et al*., 2019; Malerich and Bryant, 2022). When NASA started experimenting with meat grown in a lab, they referred to their creation as ‘edible *in vitro* muscle protein’. The term *in vitro meat* was soon adopted by the scientific community and even popularised by Van Eelen, who in 2005 created the *Invitromeat Foundation* (Stephens *et al*., 2019). However, this changed in 2011, following the *European Science Foundation Exploratory Workshop in In Vitro Meat* conference where discussions led to a shift in nomenclature to *cultured meats*. While the *in vitro* prefix was considered essential to scientifically describe the product, scientific descriptors were shown to reduce consumer acceptance and increase disgust (Siegriest *et al*., 2018). *Cultured meat*, on the other hand, appealed to consumers as a classy product sounding superior to traditional meat, which conveyed the connotation of cell culture (Stephens *et al*., 2019). However, *cultured meat* had drawbacks too, as traditional seafood aquacultures technically also involve culturing foods, hence the descriptor was shown to be misleading in relation to grown seafood (Malerich and Bryant, 2022). In 2016, the term *clean meat*, which evokes *clean energy*, was popularised by GFI and was well-received by both scientists and prospective consumers but it was strongly disliked by traditional meat producers as it could be understood to imply that traditional meat is unclean or dirty (Malerich and Bryant, 2022). In 2018, the USDA and FDA started referring to lab-grown meat as *cell-based* as part of their regulatory

approval vocabulary, however the descriptors did not include the word *meat*. *Cell-based meats* was used by GFI but studies showed that the term lacked consumer appeal. Finally in 2019, the term *cultivated meat*, made an appearance and was heavily promoted by GFI and widely adopted (Friedrich, 2019). In 2021, it was shown that 75% of start-ups in the field preferred the term *cultivated* (GFI, 2021), nevertheless, other terms are still used, especially *cultured* and *cell-based*.

Overall, development of cultivated meat has come a long way but still has to face many legal, ethical, philosophical, cultural, and scientific challenges and limitations in order to create an appealing successful meat alternative and bring cultivated meat to market for all. Scientific research to guide further development in CM should help to overcome some of these issues.

1.5 Review of scaffolding methods for cultivated meat production

1.5.1 Cell types

Meat is defined as the flesh and other edible parts of an animal, typically mammal or bird, used for food which generally include skeletal muscle, organs, fat, and connective tissues. To match consumer expectations, cultivated meat are engineered to mimic the cellular and nutritional composition of traditionally farmed meat, as well as to match the sensory and textural properties of particular meat products (Verbeke *et al.*, 2015; Pakseresht *et al*., 2022). The anatomical, physiological and molecular properties of meat all influence its organoleptic properties and depend on many factors such as the animal species and subspecies (Bender, 1992; Chriki *et al*., 2013), type (*e.g.* skeletal muscle, organs*)*, location (*e.g.* specific cut)*,* function of tissue (Zhang *et al.,* 2017; Lee *et al*., 2023), as well as environmental factors (*e.g.* animal diet and activity) and post-mortem maturation (Tornberg, 1996; Starkey *et al*., 2016).

For cultured meat to replicate the sensory attributes of meat, it should be composed of the appropriate cells and tissues found in the native meat. It is estimated that skeletal muscle is composed of 90% muscle fibres, 10% fat and connective tissues and 0.3% blood mostly as myoglobin (Listrat *et al.*, 2016). Various cell lines have been used to grow skeletal muscle *in vitro*, each having their own advantages and drawbacks, summarised in **Table 1**.

Table 1: Properties of stem and progenitor cells used for cultivated meat production.

Cell types	Description	Advantages	Disadvantages	References
Satellite cells (SC)	Myocyte progenitor cells involved in muscle tissue maintenance and repair.	Naturally programmed to differentiate into muscle cell. Can be harvested from carcasses or live animal biopsies.	Differentiates only into muscle tissue. Aging requires constant isolation (low cost-effectiveness). Requires co-culture with other progenitor cells to grow fat and connective tissue.	Post *et al.*, 2014; Stout *et al.*, 2022; Stout *et al.*, 2023; Skrivergaard *et al.*, 2023
Embryonic stem cells (ESC)	Pluripotent stem cells derived from blastocyst.	Unlimited cell division. Creation of cell banks removing need to re-isolate cells. Pluripotent.	Difficulty in controlling specific lineage differentiation. Low myogenic differentiation potential. Ethical concerns with harvesting of embryos for ESC isolation.	(Li *et al.*, 2003; Cao *et al.*, 2009; Bogliotti *et al.*, 2018; Zehorai *et al.*, 2024)
Mesenchymal stem cell (MSC)	Multipotent adult stem cells from various mesoderm tissues.	Can differentiate into myogenic and fibro-adipogenic lineages. Abundant and easily isolated from live animal biopsy. Differentiation easier to control than ESCs. Can build cell banks under the right conditions.	Limited cell divisions and undergoes senescence *in vitro*. Can require repeated isolations.	(Hanga *et al.*, 2020; Hanga *et al.*, 2021; Zaguri *et al.*, 2022)
Induced pluripotent stem cell (iPSC)	Somatic cells that are genetically reprogrammed to induce pluripotency.	All cell types can be converted into iPSC. Isolation from live animals. Easier and less invasive.	May not replicate the behaviour of primary stem cells. Issues regarding GMO consumer acceptance and food regulation.	(Talluri *et al.*, 2015; Genovese *et al.*, 2017; Su *et al.*, 2021)
Transdifferentiated cells	Somatic cells (often fibroblasts) that are differentiated into muscle/fat via ectopic expression of myogenic/adipogenic determinants.	Like with iPSC any cell can be transdifferentiated. Isolation from live animals. Easier and less invasive.	Issues regarding GMO consumer acceptance and food regulation.	(Patiska *et al.*, 2022; Kim *et al.*, 2024; Ma *et al.*, 2024)
Immortalised cells	Immortal cell lines are created by engineering genes involved in senescence and division in aging cells.	Isolation from live animals easier and less invasive. Cost-effective.	Issues regarding GMO consumer acceptance and food regulation.	(Patiska *et al.*, 2022; Stout *et al.*, 2023; Ma *et al.*, 2024)

1.5.2 Scaffolds and Microcarriers for cultivated meat production

In their native environments, cells are surrounded by a naturally secreted matrix providing the mechanical, chemical, and physical needs of the cells present in the microenvironment (Molina *et al.*, 2020). This highly porous and nanofibrous material, referred to as the extracellular matrix (ECM), provides a cell-specific niche and plays a crucial role in the natural development, maintenance and repair of tissue. The ECM is composed of hundreds of proteins and proteoglycans, helping in cell attachment, migration, proliferation, and differentiation (Gillies and Lieber., 2011). *In vivo*, the ECM provides a natural scaffold for cells to grow, proliferate, differentiate and mature in 3D (Gattazzo *et al.*, 2014).

In vitro, anchorage-dependent cells, such as MSCs, require a surface to attach to and proliferate on. Although this could be achieved on planar surfaces using cell culture flasks or well plates, tissues grown in 2D form monolayers, and monolayers do not efficiently mimic the natural structure or function of native tissue (Kapałczyńska *et al*., 2018). In addition, 2D cultures, owing to the low surface-to-volume ratio of flat surfaces, are poorly scalable and unsustainable as huge amounts of culture media and single-use plastics are needed to generate a sufficient cell biomass to create meat (Bodiou *et al.,* 2020). Instead, supports with higher surface-to-volume ratio, such as scaffolds, microcarriers and hydrogels are engineered to provide a 3D architectural foundation that can replicate the physical, biochemical and biomechanical properties of the native ECM and therefore provide a microenvironment that is tailored for cell attachment, growth and maturation (Lee and Choi, 2024). Using 3D supports also allows the creation of thick tissues that can replicate the structural and textural properties of meat (Fasciano *et al*., 2024).

1.5.2.1 Scaffold production methods

In general, scaffolds refer to any 3D support used to grow cells *in vitro* whatever their size or function. In the last few years, several techniques, mostly adapted from the wider field of tissue engineering, have been used to fabricate an array of scaffold types for cultivated meat production (**Table 2**).

Table 2: Advantages and drawbacks of scaffold fabrication techniques used in cultivated meat and tissue engineering.

Method	Description	Advantages	Drawbacks	References
3D bioprinting (Extrusion bioprinting, stereolithography, laser assisted bioprinting, droplet-based bioprinting)	Polymer solutions or bioinks are deposited on substrate layer-by-layer.	Highly versatile and tuneable. Computer-aided designs can be generated from MRI and CT scans.	Not all biomaterials can be bioprinted. Poor resolution (100 µm) makes it hard to replicate ECM with high fidelity. Expensive equipment.	(Ianovici *et al.*, 2022; Zagury *et al.*, 2022; Su *et al.*, 2023)
Electrospinning (dry, wet, melt, needless, iRJS)	Electrostatic forces draw fibres from the polymer solution after applying a high voltage. The fibres are then collected as a mesh on a grounded collector.	Uniform and tuneable nano-to-microscale fibres. High porosity and interconnectivity. ECM-like structures. High mechanical properties. Relatively cheap, simple, and reliable process. High cell viability.	Potentially toxic solvents. Spun mats are fragile and difficult to handle or store. Needs high voltage generator.	(MacQueen *et al.*, 2019; dos Santos *et al.*, 2024)
Phase separation (Thermally induced, diffusion induced)	Two or more polymers with different solubilities separate in their respective solvents.	Relatively high porosity. Can control scaffold thickness. Simple process.	Potentially toxic solvents. Poor control over architecture. Limited pore size.	(Ogawa *et al.*, 2024)
Gas foaming	Gas is dissolved in polymer under high pressure. Pressure is then lowered for gas to escape and form pores in the scaffold.	Solvent-free process. Keeps bioactive molecules in the scaffold.	Poor interconnectivity of porosity. Needs high pressure. Poor reproducibility.	(Tang *et al.*, 2024)
Solvent casting (Particulate leaching, salt or porogen leaching)	A polymer and porogen composite is cast. The solvent is then evaporated and water-soluble porogens are removed by washing the scaffolds, revealing porous structure.	Simple fabrication. High mechanical stability.	Uncontrolled structure. Low reproducibility.	(Su *et al.*, 2024)
Freeze drying	A polymer solution is mixed in water then frozen. Using a low temperature and vacuum, ice crystals in the polymer are sublimated leaving a porous network.	Moderately high porosity. Can produce nano-fibres. High cell viability. No separate leaching steps.	Irregular porosity and low pore size. Long process time. Needs freeze-dryer.	(Xiang *et al.*, 2022; Chen *et al.*, 2024)
Decellularised tissues (Animal, plant, mycelium)	Cells and nucleic acid of a tissue are removed using chemicals and enzymes until only the native ECM remains.	Decellularised ECM mimics native cell microenvironment. Excellent physical structure, biochemical and mechanical properties. Perfusion possible. Decellularised plants and fungi are more scalable. GMO plants can express natural cell adhesion motifs, increasing cell attachment.	Limited scalability. Decellularised animal tissues are expensive and risk immune response. Harsh chemicals can damage ECM proteins. Potentially toxic.	(Thyden *et al.*, 2022; Murugan *et al.*, 2024; Sood *et al.*, 2024)
Cell sheet technology (Scaffold-free)	Monolayer "sheets" are lifted by changing the temperature. The sheets are then stacked to create volume.	Mimics natural self-organisation. High cell viability. Final product is 100% meat without detaching or degrading scaffolds. Sustainable.	Complex process. Low scalability. Poor control over tissue structure.	(Yang *et al.*, 2005; Tanaka *et al.*, 2022)

Hydrogels that are capable of absorbing and retaining large amounts of water are often used as scaffolds as they promote cell attachment and proliferation. Through physical or chemical crosslinking, their physical and mechanical properties are tuneable, allowing the resulting constructs to provide

structures which facilitate organised tissue formation. In addition, hydrogels can mimic the textural properties of meat, owing to their high-water content. Hydrogels can also be used as bioinks for 3D printing where the cells are encapsulated within the hydrogel and then deposited layer-by-layer with precise control by the printer. Zagury *et al*. (2022) used alginate hydrogels to differentiate adipose-derived bovine mesenchymal stem cells into mature adipocytes. The hydrogels were subsequently dissolved, and the adipocytes were added to muscle cells in an alginate, soy and pea protein bioink that was 3D printed to form marbled steak (Ianovici *et al*., 2022; Zagury *et al*., 2022).

More traditional scaffolds have been engineered to mimic the fibrous and porous structure of the ECM. Porous scaffolds constructed using solvent casting, freeze drying, or gas foaming are characterised by their large porous network that facilitates oxygen (O_2) and nutrient diffusion. Their large pores (50-250 µm), also allow cell infiltration into the scaffolds, facilitating attachment, migration and differentiation, and resulting in the formation of thicker tissues. Xiang *et al*. (2022) freeze-dried wheat glutenin to form porous sponges that supported the proliferation of bovine satellite cells without extra functionalisation or crosslinking-strategies, thereby creating efficient food-safe and cost-effective scaffolds for cultivated meat production (Xiang *et al*., 2022).

Fibrous scaffolds, on the other hand, are characterised by their nano-to-microfibrous network which mimics the ECM skeletal muscle, thus providing an ideal microenvironment for muscle and fat tissue growth. Unlike porous scaffolds, the pores of nanofibrous scaffolds are much smaller and can prevent cellular infiltration (Wu and Hong, 2016). Dos Santos *et al*., (2024) electrospun cellulose acetate to form nanofibrous sheets that promoted mouse myoblast (C2C12) and chicken satellite cell attachment, proliferation and differentiation. They then stacked up to four of the nanofibrous sheets to form 300-400 µm thick tissues (dos Santos *et al*., 2024).

Decellularised tissues are an alternative to engineered scaffolds. Whether from animal, plant or fungus tissue, decellularisation allows the use of real ECM to grow tissue *in vitro,* thereby providing a scaffold with excellent cytocompatibility that strongly mimics the native environment of the cells. Decellularised scaffolds derived from renewable sources are also sustainable and cost-effective. Sood *et al*. (2024) used decellularised apple to fabricate natural porous scaffolds that promoted the attachment and proliferation of bovine satellite cells (Sood *et al*., 2024). Finally, scaffold-free techniques are also used which allow the formation of tissues without exogenous biomaterials. One of the most common methods uses cell-sheet technology. In this method, cells are grown in 2D in temperature responsive dishes. By changing the temperature, the cells can lift in a sheet without the use of proteolytic enzymes (Yang *et al*., 2005). The cell sheets are layered one on top of the other to form thick tissues. Tanaka *et al*. (2022) grew and stacked bovine myoblast cell sheets to form

1.3 - 2.7 mm thick muscle tissue without scaffolds (Tanaka *et al*., 2022). Other scaffold-free methods such as the use of self-assembling peptides to allow cells to secrete their own ECM have been used in tissue engineering but have yet to be explored for cultivated meat production (Lee *et al*., 2017).

1.5.2.2 Improving scaffold scalability

To generate enough cells to create meat (>10^{10} cells; Post *et al*., 2020), cells must be expanded quickly and efficiently in controllable and scalable bioprocess pipelines (Moutsatsou *et al*., 2023). For cultivated meat production, adherent cell expansion is generally achieved with the use of microcarriers cultured in suspension in bioreactors (Bellani *et al*., 2020). Microcarriers are typically micro sized beads (90-350 µm in diameter; Derakhti *et al*., 2019) that have a high surface-to-volume ratio and provide a relatively large surface for adherent cells for growth in suspension (Bodiou *et al*., 2020). The total growth surface of microcarriers can be increased by progressively adding new microcarriers to a culture. Indeed, cells have been shown to migrate to empty microcarriers via bead-to-bead transfer (Verbruggen *et al*., 2018; Rafiq *et al*., 2018; Hanga *et al*., 2021). Microcarriers come in a variety of materials, shapes and sizes. Commercial microcarriers have long been designed to mass produce cell-produced molecules such as proteins and monoclonal antibodies. Recently, developments in tissue culture, and, in particular, the advent of regenerative medicine, have driven the development of new microcarriers designed for the expansion of human stem cells (Bodiou *et al*., 2020). However, these are not designed for cultivated meat, which has very different requirements, partly dictated by food safety and the need to scale up production.

In most of the literature, cell expansion and differentiation are performed using different substrates (Bodiou *et al*., 2020). Following cell isolation, scientists use microcarriers to massively expand the cell population in bioreactors with proliferation media. Once expanded, the cells are removed from the microcarriers by either enzymatically detaching the cells or dissolving or degrading the microcarriers and recuperating the detached cells. The cells are finally seeded or encapsulated in edible scaffolds and differentiated and matured using differentiation media. The scaffolds then remain in the final product where they influence texture and nutritional content of the final product. However, the cell detachment stage, between the expansion and differentiation phases, often results in significant cell loss, and requires the use of additional chemicals and solvents, thereby increasing production costs and bioprocessing time (Derakhti *et al*., 2019).

Designing microcarriers that are edible and able to both proliferate and differentiate cells would eliminate the cell detachment stage and would make the whole process more time and cost effective. In recent years, several companies, such as Modern Meadow, Matrix Meats and Gelatex have started developing and marketing edible microcarriers for the purpose of developing cultivated meats (Marga

et al., 2015; Zinck and Vaszily, 2021; Watson, 2022) while an increasing number of studies have explored the fabrication and characterisation of edible microcarriers (Li *et al*., 2016; Thyden *et al*., 2022; Zernov *et al*., 2022; Yen *et al*., 2023). However, only a few have studied their differentiation potential on muscle or fat cells (Andreanssen *et al*., 2022; Norris *et al*., 2022; Kong *et al*., 2023; Ogawa *et al*., 2024). Andreanssen *et al*. (2022) dripped a blend of collagen and eggshell membrane into liquid nitrogen using a syringe to create edible microcarriers. They then showed that the microcarriers supported the proliferation of C2C12 cells and that the cells expressed myogenic factor 5 (MYF5) and myoblast determination protein 1 (MYOD1), indicating signs of early differentiation (Andreansson *et al*., 2022). Norris *et al*. (2022) created edible smooth and grooved gelatin microcarriers using emulsion techniques. The C2C12 cells growing on the microcarriers proliferated into small aggregates which, in turn, formed microtissues which were shown to support myogenic cell growth and differentiation (Norris *et al*., 2022). Kong *et al*. (2023) produced chickpea protein hydrolysate microcarriers treated with trypsin that were shown to proliferate and differentiate a variety of cell lines including 3T3-L1, C2C12, porcine myoblasts and chicken satellite cells. Ogawa *et al*. (2024) produced microcarriers by inoculating flasks with various strains of mycelium under constant agitation to produce pellets. The pellets were then autoclaved to inactivate them, producing porous microcarriers which supported bovine satellite cell and C2C12 cell proliferation. The cells also expressed MYOD1, and myogenic regulation factors MYOG and MYH2, which indicated potential for myogenic differentiation (Ogawa *et al*., 2024).

1.5.2.3 Scaffolding functionality

To be successful, scaffolds and microcarriers must be able to replicate the biological, physical, biochemical, and mechanical properties of the native ECM responsible for cell phenotype and tissue formation. They should promote cell attachment, migration, proliferation, and differentiation while exhibiting an environment with adequate porosity, structure, stiffness and tailorable degradation rates (Molina *et al.*, 2020).

Cellular attachment is highly dependent on the surface chemistry, topographical properties and presence of cell-binding motifs on the biomaterial surface (Derakhti *et al*., 2019). Several surface properties, including wettability, charge and chemical specificity have been shown to influence cell attachment *in vitro* (Hao *et al*., 2016; Ferrari *et al*., 2019; Fasciano *et al*., 2024) although the exact mechanism of how these properties affect attachment is poorly understood. Hao *et al*. (2014) showed that MSCs attached better on surfaces with a moderate hydrophilicity, with human and mice MSCs adhering best to surfaces with contact angles of 40-70 ° and 70-90 °, respectively. In addition, they showed that wettability also promoted MSC proliferation and differentiation on materials with a contact angle of 40-90 °, which has been in line with the results of several other studies (Ahn *et al*.,

2014; Hartriani *et al*., 2015; dos Santos *et al*., 2023). It has also been shown that cell attachment is modulated by specific proteins which are adsorbed best in moderately hydrophilic surfaces (Oliveira *et al*., 2012; Fasciano *et al*., 2024). A positive surface charge has been shown to promote attachment due to the negative charge of mammalian cells and tissues (Weiss and Zeigel, 1971; De Luca *et al*., 2016; Fasciano *et al*., 2024). *In vivo*, cell attachment to the ECM is mediated by integrins which bind to specific cell-adhesion motifs such as DGEA, IKVAV and RGD, found predominantly in collagens, laminins and fibronectin, respectively (Morwood *et al*., 2023). This functionality is mostly reserved for animal ECM proteins, and therefore synthetic and plant-based biomaterials are often coated or conjugated with RGD binding motifs in order to improve the attachment capabilities of scaffolds. Many growth factors, such as basic fibroblast growth factor (bFGF), also promote cell attachment and are often included in, or added to, culture medium to condition and coat scaffolds (Feng, *et al.*, 2017, Subbiahanadar Chelladurai *et al.,* 2021). Other functionalisation strategies such as click chemistry, used to coat RGD peptides, or polydopamine (PDA) coating are commonly used in tissue engineering to significantly improve the attachment of cells to inert scaffolds (Shin *et al*., 2003; Ku and Park, 2010; Darling *et al*., 2021). However, these techniques are expensive and have been shown to be potentially toxic (Sun *et al*., 2021; Luu *et al*., 2024) and therefore should be avoided for cultivated meat supports.

Cell attachment, migration and differentiation are also affected by the scaffold morphology and topology. To mimic the highly homogenous and interconnected porous and nanofibrous structure of the native ECM, careful consideration should be placed on several key structural parameters, including fibre diameter, fibre alignment, and pore size. Variations in these properties can influence cellular behaviours and facilitate differentiation towards various cell fates (Dolgin *et al*., 2023). Fibre diameter is an important factor to consider as it has been shown to modulate cell differentiation, expression, proliferation, infiltration, and migration (Jenkins and Little, 2019). Lee *et al.* (2017b) studied the effects of fibre diameter on randomly orientated electrospun polylactic-co-glycolic acid (PLGA). They found that unaligned nanofibres promoted cell proliferation while larger microfibres promoted cell attachment and organisation but suppressed growth (Lee *et al*., 2017b). Fibre alignment and micropatterned scaffolds have also been shown to affect cell behaviour (Thakar *et al*., 2009). Abagnale *et al*. (2015) showed that MSCs grown on 650 nm nanofibres expressed markers of adipogenic, myogenic, osteogenic and chondrogenic differentiation. However, in scaffolds with both 2 µm and 15 µm grooves, the MSCs differentiated towards chondrogenic lineages in the 2 µm grooves and adipogenic lineages in the 15 µm, without the need for differentiation media (Abagnale *et al*., 2015). Xie *et al*. (2021) studied the effects of fibre diameter and orientation of electrospun poly-L-lactic acid (PLLA) on bone marrow-derived MSCs. They showed that fibre alignment played a role in cell morphology and migration, with cells grown on aligned fibres displaying spindle shapes and migrating

along defined paths. On the other hand, cells on randomly orientated fibres were dispersed randomly and exhibited polygonal shapes. They also noted that while fibre alignment promoted cell proliferation and differentiation, the proliferation effect was minimal after 7 days of culture (Xie *et al*., 2021). Cell morphology was shown to influence differentiation, with rounder MSCs differentiating into adipocytes and spread-out flat cells into osteocytes (McBeath *et al.*, 2004). It has also been demonstrated that cell elongation is important for myogenic differentiation (Wang, *et al.*, 2015). Narayanan *et al.* (2020) showed that increasing fibre diameter of aligned electrospun polyester fibres, from a nanoscale to a microscale, enhanced myoblast proliferation and differentiation. They then showed that the fibre alignment contributed to cell elongation, muscle fibre alignment, myoblast fusion and tissue development (Narayanan *et al*., 2020).

Aside from fibre morphology, the porous architecture of the scaffolds also plays an important role on infiltration, migration, proliferation and differentiation. Estabridis *et al.* (2018) showed that pores exceeding the size of cells promoted attachment on single fibres, which increased their migration speed, whereas pores smaller than cells promoted cell bridging on multiple fibres, slowing migration (Estabridis *et al*., 2018). Balguid *et al*. (2009) showed that increased fibre diameter directly correlates to increased pore size, hence cellular infiltration in electrospun scaffolds was proportional to fibre diameter (Balguid *et al*., 2009). It is worth noting that pore size affects cells differently depending on their type and scaffold material (Nunes-Pereira *et al*., 2015).

The mechanical properties of the scaffold also play an important role in cell differentiation, as well in influencing the texture of the engineered tissue. In a process called mechanotransduction, the ECM stimulates cells to differentiate via mechanical cues, such as varying stiffness (Burkholder, 2007; Sun, *et al.*, 2016; Raman *et al*., 2022). The ECM stiffness is dependent on tissue type. The Young's modulus (which defines stiffness as a ratio of stress to strain) of adipose tissue is between 0.2 and 1.0 kPa, while it is at 10 kPa for skeletal muscle and 30-40 kPa for bone tissue (Lv, *et al.*, 2015). Varying the stiffness of a scaffold *in vitro* can cause a cell to differentiate into varying lineages. MSCs differentiate towards adipogenic lineages on soft surfaces and osteogenic lineages on hard surfaces (Engler, *et al.*, 2006). When transplanting a tissue *in vivo*, it is important for the stiffness of the engineered tissue to match the stiffness of the native tissue. However, for cultivated meats, scaffold stiffness should match the expected mechanical properties of traditional meat (Bonkamp, *et al.*, 2021).

Several mechanical testing methods have been used to describe the texture of traditional and cultivated meat, including the Warner-Bratzler shear force (WBSF) measurement of the forces applied when cutting a sample with a V-shaped knife, texture profile analysis (TPA) which measures several organoleptic properties including hardness and chewiness by mimicking successive bites (Tejerina, *et*

al., 2021; Nasrollahzadeh *et al.*, 2024; Souppez *et al*., 2025), and tensile testing to measure sample tearing (James and Yang, 2011; Paredes *et al*., 2022). Understanding the mechanical properties that are associated with meat quality can inform the production of cultivated meat to meet consumer expectations and acceptance (Souppez *et al*., 2025).

1.5.3 Electrospinning

Electrospinning is a widely used method for fabricating nanofibrous meshes in textile, filtration and food preservation applications (Liu *et al*., 2020; Sameen *et al*., 2022; Zhou *et al*., 2022; Nurul Alam *et al*., 2024b), and is commonly used to design nanofibrous scaffolds for tissue engineering (Lyu *et al*., 2013; Politi *et al*., 2020; Sharma *et al*., 2023; dos Santos *et al*., 2024b). It is the most controllable and efficient method used for creating ECM-like scaffolds that possess a nanofibrous and porous network of isotropic or anisotropic fibres (Lee and Choi, 2024). Electrospinning is a relatively simple and cost-effective method to produce homogenous polymeric scaffolds (Rahmati, *et al.*, 2021). Despite a recent drive for developing green electrospinning strategies across all fields of study, using natural polymers and non-toxic solvents and crosslinkers (Jalaja *et al*., 2015; Lv *et al*., 2018; Gao *et al*., 2018; Guo *et al*., 2019; Perez-Puyana *et al*., 2021; Melzener *et al*., 2023), very few studies have applied these methods to produce scaffolds for cultivated meat production (MacQueen *et al*., 2019; Kawecki *et al*., 2023; dos Santos *et al*., 2024; Dagès *et al*., 2025) despite its clear potential (Bonkamp *et al*., 2022; Nurul Alam *et al*., 2024b; Fasciano *et al*., 2024). MacQueen *et al*. (2019) used a rotary jet spinning method similar to wet spinning to produce fibrous edible gelatin scaffolds that supported the proliferation of rabbit myoblasts (MacQueen *et al*., 2019). Kawecki *et al*. (2023) combined myocytes grown on electrospun edible gelatin scaffolds with adipocytes grown on edible gelatin microcarriers, creating a spontaneous adhesion of myogenic and adipogenic tissues with mechanically distinct properties. The resulting multicomponent tissue had the appearance of marbled meat (Kawecki *et al*., 2023). Dos Santos *et al*. (2024) electrospun randomly aligned cellulose acetate nanofibres that supported the proliferation and differentiation of C2C12 cells and chicken satellite cells. They then stacked the electrospun sheets to produce 300-400 µm thick constructs, which through perfusion were able to differentiate cells without switching from growth to differentiation media (Dos Santos *et al*., 2024). In the manufacturing sector, Matrix Meats have started the development and production of electrospun nanofibres of a variety of edible biomaterials including chitosan, collagen and cellulose (Bonkamp *et al*., 2022).

1.5.3.1 Needle Electrospinning

Electrospinning uses electrostatic forces to draw a polymer solution into fibres. The standard laboratory electrospinning setup consists of a syringe pump holding a metallic needle-tipped syringe connected to a direct current (DC) high-voltage generator, and a grounded flat metal plate placed

perpendicular to the needle setup that acts as a fibre collector (**Figure 6**). To electrospin a biomaterial, it is first dissolved in a highly volatile solvent to form a polymer solution. The polymer solution is then loaded into the electrically charged metallic needle-tipped syringe and a syringe pump pushes out the solution droplet by droplet at a constant flow rate. When the electric current is switched on, the polymer solution droplet at the tip of the needle elongates to form a Taylor cone which emits jets that travel towards the collector plate. As the jets are in flight, the solvent evaporates leaving the dry fibres to whip across the collector to form a randomly aligned fibrous mesh. The resulting fibre morphology is highly dependent on ambient conditions (*e.g.* temperature and relative humidity), polymer solution properties (*e.g.* concentration, viscosity, surface tension, conductivity and volatility) and operating parameters (*e.g.* voltage, tip-to-collector distance and flow rate) that are explained in **Table 3**.

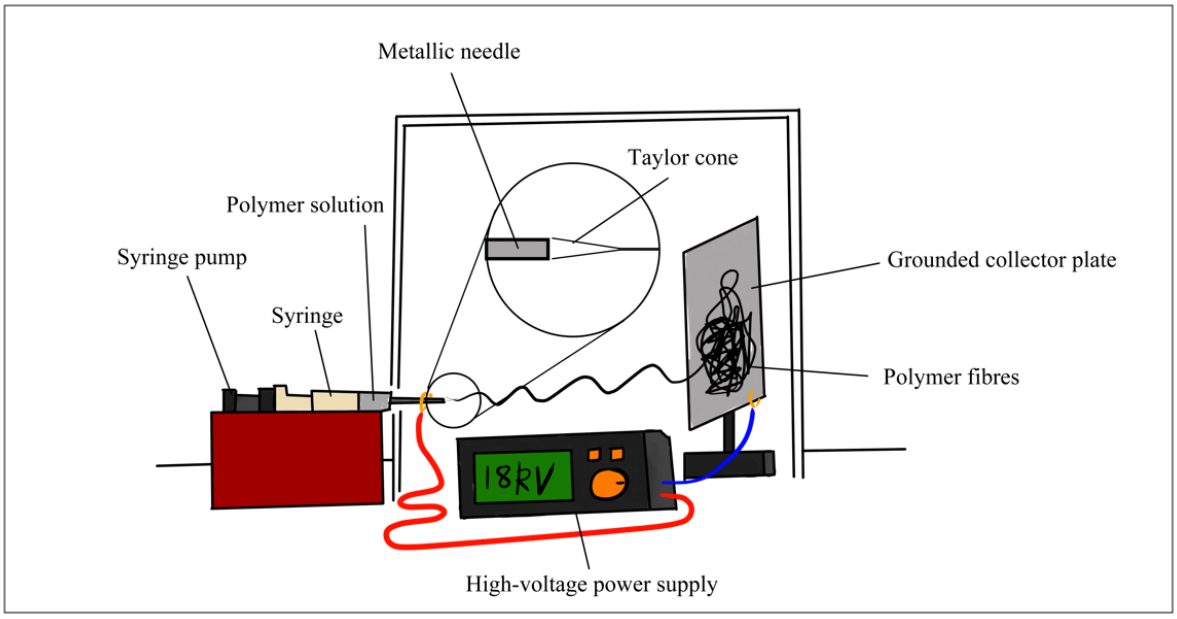

Figure 6: Standard needle electrospinning setup

There are numerous ways in which researchers have modified the electrospinning setup to handle different materials. For instance, materials that dissolve poorly can be assisted with heat, using melt electrospinning (Ibrahim *et al.*, 2019), and those with low conductivity can either be propelled with gas using solution blow spinning (Daristotle *et al.*, 2016; Carriles *et al.*, 2023) or centrifugal forces using rotary jet spinning (MacQueen *et al.*, 2019; Rogalski *et al.*, 2017). In addition, some setups may involve a coagulation bath to crosslink the fibres as they are ejected or deposited as is the case with wet-spinning, dry-wet spinning, immersed rotary jet spinning (MacQueen *et al.*, 2019; Shirvan *et al.*, 2022). Alternatively, electrospinning can produce fibres of varying morphology by switching the spinneret type, modifying the electric or magnetic field or simply altering the collector shape and movement (Maran *et al.*, 2024). Coaxial electrospinning, for example, employs two or more syringes with a single

coaxial needle consisting of concentric inner and outer openings. This allows the formation of either core-sheath or hollow nanofibres. With core-sheath fibres, the polymer at the core can provide structure while the outer layer provides functionality. Zhao *et al*. (2007) coaxially electrospun PCL/gelatin nanofibres to form non-toxic scaffolds, capable of supporting fibroblast attachment and proliferation, which benefitted from the mechanical properties of PCL at their cores (Zhao *et al*., 2007). Alternatively, coaxial electrospinning can allow a carrier material to form the core and use a non-electrospinnable material on the outer layer. Jalaja *et al*. (2016) coaxially electrospun gelatin/chitosan nanofibres, with electrospinnable gelatin serving as the core and non-electrospinnable chitosan providing the outer layer functionality which improved cytocompatibility, cell attachment and proliferation (Jalaja *et al*., 2016).

Near-field electrospinning is another original adaptation of the traditional setup in which the collector distance is so small (500 µm – 3 mm) that the fibres deposit without whipping. Similarly to 3D printing techniques, the spinneret is mounted on a controllable 3D motion platform, enabling precise deposition of fibres in the X-, Y- and Z- axis (Huang *et al*., 2024). Finally, a degree of fibre alignment (anisotropy) can be achieved with all electrospinning setups by switching out the collector plate with a fast-rotating mandrel, drum, disc or wire. At a slow rotating speed, deposited fibres form a more homogenised randomly orientated mesh. In contrast, increasing the speed augments the pull of fibres as they are being deposited, thereby reducing whipping instability and producing some alignment. To produce scaffolds of near perfect alignment, the rotation speed of the drum should match or slightly exceed the ejection rate of the fibre. Kiselev and Rosell-Llompart (2011) electrospun polyethylene oxide (PEO) nanofibres with near perfect alignment (>95% of fibres within 1 °) using a cylindrical collector with rotational speeds of 15 m/s (Kiselev and Rosell-Llompart, 2011).

1.5.3.2 Electrospinning at scale

Needle electrospinning has many advantages thanks to its versatility, ease of use, simplicity and cost-effectiveness. However, its slow production rates, averaging around 0.01-0.1 g/h of polymeric fibres, and needle clogging issues that inhibit continuous jet formation, and can even at times impede the electrospinning process altogether, prevent standard needle electrospinning setups from being used at scale (Partheniadis *et al*., 2020).

Table 3: List of parameters that should be optimised for successful electrospinning

	Parameter	Description	Effect of increase in parameter	Effect of decrease in parameter
Polymer properties	Concentration	A critical concentration is needed for polymer chain entanglement and generate viscoelastic behaviour needed for fibre formation.	Increases polymer chain proximity and entanglement. Increases fibre diameter. Decreases fibre tensile strength.	If too low, prevents chain entanglement forming droplets. Can produce electrospraying effect or transfer of large droplets.
	Viscosity	A minimum polymer viscosity is needed for electrospinning. Viscosity can be increased with concentration.	If too high, will prevent polymer solution from flowing efficiently.	If too low, cannot form uniform and smooth fibres.
	Surface tension	Fibres can only be formed once surface tension is broken. Surface tension can be overcome by increasing the voltage.	If too high, can cause unstable jets and droplet transfer.	Can allow electrospinning at lower voltages.
	Conductivity	Conductivity allows current to flow through the polymer solution.	Can be increased by adding salts such as NaCl to increase electrolytes in solution.	
	Solvent evaporation	As the solvent evaporates from the polymer jets, the fibres harden. Solvent evaporation time is dependent on tip-to-collector distance, temperature and %RH.	Fibres will have time to fully dry before reaching collector.	Fibres hitting the collector while they are wet have a larger fibre diameter and flatter morphology.
Operating parameters	Voltage	Needs to be high enough to break the surface tension and cause electrostatic effect to draw fibres.	Decreases fibre diameter. If too high, can prevent the formation of stable jets.	Increases formation of beads and transfer of droplets.
	Tip to collector distance	Affects the time needed for fibres to dry.	Decreases fibre diameter.	Increases fibre diameter.
	Flow rate	Should be adjusted to match solvent evaporation time.	Solvent will not evaporate enough.	Solvent will evaporate fully before reaching collector. If too low, can prevent continuous fibres.
Environmental conditions	Temperature	Temperature can affect polymer viscosity.	Decreases fibre diameter. If too high, can lower viscosity preventing uniform and smooth fibres.	Increases fibre diameter.
	Relative Humidity (%RH)	Relative humidity can affect solvent evaporation time.	Fibres take longer to solidify. Increases fibre diameter.	Fibres solidify faster. Decreases fibre diameter.

To increase productivity, various scalable electrospinning systems have been developed notably using multi-needled and needleless spinnerets (Partheniadis *et al*., 2020). Multi-needle electrospinning operates in a similar manner to standard single needle electrospinning, but the polymer solution is pushed out at a higher flow rate through a higher number of needles. With more Taylor cones being produced, more jets are formed, and more fibres can be collected within the same timeframe. However, multi-needle setups have drawbacks, with needle-clogging still posing a potential issue with viscous polymer solutions, and it has been shown that Coulombic repulsion between the charged jets and needles can result in an irregular electrical field reducing the homogeneity of the electrospun fibres (Beaudoin *et al*., 2022). To improve the overall electric field several strategies have been

investigated including careful positioning of the needles, varying needle arrangements and spacing, placing auxiliary electrodes laterally or perpendicularly to the needles, and even using coaxial needles with sheath gas to stabilise the jets (Theron *et al*., 2005; Zhu *et al*., 2018; Zheng *et al*., 2020; Beaudoin *et al*., 2022). Despite these difficulties, large-scale and industrial-scale multi-needle systems have been developed and commercialised that use thousands of needles and can produce up to 6.5 kg/h of fibres (Luo *et al*., 2012; Hosseini Ravandi *et al*., 2022).

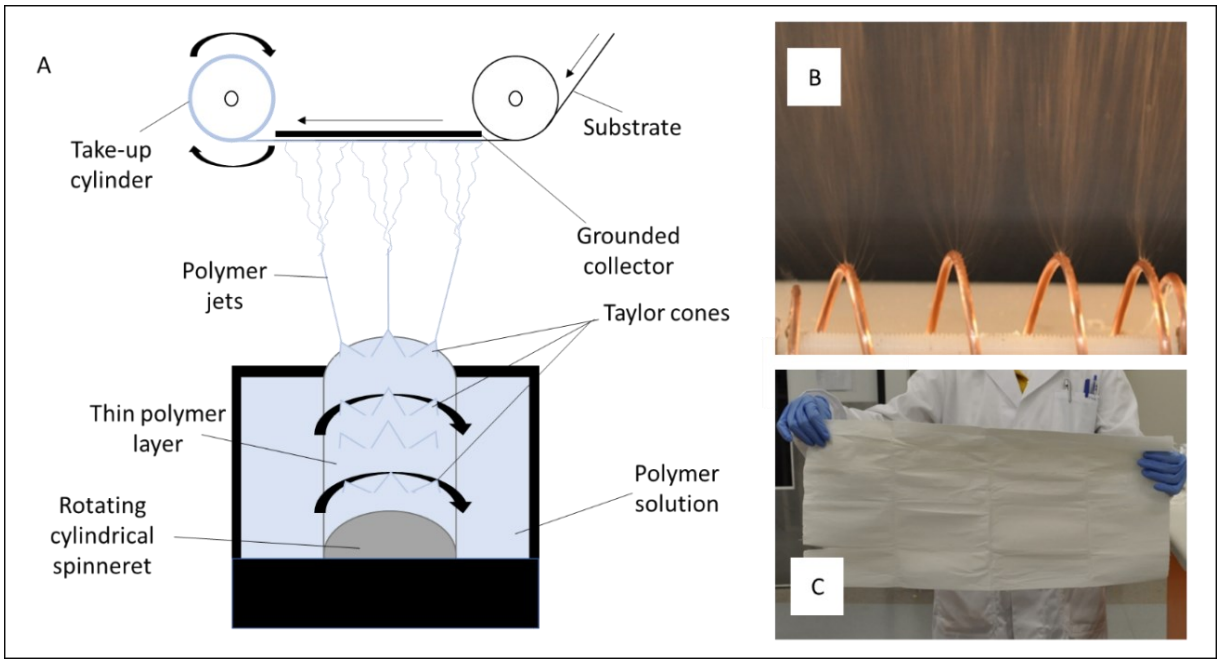

Figure 7: Needleless electrospinning setup using a rotating cylindrical spinneret.
A) Rotating spinneret setup, B) Photo of rotating coil setup during electrospinning (Niu and Lin, 2012), C) Needleless electrospun mats (Niu and Lin, 2012).

Alternatively, large scale electrospinning can be achieved without the use of any needle, removing all needle-related issues entirely. Needleless electrospinning relies on the principle that highly charged liquid surfaces can produce jets over a large area (**Figure 7**). Unlike needle electrospinning, needleless electrospinning uses very high voltages to break the liquid surface tension and create conical spikes which act similarly to Taylor cones in initiating the jet formation. Various charged rotating spinnerets have been used such as cylinders, discs, coils, and balls, that are partly immerged in the polymer solution to continuously wet with a thin layer of solution the emerged part of the spinneret from which fibres are drawn (Jirsak *et* al., 2009; Liu *et al*., 2014; Sasithorn and Martinová, 2014; Moon *et al*., 2017; Maryskova *et al*., 2019). Moreover, modern setups such as the Nanospider^{TM} use a charged wire on which a cassette, moving up and down the wire, deposits the polymer solution using capillary action. Using this technique maintains polymer solution viscosity as the solvent cannot evaporate in the cassette (Omer *et al*., 2021). Alternatively, rotating spinnerets can be removed entirely and replaced by external forces such as gravity, magnetism, pressurised gas or ultrasounds used to perturbate the

electrified polymer solution surface and initiate jet formation (Liu *et al*., 2008; Huang *et al*., 2017; Nieminen *et al*., 2018). Several commercial laboratory-, pilot- and industrial-scale needleless electrospinners have been developed that can produce from 10 - 6500 g/h of nanofibres (Omer *et* al., 2021; Hosseini Ravandi *et al*., 2022).

Finally, AC electrospinning, is an up-and-coming needleless electrospinning system that uses an alternative current (AC), rather than direct current (DC), to excite a fluid surface into producing Taylor cones and initiating jet formation (Batka *et al*., 2024). Unlike DC electrospinning strategies, AC electrospinning does not require a grounded or charged collector since half the jets are formed positively charged and half negatively charged. Therefore, each jet acts as a collector to the subsequent inversely charged jet (Sivan *et al*., 2022). Spinnerets used for AC electrospinning generally involve an electrified rod through which the polymer solution passes at a constant rate, using a screw pump or other automated systems (Valtera *et al*., 2015; Valtera *et al*., 2019), although other combinations, such as bubble electrospinning have been used with AC (Erben *et al*., 2020). As the solution is excited, jets are ejected and form an electrically neutral plume that ascends and stabilises as shown in **Figure 8** (Batka *et al*., 2024). To retrieve the fibres a neutral collector material such as a wire, stick or spun-bond can be used depending on desired fibre function and morphology. As the technology is still in its infancy, no commercial systems have been developed yet.

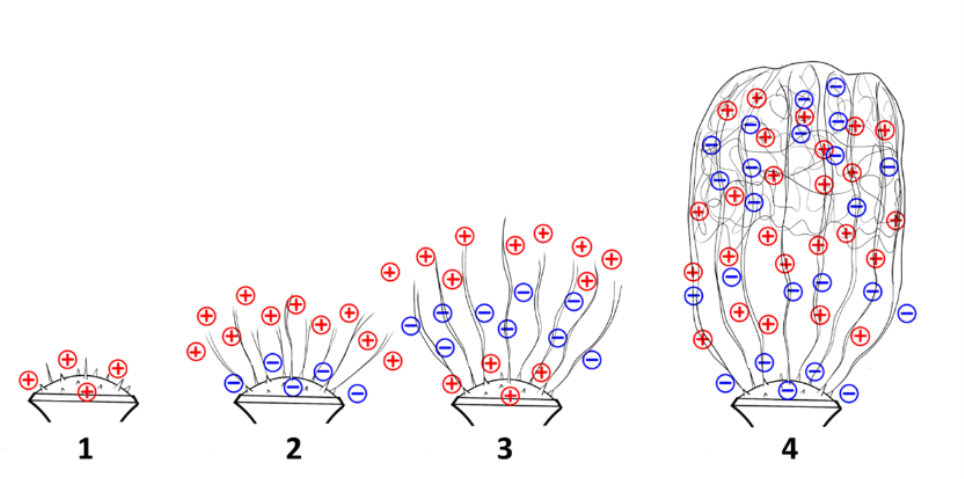

Figure 8: Concept of AC electrospinning. 1) As current is switched on the hydrodynamic effect on the polymer solution initiates jet formations. 2) as the charge is alternated, the negatively charged polymer solution is attracted to the positively charged jet previously ejected, 3) with every change in voltage polarity, jets become longer, forming fibres with positive and negative charge that end up cancelling each other out in an electrically neutral fibrous plume (4).

1.5.4 Material selection for cultured meat scaffold

The science behind cultivated meat production stems from a combination of tissue engineering and food science. The materials used in scaffolding must have key tissue engineering properties such as functionality and compatibility with the scaffold fabrication and tissue culture process, and at the

same time they should be edible, cheap and acceptable to consumers just like any other food ingredient. Materials that satisfy these properties should therefore be prioritised in the material selection process. Some important considerations when choosing biomaterials for cultivated meat scaffolding are presented in **Figure 9**. A list of edible materials with potential in cultivated meat scaffolding is displayed in **Table 4**.

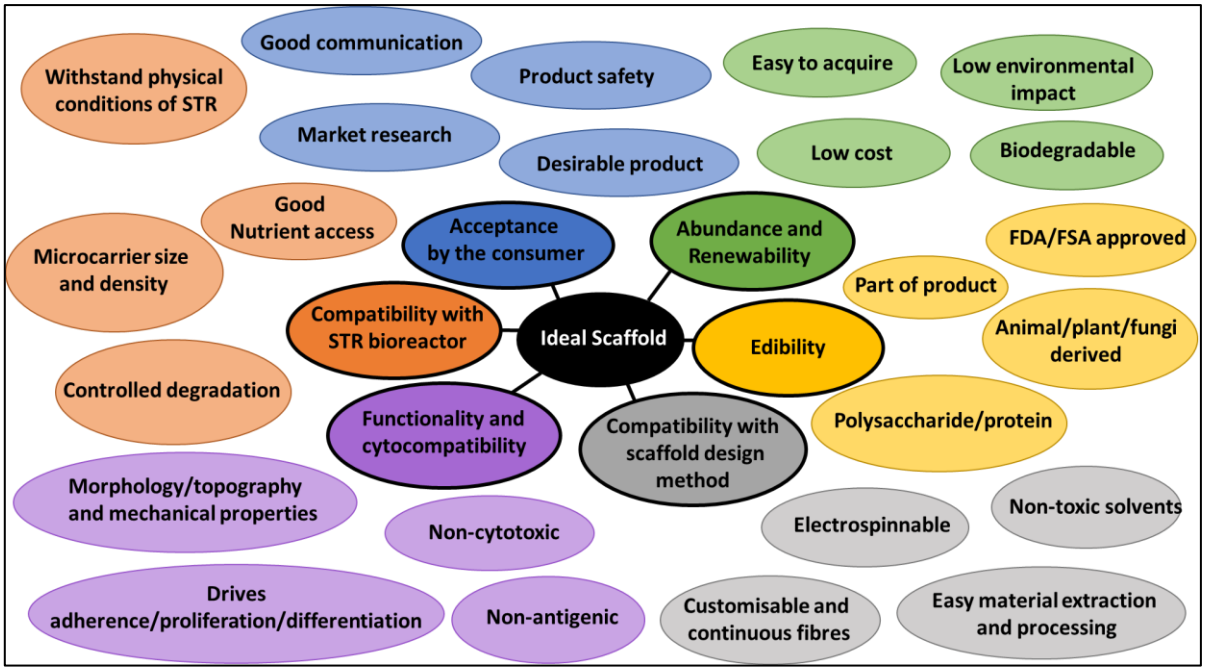

Figure 9: Ideal scaffold biomaterial considerations.

1.5.4.1 Biomaterial scalability

One of the most important factors to consider during material selection is scalability from small quantities used in a research laboratory to the large amounts required in industrial-scale production. It is, therefore, important that the material is abundant, relatively cheap and easy to procure and extract (Bodiou *et al.*, 2020). By decreasing the amount of steps in the material processing and refinement, the relative cost of production is lowered, which in turn reduces the price of the final product. Finally, to increase the sustainability of cultivated meat, materials used in its production should also be renewable with a low environmental or ecological impact. Many natural polymers fit these requirements, whereas many synthetic polymers favoured in tissue engineering applications have a detrimental effect on the environment (Jahangirian *et al.*, 2019). Natural polymers obtained from massively produced waste products are excellent candidates as they are cheap recycled materials. For example, chitosan and zein, which are waste products from the fishing and alcohol industries, respectively, have been used in a wide range of biomedical applications (Li *et al.*, 2022; Wang *et al.*, 2024). In addition, ubiquitous materials, such as cellulose in all plants and alginate in seaweeds, are easily obtainable from a large variety of sources (Jahangirian *et al.*, 2019).

1.5.4.2 Biomaterial food safety

As most scaffolds for cultivated meat production remain in the final product, food safety is of the utmost importance. The scaffold material also plays a role in altering the organoleptic properties of the final product, and therefore tasteless or flavour-enhancing polymers are desirable. Ulagesan *et al*. (2024) used a mixture of sodium alginate and carrageenan gum to 3D-print hydrogels with a strong umami taste that was described as enhancing the flavour of cultivated fish products (Ulagesan *et al*., 2024). Lee *et al*. (2024) designed a gelatin scaffold conjugated with switchable flavour-compounds that supported the attachment, proliferation and differentiation of bovine myoblasts. When cooked, the cultivated meat product released meaty flavours that mimicked the Maillard reactions (non-enzymatic browning during cooking) of traditional meat cooking (Lee *et al*., 2024). It is worth noting that materials can be edible without being digestible, as is the case for dietary fibres such as cellulose and arabinoxylans, and low-toxicity synthetic polymers such as polyethylene glycol (PEG), polyethylene oxide (PEO) and polymethyl methacrylate (PMMA; Shit and Shah, 2014). In addition, using GRAS status biomaterials can facilitate regulatory approval of the final product as well as improve consumer satisfaction (Lanzoni *et al*., 2024). Silk fibroin, for example, is a GRAS status natural biopolymer that is commonly used in tissue engineering applications due to its synthetic-like properties such as controllable degradation, tensile strength and other mechanical properties. In addition, silk fibroin is tasteless and digestible, making it auspicious for cultivated meat scaffolding (Sun *et al*., 2021b).

1.5.4.3 Biomaterial functionality

Material functionality is also very important as it will help cells attach, proliferate, migrate and differentiate on the engineered scaffold. ECM components, such as collagen, fibrinogen, hyaluronic acid and their derivatives like gelatin, possess cell adhesion motifs. In addition, scaffolds produced from ECM proteins have been shown to replicate native cell niches and modulate cell fate. However, reliance on animal protein should be avoided as the removal of animals from meat production is a hallmark of cultivated meat. Instead, many ECM proteins could eventually be produced recombinantly and at scale using bacteria, plants and fungi (Post *et al*., 2020). It is worth noting that cell adhesion motifs are not unique to the ECM surrounding animal cells, with several plant and fungi displaying RGD and RGD-like peptide motifs (Senchou *et al*., 2004). Kong and Huang (2024) produced alginate microcarriers coated with pumpkin seed protein that is known to be rich in RGD motifs. The microcarriers supported the attachment and proliferation of C2C12 cells, chicken satellite cells, porcine myoblasts and 3T3-L1 adipocytes, performing as efficiently as animal gelatin microcarriers (Kong and Huang, 2024). Biomaterials can also possess other desirable properties that can enhance scaffolds used for cultivated meat production. Plath *et al*. (2021) demonstrated that zein promoted

cell adhesion, proliferation and differentiation on PCL/zein electrospun scaffolds. In addition, zein was shown to be bactericidal and antiadhesive, preventing *E. coli* and *S. aureus* from colonising the scaffolds (Path *et al*, 2021). Many dietary fibres also have health benefits, playing a role in digestive health (Gill *et al*., 2021). Psyllium husk, for instance, which is often prescribed to relieve constipation, has been used to treat an array of colonic disorders including bacterial infections and colorectal cancer (Bacha *et al*., 2022). In addition, as a soluble fibre with antimicrobial properties, psyllium husk acts as a hydrogel capable of being used in drug delivery systems (Sharma *et al*., 2024) and wound dressings (Fernandes *et al*., 2018). By countering some of the negative effects of red meat consumption, psyllium husk scaffolds could make cultivated meat healthier and improve consumer acceptance.

1.5.4.4 Bioprocess compatibility

Compatibility of the biomaterials used with the scaffold fabrication process and the cell culture bioprocess is also essential. Compatibility significantly limits the number of polymers that can be used for specific applications. For instance, many natural polymers lack the mechanical strength needed for 3D bioprinting. Moreover, polyionic materials such as alginate, chitosan and some dietary fibres have been shown to interfere with the electric field during electrospinning, preventing them from being electrospun without a carrier material (Dierings de Souza *et al*., 2021; Stijman *et al*., 2011). In addition, most of the bioprocess takes place in aqueous conditions, making water-soluble materials such as zein unusable. Although the hydrolytic stability of zein can be improved, its crosslinkers are toxic and should be avoided in food products (Huang *et al*., 2015). Finally, the biomaterial should have sufficient integrity to withstand shear stresses imparted by bioreactor impellors. While shear stress present in spinner flasks and laboratory-scale bioreactors is relatively low, the biomaterial should also be able to endure the shear stresses of industrial-scale reactors (Li *et al*., 2020).

1.5.4.5 Consumer acceptance

Lastly, and possibly most importantly, the material must have consumer acceptance, as no matter how good a product may be, it cannot be successful without this. To this end, it is important to conduct market research on what the public is willing to consume and how cultivated meat could impact dietary habits, and cultural or religious traditions. Psychology and social sciences will have a huge role in bringing cultivated meats to market.

Table 4: Advantages and disadvantages of edible biomaterials with potential in cultivated meat scaffolding.

Material	Origin	Advantages	Disadvantages	References
Sodium alginate	Brown seaweed	Can produce ultrathin fibres Abundant Extensive use in food and medical sectors Hydrophilic	Difficult to electrospin Relatively poor mechanical strength Low biodegradability Polyanionic character	Pan *et al.*, 2020; Li *et al.*, 2022; Chen *et al., 2023*
Chitosan	Crustacean, fungi	Already used in meat replacement products and clean meats Has the ability to regulate and modulate bioactive factors	Difficult to electrospin Low solubility Poor mechanical strength Polycationic character	Jalaja *et al.*, 2016; Li *et al.*, 2022; Wang *et al.*, 2024
Zein	Corn	Good mechanical strength	Fast biodegradation Poor stability in aqueous environments	Perez-Guzman and Castro-Munoz, 2020; Melzener *et al.*, 2023; Jeong *et al.,* 2024
Cellulose	Plants	Tuneable physical and chemical properties Extremely abundant	Non-biodegradable in Humans Methylcellulose is a laxative	Hickey and Pelling, 2019; Tang *et al.*, 2024; Dos Santos *et al.*, 2024
Gums (Pectin, dextran, psyllium husk)	Plants	Hydrophilic Mimics natural ECM High elasticity Good cell attachment and proliferation Abundant	Cannot control hydration Possible antigenicity Poor mechanical strength Polyionic character Difficult to electrospin	Mohammadinejad *et al.*, 2020; Wollshlger *et al.*, 2022; Kirsch *et al.*, 2023
Collagen	Animal	Natural component of ECM Good cell attachment Easy processing	Poor mechanical strength Expensive Low solubility	Murphy *et al.*, 2010; Shepherd *et al.*, 2018
Gelatin	Denatured collagen	Similar structure to collagen Good cell attachment Cheaper than collagen Water soluble	Degrades too fast for cell differentiation Poor mechanical strength	MacQueen *et al.*, 2019; Rao *et al.*, 2023; Lee *et al.*, 2024
Fibrinogen	Animal	Hydrophilic Excellent cell attachment and differentiation abilities	Poor mechanical strength Expensive	McManus, 2006; Linnes *et al.*, 2007; Kang *et al.*, 2021
Hyaluronic Acid	Animal	ECM Glucosaminoglycan Biocompatibility High elasticity Water soluble	Poor mechanical strength Rapid enzymatic degradation	Singh *et al.*, 2023
Silk Fibroin	Silkworms	Very good cell attachment and proliferation Very good mechanical strength Amphiphilic Tuneable physical and chemical properties Controllable biodegradibility	Relatively fast degradation without modification or crosslinking	Nguyen *et al.*, 2019; Ma *et al.*, 2024; Dagès *et al.*, 2025
Sericin	Silkworms	Good elasticity Hydrophilic Good cell attachment	Very fragile, cannot make scaffold on its own Moderate antigenicity	Jo, *et al.*, 2020; Chachlioutaki *et al.*, 2022; Demiray *et al.*, 2024
Wheat (Gliadin, Glutenin)	Wheat	Good mechanical strength Excellent elasticity	Common allergies or intolerances Needs physical or chemical modifications to dissolve	Ba *et al.*, 2018; Wu *et al.*, 2024; Yao *et al.*, 2024
Soy Protein	Soy	Good mechanical strength Good cell attachment Stable to hydrolysis	Hard to dissolve in most solvents Relatively fast degradation Needs blending to produce fibres	Ben-Arye *et al.*, 2020; Phelan *et al.*, 2020; Wei *et al.*, 2023
Polyethylene Glycol (PEG)	Synthetic polymer	Edible Biocompatible Water soluble Good mechanical properties Tuneable physical and biochemical properties	Non-biodegradable Toxic in high quantities	Shit and Shah, 2014

1.5.5 Silk Fibroin

It is evident from **Table 4** that silk fibroin stands out as an abundant, relatively cheap and easily extractable protein with GRAS status, and excellent versatility, cytocompatibility and mechanical properties. Furthermore, silk fibroin has been extensively researched as a scaffold biomaterial for tissue engineering, with applications in skin, bone, skeletal muscle, smooth muscle, and neural cell regeneration (Chaturvedi *et al*., 2016; Safonova *et al*., 2021; Yonesi *et al*., 2021; Hu *et al*., 2022; Polakova *et al*., 2022). Silk fibroin is also compatible with electrospinning and is commonly used in scaffolds, wound dressings, drug delivery systems, filtration applications and textiles (Faroki *et al*., 2018; Chomachayi *et al*., 2018; Gao *et al*., 2018; Sencadas *et al*., 2019; Polakova *et al*., 2022; He *et al*., 2023). Although silk fibroin electrospun nanofibres are water-soluble, they can be stabilised with non-toxic and food-safe physical crosslinkers such as ethanol and water vapour, making silk fibroin scaffolds suitable for use in aqueous environments (Huang *et al*., 2014; Terada *et al*., 2016). Another advantage of silk fibroin is that it is comestible and tasteless. Moreover, it is already used in the food industry as biodegradable food packaging and as a preservative for apples and strawberries (Marelli *et al*., 2016; Gianelli e*t al*., 2021; Low *et al*., 2022). In addition, a recent study has shown that silk fibroin has no allergenic potential, nor does it pose any toxicity risk at 500 mg/kg per day (Yigit *et al*., 2021). All these properties make silk fibroin a promising biomaterial for cultivated meat scaffolding.

Silk fibroin is a natural biopolymer present in the silk secreted by *Leptidoptera spp.* (*i.e.* butterflies and moths), *Hymenoptera spp.* (*i.e.* bees and wasps), and *Araneae spp.* (*i.e*. spiders) (Sehnal and Sutherland, 2008). Silk is composed of silk fibroin (70-80% w/w) and silk sericin (20-30% w/w). Silk fibroin is a fibrous protein that runs at the core of the silk filament and provides mechanical structure and tensile strength, and the silk sericin (20-30% w/w), a globular protein that acts as a glue-like substance surrounding silk fibroin and providing elasticity to the silk (**Figure 10C**; Nguyen *et al*., 2019). Depending on the function of the silk, the properties of silk fibroin can vary significantly. For instance, the silk of spiders used for cobwebs to catch prey often feature extremely tough silk fibroin that can exceed the toughness of synthetic nylon or Kevlar (Römer and Scheibel, 2008). However, the lack of domestication amongst spider species makes obtaining spider silk quite challenging. On the other hand, silkworms, mostly from moth species, have been domesticated and farmed for millennia to harvest silk for clothing and accessories (Gong *et al*., 2016), and, since antiquity, for skin care and medical sutures as famously described by Galen of Pergamum in 150 AD (Galen, 150/2011). Nowadays, raw silk is primarily harvested from mulberry silkworms (*Bombyx mori*; **Figure 10A,B**) cocoons for the textiles industry with over 90% of its global production emerging from China and India. To obtain raw silk, sericulture farmers hatch silkworm eggs on disinfected rearing beds and feed the larvae until they spin their silk cocoons, a process taking approximately 28 days (Bitar *et al*., 2024).

Once spinning is complete, but before eclosion of the moth, the cocoons are harvested and dried using hot air, killing the silkworm pupae in the process. The cocoons are then generally boiled or steamed to reel the silk onto spools and various treatments are then used to process the raw silk for use in garments (Astudillo *et al*., 2014). Although, silk is often considered environmentally friendly, there is debate on its global warming potential (GWP). While most studies set the GWP of raw silk around 18 – 25 kg of CO_2 equivalent per kg of product (CO_2eq/kg; Ren *et al*., 2016; Holland *et al*., 2019; Liu *et al*., 2022), two recent studies have shown that the whole process of silk production, from mulberry cultivation and silkworm rearing to raw silk processing had a GWP of around 80 kg CO_2eq/kg (Astudillo *et al*., 2014; Wu *et al*., 2025), a figure far exceeding the GWP of beef farming (approximately 30 kg CO_2eq; Mattick *et al*., 2015). With the culture of mulberry fields and silkworms representing 20-70% of that figure, it should be noted that this high global warming potential is linked to inefficiencies in the culture process (Astudillo *et al*., 2014; Wu *et al*., 2025). With a primary focus of yields, mulberry trees are generally over-fertilised using manure or chemical fertilisers with ammonia and potassium chloride, contributing to N_2O emissions and soil, freshwater and marine ecotoxicity (Wu *et al*., 2025). In addition, the high energy input mostly as electricity required for heating, ventilation and illumination represents 70% of the environmental impacts of silkworm rearing. While the use of more efficient systems such as water-fertiliser irrigation technology, drip-irrigation, renewable energy and smart management systems for climate control could easily and considerably reduce production costs and pollution (Siddalingaswamy *et al*., 2007; Wu *et al*., 2025), these technologies may be too costly for most sericulture farms in China and India without significant government subsidies and incentives (Astudillo *et al*., 2014; Wu *et al*., 2025). To mitigate some of the environmental damages and ethical concerns of sericulture and to improve the purity and quality of silk proteins, research has been conducted to engineer silk proteins using precision fermentation. As such, silk fibroin, especially from non-domesticated silkworm and spider species, has been recombinantly produced using a range of host organisms including bacteria (Bowen *et al*., 2018; Xiao *et al*., 2023), yeast (Jansson *et al*., 2016), transgenic animals and plants (Scheller *et al*., 2004; Wen *et al*., 2010), however none of these methods have yet to be scalable due to high metabolic burdens limiting protein expression, leading to high production costs and low titers (Xiao *et al*., 2023). Although recombinant silk fibroin could be produced at cost parity with farmed raw silk (~$100/kg; Flaibam *et al*., 2025; Wu *et al*., 2025), there is still a lot of doubt on whether precision fermentation could be environmentally friendlier than sericulture farms. With a significant electricity consumption to warm cell culture media, other recombinant proteins and growth factors used in the production of cultivated meat have had GWPs ranging 10 kg CO_2/kg to 100,000 kg CO_2eq/kg depending on the protein molecular weight and host organism (Xiao *et al*., 2023). In addition, while the carbon footprint of cultivated meat is predicted to be around

14 – 25 kg CO_2eq/kg of meat, the use of renewable energies could bring this down to 3-6 kg CO_2eq/kg (Tuomisto *et al*., 2022; Sinke *et al*., 2023). Consequently, as scaffolds are expected to represent 10% of the final meat product (Sinke *et al*., 2023), it could be deduced that the production of cultivated meat using silk fibroin scaffolds would increase to approximately 22 – 33 kg CO_2eq/kg with the current energy infrastructures and farming inefficiencies, or 7 – 10 kg CO_2eq/kg with renewable energy, drip irrigation and efficient fertiliser systems (Tuomisto *et al*., 2022; Sinke *et al*., 2023; Wu *et al*., 2025).

Structurally, the silk fibroin protein is composed of hydrophobic heavy chains connected to hydrophilic light chains by a single disulfide bond (**Figure 10D**). In the heavy chain, predominantly hydrophobic amino acids (AA) such as alanine (Ala), glycine (Gly) and serine (Ser) form highly repetitive and ordered antiparallel β-sheets interspaced by hydrophilic anamorphous regions (Nguyen *et al.*, 2019). These β-sheet regions characterised by Gly-Ala-Gly-Ala-Gly-Ser repeats, form the crystalline structure of silk fibroin (**Figure 10E**). Depending on its physical state, silk fibroin can present different crystalline structures referred as Silk I (liquid state) and Silk II (solid state). In its naturally liquid state, as stored in the secretory glands of insects, the fibroin displays a Silk I conformation and is mainly composed of water-soluble irregular structures of random coils and α-helices. As the silk is naturally spun, the fibroin solidifies and presents a Silk II conformation characterised by a high density of parallel and antiparallel β-sheets (Nguyen *et al*., 2019). The natural transition from Silk I to Silk II conformations has been shown to impact the protein's solubility, degradation rate, mechanical strength, and chemical properties (Hu *et al*., 2012; Sun *et al*., 2021). Most importantly, the conformational transition can be initiated artificially without the use of toxic crosslinkers making silk fibroin a particularly versatile and tuneable biomaterial.

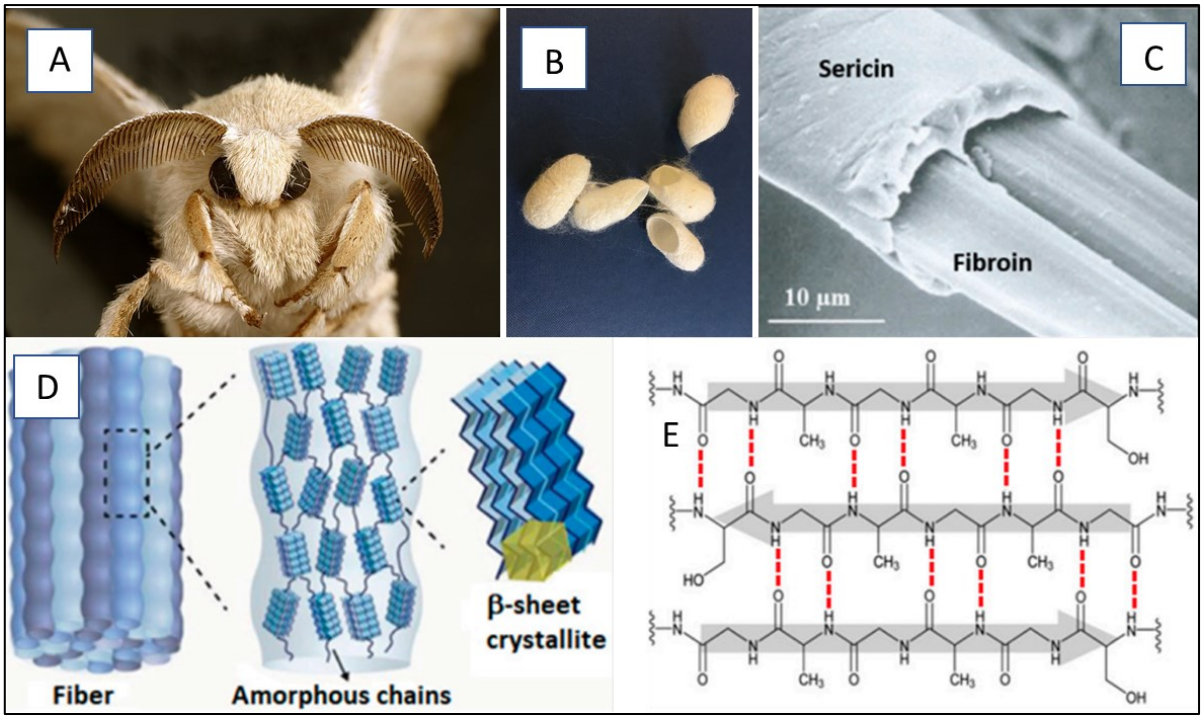

Figure 10: The origin and structure of *B. mori* silk fibroin.
(A) Adult Bombyx mori *silkworm (CSIRO, 2010), (B)* B. mori *cocoons, (C) SEM image of a silk fibre (Nguyen,* et al.*, 2019), (D) Heavy chain composition of silk fibroin (Nguyen,* et al.*, 2019), (E) Hydrogen bonds connect hydrophobic amino acids forming anti-parallel β-sheets (Nguyen,* et al.*, 2019).*

There are also drawbacks to silk fibroin as a material for scaffold engineering, however, these could be remediated. For instance, *B. mori* silk fibroin is devoid of cell adhesion peptide motifs which could inhibit cell attachment to the scaffold, and its high tensile properties could induce unwanted spontaneous differentiation of MSCs into bone lineages (Fernández-Muiños *et al*., 2014; Nguyen *et al*., 2019; Yamazaki *et al*., 2020). This could, however, be corrected by blending silk fibroin with highly functional polymers such as chitosan, zein, pumpkin seed protein or gelatin. Alternatively, this could be achieved using co-axial electrospinning with silk fibroin at the core carrying another softer sheath material with high functionality.

Another concern is the public perception of silk fibroin in food products, which has yet to be investigated. Despite this, it can be anticipated that many prospective consumers would negatively regard foods with insect-derived additives and cultivated products that are not slaughter-free. Many studies have shown that insect-based protein in foods disgust consumers in western societies who would likely represent the dominant market for cultivated meat products in the near future (Bryant, 2020; Castro *et al*., 2019; Hopkins *et al*., 2023; White *et al*., 2023). In addition, silkworm pupas are killed to obtain the cocoons from which silk fibroin is extracted and, despite the low amounts of polymer needed for electrospinning, production at an industrial scale would result in the deaths of thousands, if not millions, of silkworms per day. This could also be remedied by producing silk fibroin

recombinantly at scale, driving the cost down and eliminating the cruelty factor entirely (Post *et al*., 2020). However, as a genetically modified product, public perception would be challenged yet again by a distrust of genetically modified organisms (GMO; Siegriest and Hartmann, 2020).

1.6 Conclusion

In summary, cultivated meat, grown from stem cells *in vitro*, represents a sustainable alternative to the environmentally damaging and morally unethical intensive animal farming model, for feeding an ever-growing population with an increasing demand for meat. Despite, recent advances and major breakthroughs led by industry, including legalisation of less than a handful of cultivated meat products in a few countries, the scalable production of cultivated meat remains one of the largest challenges to be resolved to improve accessibility to the general public.

One way of improving scalability is to develop edible scaffolds that play a role in the expansion, differentiation and maturation of cells and are incorporated into the final meat product, contributing to its texture, taste and appearance. This thesis explores the possible use of scaffolds made from non-woven electrospun mats made of edible biomaterials, using scalable methods and non-toxic materials in the process.

Silk fibroin, a material used extensively in tissue engineering and food science, was chosen as the default biomaterial for the fabrication of scaffolds and microcarriers due to its abundance, digestibility, excellent cytocompatibility, mechanical properties and food-safe status. Electrospinning was chosen as a scalable method for the fabrication of nanofibrous supports that can mimic the native ECM of skeletal muscle (the predominant type of meat). Ground beef was chosen as the target meat model, as beef is one of the most consumed meats in the world, frequently enjoyed in minced form, which corresponds well to unstructured cultivated meat, while at the same time beef farming is one of the most environmentally damaging forms of agriculture. In addition, as most tissue engineering studies having been performed on mammalian cell lines, there is a wealth of documented research on adaptation of media formulation and cell culture protocols to build on when working with mammalian cells. Mesenchymal stem cells were chosen because of their simple and ethical isolation from live animal biopsies and their ability to differentiate into all meat tissue components (skeletal muscle, fat, connective tissue, tendons, bone) is relatively easy to control.

1.7 Research aims

The aim of the research presented in this thesis is to develop novel electrospun silk fibroin microcarriers that support the expansion of bovine mesenchymal stem cells and improve the

scalability of cultivated meat production and are cost-effective, food safe and acceptable to future consumers.

Chapter II lays out the groundwork for the production of stable electrospun silk fibroin nanofibres. In this chapter, polymer solution properties and electrospinning parameters are optimised to produce randomly orientated, continuous and homogenised nanofibres. The fibres are then stabilised, using either ethanol or methanol, and characterised chemically, physically and mechanically to identify the best treatment method.

Chapter III builds on the results of Chapter II by seeking to improve the cost-effectiveness and scalability of fibre production. First, degumming strategies are explored to improve silk fibroin yields during extraction and regeneration in order to reduce costs, and the resulting regenerated silk fibroin is compared to the commercially available protein characterised in Chapter II. Then, various DC and AC needless electrospinning technologies are tested to produce fibres at scale and the resulting mats are characterised. Finally, the electrospun mats are biologically characterised to evaluate material cytotoxicity and study the growth kinetics of bovine mesenchymal cells on the electrospun fibres when seeded at different densities.

Chapter IV aims to improve the expansion of bovine mesenchymal stem cells by functionalising the silk fibroin scaffolds and converting these into novel electrospun nanofibrous non-spherical microcarriers. First, the surface properties of the electrospun fibres are modified using either ultraviolet light or silk fibroin blended with plant-based biopolymers with additional nutritional, health and antimicrobial properties. The proliferation of bovine mesenchymal cells is then measured on these functionalised scaffolds to identify best functionalisation strategies. Next, electrospun mats are converted into microcarriers that are then characterised and compared to commercially available microcarriers in static conditions.

Chapter V seeks to quantify the mouthfeel of traditional meat and plant-based analogue burgers to inform future work on cultivated meat production, where edible scaffolds might be used to enhance the texture of cultivated meat products. A range of mechanical and textural tests are employed to measure the properties of raw and cooked burgers to gain insights into properties relevant to mouthfeel and handling which could help to improve novel products so that they gain increased consumer acceptance.

CHAPTER II

ELECTROSPUN SILK FIBROIN MATS FOR THE EXPANSION OF BOVINE MESENCHYMAL STEM CELLS

2.1 Introduction

In vivo, the extracellular matrix (ECM) provides anchorage and functionalisation cues for stem cells to grow and differentiate (Zhang *et al.,* 2021). To grow tissues *in vitro*, scientists engineer support materials that mimic the ECM properties and structure, in the form of scaffolds or hydrogels (Molina *et al.*, 2021). Electrospinning is a popular choice for fabricating scaffolds and meshes for biomedical and tissue engineering applications, as it can form sheets of nanofibrous and interconnected porous networks which closely resemble the structure of the ECM (Rahmati *et al*., 2021).

While many materials electrospun for tissue engineering applications have been either non-edible synthetic polymers (Guo & Ma, 2014) or composites, a recent drive for environmentally friendly and biodegradable biomaterials has put the spotlight on natural polymers such as proteins (Bonkamp *et al*., 2022). Silk fibroin is a food safe (GRAS status; Yigit *et al*., 2021) fibrous protein derived from *Bombyx mori* silkworm silk, that has similar mechanical stability to synthetic polymers. Silk fibroin has been used in numerous applications such as drug delivery (Mottagitalab *et al*., 2015), filtration systems (Konda *et al*., 2020; Wang *et al*., 2021), regenerative medicine (Kaur *et al*., 2019; Polakova *et al*., 2022) and most recently food engineering (Marelli *et al*., 2016; Ruggeri *et al*., 2020). At first glance, it may not be an obvious choice of material for cultivated meat supports because its insect origin may evoke disgust in consumers, however, its excellent and tailorable physicochemical, mechanical, and biological properties could in fact make silk fibroin electrospun supports an excellent material for cultivated meat.

This chapter presents a proof-of-concept study of the production of silk fibroin electrospun non-woven mats. This proof-of-concept study employs a benchtop low-productivity needle-electrospinner and commercially obtained silk fibroin (as a readily available and consistent source of starting material, despite its high price). Following investigation of the effects of electrospinning conditions (*i.e.* polymer concentration, voltage, tip-to-collector distance, and flow rate) the electrospun mats are stabilised by immersion in monohydric alcohols, namely ethanol (EtOH) or methanol (MeOH), to render them

insoluble while maintaining their highly porous and fibrous structure in culture conditions. The effects of the alcohol treatments on the chemical, morphological and mechanical properties of the silk fibroin fibres are then characterised and compared, in order to identify the best method for the creation of electrospun non-woven mats.

2.2 Materials and Methods

2.2.1 Materials

Ethanol (99.8%), methanol (HPLC grade, 99.8%) and formic acid (98+%) (Acros Organics) were purchased from Fisher Scientific Ltd. (UK) and aqueous silk fibroin (50 mg/mL) (Sigma-Aldrich) was obtained from Merck Life Science (UK). Deionised water was used in all experiments unless otherwise stated.

2.2.2 Needle electrospinning of silk fibroin

Aqueous silk fibroin was oven dried (SQ Oven-80HT, SciQuip, UK) at at 40 °C for 24 h to form silk fibroin films. The polymer solutions were then prepared by dissolving the silk fibroin films in formic acid (FA) to a final concentration of 10%, 12% and 15% (w/w), under magnetic stirring for 24 h at room temperature The solutions were stored at 4 °C and used within 72 h to electrospin silk fibroin non-woven mats.

The electrospinning set-up for obtaining the non-woven mats is shown schematically in **Figure 11**. A syringe containing the polymer solution was mounted to a syringe pump (NE-300, New Era Pump Systems Inc., USA) and combined with a 22-gauge blunt needle (Hamilton Kel-F Hub Blunt Point Needle, ga22/51 mm/pst3, Fischer Scientific, UK). A metal collector plate was placed vertically and covered with non-stick baking paper to easily amass, and later lift, the electrospun mats. The positive and grounded wires of a high voltage generator (Genvolt High Voltage Power Supplies, UK) were connected to the needle and collector plate. During all runs, the temperature and relative humidity were measured at 20 °C (± 2 °C) and 30% (± 2%), respectively. The electrospinning parameters and the polymer solution concentration were optimised by varying the voltage (15-20 kV), tip-to-collector distance (10-15 cm) and polymer concentration (10-15% (w/w) in FA). The flow rate was adjusted between 0.1 mL/h and 0.2 mL/h on every run to match the polymer transfer rate.

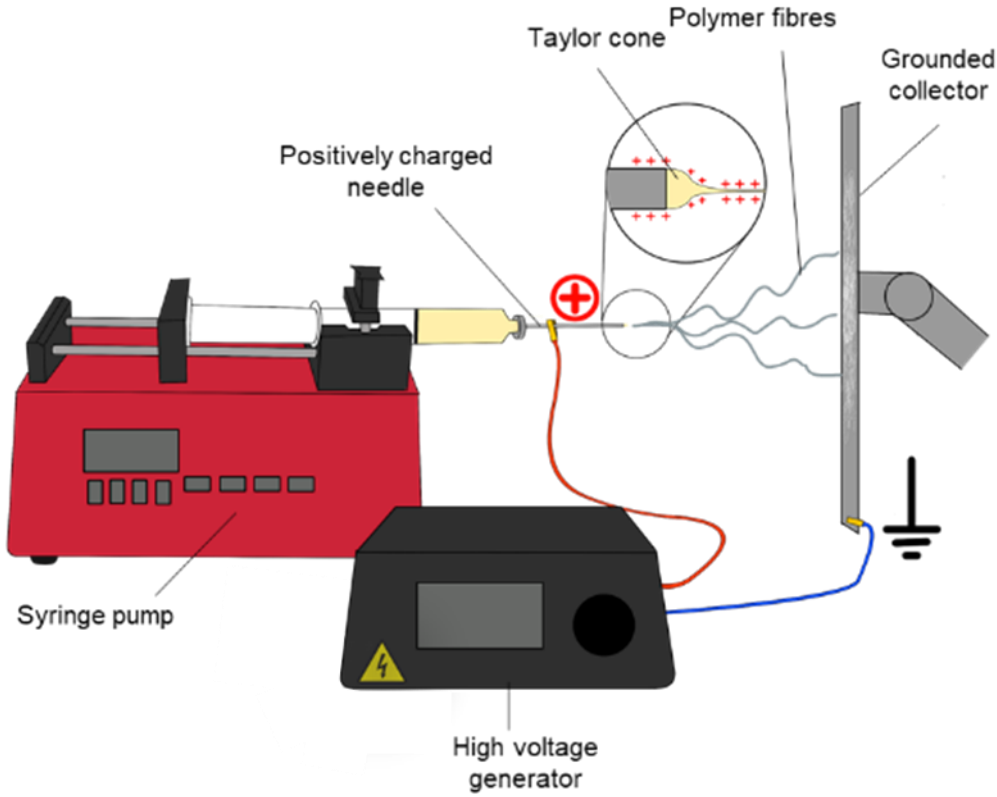

Figure 11: Horizontal needle-electrospinner setup. The syringe pump pushes the polymer solution out of the electrified syringe at a constant flow rate. As the solution exits the needle, electrostatic forces draw the polymer solution into jets that travel towards the grounded collector plate. While in flight, the solvent evaporates from the jets and whipping instability causes dry fibres to amass on the collector as a randomly aligned fibrous mesh. Over time the mesh thickens to produce an electrospun non-woven mat.

The resulting SF_{10} (10% (w/w)), SF_{12} (12% (w/w)) and SF_{15} (15% (w/w)) electrospun mats were left to air dry overnight before stabilisation or characterisation.

2.2.3 Electrospun mat stabilisation

To introduce conformational changes and reduce solubility in water (Kaewpirom and Boonsang, 2020), the electrospun silk fibroin mats were stabilised by physically crosslinking them with monohydric alcohols (ethanol or methanol) for 20 min at room temperature. To reduce structural damage to the crosslinked mats, the mats were first cut into smaller rectangular shapes using a rotary blade on a precision cutting pad. A strip of non-stick aluminium foil (larger than the mat cut) was placed flat in a petri dish with the non-stick side facing upwards. The petri dish was subsequently filled with ethanol (EtOH) or methanol (MeOH) at different concentrations (between 70% and >99.8%) keeping the aluminium foil submerged. The piece of electrospun mat was then carefully placed flat onto the alcohol surface and sunk onto the foil where it remained immersed for 20 min. The aluminium foil and mat were subsequently removed from the alcohol solution and left to dry at room temperature under

a fume hood to allow for rapid alcohol evaporation. The mats were easily separated from the foil following drying of the fibres and placed in a desiccator at low pressure (< 50 mbar) for an additional 24 h. The stages involved in the stabilisation process are depicted in **Figure 12.**

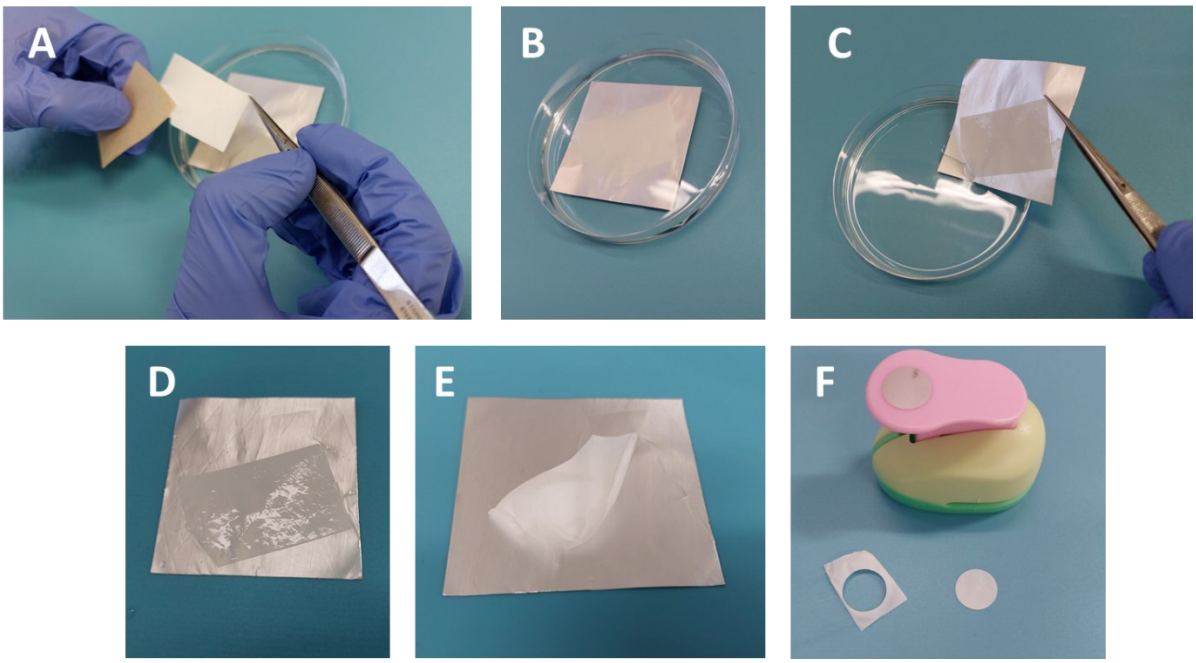

Figure 12: Stabilisation of electrospun silk fibroin mats. (A) The electrospun mats were carefully removed from the baking paper collector and immersed flat on a sheet of aluminium foil in EtOH or MeOH (B), (C) After 20 min of immersion, both the mats and the foil were removed from the alcohol solution and left to dry in a fume hood (D). (E) As the mats dried, they were easily lifted from the foil. (F) The stabilised mats were then cut into the desired sample shape and desiccated for 24h.

2.2.4 Physicochemical characterisation of electrospun scaffolds

2.2.4.1 Fourier Transform Infrared Spectroscopy (FTIR)

FTIR was carried out on a Frontier Spectrometer (PerkinElmer Ltd., USA) combined with an attenuated total reflectance (ATR) accessory (GladiATR; Pike Technologies, USA), to identify chemical changes and protein secondary structure rearrangements caused by the electrospinning method and the subsequent alcohol treatments. A total of 16 scans were performed from 4000 cm^{-1} to 400 cm^{-1} with a resolution of 4 cm^{-1} for each sample. The following method described by Boulet-Audet *et al*. (2015) was then used to normalise the FTIR spectra (see ***Appendix A, Figure S1***) and identify functional groups and determine conformational changes in the secondary structure of silk fibroin. First, an offset was performed by subtracting the average absorbance values of the region spanning 1950 – 1900 cm^{-1} for each data set. The spectra were then normalised using the integrated absorbance of the region spanning 1900 – 800 cm^{-1} to compensate for signal intensity variations caused by varying contact with the electrospun fibres (Boulet-Audet *et al*., 2015). The interpretation of the amide bands was based on the relevant literature (Biagiotti *et al*., 2022; Hu *et* al., 2006; Kong and Yu, 2007; Tretinikov *et al*., 2001; Zhang and Pan, 2019; Carissimi *et al*., 2019).

Table 5: Peak assignments in amide bands I, II and III.

Silk Conformations	Assignments	Amide I	Amide II	Amide III
Silk II	β-sheets	1612-1638 and 1697-1703	1555 and 1515-1525	1260
Silk I	Random coils	1638-1655	1535-1545	1235
	α-helices	1650-1662	1545	1240
	β-turns	1663-1696		

The percentage of β-sheets in the amide I band was calculated using a combination of second derivative analysis, deconvolution and curve fitting strategies (**Figure 13**). To achieve this, the FTIR absorbance spectra of the amide I band (f_a) was first plotted between 1600 and 1708 cm^{-1} by converting transmittance values ($\%T$) into absorbance (A; **Equation 1**) and then smoothed by a factor of 3.

$$A = 2 - \log(\%T) \tag{1}$$

Then second derivative analysis of the amide I band (f_a'') was undertaken where w and A represents wavenumber and absorbance values, respectively (**Equation 2**). The local minima of the second derivative of the amide I (μ_i) in the resulting function were identified and assigned a conformation based on the data presented in **Table 5**.

$$f_a'' = \frac{d^2w}{dA^2} \tag{2}$$

The amide I spectra was then decomposed into Gaussian distributions (X_i), with a density f_{X_i}, centred on μ_i, with unknown standard deviation σ_i. The density of the Gaussian distribution ($f_{X_i}(w)$; **Equation 3**) was computed as follows:

$$f_{X_i}(w) = \frac{e^{-\frac{(w-\mu_i)^2}{2\sigma_i^2}}}{\sigma_i\sqrt{2\pi}} \tag{3}$$

The distribution of the amide I band (f_a) was then fit with a weighted average of the Gaussian distributions f_{X_i}, weighted by their respective unknown relative areas (RA_i). Both the relative areas and standard deviations were selected to minimise the mean square error of the fit.

The weighted average of densities $f_{weighted}$ (**Equation 4**) was computed as follows:

$$f_{weighted}(w_j) = \sum_{i=1}^{n} (RA)_i f_{X_i}(w_j) \tag{4}$$

The mean square error (MSE) of the fit between the amide I function and the weighted average of Gaussian distributions $f_{weighted}$, was calculated as the sum of the square differences between the values of the weighted distribution and the amide I distribution and at every wavenumber in the dataset (**Equation 5**). In other terms, the difference between $f_{weighted}(w_j)$ and $f_a(w_j)$, for all wavenumber values (w_j). The MSE was minimised by choosing optimal relative areas RA_i and standard deviation σ_i for the Gaussian distributions that make up the weighted average $f_{weighted}$, under the constraint that each standard deviation should be equal or less than 5 cm^{-1}. The maximum standard deviation was used to reduce the width of the Gaussian distributions and prevent too much overlapping into regions assigned to different conformations.

The MSE is calculated as:

$$MSE = \sum_{j=1}^{k} (f_{weighted}(w_j) - f_a(w_j))^2 = \sum_{j=1}^{k} (\sum_{i=1}^{n} (RA)_i f_{X_i}(w_j) - f_a(w_j))^2 \quad (5)$$

The MSE was minimised by choosing optimal relative areas summing up to 1 and optimal standard deviations under the constraint that they should be equal or less than 15 cm^{-1} (**Equation 6**).

$$\begin{cases} RA_1, \dots, RA_n \in [0,1] \; such \; that \; \sum_{i=1}^{n} (RA)_i = 1 \\ and \; optimal \; \sigma_1, \dots, \sigma_n \; less \; than \; 15 \; cm^{-1} \in [0,15] \end{cases} \quad (6)$$

Finally, the percentage of Silk II conformations in the amide I band was calculated as the sum of the relative areas of the Gaussian distributions assigned to β-sheets.

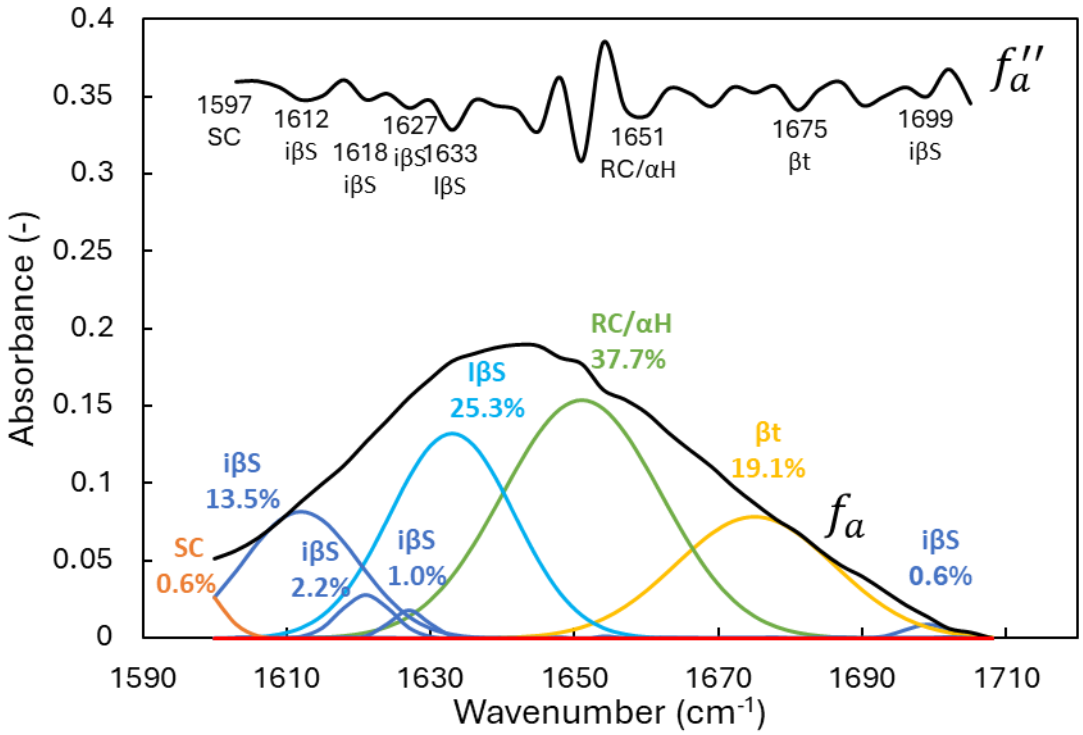

Figure 13: Example deconvolution of the amide I band of electrospun silk fibroin. At the top, the black line represents the second derivative function of the amide I band (f_a''), the peaks have been matched to protein conformations (SC: Tyrosine side chains; iβS: inter-molecular β-sheets; IβS: intra-molecular β-sheets, RC/αH: random coils and α-helices; βt: β-turns). At the bottom, the black line represents the amide I function (f_a), the relative area of the Gaussian distribution for each peak was solved by minimising the mean square error of the data set so that the total relative areas of the sum of the peaks equals the area of the amide I band function. The percentage of β-sheets in the silk can then be found by summing the relative area of every peak assigned to inter- and intra-molecular β-sheets.

2.2.4.2 Scanning electron microscopy

Imaging of the silk fibroin mats before and after alcohol treatment was performed on a Thermo Fisher Quattro S (Thermo Fisher Scientific, USA) environmental scanning electron microscope (SEM) with a field emission filament and a low vacuum detector. The pressure was set to 10 Pa and samples were scanned at 5-15 kV by measuring secondary electron emission. Electrospun samples were stuck to double-sided copper tape without sample coating. The average fibre diameter was determined using ImageJ software (National Institutes of Health, USA) and presented as an average value of 100 independent measurements.

2.2.4.3 Estimation of porosity

The porosity of scaffolds can be critical for cell culture, as it allows cells to penetrate pores and align alongside fibres, while ensuring adequate flow of nutrients (Rahmati *et al*., 2021; Yadav *et al*., 2021). The porosity of the electrospun samples (φ) was estimated by comparing their apparent density (ρ) to the density of mulberry silk fibroin (ρ_{SF} = 1.40 kg/m^3; Warwicker, 1954) (**Equation 7**). Discs (n=5) were cut using a 6mm diameter puncture tool and their thickness was determined with a micrometre

to calculate the volume. Each disc was weighed on a microbalance (XPR2, Mettler Toledo, UK) and the apparent density was calculated as the product of mass over volume.

$$\varphi = 100\left(1 - \frac{\rho}{\rho_{\mathrm{SF}}}\right) \tag{7}$$

2.2.4.4 Assessment of aqueous stability

The effect of incubation in aqueous conditions on the solubility and therefore structural integrity of the electrospun mats was assessed by immersing untreated and alcohol-treated silk fibroin electropsun samples in H_2O for various time periods (from 1 min and up to 2 weeks). The samples (n=3) were weighed in aluminium foil containers that were then filled with 2 mL diH_2O. At the end of the contact time, the excess water was carefully removed, the samples were dried in a fan assisted high temperature oven (SQ Oven-80 HT; SciQuip, UK) at 60 °C and weighed once again. The weight difference was calculated as a percentage of scaffold weight integrity at the end of the experiment (W_{end}) compared to that at the start (W_{start}) (**Equation 8**).

$$W = 100\left(1 - \frac{W_{\mathrm{end}}}{W_{\mathrm{start}}}\right) \tag{8}$$

2.2.4.5 Tensile testing

An ElectroForce 3200 series III Extended Stroke (TA Instruments, USA) with a 1000 g load cell was used to measure the force and displacement to compute the stiffness, strength, and elasticity of the silk fibroin electrospun mats ($n = 10$). In the absence of specific standards for nanofibrous materials, the ASTM International D368-14 tensile testing method for the properties of plastics (ASTM International, 2014) was followed with modifications to strip dimensions. Instead of using the narrow dog-bone shapes of specific dimensions, rectangular strips 10 mm wide by 50 mm long were employed corresponding to common practice found in the published literature (Amiraliyan *et al*., 2010; Cai *et al*., 2010; Yin and Xiong, 2017). The parameters were set to 30 mm gauge length, 0.5 mm/min displacement and 100 Hz recording frequency, to ensure the range specified by the standard was met. The cross-section of each strip was measured using a calliper and micrometre. A stress-strain curve was plotted, from which the Young's modulus (E) was calculated as the slope of the linear portion of the curve during the elastic deformation stage (**Equation 9**), with the stress (σ) measured as the force (F) over the cross-sectional area (A) of the samples (**Equation 10**), and strain (ε) measured as the recorded displacement (ΔL) over the gauge length (L; **Equation 11**). The ultimate tensile strength (σ_{max}) was recorded as the highest value on the Y-axis, and the yield strain (ε_y) was measured as the X-intercept.

$$E = \frac{\sigma}{\varepsilon} \tag{9}$$

$$\sigma = \frac{F}{A} \tag{10}$$

$$\varepsilon = \frac{\Delta L}{L} \tag{11}$$

The shear modulus was calculated assuming that the randomly orientated fibres would make the electrospun mats isotropic, as commonly assumed with unwoven (random orientation) fibrous materials employed in composites. This is a valid assumption in-plane, and the shear modulus (μ) was calculated from the Young's modulus (**Equation 12**) in reference to the Poisson's ratio of silk fibroin ($\nu = 0.25 - 0.3$; Ansys GRANTA EduPack, ANSYS Inc, UK).

$$\mu = \frac{E}{2(1+\nu)} \tag{12}$$

2.2.5 Statistical analysis

Statistical analysis was carried out using Microsoft Excel version 2208, with a confidence interval of 95%, to determine mean and standard deviation (SD). Bar charts are shown as mean ± SD ($n \geq 3$). The statistical significance of the results was calculated using a one-way analysis of variance (ANOVA) followed by Tukey's honestly significant difference (HSD) test (**Equation 13**). The Tukey criterion (T) was measured as the product of the studentised range (q) and the square root of the ratio of the mean square error (MSE) and the number of fewest observations in a single group (n_i).

$$T = q_{\alpha(k,df)} \sqrt{\frac{MSE}{n_i}} \tag{13}$$

The value of the q statistic for each test was identified from a table of critical values of the studentised range distribution that depended on the level of significance (α; α = 0.05), the number of categories (k) being compared and the degrees of freedom (df) calculated as the difference between the total number of observations (n) and the number of categories compared (k; **Equation 14**).

$$df = n - k \tag{14}$$

Finally, the difference between the means of two categories was considered significant (p<0.05) when the absolute mean difference $|\bar{x}_1 - \bar{x}_2|$ was larger than the Tukey criterion. In the bar charts presented in chapters II, III and IV, values are shown as means ($n \geq 3$) with error bars representing standard deviation (± SD). Letters above the bars indicate statistical difference. Categories with the

same letter have means that are not significantly different from each other. Different letters show significant difference between categories.

2.3 Results & Discussion

2.3.1 Lab-scale calibration and optimisation of needle electrospun silk fibroin

Several polymer, operating and environmental properties affect the effectiveness of electrospinning and play an important role in fibre morphology and orientation (as explained in Chapter I, *section 1.5.3.2* and **Table 3**). For electrospinning to take place, it is essential that polymer chains entangle tightly (minimum 2.5 chains) and the polymer solution concentration, molecular weight, viscosity, surface tension and conductivity all affect its electrospinnability (Shenoy *et al.*, 2005). To ensure that silk fibroin could be efficiently electrospun to form mats with continuous, uniform and randomly orientated fibres, the properties of the polymer solution were tailored to meet the critical concentration needed for jet formation without frequent needle clogging (Haider *et al*., 2018). Based on the literature, silk fibroin concentration was set between 10% and 15% (w/w) in formic acid (Kim *et al*., 2003; Amiraliyan *et al*., 2015; Saltik-Cirkin & Yuksek, 2021).

The operational ranges of the needle electrospinner were defined by visually observing the effect of voltage (8-23 KV), collector distance (5-20 cm) and flowrate (0.01-1 mL/h) on the behaviour and geometry of the polymer droplet at the tip of the needle, and by visualising the presence of fibres on the collector for the 10%, 12% and 15% (w/w) silk fibroin polymer solutions. Slowly increasing the voltage from 8 kV, with a constant collector distance of 15 cm, caused the polymer drop at the tip of the needle to elongate until a defined Taylor cone appeared at around 13 kV for all polymer solutions and remained present up to 23kV, although setup limitations prevented reliable experimentation above 20 kV due to frequent arcing between the electrified needled and the metallic syringe pump. Transfer of droplets (electrospraying) was observed between 11 and 15 kV, beyond which only fibres were observed on the collector plate. In terms of collector distance, material was seen collecting 5 to 20 cm from the tip, although the distribution of fibres differed considerably between those distances. Below 7 cm, electrical crackling could be heard, and a blue glow was observed in the dark between the needle and collector plate which intensified considerably when increasing the voltage. In contrast, with a collector distance above 15 cm the area of fibre collection became larger than the collector plate and fibres were lost. Therefore, a collector range of 10 cm to 15 cm and voltage of 15 kV to 20 kV was chosen to characterise electrospun fibres. Depending on collector distance, voltage and ambient conditions, the flowrate was adapted for each experiment and polymer solution so that the

polymer droplet at the tip of the needle stayed a constant size during electrospinning, thereby matching the jet formation rate. In practice, the flowrate ranged from 0.1-0.2 mL/h. While all three polymer solutions could be electrospun within the defined parameter ranges, the higher viscosity of the 15% (w/w) polymer solution resulted in frequent needle clogging and rapid solidification of the electrospinning droplet preventing reliable and continous electrospinning for longer periods of time (>30 min). Therefore, characterisation of the electrospun fibres was performed with the 10% (w/w) and 12% (w/w) silk fibroin polymer solutions only.

Non-woven electrospun mats using the 10% (w/w) polymer solution (SF10-U; **Figure 14A**) exhibited continuous and randomly orientated fibres of relatively thin diameters averaging 90 ± 58 nm across all tested operating parameters. These mats also displayed relatively high amounts of defects, notably elongated beads, and split and branched fibres that were symptomatic of suboptimal electrospinning conditions. Beads are generally a sign of low polymer concentration, and result from a breaking of fibres mid-flight owing to the current and high surface tension. By increasing the polymer concentration, and therefore its viscosity, the polymer chains can tangle more tightly and overcome the polymer surface tension to form uniform and bead-free fibres (Haider et al., 2018). In contrast, non-woven mats electrospun from the 12% (w/w) polymer solution (SF12-U; **Figure 14B**) displayed consistent, straight, uniform and randomly orientated continuous nanofibres that averaged 134 ± 13 nm across all tested operating parameters. Minor defects including split and branched fibres were occasionally observed. Interestingly, no correlation was observed between the fibre diameter and the voltage (15-20 kV) or collector distance (10-15 cm) for either SF10-U or SF12-U ($p>0.05$). However, there was a significant increase in fibre diameter for most electrospinning parameter between SF10-U and SF12-U ($p<0.05$; Figure 15) with the exception of the 15 kV, 12.5 cm and 17.5 kV, 15 cm which were abnormally high and should be repeated. As thicker fibres have been shown to improve cell attachment, migration, proliferation and differentiation of mesenchymal stem cells (Lee et al., 2017b; Jenkins et al., 2019), the 12% (w/w) silk fibroin in formic acid formulation was chosen as the default electrospinning polymer solution for all subsequent experiments. In addition, the 15 kV and 10 cm collector distance were chosen as the default electrospinning operating parameters, as the resulting mats displayed thick and uniform fibres with no apparent defects. Finally, owing to the higher viscosity of the 12% (w/w) polymer solution, the flowrate could be increased from 0.1 to 0.2 mL/h at 15 kV and 10 cm collector distance, in turn doubling productivity and producing mats with improved handleability.

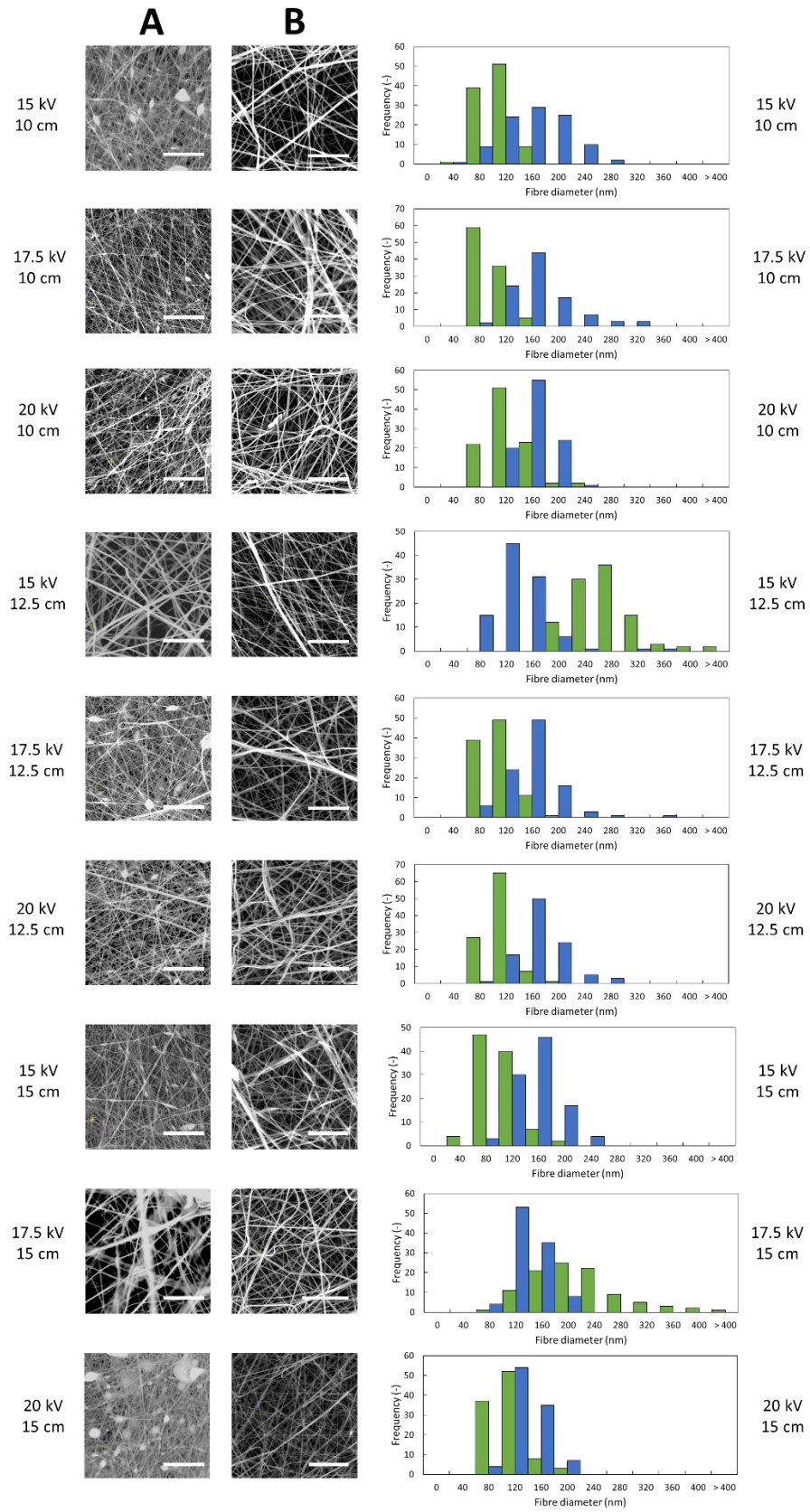

Figure 14: SEM images (left) and fibre distribution (right; n=100) of needle electrospun non-woven silk fibroin mats using either (A) 10% (w/w; green) or (B) 12% (w/w; blue) silk fibroin in formic acid, at various tip-to-collector distances and voltages. Scale bars = 5 µm.

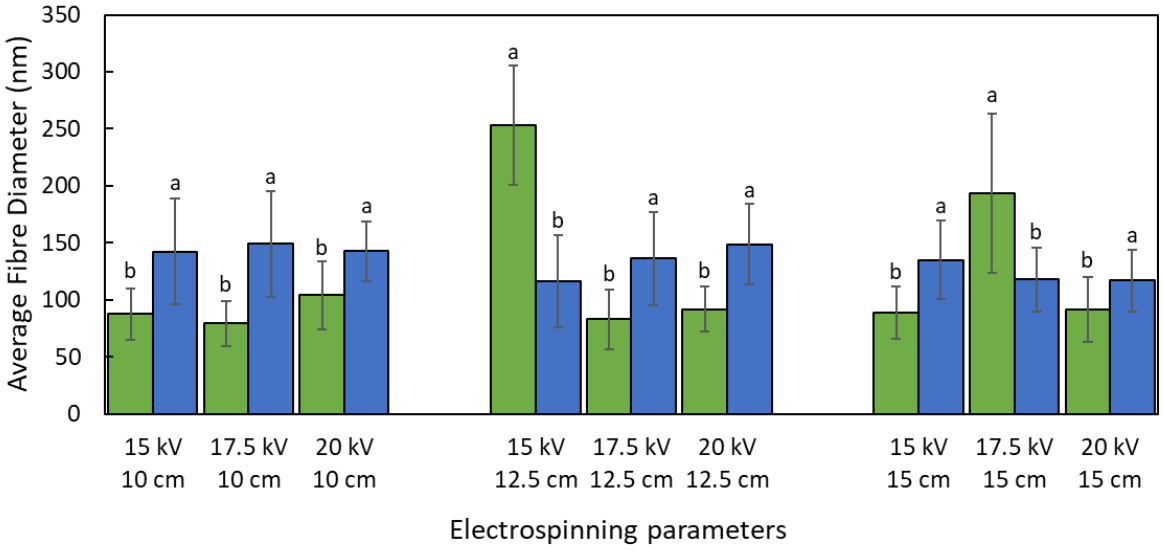

Figure 15: Effect of voltage and tip-to-collector distance on average fibre diameter for SF_{10} (green bars) and SF_{12} (blue bars). Results displayed as mean $\pm SD$ (n = 100 fibres). Different letters show statistical differences ($p<0.05$) between SF_{10} and SF_{12} for each set of electrospinning parameters.

2.3.2 Physicochemical characterisation of non-woven needle electrospun silk fibroin mats

2.3.2.1 Chemical characterisation

The effects of EtOH- and MeOH-induced crosslinking on SF electrospun mats were measured using FTIR spectroscopy. FTIR spectra are interpreted as the vibrations of structural repeat units in a polymer. In proteins, these repeat units induce nine characteristic IR bands referred to as the amide A, B and I-VII, which give information on the secondary structure of the protein (Kong and Yu, 2007). The main peaks of interest in silk fibroin are present in amides I, II, III and somewhat in the V and VI bands (**Figure 16A**). The Amide I band is the most sensitive to protein secondary structure (1600-1700 cm^{-1}), which corresponds to C=O stretching vibration (Koperska *et al*., 2014) and is often used for quantitative analysis of protein crystallinity. The Amide II (1500-1600 cm^{-1}) and Amide III (1200-1300 cm^{-1}) bands, which both correspond to C-N stretching and N-H bending vibrations, are also important indicators for protein secondary structure. The Amide V (600-700 cm^{-1}) and Amide VI (490-590 cm^{-1}) are thought to correspond to the out-of-plane N-H and C=O bending, respectively, of the -CONH peptide backbone (Wang *et al*., 2005; El Khoury *et al*., 2011; Qu *et al*., 2018). The Amides A (3300 cm^{-1}) and B (3100 cm^{-1}) corresponding to N-H stretching (Naskar *et al*., 2019), IV (700-800 cm^{-1}) relating to -OCN bending, and VII (<250 cm^{-1}), representing out-of-plane skeletal torsions, are considered less sensitive to structural conformations in silk fibroin (El Khoury *et al*., 2011; Kong and Yu, 2007; Liu *et*

al., 2022). The changes in peak positions (wavenumber) or intensities (transmittance or absorbance) help interpret conformational changes between samples qualitatively and quantitatively. In this study, the overall conformational transitions between untreated (SF_{12}-U) and EtOH-treated silk fibroin (SF_{12}-E) and between SF_{12}-U and MeOH-treated silk fibroin (SF_{12}-M) treated silk fibroin non-woven mats were qualitatively interpretated by comparing peak locations in the normalised spectra of the samples and comparing these to their corresponding protein secondary structure conformations (**Table 5**).

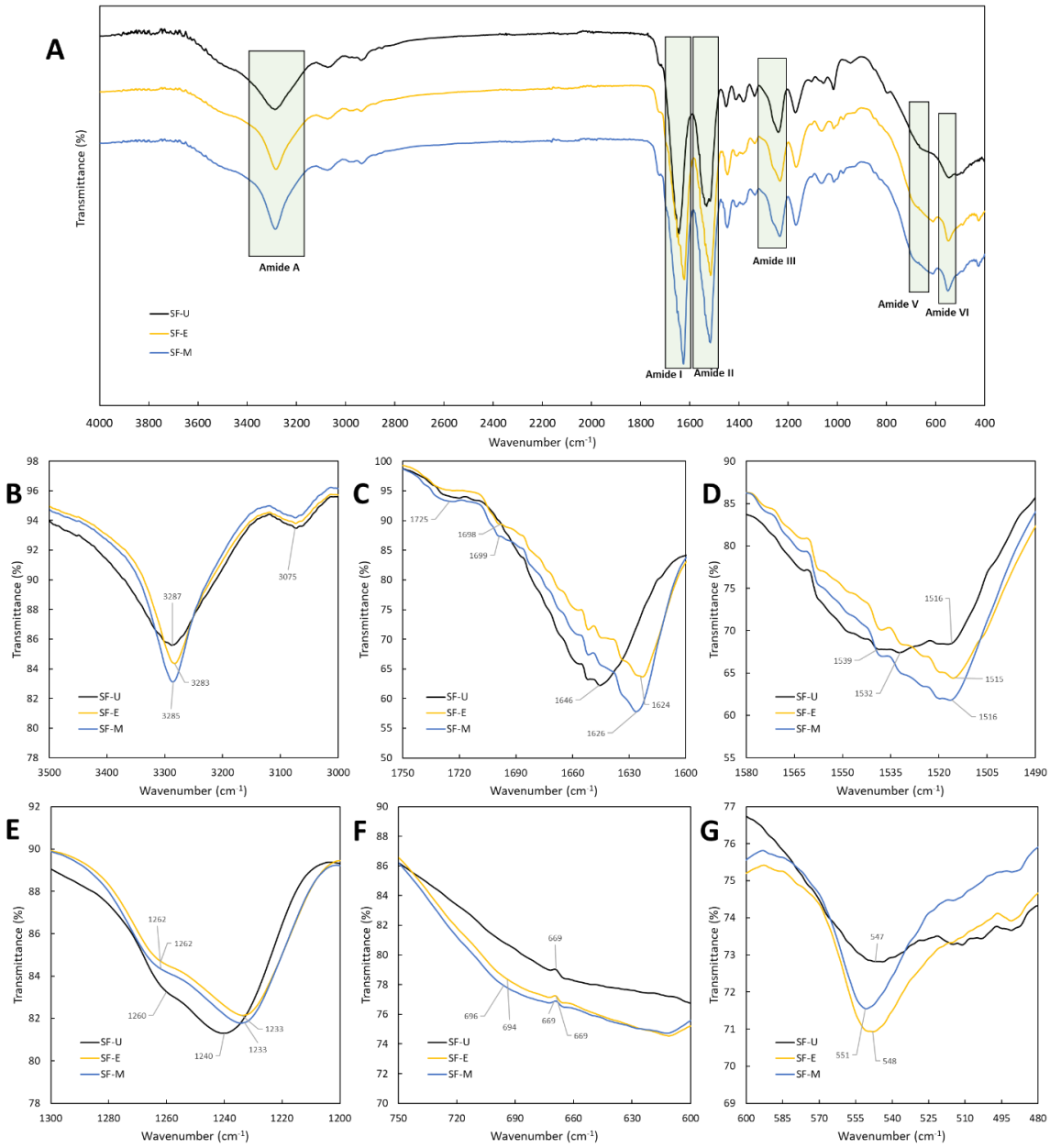

Figure 16: FTIR Spectra of needle electrospun silk fibroin, before (SF_{12}-U) and after treatment with EtOH (SF_{12}-E) and MeOH (SF_{12}-M). (A) Whole FTIR spectra with the bands of interest highlighted in green. Close ups of: amide A (B); amide I (C); amide II (D); amide III (E); amide V (F); and amide VI (G).

Major differences were observed in the form of band shifts between untreated SF_{12}-U and EtOH- or MeOH-treated SF_{12}-E and SF_{12}-M, respectively (**Figure 16B-G**). A broad band was observed at 3287 cm^{-1} for SF_{12}-U corresponding to the N-H stretching of secondary amides (**Figure 16B**). The band was intensified and narrowed for SF_{12}-E and SF_{12}-M (3283 and 3285 cm^{-1}). This intensification may be caused by the -OH stretching of bound alcohols following treatment. A smaller second band, corresponding to Amide B, was spotted at 3075 cm^{-1} in SF_{12}-U, but there was no shift or increase in intensity for SF_{12}-E or SF_{12}-M. In the amide I (**Figure 16C**), a substantial shift occurred from 1646 cm^{-1} (random coils) in SF_{12}-U, to 1624 cm^{-1} and 1626 cm^{-1} (β-sheets) in SF_{12}-E and SF_{12}-M, respectively. In addition, a small peak at 1698 cm^{-1} and 1699 cm^{-1} in SF_{12}-E and SF_{12}-M corresponding to inter-molecular β-sheets, was absent in SF_{12}-U. In the amide II (**Figure 16D**), a broad band of two peaks at 1539 cm^{-1} (random coils) and 1516 cm^{-1} (tyrosine) in SF_{12}-U was replaced by a single and more intense narrow band at 1515 cm^{-1} and 1516 cm^{-1} (tyrosine) in SF_{12}-E and SF_{12}-M. As tyrosine (Tyr) is an essential amino acid in the assembly of β-sheets, several studies have linked the Tyr absorption peak at 1515 cm^{-1} as a marker for β-sheets (Asakura *et al*., 2004; Xue *et al*., 2020). There was also a marked reduction in the 1530-1560 cm^{-1} band in SF_{12}-M and SF_{12}-E corresponding to a reduction in irregular structures (*e.g.* α-helices, β-turns and random coils) and a rearrangement into β-sheets (Puerta *et al*., 2019). In the Amide III (**Figure 16E**), a shift from 1240 cm^{-1} in SF_{12}-U to 1233 cm^{-1} in both SF_{12}-E and SF_{12}-M showed another conformational shift from random coils to β-sheets. Moreover, the reduction in intensity of the band from 1240 to 1260 cm^{-1} in both SF_{12}-E and SF_{12}-M showed a marked reduction of random coils. In the Amide V (**Figure 16F**), the whole band spanning 600-700 cm^{-1} was intensified in SF_{12}-E and SF_{12}-M. The ranges spanning 670-700 cm^{-1} and 650-667 cm^{-1} showed an increase in β-sheets and random coils respectively, while the inverted peak at 669 cm^{-1} corresponded to α-helices. Finally, in the Amide VI (**Figure 16G**), which has yet to be studied in silk fibroin and is therefore a less reliable indicator of conformational transitions, no difference was observed between SF_{12}-U at 547 cm^{-1}, thought to correspond to both random coils and β-sheets, and SF_{12}-E and SF_{12}-M at 548 cm^{-1} and 551 cm^{-1} (El Khoury et al., 2011).

Although EtOH and MeOH significantly affected the conformational state of electrospun silk fibroin, the absence of ethanol characteristic peaks at 1088/1046 cm^{-1} (C-O stretching) and 880 cm^{-1} (C-O-C stretching) in SF_{12}-E and methanol characteristic peaks at 1118/1021 cm^{-1} (C-O stretching) in SF_{12}-M, indicate that neither EtOH nor MeOH remain in silk fibroin following treatment (see ***Appendix A***, ***Figure S2***). This is expected as both EtOH and MeOH are physical crosslinkers of silk fibroin and therefore do not covalently bond to the protein chains (Kaewpirom and Boonsang, 2020).

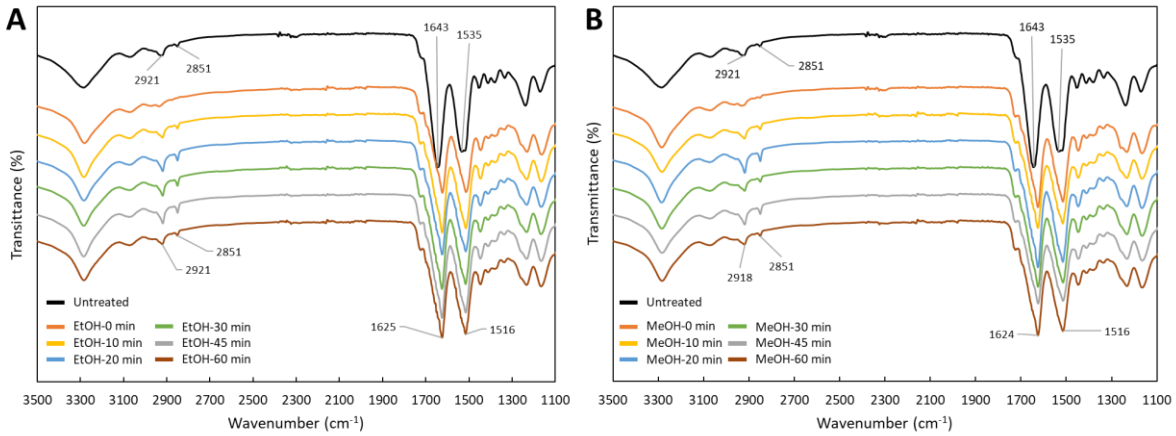

Figure 17: Effects of (A) EtOH and (B) MeOH immersion time on the chemical structure of electrospun silk fibroin fibres.

Figure 17 shows the effects of immersion time in EtOH or MeOH on the chemical structure of the silk fibroin electrospun fibres. Interestingly, EtOH- and MeOH-induced structural changes occurred within seconds of the mats being immersed, causing the fibroin to shift from Silk I to Silk II conformations. Peaks at 2921 cm^{-1} and 2851 cm^{-1}, corresponding to C-H stretching vibrations of aliphatic functional groups, slightly increased in intensity following immersion in both EtOH and MeOH. This could have resulted from the aggregation of aliphatic amino acids such as alanine and glycine responsible for the formation of β-sheets. To further quantify the effects of alcohol treatment on electrospun silk fibroin mats, second derivative analysis and spectral decomposition of the amide I band was carried out (see ***Appendix A, Figures S3, S4, S5***). As shown in **Figure 18A**, the total β-sheet content rose from 46% in SF_{12}-U to 53% in SF_{12}-E and 53% SF_{12}-M the moment the silk fibroin mats came into contact with the alcohol solutions. Moreover, the proportion of inter-molecular β-sheets increased considerably from 16% in SF_{12}-U to 62% in SF_{12}-E and 58% in SF_{12}-M indicating a transition from intra-molecular parallel β-sheets to inter-molecular antiparallel β-sheets, a hallmark of the Silk II conformational state. Interestingly, increasing the alcohol-treatment time had no effect on the composition of the crystalline structure of silk fibroin up to 1 h of immersion in 99.8% EtOH or MeOH. These results align well with the literature. Wei *et al*. (2011) showed that crystallinity in silk fibroin β-sheets increased rapidly upon immersion in EtOH, although they reported that crystallinity continued to increase up to 30 min of immersion (Wei *et al*., 2011). In addition, Puerta *et al*. (2020) showed no significant changes to β-sheet crystallinity beyond 15 min of immersion in EtOH, however they did note an increase in β-sheets from 15 min to 60 min of immersion in MeOH (Puerta *et al*., 2020).

To investigate the effects of different alcohol concentrations on protein crystallinity, silk fibroin was immersed in successively decreasing concentrations of EtOH and MeOH. As shown in **Figure 18B**, no difference in crystallinity was observed when decreasing the EtOH concentration to 70% (v/v), however decreasing the concentration of MeOH led to an increase in β-sheets from 50% in 99.8%

MeOH to 62% in 70% MeOH. In addition, when immersed in 70% MeOH, a strong decrease in random coils from 30% to 21%, was accompanied by a change in β-sheet composition, with a share intra-molecular β-sheets of total β-sheets rising from 43% to 54%, indicating a transition from random coils to intra-molecular β-sheets and therefore increasing in silk fibroin crystallinity. It is suggested that water plays an important role in the formation of β-sheets and that using lower concentrated alcohol solutions enhances silk fibroin crystallinity. Terada *et al*. (2016) showed that using lower concentrated alcohol solutions increased alcohol diffusion in silk fibroin films, enabling a more rapid crosslinking effect but also causing fibres to swell more noticeably. In fact, when silk fibroin films were immersed in highly concentrated alcohols (>95% (v/v)) fibre morphology was less impacted than when immersed in lower concentrated alcohols (<80% (v/v)) which caused the fibres to swell and fuse (Terada et al., 2016).

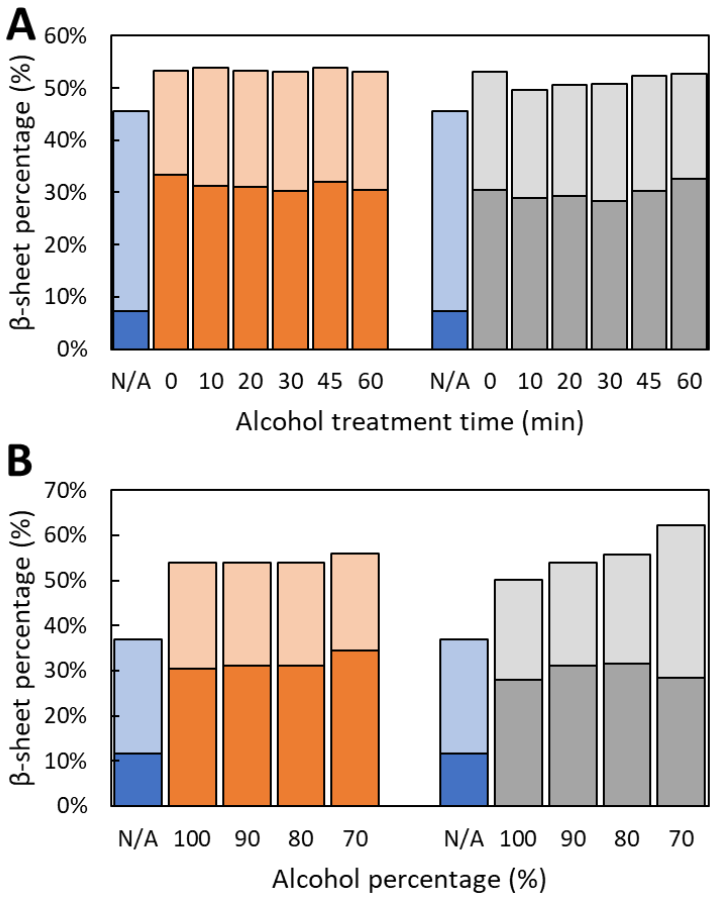

Figure 18: Effects of (A) alcohol-treatment time and (B) alcohol percentage on β-sheet crystallinity (whole bar), intermolecular β-sheets (dark) and intramolecular β-sheets (light). Untreated samples are blue (labelled N/A), EtOH-treated are orange and MeOH-treated electrospun samples are grey.

Overall, analysis of the secondary structure of electrospun silk fibroin mats demonstrated a consistent transition from Silk I to Silk II conformations following immersion in EtOH or MeOH solutions, as a result of structural shifts, causing amorphous structures composed of random coils and β-turns to

form densely packed ordered anti-parallel β-sheets (Nguyen *et al*., 2019), thereby increasing crystallinity.

It is worth noting that a peak at 1725 cm^{-1} (**Figure 16C**), identified as the C=O bond of formic acid, was present in all electrospun samples (Biagiotti *et al*., 2022), indicating that traces of formic acid remained within the electrospun fibres. Biagiotti *et al*. (2022) studied the effects of formic acid on cell culture and quantified its toxicity when present in electrospun silk fibroin mats. Using Head-Space Gas Chromatography/Mass Spectrometry, the team measured approximately 250 µmol of formic acid per gram of silk fibroin, which represents about 1 µL or 1.2 mg per gram of silk fibroin. With a tolerable exposure of 65.4 mg/day (Biagiotti *et al*., 2022) and assuming a 10% scaffold to cultivated meat ratio (Sinke *et al*., 2023), a person would only be able to eat around 54 g of cultivated meat per day. However, as formic acid rapidly dissociates into formate anions in aqueous solutions at neutral pH or bodily fluids, it can be asserted that any trace of formic acid would be removed during cell culture, and therefore there should be no concern for human health (Biagiotti *et al*., 2022). In addition, formic acid, which has GRAS status, has widely been used in the food industry for packaging and food preservation due its antimicrobial effects (Yadav *et al*., 2021). Therefore, the use of formic acid in the processing of cultivated meat scaffolds should neither pose health and safety risks nor cause concerns during regulatory approval.

2.3.2.2 SEM morphology and porosity

Fibre morphology and overall surface topography plays a major role in scaffold functionality, and has been shown to affect the attachment, migration, proliferation and differentiation of mesenchymal stem cells (Jenkins and Little, 2019; Molina *et al*., 2020). SEM was employed to visualise the effects of EtOH and MeOH treatment on electrospun silk fibroin fibres (**Figure 19**). The untreated SF_{12}-U fibres displayed thin (98 ± 33 nm), straight and randomly aligned nanofibers with occasional defects (mostly beads). However, following EtOH and MeOH treatments, stabilisation caused the electrospun fibres to swell and flatten, significantly increasing the thickness of the fibres to 166 ± 44 nm and 160 ± 55 nm (p<0.05), respectively. The fibre swelling also led to a noticeable reduction in voidage which was further confirmed by measuring scaffold porosity (**Figure 20A**). While the untreated electrospun SF_{12}-U scaffolds were highly porous structures with 82 ± 1.7% porosity, stabilisation resulted in a reduction of the porosity to 51 ± 2.2% in SF_{12}-E and 52 ± 0.3% in SF_{12}-M (n=5).

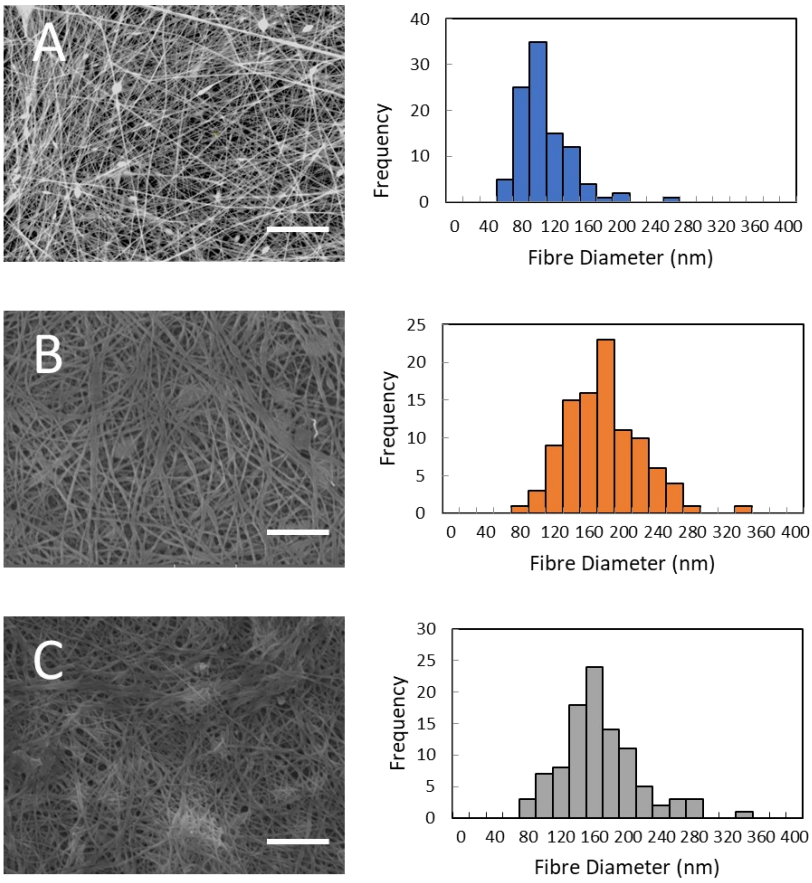

Figure 19: SEM images (left) and fibre distribution (right; n=100) of needle electrospun non-woven silk fibroin mats (A) untreated (SF_{12}-U), (B) after EtOH-treatment (SF_{12}-E) or (C) after MeOH-treatment (SF_{12}-M). Scale bars: 5 µm.

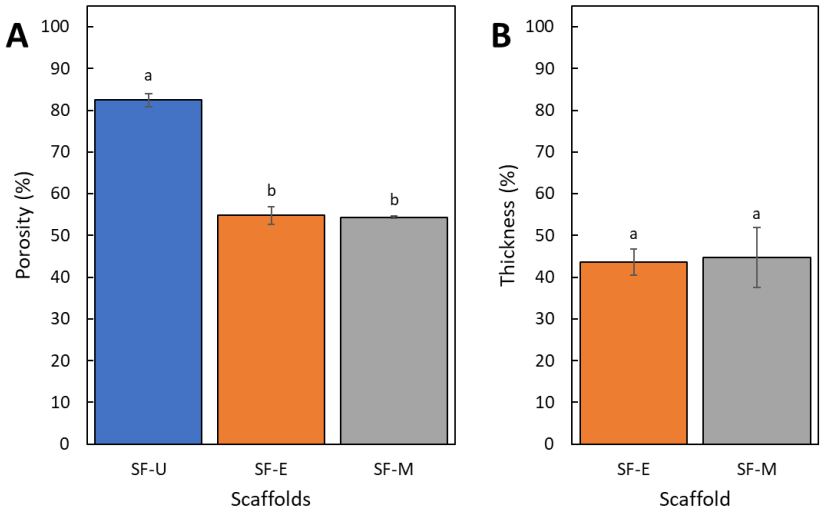

Figure 20: Effects of MeOH and EtOH stabilisation on silk fibroin electrospun mat (A) porosity and (B) thickness (n=5). Different letters show statistical differences between samples ($p<0.05$).

EtOH- and MeOH-treatment also caused visible damage to the electrospun mats, causing them to fold onto themselves and tear during the drying process. This effect was markedly reduced when immersing the electrospun mats on a layer of non-stick foil. At the end of the immersion time, the

alcohol solution was removed, and the samples were left to air dry flat on the foil under a laminar flow. As the fibres dried, the samples gently detached from the foil layer conserving their macroscopic morphology and size in the x- and y-axis, although a significant reduction in scaffold thickness was observed in the z-axis (**Figure 20B**). As such, electrospun mats stabilised with EtOH- and MeOH-treatment shrank by 56.4 ± 3.1% and 55.4 ± 7.2%, respectively, in thickness.

2.3.2.3 Solubility

As scaffolds used for cell culture are typically exposed to aqueous environments for long periods of time, the effects of EtOH and MeOH stabilisation on the ability of the silk fibroin scaffolds to remain intact under those conditions was measured over a period of 2 weeks. As shown in **Figure 21**, the untreated samples lost 55% of their weight within 1 min of contact with water, followed by a steady decrease until they stabilised at 20% of their original weight after 30 min. Upon 72 h of immersion, however, the SF_{12}-U mats started regaining part of their lost weight, reaching 70% of their original weight after 2 weeks of immersion. In contrast, both the SF_{12}-E and SF_{12}-M mats retained >85% of their weight over the whole time period, due to their higher densities of Silk II conformations.

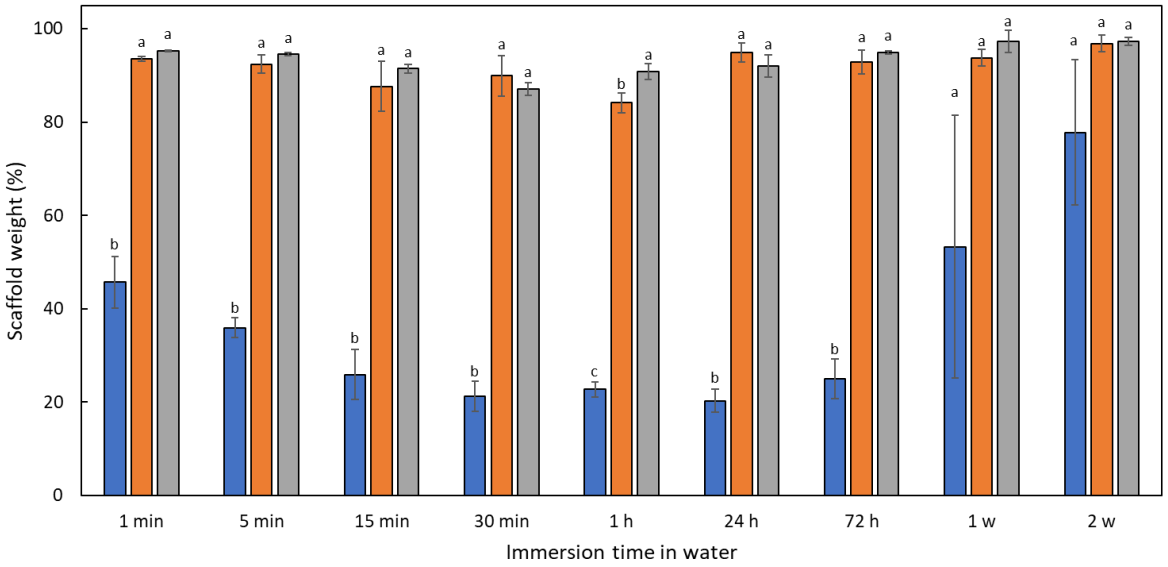

Figure 21: Solubility of untreated (blue) and EtOH- (orange) or MeOH- (grey) stabilised electrospun silk fibroin mats following immersion in water for different time intervals. Data shown as mean ± SD (n=3). Different lower-case letters show statistical differences ($p<0.05$) between SF_{12}-U, SF_{12}-E and SF_{12}-M at each time interval.

It has been shown that polar solvents promote the aggregation of hydrophobic amino acids (such as glycine and alanine, which are the main amino acids in silk fibroin's heavy chains) to form the β-sheet crystallites. In turn, the stable intramolecular bonds of the anti-parallel β-sheets reinforce the hydrophobicity of the protein heavy chains and reduce solubility in water (Cheng *et al*., 2014; Nguyen *et al*., 2019). It is also worth mentioning that water acts as a plasticising agent that increases chain

motility in silk fibroin and can also induce conformational transitions without needing organic solvents (Terada et al., 2016). This process, called water annealing, is often performed with water in a vacuum (Hu *et al*., 2011; Marelli *et al*., 2016; Jaramillo-Quiceno & Restrepo-Osorio, 2019) but could occur in liquid form (Lu, *et al*., 2010). Rather than fully dissolving, after longer periods of time, the aggregation of chains and swelling of amorphous regions could give rise to silk fibroin hydrogels. This would explain the increase in weight of the untreated SF_{12}-U samples beyond 72 h immersion time. Additionally, Lu *et al*. (2010) showed that films with predominantly Silk I conformations could be made insoluble in water with longer drying times exceeding 12 h (Lu *et al*., 2010). This could also be the case for the alcohol treated supports, but due to their predominantly Silk II form, the amount hydrogel would likely be much lower. Although SF_{12}-U never fully dissolved in water, the considerable loss of material and collapse of the scaffold structure made the untreated scaffolds unusable for cell culture-based applications, and so the alcohol treatment was deemed necessary to stabilise the scaffolds prior to their use in the aqueous cell culture environment.

2.3.2.4 Tensile Properties

Tensile testing of silk fibroin electrospun scaffolds was performed to investigate whether the material could tolerate the high shear environment of a stirred tank reactor and promote cellular mechanotransduction without adversely affecting the edibility of the final product. As shown in **Figure 22,** untreated SF_{12}-U mats displayed relatively low stiffness (103.3 ± 18.4 MPa) and ultimate tensile strength (2.4 ± 0.5 MPa), which increased significantly when treated with EtOH (400.0 ± 111.7 MPa stiffness and 11.7 ± 1.9 MPa strength) and with MeOH (441.6 ± 128.7 MPa stiffness and 13.4 ± 4.4 MPa strength) (p<0.05). Inversely, SF_{12}-U scaffolds had the highest yield strain (>26.8%), with most samples reaching the maximum displacement limit without breaking, and this decreased significantly (p<0.05) with EtOH- (6.4 ± 1.6%) and MeOH-treatment (5.5 ± 1.4%). Finally, the shear modulus increased from 62.7% in SF_{12}-U to 376.1 MPa in SF_{12}-E and to 400.0 MPa in SF_{12}-E, although it is worth noting that these values far exceeded the maximal sheer stresses encountered in stir tank bioreactors (< 1 kPa; Wang *et al*., 2022). No significant differences (p>0.05) were identified between the effects of EtOH- or MeOH-treatment on any of the measured mechanical properties due to the relatively high variance between samples. Moreover, following alcohol stabilisation, the frequent appearance of defects in the macrostructure of the materials (such as undulations, ripples, and occasional minor tears) had an impact on their failure mechanism and, in turn, the reproducibility of the test. Despite this, the values and trends were consistent with those reported in the literature (Amiraliyan *et al*., 2010; Allardyce *et al*., 2015; Johari et al., 2020) and confirm that EtOH- and MeOH-stabilisation causes silk fibroin fibres to transition from a highly elastic to brittle state as the protein crystallises.

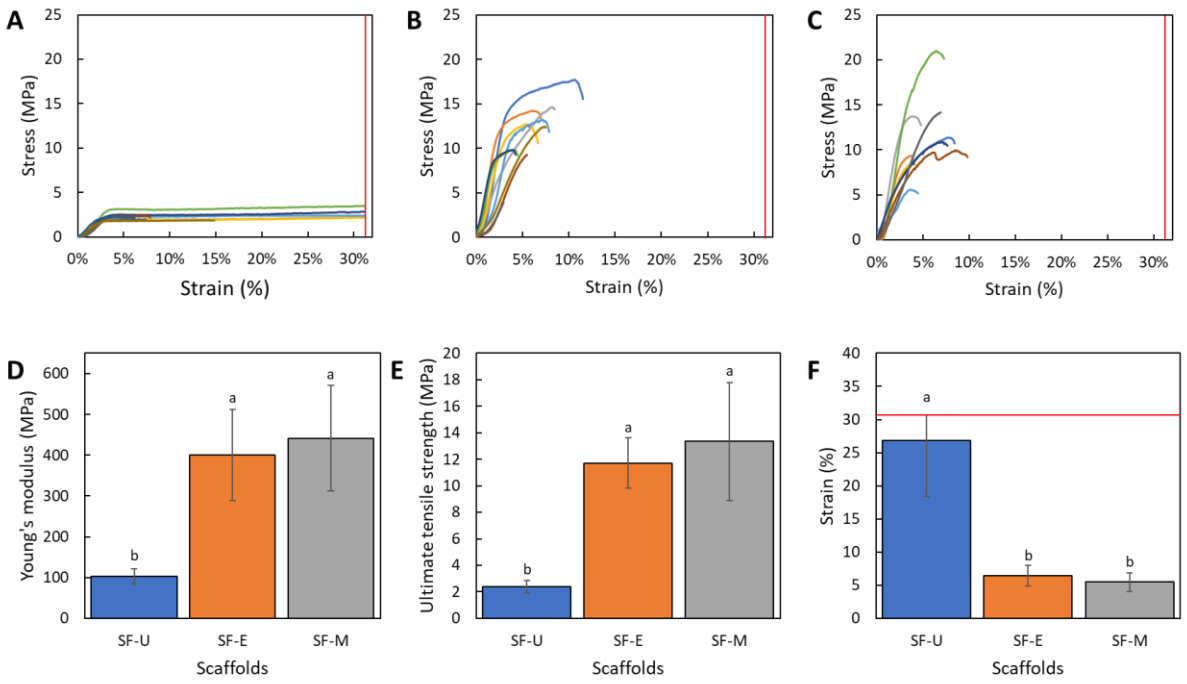

Figure 22: Stress-strain curves of (A) SF_{12}-U, (B) SF_{12}-E, (C) SF_{12}-M, and average (D) Young's modulus, (E) ultimate tensile strength and (F) yield strain of untreated and EtOH- and MeOH- stabilised electrospun silk fibroin non-woven mats. Data shown as mean ± SD ($n \geq 8$) Different lower-case letters show statistical differences ($p<0.05$) between samples.

In vivo, the stiffness (Young's modulus) of the ECM plays an important role in cell development and fate. The process of mechanotransduction stiffens the ECM to promote stem cell differentiation into the desired cell lineages (D'Angelo *et al*., 2011; Kim *et al*., 2021). It has been shown that softer tissues, such as fat and muscle, differentiate better on flexible surfaces (0.1-10 kPa), while harder tissues, such as bone, prefer stiffer conditions (>30 kPa) (Lv *et al*., 2015). Designing scaffolds to mimic the stiffness of the ECM can strongly improve cell differentiation (Engler *et al*., 2006), although specific media formulations can drive differentiation on materials with non-optimal stiffness using molecular cues (Park *et al*., 2011). In the context of cultivated meat, where media components are known to be one of the main drivers of cost (O'Neill *et al*., 2021; Venkatesan *et al*., 2022), the ability to promote differentiation through physical means by tuning the stiffness of scaffolds rather than using molecular cues, could be a more economic option. The extremely high stiffness (approximately 400 MPa) of alcohol-treated silk fibroin electrospun surfaces could be reduced by blending silk fibroin with softer biomaterials, such as plant-based gums (Eslami *et al*., 2021). Furthermore, although such high stiffness could be assumed to negatively impact the sensory properties and mouthfeel of the final product (Paredes *et al*., 2022), reducing the microcarrier dimensions might overcome this limitation, due to the smaller scaffold to meat ratio. It is worth noting that commercially available microcarriers, such as Cytodex-1, have much lower elastic modulus (50 kPa), which nevertheless is still better suited for hard tissue formation (Norris et al., 2022). Finally, it is not known how the high temperatures used during cooking would further influence the stiffness of the scaffold component of the cultivated meat

product. Silk fibroin has been reported to be thermally stable up to 260-280 °C (Hashimoto et al., 2020; Zhao, *et al*. 2021), above which the secondary structures in the protein break down, impacting its mechanical properties. However, such temperatures would not be attained during normal cooking.

2.3.3 Sterilisation of electrospun silk fibroin mats

As with any material used for tissue culture purposes, it is essential that electrospun mats are sterilised before coming into contact with cells. Several methods, including physical (*e.g*. heat, plasma and irradiation) and chemical (ethylene oxide, ethanol, acids) have previously been used for the sterilisation of silk fibroin nanofibres (Rnjack-Kovacina *et al*., 2015; Dai *et al.*, 2016). However, to avoid the accumulation of toxic residues and prevent further conformational changes to the silk fibroin protein, only heat treatments were investigated in this study. As such, electrospun mats were either sterilised using dry heat (160 °C for 30 min) in a convection oven or moist heat (steam under pressure - 121 °C for 20 min) in an autoclave.

As shown in **Figure 23**, FTIR was used to measure chemical and conformational changes to SF_{12}-E and SF_{12}-M mats following heat sterilisation treatments. Interestingly, both oven-sterilisation and autoclaving had no impact on the silk fibroin conformational structure. However, autoclaving caused a noticeable decrease in intensity at 1733 cm^{-1} and at 1165 cm^{-1}, corresponding to C=O and C-O stretching vibrations of formic acid residues in the electrospun fibres (***Appendix A***, ***Figure S6***). As autoclaving appeared to reduce formic acid residues, it was adopted as the preferred heat sterilisation method for all subsequent experiments.

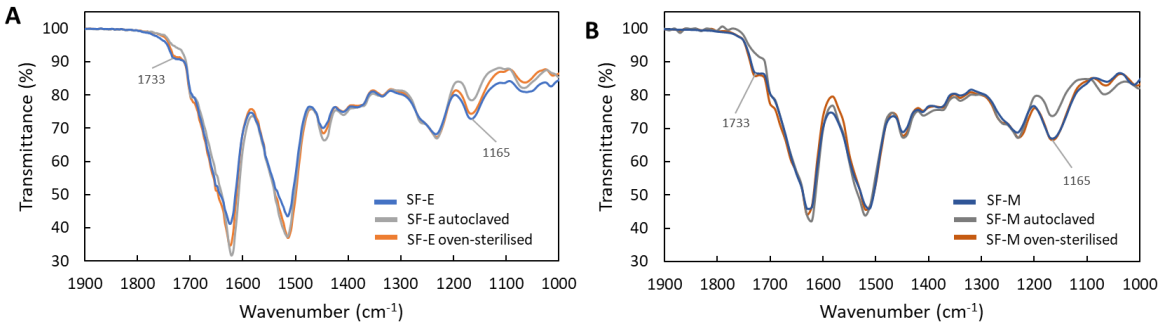

Figure 23: FTIR spectra of (A) SF-M samples before and after sterilisation using dry heat at 160 °C for 30 min (top) or autoclaving at 121 °C for 20 min (bottom), (B) SF-M samples before and after UV sterilisation for 8h.

It should be noted that there are limitations to heat sterilisation as high temperatures can denature certain proteins. While the silk fibroin protein is stable up to temperatures of 260-280 °C (Hashimoto et al., 2020; Zhao *et al*. 2021), most ECM proteins denature at much lower temperatures (Latorre and Velazquez, 2021), making dry heating and autoclaving unsuitable for scaffolds functionalised with ECM proteins (Tao et al., 2021). Other methods which do not denature proteins, such as ethylene oxide

(EtO) and hydrogen peroxide (H_2O_2) gas plasma can be used to sterilise electrospun fibres (Dai *et al.*, 2016). However, the toxic residues that remain for some time after sterilisation limit the practicality of these methods for use with edible products

2.4 Conclusion

Non-woven silk fibroin mats were successfully electrospun using needle electrospinning and commercially available silk fibroin. The polymer concentration as well as the electrospinning operating parameters, voltage, collector distance and flowrate, were optimised to produce straight, uniform and relatively thick (142 ± 47 nm), randomly aligned nanofibres with a degree of consistency. The electrospun mats were then treated with monohydric alcohols (EtOH and MeOH) to induce conformational changes in the secondary structure of the silk fibroin protein. The effects of alcohol treatment were investigated and fully characterised in terms of chemical, morphological, and mechanical properties. FTIR analysis of the amide I, II, and III showed systematic conformational transitions from dominant Silk I to Silk II conformations following alcohol treatments. Consequently, the conformational transition from hydrophilic Silk I conformations to hydrophobic β-sheets resulted in the near insolubisation of silk fibroin mats in water, allowing the use of electrospun silk fibroin scaffolds in aqueous environments for up to 2 weeks. This is more than sufficient for the expected time needed for expansion (four days) and myogenic differentiation (seven days) of bovine mesenchymal stem cells (bMSC) to produce cultivated meat (Moutsatsou *et al.*, 2023). Stabilisation also affected fibre and scaffold morphology, significantly increasing fibre diameter from 98 ± 33 nm in SF_{12}-U to 166 ± 44 nm in SF_{12}-E and 160 ± 55 nm in SF_{12}-M, due to fibre swelling and flattening, which also resulted in a loss of porosity of 33.5% in SF_{12}-E and of 34.0% in SF_{12}-M and thickness of 56.4 ± 3.1% in SF_{12}-E and of 55.4 ± 7.2% SF_{12}-M. Nevertheless, the scaffolds retained an overall nanofibrous and interconnected microporous architecture. The transitions from irregular conformations to highly stable and ordered β-sheets also resulted in a strong decrease in material ductility. Tensile testing revealed average stiffnesses of 400.0 ± 111.7 MPa and 441.6 ± 128.7 MPa for EtOH- and MeOH-treated silk fibroin non-woven mats, respectively, more than 4 orders of magnitude higher than the values recommended for soft tissue differentiation (Lv *et al.*, 2015). Despite this, modifications in media formulation, polymer composition, scaffold geometry and surface chemistry could still promote stem cell differentiation on stiff surfaces (Park *et al.*, 2011; Sionkowska, 2011; Derakhti *et al.*, 2019). No significant differences were detected between the effects of 20 min treatments in 99.8% EtOH or 99.8% MeOH on protein crystallinity, solubility, fibre and scaffold morphology and mechanical properties. However, the presence of MeOH in food production could be concerning due to its high toxicity when ingested (Nekoukar *et al.*, 2021). Although it would be unlikely to remain in the

cultivated meat product, and it is authorised for use in food preparation in the US and EU (Pharmco, 2018), little is known about the frequent ingestion of trace amounts (COT, 2011) or its acceptability to consumers (van der Vossen-Wiljmenga *et al*., 2022). These food safety concerns make EtOH the preferred alcohol for the preparation and stabilisation of electrospun silk fibroin scaffolds for cultivated meat production. EtOH immersion will remain the default stabilisation method for all subsequent experiments in this thesis.

Overall, electrospun silk fibroin non-woven mats showed promise as scaffolds for cultivated meat, owing to their compatibility with the tissue engineering bioprocess and ECM-mimicking structure. However, the high cost of commercial silk fibroin (£325/g) and slow productivity rate of needle electrospinning (0.024 g/h at 0.2 mL/h) make this proof-of-concept unscalable productively and financially. To develop electrospun silk fibroin non-woven mats at scale, cheap sources of renewable silk fibroin should be investigated, including degumming strategies of farmed *Bombyx mori* silk cocoons and the production of recombinant silk fibroin at scale. In addition, fibre productivity could be increased using scalable electrospinning methods including multi-needle and needleless electrospinning platforms. Chapter III will focus on the scalability of electrospun scaffolds production and first steps towards using them for expansion of bMSCs.

CHAPTER III

Evaluation of electrospinning methods and silk fibroin sources on bovine mesenchymal stem cell 2D culture

3.1 Introduction

Silk fibroin was selected as a promising material with which to electrospin edible supports for cultivated meat production. However, the high price of the material, which is only available commercially as a costly pharmaceutical grade protein, prevents scalability. It was therefore necessary to find an alternative source. Silk fibroin is typically obtained by degumming the silk of domesticated *Bombyx mori* cocoons, produced by silkworms during their pupal life stage (Blossman-Myer & Burggren, 2010), to remove fats, ash and the outer sericin protein that envelopes the silk fibroin fibres (Nguyen *et al*., 2019). The resulting silk fibroin fibres are then dissolved and dialysed to obtain the final regenerated silk fibroin film used to prepare the electrospinning polymer solution (Nguyen *et al*., 2019). The temperature, chemicals and other parameters used during the degumming and regeneration process have been shown to significantly affect the properties of the silk fibroin (Allardyce *et al*., 2015; Zhao *et al*., 2018; Carassimi *et al*., 2019; Zhao *et al*., 2021). Moreover, while many degumming strategies have been developed to prioritise either the degumming efficiency (using proteases, alkali or acidic solutions) or ease of degumming (using hot water with Marseille soap), the food safety, associated costs and scalability of these strategies have not always been prioritised (Dou and Zuo, 2015; Feng *et al*., 2020; Liu *et al*., 2023). For example, silk fibroin is generally dissolved in 9.3 M lithium bromide which is known to be environmentally detrimental, expensive and toxic (Cheng *et al*., 2022). Nevertheless, research has shown that degumming silk fibroin with sodium carbonate and then regenerating it in a ternary solution of water, ethanol and calcium chloride provides a highly efficient, low cost and food-safe method for the extraction and purification of silk fibroin for electrospinning purposes (Ajisawa, 1998; Dou and Zuo, 2015; Cheng *et al*., 2022).

Another hurdle to scalability was the low productivity of the needle-electrospinning method. Although SF scaffolds were prepared and characterised with ease, their low reproducibility, due to changing ambient conditions, as well as the slow rate of fibre generation (0.01-0.02 g/h) made this method unsuitable for scaffold production at scale. It was therefore decided to adopt needleless electrospinning, which uses the electrohydrodynamic agitation of the polymer solution, rather than extrusion through a needle, to initiate the electrospinning process. This method has been shown to produce fibres at extremely high rates (up to 1000-fold increase compared to single needle setups) in controlled environments (Partheniadis *et al*., 2020; Omer *et al*., 2021).

Finally, it was important to select biomaterials that could promote the expansion and differentiation of stem cells. Mesenchymal stem cells (MSCs) are adult multipotent stem cells, capable of differentiation into myogenic and adipogenic lineages to produce muscle and fat, the main components of meat (Reiss *et al*., 2021). Thus, bovine mesenchymal stem cells (bMSCs) were selected for the cell culture.

This chapter covers the extraction and regeneration of silk fibroin from *B. mori* cocoons and compares it with its commercial counterpart. Then needleless electrospun mats using regenerated silk fibroin are produced[1] and characterised. Finally, bMSCs are seeded onto the resulting non-woven scaffolds to measure cytocompatibility and cell growth kinetics.

3.2 Materials and Methods

3.2.1 Materials

Bovine adipose-derived mesenchymal stem cells (bMSCs) were purchased from Quest Meat Ltd (UK) at passage 1. Ethanol (99.8%), calcium chloride (97%), sodium carbonate (≥99.5%), paraformaldehyde in PBS (4%), and formic acid (98+%) (Acros Organics) were purchased from Fisher Scientific (UK). Invitrogen™ LIVE/DEAD™ viability/cytotoxicity kit, Invitrogen™ PrestoBlue™ Cell Viability Reagent, Alpha-modified Eagle medium (α-MEM; Gibco™), Dulbecco's phosphate buffered saline (DPBS; Gibco™), penicillin-streptomycin (Gibco™), Trypan Blue solution 0.4% (Gibco™) and ultraglutamine (Gibco™) were purchased from Thermo Fisher Scientific. Trypsin-EDTA and foetal bovine serum (FBS) were obtained from Merck Life Science (UK). *Bombyx mori* silkworm cocoons (brand TMISHION) were

[1] *All needleless-electrospinning experiments were performed during a visit at the Technical University of Liberec (TUL; Czech Republic) and the electrospinners were operated by TUL researchers (Dr Miroslava Risová for DC electrospinning & Dr Jan Valtera for AC electrospinning). All characterisation and cell culture experiments were performed at Aston University.*

bought on Amazon (UK). Basic fibroblast growth factor (bFGF) was acquired from PeproTech (UK). Deionised water was used in all experiments unless otherwise stated.

3.2.2 Extraction of silk fibroin from raw silk, and subsequent degumming

Silk fibroin was extracted and purified by degumming *Bombyx mori* virgin silk of silk sericin and other impurities, following a protocol described by Polakova *et al*. (2022) with modifications to the concentration of sodium carbonate (Polakova *et al*., 2022). First, *B. mori* silk cocoons were cut into small pieces and soaked in water for 3 h to remove impurities. The cocoon pieces were then soaked in a 0.05% (w/v) sodium carbonate (Na_2CO_3) aqueous solution overnight to loosen and further wash the silk fibres. The cocoon pieces were then boiled in 0.2%, 0.5% or 5% (w/v) Na_2CO_3 for 30 min under constant stirring in a boiling flask. The fibres were then collected and washed thoroughly with diH_2O. The boiling and washing process was repeated two more times before the resulting degummed silk fibroin fibres were laid out to dry overnight at room temperature under a fume-hood. The following day, the degummed fibres were weighed to determine the degumming ratio and assess the degree of sericin removal. The degumming ratio (D_r(%)) was expressed as the percentage weight loss from silk following degumming, where W_0 represents the initial cocoon weight and W_1 represents the weight of degummed fibres (**Equation 15**).

$$D_r(\%) = \frac{W_0 - W_1}{W_0} \times 100 \tag{15}$$

The silk fibroin fibres were then regenerated by dissolving them in Ajisawa's solution, a solution consisting of $CaCl_2$:EtOH:diH_2O in a 1:2:8 molar ratio at 80 °C ± 3 °C for 1 h. The resulting solution was then dialysed against deionized water (diH_2O) using 14 kDa molecular weight cut-off cellulose membrane tubing (Merck Life Science, UK) with changes in the diH_2O every 15 min for the first 2 h, then twice daily for 3 days. The regenerated solution was poured into petri dishes and oven dried (SQ Oven-80HT, SciQuip, UK) at 40 °C for 72 h to cast silk fibroin films. These films were stored at room temperature, away from direct sunlight, until further use. The regeneration ratio ($R_r(\%)$) was expressed as the percentage weight loss between degumming and regeneration (W_2; **Equation 16**), and the final regeneration yield ($Y_f(\%)$) was calculated as the percentage of weight remaining between the initial cocoon weight and regeneration (**Equation 17**).

$$R_r(\%) = \frac{W_1 - W_2}{W_1} \times 100 \tag{16}$$

$$Y_f(\%) = 100 - \frac{W_0 - W_2}{W_0} \times 100 \tag{17}$$

The price of regenerated silk fibroin (P_{RSF}), excluding the negligible costs of processing and other reagents, was calculated as the price per gram of the cocoons (P_c = 0.91 GBP/g) divided by the final regeneration yield (**Equation 18**).

$$P_{RSF} = \frac{P_c}{Y_f(\%)} \quad (18)$$

Polymer solutions were prepared by dissolving the regenerated silk fibroin (RSF) films in formic acid to a final concentration of 12% (w/w) under magnetic stirring for 24 h at room temperature. The polymer solutions were stored at 4 °C and used within 72 h.

3.2.3 Needle Electrospinning

As in Chapter II, *section 2.2.2*, a benchtop needle-electrospinner was operated at 15 kV with a 10 cm collector distance. A 12% (w/w) regenerated silk fibroin in formic acid polymer solution was used with all needle electrospinning platforms. All needle electrospinning experiments were conducted at 20 ± 2 °C and 30 ± 2 %RH and polymer flowrate was adjusted to match the jet formation and solvent evaporation rate.

3.2.4 Needleless Electrospinning

A 12% (w/w) regenerated silk fibroin in formic acid polymer solution was also used with all needleless electrospinning platforms. All needleless electrospinning experiments were conducted at 20 ± 2 °C and 30 ± 2 %RH.

3.2.4.1 DC Electrospinning methods

Non-woven nanofibre mats were obtained using 12% (w/w) regenerated silk fibroin in formic acid and either a benchtop set up (**Figure 24A**) or a semi-industrial Nanospider™ NS1S500U device (Elmarco, Czechia; **Figure 24B**).

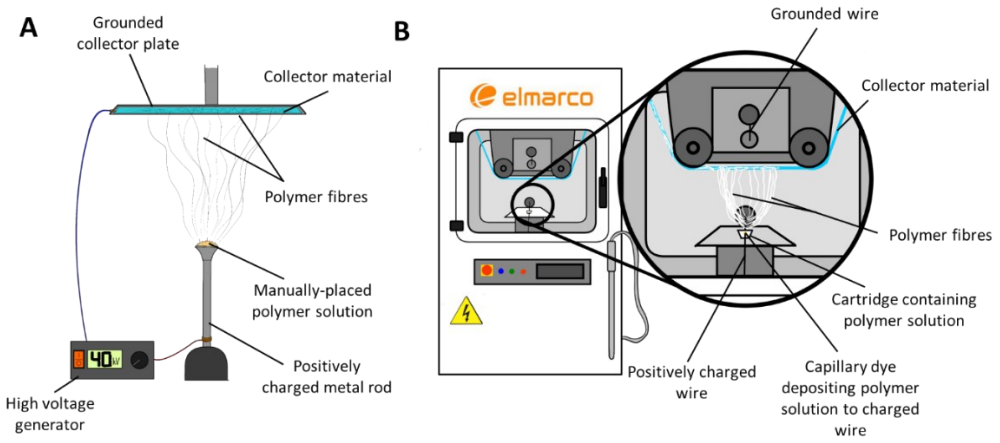

Figure 24: DC Needleless electrospinning setups. (A) Benchtop needleless electrospinner, (B) pilot-scale Nanospider™ NS1S500U (Elmarco, Czechia).

The benchtop setup consists of a flat-topped steel rod connected to a high voltage generator (40-55 kV), above, a silicone-coated paper was placed directly below a grounded collector plate (10-12 cm). To start the electrospinning process, a droplet of polymer solution was manually placed at the top of the rod using a Pasteur pipette. The voltage was then switched on and turned off up to 5 seconds later as most of the polymer solution was transferred towards the collector. The current was then switched off and the residual charge in the rod was removed using a discharge rod before the remaining polymer solution was wiped off. This process was repeated many times to generate non-woven electrospun mats.

The needle-free Nanospider™ technology relies on placing the polymer solution into a cartridge moving at high speed across a positively charged horizontal wire. Above which, a grounded (or negatively charged) wire runs parallel. A slowly moving spunbond fibrous support which collects the fibres is placed between the two wires. A capillary die at the cartridge-wire interface dispensed the polymer solution onto the charged wire while travelling back and forth on the wire, immediately initiating jet ejection and fibre formation. By passing rapidly from one end of the wire to the other, the polymer solution is constantly resupplied homogeneously in order to maximise the fibre output. All experiments using the Nanospider™ were carried out at 40 kV and with a 10 cm collector distance, whilst the temperature and relative humidity were controlled and maintained at 22 °C and 30%, respectively.

3.2.4.2 AC Electrospinning methods

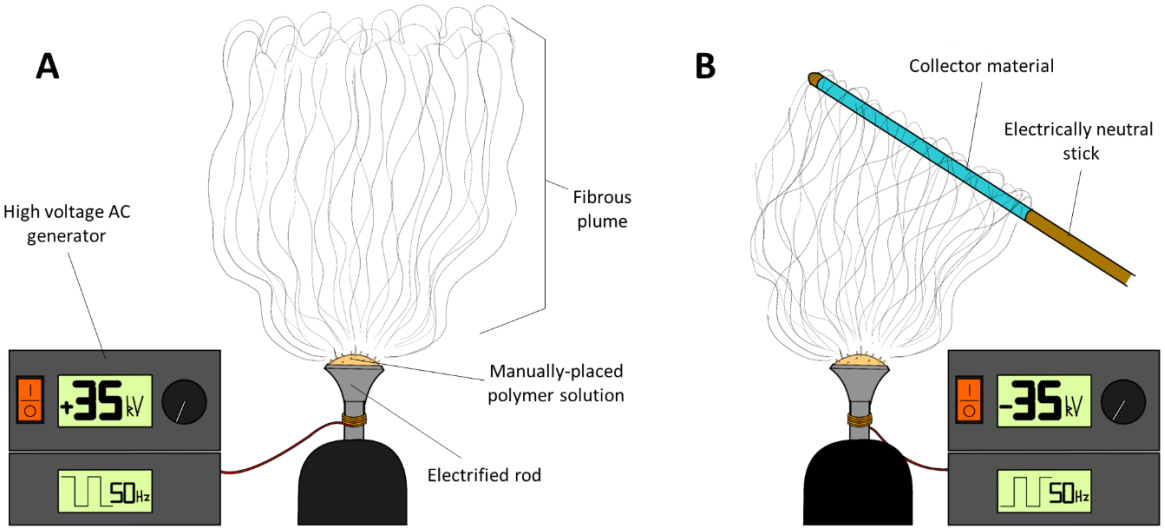

Figure 25: (A) Needleless AC electrospinning setup, (B) Fibre collection during needleless AC electrospinning process.

The AC needleless electrospinner (**Figure 25**) developed by TUL (Kocis *et al*., 2018) employs a rod-like electrode connected to an AC high voltage generator (35 kV, 50 Hz). Approximately, 0.5 mL of polymer solution was manually placed at the top of the 22 mm diameter rod emitter using a Pasteur pipette. As the current was switched on an ascending plume of fibres formed and stabilised mid-air. The fibres were then collected using an electrically neutral stick and deposited onto spunbond fabric.

3.2.5 Electrospun mat stabilisation

As in Chapter II, *section 2.2.3*, electrospun silk fibroin mats were treated by immersion in 99.8% EtOH for 20 min and then air dried under laminar flow.

3.2.6 Physicochemical characterisation of electrospun scaffolds

As in Chapter II, *section 2.2.4*, Fourier-transform infrared spectrometry (FTIR), scanning electron microscopy (SEM), tensile testing, and measurements of porosity and aqueous stability were conducted to characterise the regenerated silk fibroin mats produced by needle- (SF_{12}-U and SF_{12}-E) and needleless-electrospinning ($NLSF_{12}$-U, $NLSF_{12}$-E, NSF_{12}-U and NSF_{12}-E).

3.2.6.1 Static contact angle measurements

Films of 12% (w/w) regenerated silk fibroin in formic acid (RSF_{12}-U) were prepared. The RSF_{12}-U films were subsequently stabilised by immersion in 99.8% EtOH for 20 min (the same stabilisation treatment as used for electrospun fibres described in Chapter II, *section 2.2.3*) to produce EtOH-treated regenerated silk fibroin films (RSF_{12}-E). The surface wettability of RSF_{12}-U and RSF_{12}-E was measured

with a sessile drop method on a tensiometer (Theta Flex, Biolin Scientific, UK) with a built-in high-resolution camera and then analysed using OneAttension software. First, films were laid flat on the tensiometer platform and lined up with the camera to create a horizontal baseline across the sample. A 5 µL sessile drop of diH_2O was then automatically lowered onto the films and released from the pipette. The contact angles (left and right) were averaged to measure the surface wettability of the films 1 s after droplet release from the pipette tip (**Figure 26**).

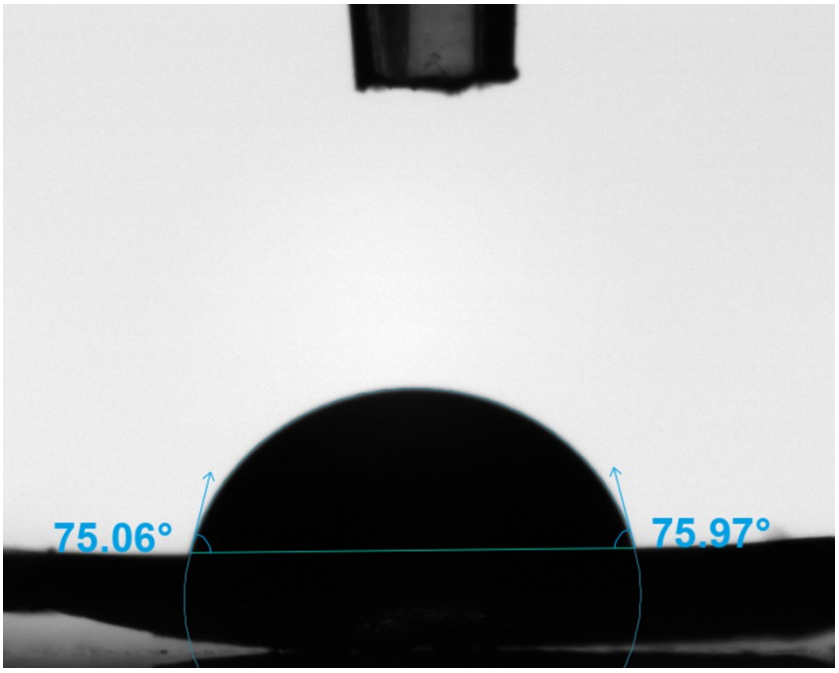

Figure 26: Photograph of a diH_2O sessile drop 1 s after release from the pipette tip (top) on the surface of an RSF_{12}-U film.

3.2.8 Biological characterisation

3.2.8.1 Cell culture in tissue culture flasks

Adipose-derived bovine mesenchymal stem cells (bMSCs) were thawed from cryopreservation at -180 °C in 10% (v/v) FBS in Dimethylsulfoxide (DMSO). bMSCs were then seeded at 1500 cells/cm^2 and cultured in tissue culture vessels in a growth medium comprising α-MEM supplemented with 2 mM UltraGlutamine, 10% (v/v) FBS, 1 ng/mL bFGF and 1% (v/v) penicillin-streptomycin. The cells were cultured in a humidified incubator at 37 °C, 5% CO_2 until they reached 80-90% confluency. Subculturing was carried out by adding 0.25% trypsin-EDTA and incubating for 5 min at 37 °C, 5% CO_2 until complete detachment. The trypsin-EDTA was then neutralised by adding more prewarmed growth medium at a 2:1 ratio. The cell suspension was then centrifuged at 200 *g* for 5 min following which the supernatant was discarded, and the cell pellet was resuspended in a 1 mL of growth medium.

To count cells, 10 µL of the cell suspension was first diluted in a 1:1 ratio with trypan blue, a dye that stains dead cells making it easier to visually differentiate between live and dead cells. 10 µL of the diluted solution was then injected into a haemocytometer used to count cells manually. To then estimate the live cell concentration in the original cell suspension ($C_{live\ cells}$; **Equation 19**), the average number of cells ($N_{live\ cells}$) per large haemocytometer square (n) was multiplied by the dilution factor (DF) and divided by the holding volume of a haemocytometer square (V_s = 0.0001 mL).

$$C_{live\ cells} = \frac{DF}{nV_s}\sum_{i=1}^{n} N_{live\ cells_i} \tag{19}$$

3.2.8.2 Scaffold preparation and sterilisation

EtOH-treated needle-electrospun silk fibroin mats (SF_{12}-E) and needleless-electrospun silk fibroin mats (NSF_{12}-E) are referred to as scaffolds when they are used to culture cells. To prepare scaffolds for cell culture, the stabilised SF_{12}-E and NSF_{12}-E mats were cut out using a 16 mm diameter puncture tool. The surface area (SA) of the scaffold was calculated as the surface area of a cylinder (**Equation 20**).

$$SA = 2\pi r^2 + 2\pi rh \tag{20}$$

Prior to use, the scaffolds were autoclaved at 121 °C for 20 min and then conditioned in growth media (α-MEM supplemented with 2 mM UltraGlutamine, 10% (v/v) FBS, 1 ng/mL bFGF and 1% (v/v) penicillin-streptomycin) in Corning™ Costar™ ultra-low attachment 24-well microplates (Thermo Fisher Scientific, UK) for 1 h at 37 °, 5% CO_2.

3.2.8.3 Cytotoxicity assay

Bovine MSCs were seeded at 3000 cells/cm^2 on the previously conditioned scaffolds. A full medium exchange was performed every 48 h. On the eighth day of culture, cell viability was measured using live/dead staining according to the manufacturer's protocol. Briefly, the growth medium was removed from the wells and replaced with an equal volume of a solution containing 5 mM calcein-AM and 20 mM ethidium homodimer in DPBS. The samples were then incubated in the dark at 37 °C, 5% CO_2 for 40 min, and imaged using a fluorescent microscope (EVOS M5000, Thermo Fisher Scientific, UK). The autofluorescence of the scaffolds was subtracted from the images to only display the cells. Cells fixed and permeabilised with 4% paraformaldehyde (PFA) served as negative controls.

3.2.8.4 Cell proliferation assay

To quantify the rate of bMSC expansion on electrospun (NSF_{12}-E) scaffolds, a PrestoBlue™ assay was performed every two days for 9 nine days. On day 0, cells were seeded on previously conditioned scaffolds of known surface areas at densities of 3000, 6000 and 10000 cells/cm^2. At the start of each assay, spent media was removed from sample wells and calibration wells and replaced with 10% (v/v) PrestoBlue in fresh complete growth medium and then incubated in the dark for 2 h at 37 °C, 5% CO_2

in a humidified incubator. At the end of the incubation time, 100 µL of the media was transferred to a Corning™ Costar™ 96-well microplate (Thermo Fisher Scientific, UK) and its fluorescence was measured using a microplate reader (FLUOstar Omega, BMG LABTECH, Germany) with excitation and emission wavelengths set to 560 nm and 590 nm respectively. A calibration curve was plotted for each assay to determine the concentration slope and quantify cell concentrations in samples. After each assay, the remaining 10% PrestoBlue™ solution in sample wells was removed and scaffolds were washed twice in DPBS, before being replaced by fresh growth medium and incubated at 37 °C, 5% CO_2 in a humidified incubator.

To measure the growth kinetics of bMSCs on electrospun silk fibroin scaffolds, the seeding efficiency (E_s), growth rate (GR), doubling time (DT) and fold increase (FI) were estminated using cell densities obtained from the PrestoBlue™ assay calibration curve (***Appendix B, Figure S8***). The seeding efficiency (E_s; **Equation 21**) was measured by dividing the cell density at day 1 (N_1) by the seeding density (N_0).

$$E_S = \frac{N_1}{N_0} \times 100 \tag{21}$$

The fold increase (FI) was measured by dividing the maximum (or final) density (N_{max}) by the initial seeding density (**Equation 22**).

$$FI = \frac{N_{max}}{N_0} \tag{22}$$

The doubling time (DT; **Equation 23**) during the exponential growth phase was measured using the specific growth rate (GR; **Equation 24**) where N_e represents the density of cells measured at the end of the exponential growth phase and t represents the time span in hours between N_0 (on day 0) and N_e.

$$GR = \frac{\ln\left(\frac{N_e}{N_0}\right)}{t} \tag{23}$$

$$DT = \frac{\ln(2)}{GR} \tag{24}$$

3.2.9 Statistical analysis

Statistical analysis was carried out using Microsoft Excel version 2208 to determine the mean and standard deviation (SD), with a confidence interval of 95%.

Biological characterisation experiments were conducted in triplicates four separate times (n = 12). All other experiments were performed once with 3 to 8 replicates ($n \geq 3$). All results were displayed as mean ± SD ($n \geq 3$).

The statistical significance of the results was calculated using a one-way ANOVA followed by Tukey's HSD test. Different letters were used to display groups that were statistically different from one another.

3.3 Results and Discussion

3.3.1 Degumming efficiency

The first step towards improving the scalability of electrospun silk fibroin scaffolds is to obtain a cheap, reliable and abundant source of silk fibroin. To achieve this, silk fibroin was degummed from the virgin silk of *B. mori* cocoons to detach and wash off the sericin, fats and ash components from the core silk fibroin fibrils and then purified to produce regenerated silk fibroin that could be electrospun. Although many strategies have been developed to efficiently degum and regenerate silk fibroin, it has been shown that boiling cocoons in sodium carbonate (Na_2CO_3) for 30 minutes and then rinsing three times was one of the most cost effective, high yield, easy and quick method to produce silk fibroin with minimal structural damage to the degummed fibres (Feng *et al*., 2020). However, it has also been shown that the concentration of the Na_2CO_3 degumming solution affected the physicochemical and mechanical properties of silk fibroin as well as its electrospinnability (Dou and Zuo, 2015; Wang *et al*., 2013). Here 0.2%, 0.5% and 5% (w/v) aqueous Na_2CO_3 solutions were used to degum the silk fibroin fibres and the degumming and regeneration ratios were used to measure the percentage weight loss resulting from the degumming and regeneration steps respectively (**Figure 27**). As shown in **Figure 27A**, degumming ratios of 29.8 ± 1.9%, 31.1 ± 0.2% and 47.9 ± 6.7% (n=3) were achieved using 0.2%, 0.5% and 5% (w/v) Na_2CO_3 solutions, respectively, matching or exceeding the upper limit of the 20-30% weight of non-silk fibroin components in silk, and indicating the complete degumming of the degummed silk fibroin (DSF) fibres. However, while the use of the 0.2% and 0.5% (w/v) Na_2CO_3 solutions resulted in little-to-no loss of silk fibroin, the significant increase in degumming ratio of the 5% (w/v) Na_2CO_3 demonstrated a significant loss of silk fibroin in the degumming stage, likely resulting from damage caused by the harshness of the more concentrated Na_2CO_3 solution.

Additionally, regeneration ratios (**Figure 27B**) of 26.8 ± 13.8%, 50.9 ± 6.9% and 62.1 ± 4.5% (n = 3) were obtained using the 0.2%, 0.5% and 5% (w/v) Na_2CO_3 solutions, respectively. Thus, indicating that dissolved silk fibroin chains with a molecular weight below 14 kDa (the molecular weight cut-off of the dialysis tubing used during the dialysis period) were lost during the silk fibroin regeneration stage. Furthermore, final regenerated silk fibroin (RSF) yields of 51.6 ± 7.7%, 33.8 ± 4.8% and 19.9 ± 4.1% obtained with the 0.2%, 0.5% and 5% (w/v) Na_2CO_3 solutions, respectively, demonstrated a negative correlation between final yield and Na_2CO_3 degumming solution concentration (**Figure 27C**). It should

be noted that the final yield also correlated negatively with the cost of silk fibroin extraction and purification, with estimated prices at 1.81 ± 0.29 £/g, 2.74 ± 0.40 £/g and 4.77 ± 1.03 £/g for RSF films obtained with the 0.2%, 0.5% and 5% (w/v) Na_2CO_3 solutions, respectively (**Figure 27D**). While these prices were much lower than the price of commercial silk fibroin (325.00 £/g), it should be noted that they could be considerably further reduced by purchasing raw silk at the global market index price (55-80 £/kg as of November 2024; Business Analytiq, 2024). As such, using the 0.2% (w/v) Na_2CO_3 degumming method could yield RSF costing as little as 0.12 £/g.

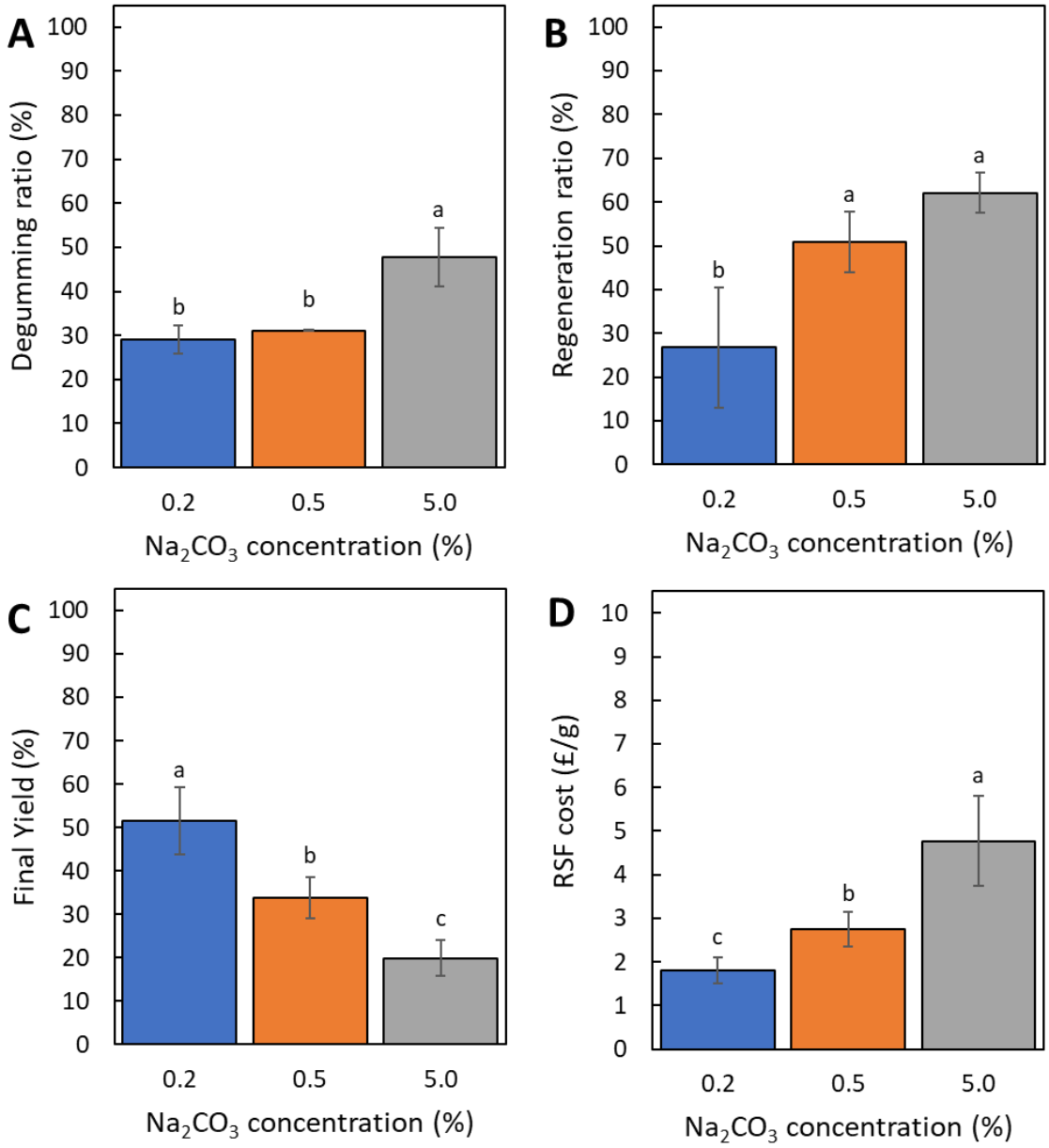

Figure 27: Effects of Na_2CO_3 concentration on (A) degumming ratio (B) regeneration ratio (C) final yield and (D) estimated cost of regenerated silk fibroin. Results displayed as mean ± SD (n=3), different lower case letters indicate statistical differences between groups ($p<0.05$).

It should also be noted that the use of different Na_2CO_3 solution concentrations impacted the effectiveness of the regenerated silk fibroin and its ability to be electrospun under normal operating conditions. RSF films degummed using both the 0.2% and 0.5% (w/v) Na_2CO_3 solutions, exhibited similarly flexible clear films that could be electrospun at a concentration of 12% (w/w) in formic acid at 15 kV with a 10 cm collector distance. In contrast, those degummed using the 5% (w/v) Na_2CO_3 solution were particularly brittle with a yellow taint, and could not be electrospun, at a concentration of 12% (w/w) in formic acid, despite the formation of a Taylor cone, indicating a possible lack of chain entanglement. Dou and Zuo (2015) quantified the molecular weight of degummed silk fibroin using Na_2CO_3 solutions of decreasing concentrations. Using SDS-page, the team found that DSF obtained using a 5% (w/v) Na_2CO_3 solution resulted in a single band at 10 kDa while DSF obtained using a 0.5% (w/v) Na_2CO_3 solution resulted in a smear from 25 kDa to 100 kDa and a minor band at 200 kDa (Dou and Zuo, 2015). In addition, Wang *et al*. (2013) showed that DSF obtained using a 0.2% (w/v) Na_2CO_3 solution exhibited a smear between 50 kDa and 200 kDa using the same method (Wang *et al*., 2013). These results demonstrate the destructive effect of Na_2CO_3 on silk fibroin chains and explain the observed differences in regeneration ratio, final yields, and electrospinnability of the RSF films. With most molecular fragments being smaller than 14 kDa in the 5% (w/v) Na_2CO_3-degummed silk fibroin, it is expected that most of the dissolved silk fibroin solution would be lost during dialysis. The absence of fibres during electrospinning may have also resulted from insufficient chain length and strength to break the surface tension of the polymer solution and pull jets continuously into fibres (Perez-Puyana *et al*., 2025). These results could explain the significant increase in regeneration ratio between the 0.2% and 0.5% (w/v) Na_2CO_3 solutions despite their similar degumming ratios. Indeed, while both Na_2CO_3 solutions removed non-silk fibroin components equally, the harsher effect of the more concentrated 0.5% Na_2CO_3 resulted in more damage to the fibres resulting in the formation of smaller protein fragments. These results therefore demonstrate that the degumming ratio, often used in the literature as a measure of degumming success is a relatively poor indicator of fibre quality compared to the regeneration ratio (Carissimi *et al*., 2019; Feng *et al*., 2020; Schmidt *et al*., 2023). Although, no differences were observed between the fibre morphology or electrospinnability of the 0.2% and 0.5% (w/v) Na_2CO_3-degummed RSF, the significantly higher yield and reduced production cost per gram of RSF made the 0.2% (w/v) Na_2CO_3 degumming method far more scalable. As such, the 0.2% (w/v) Na_2CO_3 solution was used as the default for silk fibroin degumming for all subsequent experiments.

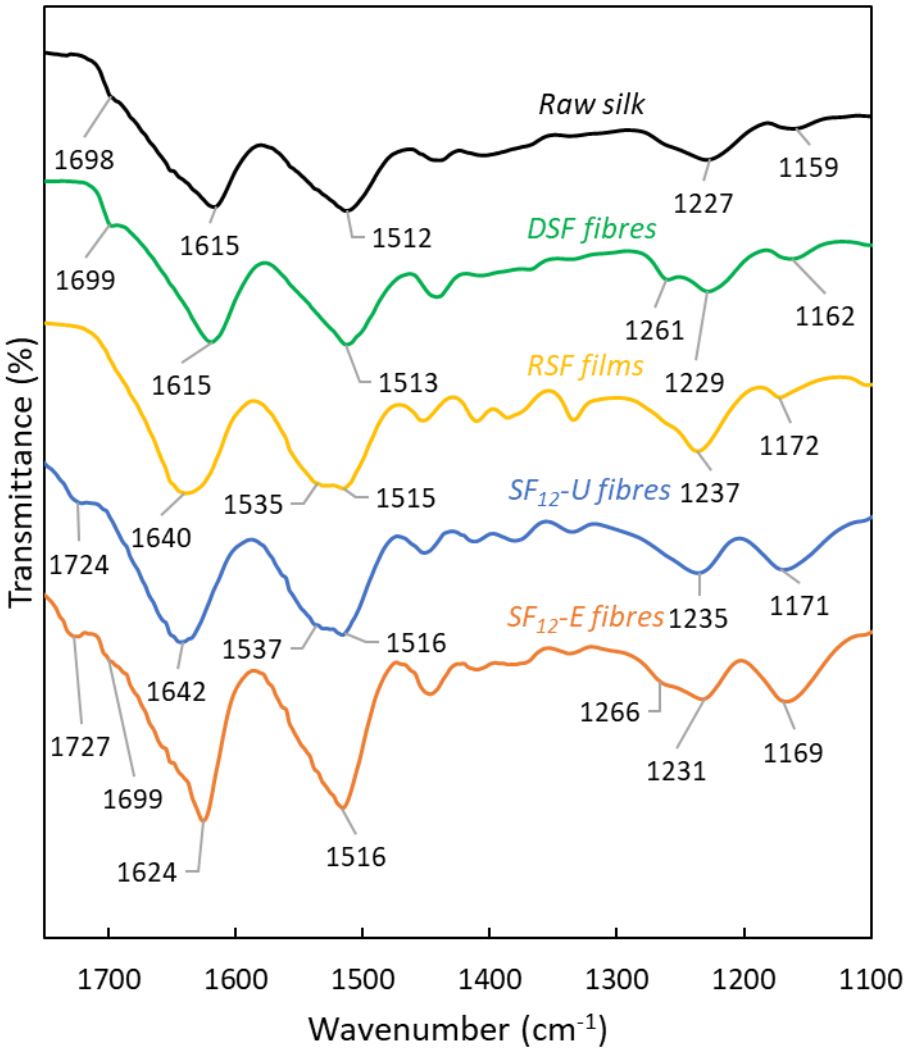

Figure 28: FTIR spectra of silk fibroin throughout the degumming, regeneration, electrospinning and stabilisation processes.

The effect of degumming and regeneration on protein secondary structure was investigated using FTIR (**Figure 28**) and spectral decomposition of the amide I band of raw silk cocoons, DSF fibres, RSF films, electrospun regenerated silk fibroin (SF_{12}-U) and EtOH-treated electrospun regenerated silk fibroin mats (SF_{12}-E; **Figure 29**). As shown in **Figure 28**, raw silk displayed peaks at 1698 cm^{-1} and 1615 cm^{-1} in the amide I band (C=O stretching vibrations) and 1512 in the amide II (C-N stretching vibrations and N-H in-plane bending deformations) corresponding to a highly crystalline structure of β-sheets (62.5% of the total protein conformations) composed of mostly inter-molecular β-sheets (45.2% of the total protein conformations). In addition, the single peak at 1229 cm^{-1} with no shoulder peaks in the amide III (C-N stretching vibrations and N-H in-plane bending deformations) was assigned to random coils and associated with the presence of sericin in raw silk due to its relatively low crystallinity in its natural spun state (Zhang and Wyeth, 2010; Boulet-Audet *et al.*, 2015). Degumming the silk fibres had no major effect on the FTIR spectrum of DSF fibres in the amide I and II bands, but a strong peak at 1261

cm^{-1} corresponding to β-sheets was observed in the amide III band, indicating the removal of sericin. In contrast, regeneration caused major shifts in the amide I from 1615 cm^{-1} in DSF to 1640 cm^{-1} in RSF, a broadening of the amide II band with a large secondary peak at 1535 cm^{-1} and the disappearance of the peak at 1261 cm^{-1} with, instead, a higher intensity peak at 1237 cm^{-1} in the amide III band, all corresponding to a transition from Silk II in DSF to Silk I in RSF. Moreover, no substantial difference was observed between the FTIR spectra of RSF and electrospun SF_{12}-U fibres. In contrast, the FTIR spectrum of SF_{12}-E resembled the spectrum of DSF fibres with strong peaks at 1699 cm^{-1}, 1624 cm^{-1}, 1516 cm^{-1} and 1266 cm^{-1} corresponding to silk II conformations.

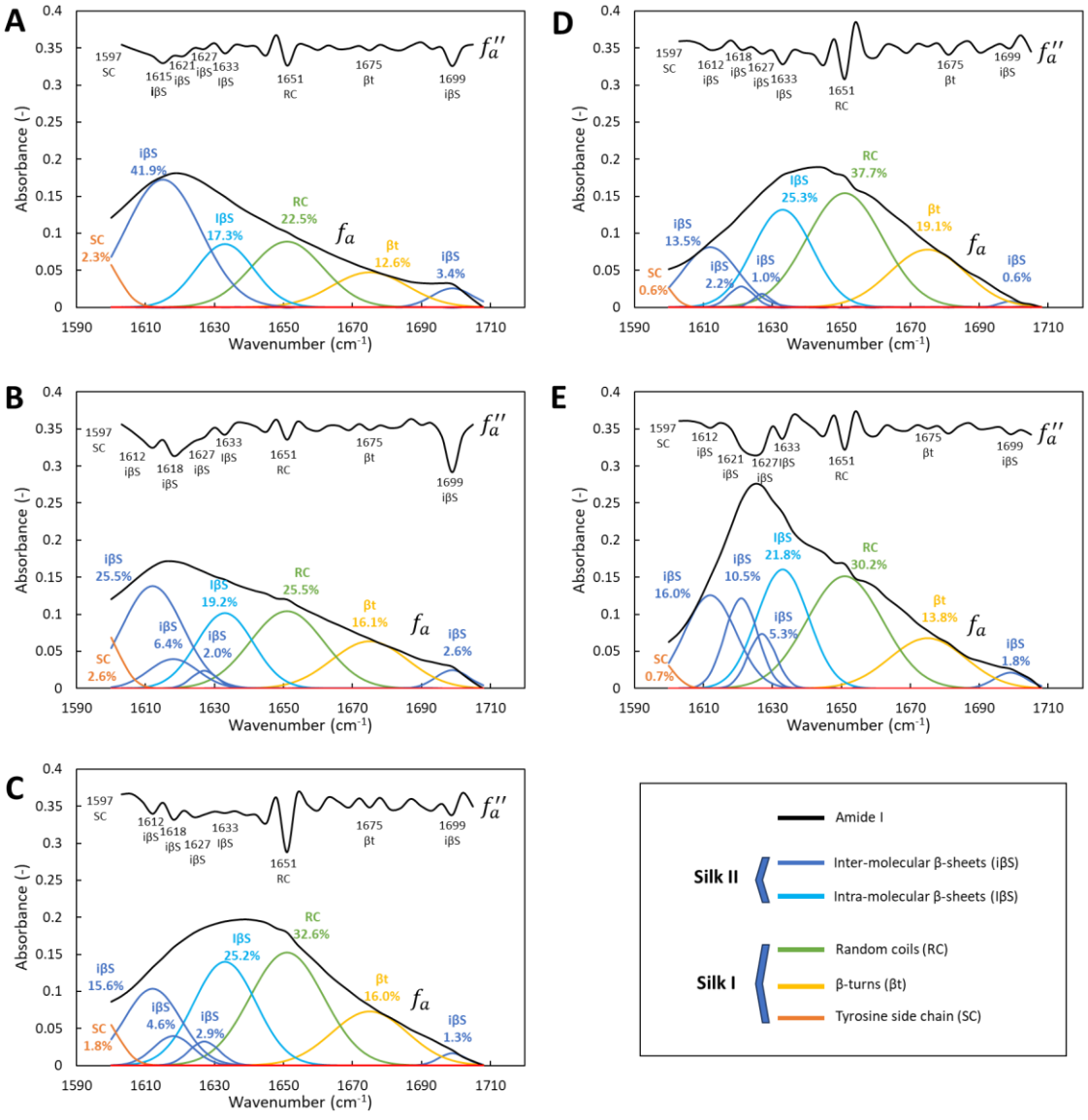

Figure 29: Spectral decomposition of the amide I band (f_a) of silk throughout the degumming, electrospinning and stabilisation process using second derivative analysis (f_a'') to identify peak locations and assignments (bottom). (A) B. mori raw silk cocoon, (B) degummed silk fibroin fibres (DSF), (C) regenerated silk fibroin films (RSF), (D) needle-electrospun regenerated silk fibroin (SF_{12}-U), (E) EtOH-treated needle-electrospun silk fibroin (SF_{12}-E).

As shown in **Figure 29** and summarised in **Figure 30**, degumming, regenerating and dissolving silk fibroin caused a progressive reduction in crystallinity and inter-molecular β-sheet content. First, degumming silk fibres caused a drop in overall crystallinity from 62.5% to 55.7% with a reduction of inter-molecular β-sheets from 72.3% to 65.6%, likely resulting from damage to the peptide chains initiated by the Na_2CO_3 degumming solution. As the DSF fibres were dissolved in Ajisawa's solution, $CaCl_2$ disrupted hydrogen bonds stabilising anti-parallel β-sheets, and caused a conversion of hydrophobic crystalline regions into hydrophilic amorphous regions, thereby improving the solubility of silk fibroin in water and organic solvents such as formic acid (Ajisawa, 1998; Belton *et al*., 2019). Silk fibroin was then maintained in this Silk I conformational state using dialysis, to quickly desalt the protein, removing $CaCl_2$ and preventing protein aggregation (Belton *et al*., 2019) and thereby, substantially reducing the crystallinity of the RSF films to 49.6% (of which 49.2% intermolecular β-sheets). When RSF films were subsequently dissolved in formic acid, the overall crystallinity of the electrospun mats dropped to 42.7% (of which 42.6% inter-molecular β-sheets). As implied by their name intra-molecular β-sheets are formed within proteins whereas inter-molecular β-sheets are formed around and between different protein chains, contributing to protein aggregation, clustering and fibre formation (Khakshoor and Nowick, 2009; Wang *et al*., 2023). As silk fibroin is dissolved, the hydrogen bonds are disrupted, disassembling the inter-molecular β-sheets and causing the peptide chains to separate, thereby loosening and exposing the hydrophilic irregular side chains and dissolving the protein (Nguyen *et al*., 2019). Finally, to improve the stability and mechanical properties of the electrospun mats they were immersed in EtOH for 20 min. This treatment largely reversed the effects of dissolution, increasing the crystallinity to 55.4% (of which 60.7% inter-molecular β-sheet).

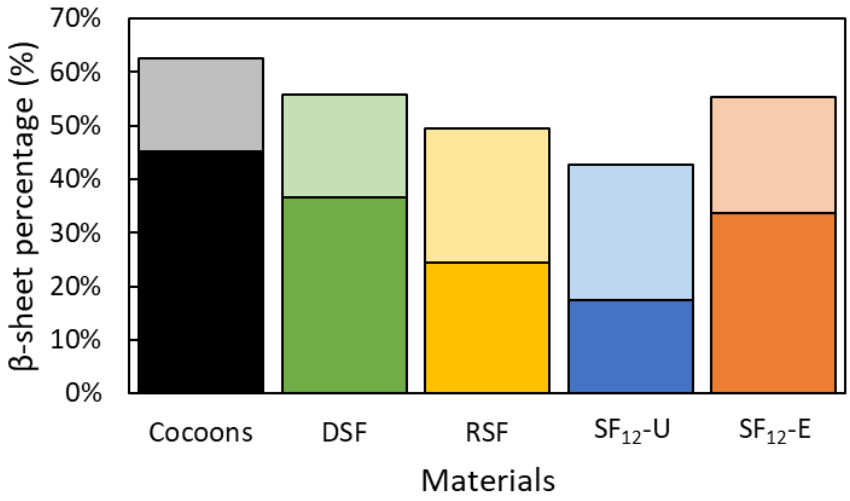

Figure 30: Changes in β-sheet content and composition (dark: inter-molecular β-sheets; light: intra-molecular β-sheets) resulting from degumming, regeneration, electrospinning and stabilisation, from B. mori cocoons to electrospun silk fibroin mats.

Non-woven needle-electrospun SF_{12}-U mats displayed smooth, continuous, uniform and randomly orientated fibres of relatively thin fibre diameter (105 ± 27 nm) that significantly increased in size following EtOH-treatment (140 ± 34 nm; p<0.05; **Figure 31**), making both treated and untreated regenerated silk fibroin fibres comparable in size to those obtained with commercial silk fibroin under the same electrospinning conditions, but with little-to-no defects (see Chapter II, *section 2.3.2.2*). In addition, characterisation of the tensile properties of regenerated silk fibroin (***Appendix B, Figure S7***), revealed a Young's modulus of 166.6 ± 20.2 MPa and ultimate tensile strength of 2.6 ± 0.5 MPa which significantly increased after EtOH treatment to 381.0 ± 80.5 MPa and 4.1 ± 1.1 MPa, respectively (p<0.05)). Interestingly, these results were not significantly different from those obtained with commercial silk fibroin before and after EtOH-treatment (see Chapter II, *section 2.3.2.4*). With no major differences in the fibre thickness and mechanical properties between the commercial and regenerated silk fibroin needle-electrospun mats, minor differences in fibre morphology (*i.e.* the presence of defects) could be due to a slight difference in protein molecular weight resulting from differing degumming strategies. Longer and undamaged molecular chains may create a stronger entanglement, allowing the jets to continuously overcome the surface tension of the polymer solution and therefore produce smooth uniform fibres with a relatively narrow fibre distribution.

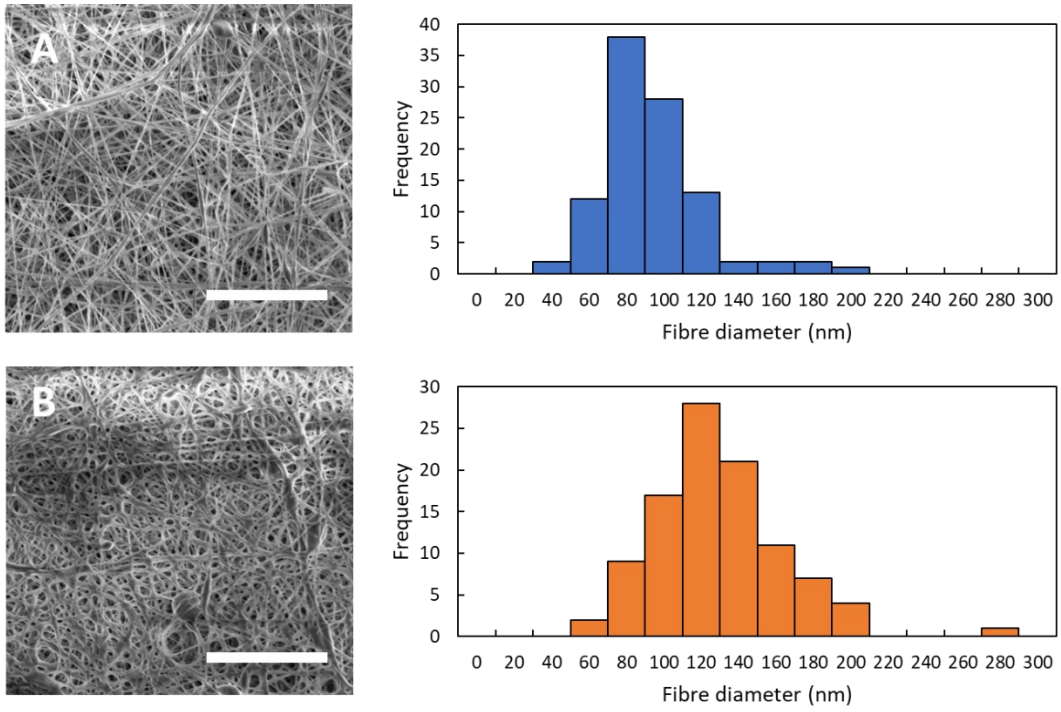

Figure 31: SEM images (left) and fibre distribution (right; n = 100) of needle electrospun regenerated silk fibroin (A) untreated (SF_{12}-U) and (B) EtOH-treated (SF_{12}-E). Scale bar = 5 µm.

The non-woven needle-electrospun SF_{12}-U and EtOH-treated SF_{12}-E mats were immersed in water to measure the solubility of the regenerated silk fibroin protein in aqueous environments for long periods

of time (**Figure 32**). Despite its dominant Silk I conformational state, SF_{12}-U dissolved slowly in water, losing up to 49.9 ± 12.5% of its weight after 1 hour but regaining 82.9 ± 3.3% of its initial weight within 24 hours (n=3). Interestingly, this level of dissolution was achieved within 1 minute using electrospun commercial silk fibroin, which could also be explained by a difference in molecular weight. Indeed, with less damage caused to the heavy chains during degumming, fewer molecular fragments of hydrophobic amino acids are lost during dialysis, making the regenerated protein more resistant to dissolution in water. In contrast, SF_{12}-E dissolved much more slowly losing only 18.9 ± 6.9% of its weight after 1 hour of immersion and regained 93.3 ± 4.7% within 24 hours. Beyond 24 hours of immersion no significant differences were observed between the weight integrity of SF_{12}-U and SF_{12}-E, indicating possible water-annealing, as explained in Chapter II, *section 2.3.2.3*.

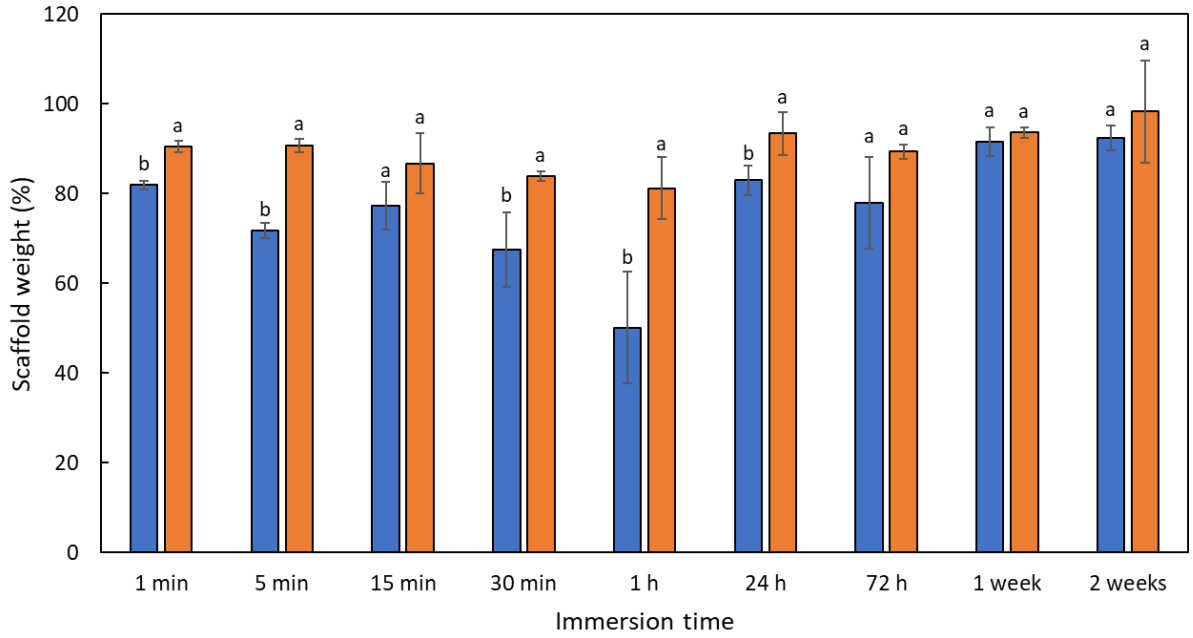

Figure 32: Solubility of needle electrospun regenerated silk fibroin before (blue) and after EtOH (orange) treatment, following water immersion for different time intervals. Data shown as mean ± SD (n=3), with lower-case letters indicating statistical differences between the mean of each group at each time point (p<0.05).

The water contact angle measurements showed a significant difference between the wettability of untreated commercial (42.6 ± 6.7°) and regenerated silk fibroin films (69.5 ± 4.6°; **Figure 33**), with the commercial untreated silk fibroin films being more hydrophilic than the regenerated one. Interestingly, no significant differences were seen between the contact angles on untreated and EtOH-treated regenerated films (61.9 ± 4.1°), nor was there any between the contact angles on regenerated and commercial (55.5 ± 8.0°) and regenerated EtOH-treated films (61.9 ± 4.1°; p<0.05). These results tie in well with the solubility results showing a significant difference between the wettability of

untreated silk fibroin degummed under different conditions, and that of stabilised silk fibroin which barely dissolves in water regardless of the degumming method. Moreover, Terada *et al*. (2016) showed that a reduction in surface hydrophilicity could be influenced by an increased molecular weight of silk fibroin. The team also found that alcohol treatment of silk fibroin films resulted in a partial dissolution of the molecular chains at the outermost layer of the film during alcohol immersion, creating a thin and more hydrophilic gel-like substance on the surface of dried films (Terada *et al*., 2016), thereby explaining the minor decrease (or lack of an increase) in contact angle that would be expected from the protein solubilisation process. Nonetheless, the results obtained here are in line with the literature indicating that silk fibroin films are moderately hydrophilic (Beena *et al*., 2022; dos Santos *et al*., 2021).

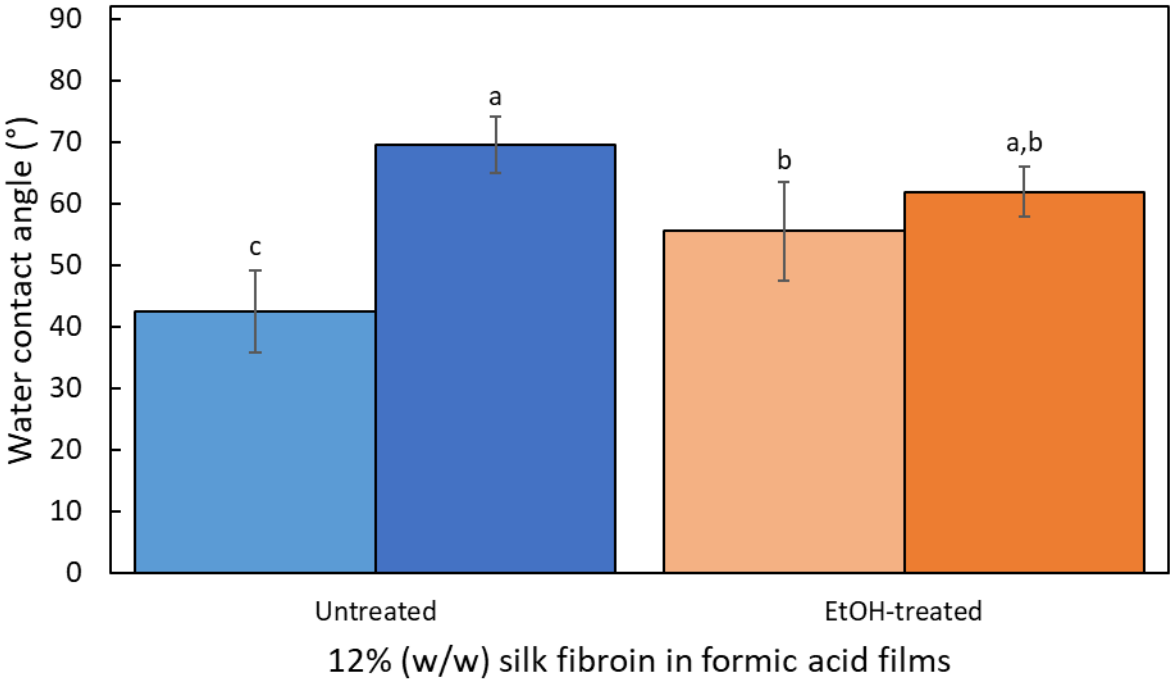

Figure 33: Water contact angle measurements on commercial (light) and regenerated (dark) silk fibroin films (12% (w/w) in formic acid) before (blue) and after ethanol (orange) treatment, displayed as mean ± SD ($n \geq 5$), with different lower-case letters indicating statistical significance ($p<0.05$).

While there are some undeniable differences between commercially purchased and regenerated in-house silk fibroin, the results obtained gave confidence in the use of the latter as a starting material for subsequent experiments. The degumming and regeneration process was quite straightforward and easy to scale up, and the resulting regenerated silk fibroin formed uniform, defect-free mats with relatively high fibre thickness. Furthermore, switching from commercial to regenerated silk fibroin significantly reduced the cost of the feedstock biopolymer, which could still be significantly lowered in scaled-up production by purchasing raw silk or cocoons in bulk at global market index prices.

Ultimately, producing silk fibroin using scalable precision fermentation systems will likely become a necessity for cultivated meats in order to achieve cost parity with traditional meat (Bonkamp *et al*., 2022; Venkatessen *et al*., 2022). In addition, future regulatory guidelines may not require precision-fermented products to be labelled as derived from genetically modified organisms (GMOs) (Dupuis *et al*., 2023), which could mitigate the stigma associated with eating 'artificial foods' (Marris, 2001; Siegriest and Sütterlin, 2017).

3.3.2 Needleless electrospinning

3.3.2.1 Needleless DC-electrospinning: Laboratory scale

To further improve the production rate of electrospun mats and scaffolds, an upgrade from the conventional small-scale needle-electrospinning to a pilot-scale needleless electrospinner (NS1S500U Nanospider™; Elmarco, Czechia), capable of producing mats measuring 0.5x1000 m in a single run, was carried out (Xiong *et al*., 2021; Omer *et al*., 2021; Homer *et al*., 2023). Due to the large volume of polymer solution (10-50 mL) needed for the Nanospider™ to run effectively, the time constraints surrounding the operation of the needleless-electrospinner and the limited staff availability for supervision, it was not feasible to optimise needleless-electrospinning conditions for the Nanospider™ directly. Instead, a benchtop needleless-electrospinner was used for this purpose, to produce five needleless-electrospun ($NLSF_{12}$-U) mats using regenerated silk fibroin polymer solution (12% (w/w) in formic acid) with voltages ranging from 35 kV to 55 kV and a collector distance of 10 cm to 12 cm. As shown in **Figure 34**, the non-woven $NLSF_{12}$-U mats exhibited randomly orientated nanofibres of relatively thick diameter (160 ± 24 nm, averaged across all mats) that significantly increased following EtOH-treatment (165 ± 22 nm). All fibres produced using needleless electrospinning were significantly thicker than needle-electrospun ones, with the thickest fibres created at 40 kV and a collector distance of 10 cm measuring 172 ± 68 nm which increased to 193 ± 60 nm following EtOH-treatment. All mats also displayed many defects, notably beaded and branched fibres, and occasional unspun droplets. These defects result from the limitations of needleless electrospinning, notably the lack of control of the Taylor cone formation, the variable charge distribution and the solvent evaporation rate which occur throughout the electrospinning process (Partheniadis *et al*., 2020). As fibres are drawn from the thin polymer solution layer on the spinneret, solvent evaporation causes the solution to dry out causing an unstable spinning process resulting in the spraying of large unspun droplets (Holopainen *et al*., 2014). Consequently, it was necessary to frequently interrupt the electrospinning process to clean the spinneret and reset the polymer solution. The inconstant charge accumulation in the polymer solution, also caused increased whipping instability which contributed to the formation of split-, branched- and beaded-fibres (Zhao and Chi, 2014). These flaws can however be mitigated using rotating spinnerets or screw pumps to

continuously replenish the polymer solution (Partheniadis *et al*., 2020). The mat with the least defects was also the one with the thickest fibres, electrospun at 40 kV with a 10 cm collector distance. Therefore, these parameters were chosen as the default operating conditions for subsequent Nanospider™ electrospinning. Curiously, upon EtOH-treatment (**Figure 35**), $NLSF_{12}$-E mats formed large fibrous structures that resembled the curd of a cauliflower in the most extreme cases (**Figure 35B**), likely resulting from fibres tightening around large unspun droplets as the mats shrank during EtOH-treatment.

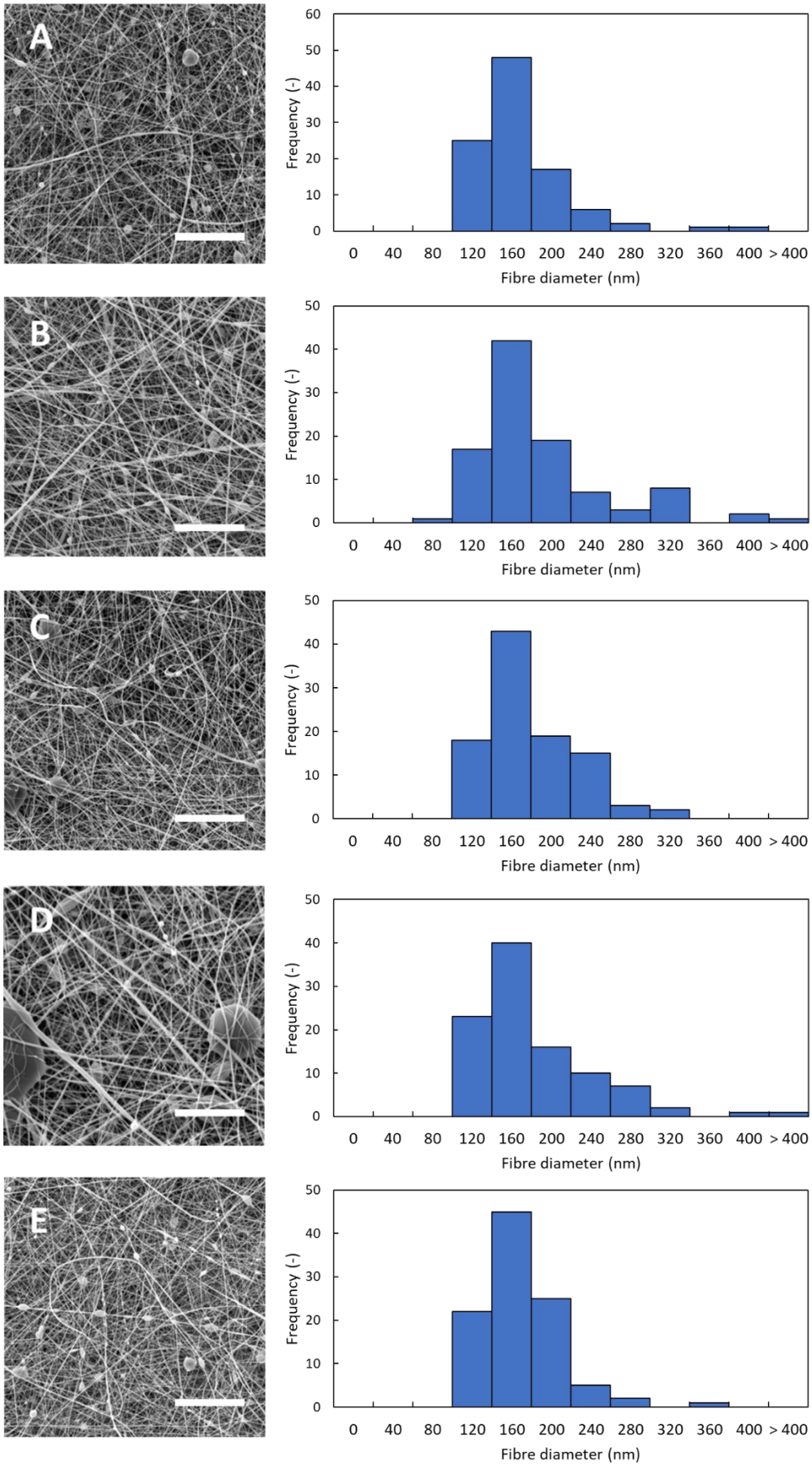

Figure 34: SEM images (left) and fibre distribution (right; n=100) of needleless electrospun silk fibroin using a benchtop setup ($NLSF_{12}$-U). (A) 35 kV, 10 cm, (B) 40 kV, 10cm, (C) 45 kV, 10 cm, (D) 45 kV, 12 cm, (E) 55kV, 12cm. Scale bar = 10 µm.

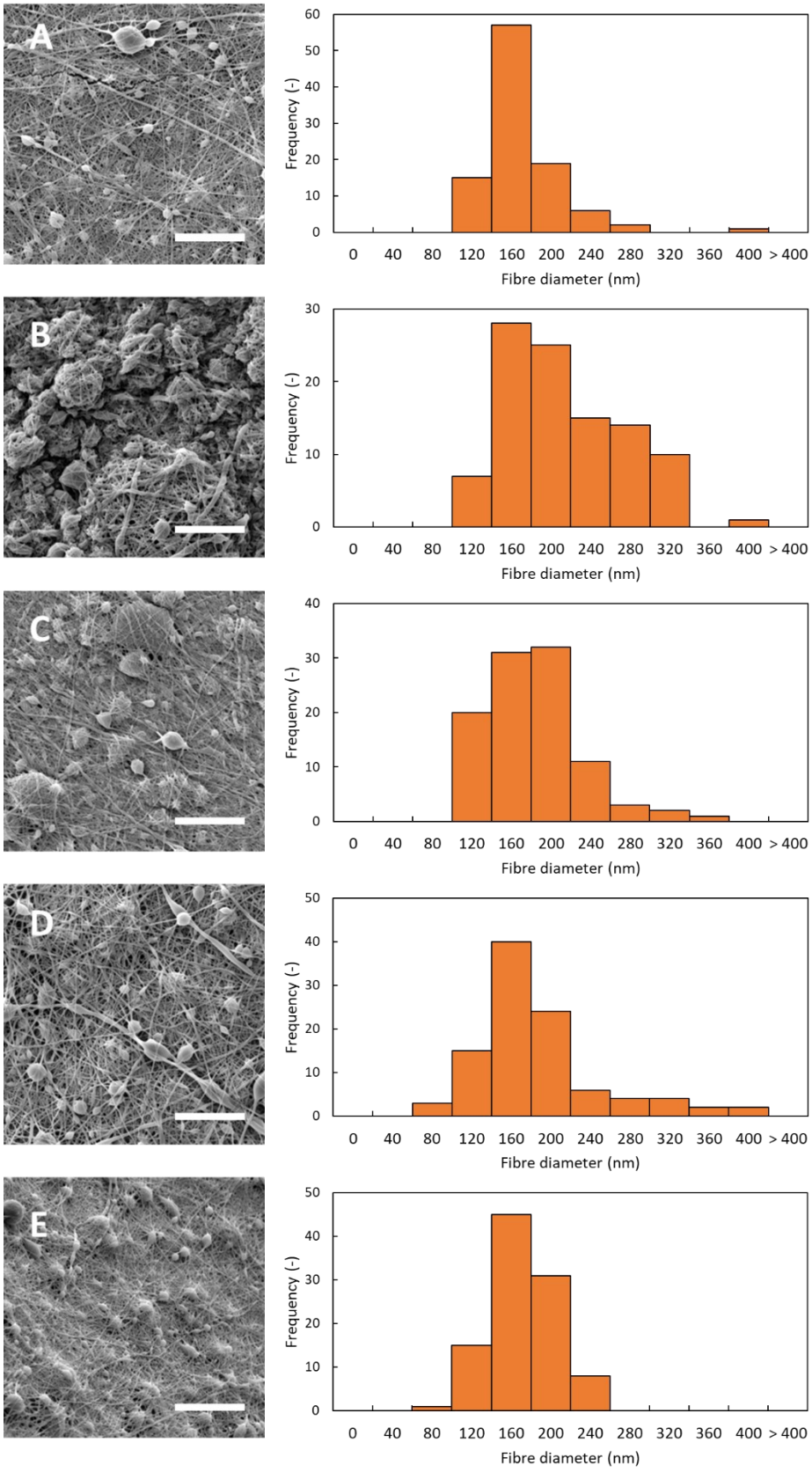

Figure 35: SEM images (left) and fibre distribution (right; n=100) of EtOH-treated needleless electrospun silk fibroin using a benchtop setup ($NLSF_{12}$-E). (A) 35 kV, 10 cm, (B) 40 kV, 10cm, (C) 45 kV, 10 cm, (D) 45 kV, 12 cm, (E) 55kV, 12cm. Scale bar = 10 µm.

3.3.2.2 Needleless DC-electrospinning: Pilot scale

Creation of functional supports for the scalable expansion and differentiation of stem cells, essential for viable production of cultivated meat, will require a manufacturing platform which is commercially mature, has high productivity and can generate materials with consistent specifications. The needleless Nanospider™ technology offers scale-up potential, is semi-automated and has an integrated climate control system which allows reproducibility in the manufacture of nanofibre-based materials. Following the optimisation experiments conducted on the needleless benchtop DC-electrospinner, the electrospinning parameters were set 40 kV and 10 cm collector distance for experiments using the Nanospider™ producing NSF_{12}-U mats from regenerated silk fibroin.

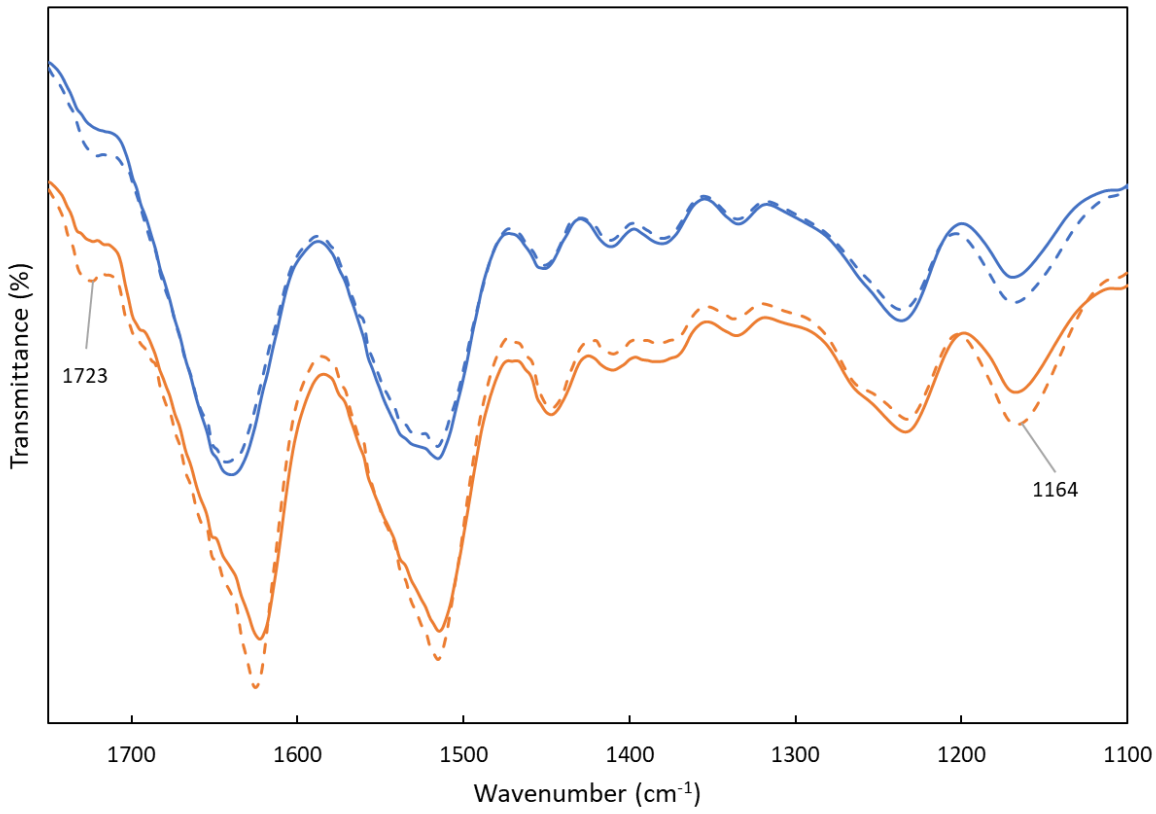

Figure 36: FTIR spectra of non-woven mats produced using a Nanospider™ (NSF_{12} - continuous line) and a needle-electrospinner (SF_{12} - dotted line) before (blue) and after (orange) EtOH-treatment.

The FTIR of mats recorded before and after alcohol treatment using the Nanospider™ platform were very similar to those produced using the needle electrospinner (**Figure 36**), confirming that the different electrospinning methods had no major impact on the secondary structure of silk fibroin. However, a difference in the intensity of the peaks at 1723 cm^{-1} and 1164 cm^{-1}, previously attributed to the C=O and C-O stretching vibrations of formic acid, was observed between SF_{12} and NSF_{12} samples. This variation may be attributed to the Nanospider's improved solvent evaporation time and better

control over processing through its integrated climate control system, as solvent evaporation time is directly influenced by ambient temperature and relative humidity (Haider *et al*., 2018).

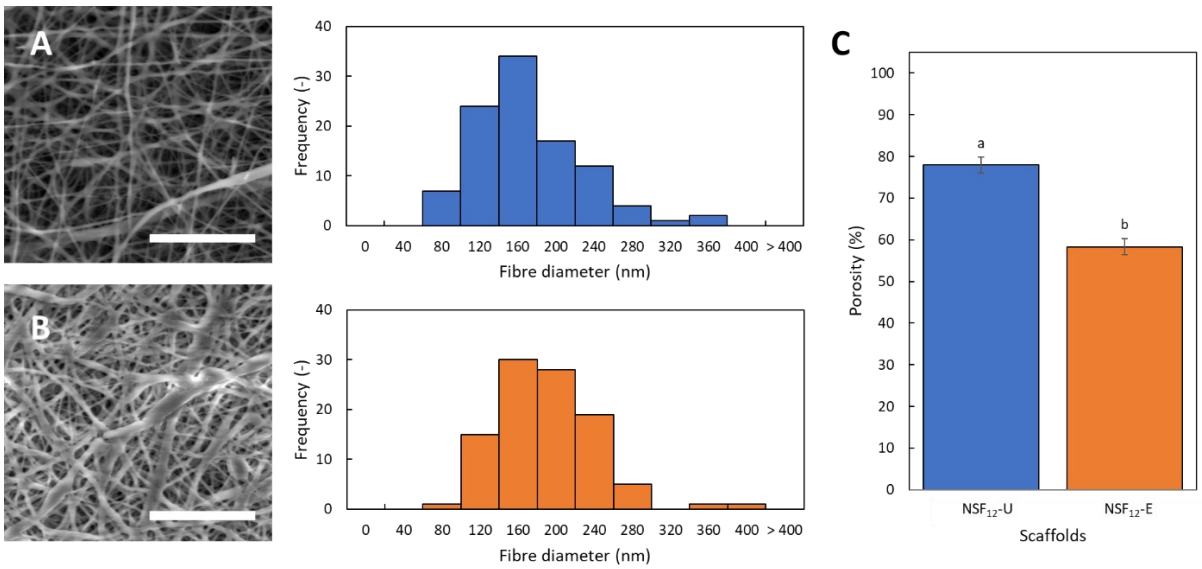

Figure 37: SEM images (left) and fibre distribution (middle; n=100) of electrospun silk fibroin mats using Nanospider™ technology (A) Untreated (NSF_{12}-U), (B) EtOH-treated (NSF_{12}-E). (C) Porosity measurements in Nanospider™ produced scaffolds before (NSF_{12}-U) and after (NSF_{12}-E) EtOH-treatment, displayed as mean ± SD (n=5), with lower-case letters indicating statistical differences (p<0.05). Scale bar = 5 µm.

Non-woven NSF_{12}-U and EtOH-treated NSF_{12}-E mats displayed uniform, continuous and randomly orientated fibres with a similar fibre distribution and diameter (151 ± 58 nm for NSF_{12}U and 170 ± 51 nm for NSF_{12}-E), to fibres produced by the benchtop needle and needleless electrospinners (**Figure 37A,B**). Unlike $NLSF_{12}$ mats, no defects were present in NSF_{12} fibres, as the Nanospider™ precisely controlled environment (relative humidity and temperature) and polymer deposition rate allowed for a continuous electrospinning process. Finally, and similarly to the results obtained with the needle electrospun supports (**Figure 37C**), scaffold porosity decreased with alcohol treatments, from 77.95 ± 1.99% for NSF_{12}-U to 58.29 ± 1.94% for NSF_{12}-E (n=5).

3.3.2.3 Needleless AC-electrospinning

In addition, to the benchtop needleless electrospinner and Nanospider™ system, an AC-electrospinner was used to generate silk fibroin fibres. AC-electrospinning, and in particular needleless AC-electrospinning, is a relatively recent innovation. Using an alternating current, the polymer solution placed at the tip of the electrified rod is subject to a high degree of hydrodynamic instability that initiates jet formation. The rapidly alternating current creates short fibres that have both positive and negative charged ends which attract jets of opposing charged ends. Due to the ionising of the ambient air, an electric wind creates a compact fibrous plume that can be collected without a physical collector (Kessick *et al*., 2004; Teo *et al*., 2011; Sivan et al., 2022). As a novel technology, most studies have

focused on the characterisation of AC-electrospun yarns and the theory behind it (Pokorny *et al*., 2014; Valtera *et al.,* 2019; Sivan *et al.,* 2022) with only a small handful of studies exploring the applications of AC-electrospun fibres in a biomedical context (Homer *et al*., 2023). As of November 2024, there are still no studies which have characterised the needleless AC-electrospinning of proteins nor have there been any investigations into the production of novel scaffolds using this technology for tissue engineering applications.

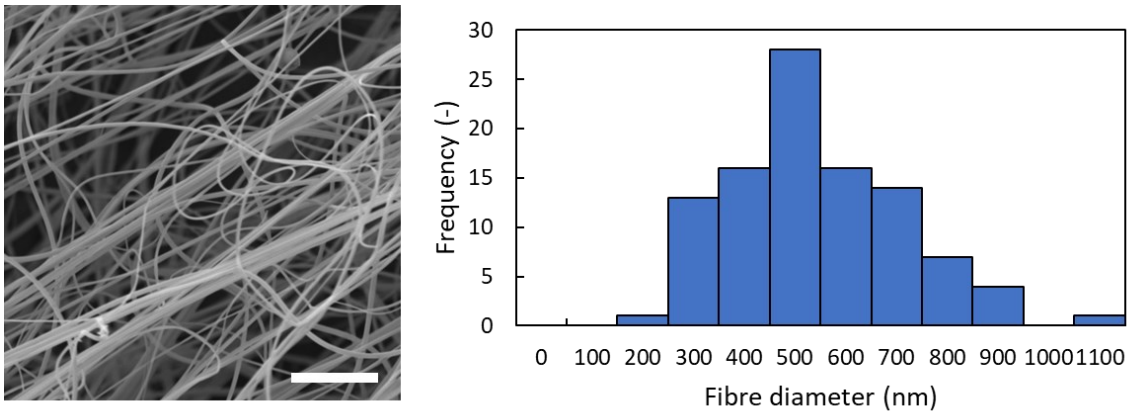

Figure 38: SEM images (left) and fibre distribution (right; n=100) of AC electrospun regenerated silk fibroin fibres ($ACSF_{12}$-U). Scale bar = 10 µm.

As a proof of concept, a small amount of 12% (w/w) regenerated silk fibroin in formic acid was tested for AC-electrospinnability. Surprisingly, silk fibroin electrospun exceptionally well with AC electrospinning, producing a very wide distribution of thick (489 ± 176 nm), smooth, uniform, and defect-free fibres (**Figure 38**). Interestingly, and despite no mats being produced, more fibre alignment was observed in the AC-electrospun ($ACSF_{12}$-U) collection of fibres due to the reduction of whipping instability generated by the neutral charged plume (Sivan *et al*., 2022). Unfortunately, and since AC electrospinning is still under development and commercial equipment is not yet available, it is considered an immature technology and was not used for further experiments.

3.3.3 Biological characterisation of regenerated silk fibroin scaffolds

To assess the suitability of silk fibroin materials in the manufacture of cultivated beef products, needleless electrospun EtOH-treated (NSF_{12}-E) supports were tested for cytotoxicity and cell proliferation with bovine mesenchymal stem cells (bMSCs) in static culture conditions. Cell viability was assessed after eight days of cell culture using a live/dead assay and fluorescent microscopy (**Figure 39**). No dead cells were detected, indicating excellent cytocompatibility of the silk fibroin nanofibres. The cells appeared to be spread out on the entire fibrous surface of the NSF_{12}-E scaffold, with rounded cell clumps visible in large grooves, and elongated and flattened cells present along single fibres or anchored on multiple fibres.

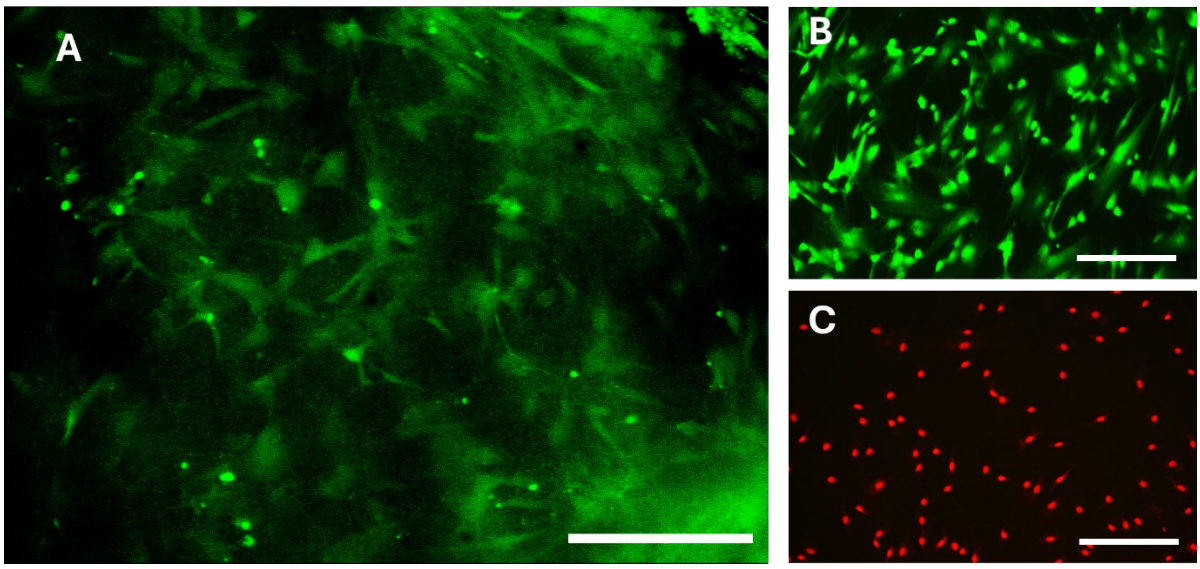

Figure 39: (A) Live/dead staining of bMSCs on NSF_{12}-E at day 8 of culture with calcein AM staining live cells green and ethidium homodimer-1 staining the nuclei of dead cells red. Positive (B) and negative (C) controls were prepared by growing bMSCs on tissue culture plastic. For the negative control, cells were fixed with 4% paraformaldehyde before live/dead staining. Scale bar = 250 µm.

The cell proliferation rate and quantification of metabolically active cells on the scaffolds was measured using a PrestoBlue assay over 11 days of culture (**Figure 40A**). Following cell seeding on day 0 at 3000, 6000 and 10000 cells/cm^2, a low fluorescence at day 1 indicated a moderate seeding efficiency of 43.2 ± 14.7%, 38.3 ± 8.6%, and 58.2 ± 11.8%, respectively. It is worth noting that the low values of culture on day 1 resulted from low to negative fluorescence values caused by, on the one hand, the reduction in metabolic activity of cells as they adapt to their fibrous environment which can take over 24 h (Beijer *et al*., 2019), and on the other hand, by the nanofibrous nature of the supports which causes resazurin and resorufin to adhere to the fibres, thereby reducing the fluorescence intensity below the background fluorescence (Podgórski *et al*., 2022). From day 1, the cells entered the exponential growth stage which ended on day 7 (R^2= 0.9939, R^2=0.9995 and R^2=0.9819, for bMSCs seeded on scaffolds at 3000, 6000 and 10000 cells/cm^2,respectively (***Appendix B, Figure S9***)). During this time the doubling rate for cells seeded at 3000, 6000 and 10000 cells/cm^2 was estimated at 47.9 ± 8.5 h, 59.1 ± 4.2 h and 76.9 ± 13.3 h, respectively, indicating a negative correlation between higher seeding densities and cell doubling time (p<0.05). These results fell in line with the doubling times of adipose-derived mesenchymal stem cells across a range of species (Chen *et al*., 2012; Zhan *et al*., 2019; Buckowska *et al*., 2020; Stout *et* al., 2022; Min *et al*., 2022). From day 7 to day 11, the cells continued to divide but at a slower rate, probably due to diminishing growth space and nutrient depletion as the cells approached confluency. On day 11, cells entered the stationary phase, resulting in lower metabolic activity as cells became confluent, as shown in **Figure 41**. The maximum yield on day 11, marked a 21.9 ± 1.1, 11.5 ± 0.8 and 7.7 ± 0.1 -fold increase on NSF_{12}-E scaffolds seeded at 3000,

6000 and 10000 cells/cm^2, respectively, and again showed a negative correlation between higher seeding densities and fold increase.

Fast doubling times are essential for tissue engineering scalability, as by producing a higher yield sooner they reduce production costs. The shorter the period of cell expansion, the less media (and media components) and energy are required (Allan *et al*., 2019; Kirsch *et* al., 2023; Cai *et al*., 2024). Therefore, to maximise cell yields, cells should be maintained in the exponential phase by controlling the culture time, seeding density and scaffold surface area. Increasing the available growth area, would make cells take longer to reach confluency, thereby extending the duration of the exponential phase. Using microcarriers instead of scaffolds could therefore be beneficial as the total growth area can be increased by progressively adding more microcarriers at critical time points in culture (Verbruggen *et al*., 2018; Rafiq *et al*., 2018; Hanga *et al*., 2021). Given the higher fold increase and doubling time, the 3000 cells/cm^2 seeding density was chosen as the default for all subsequent cell culture experiments on scaffolds in this study.

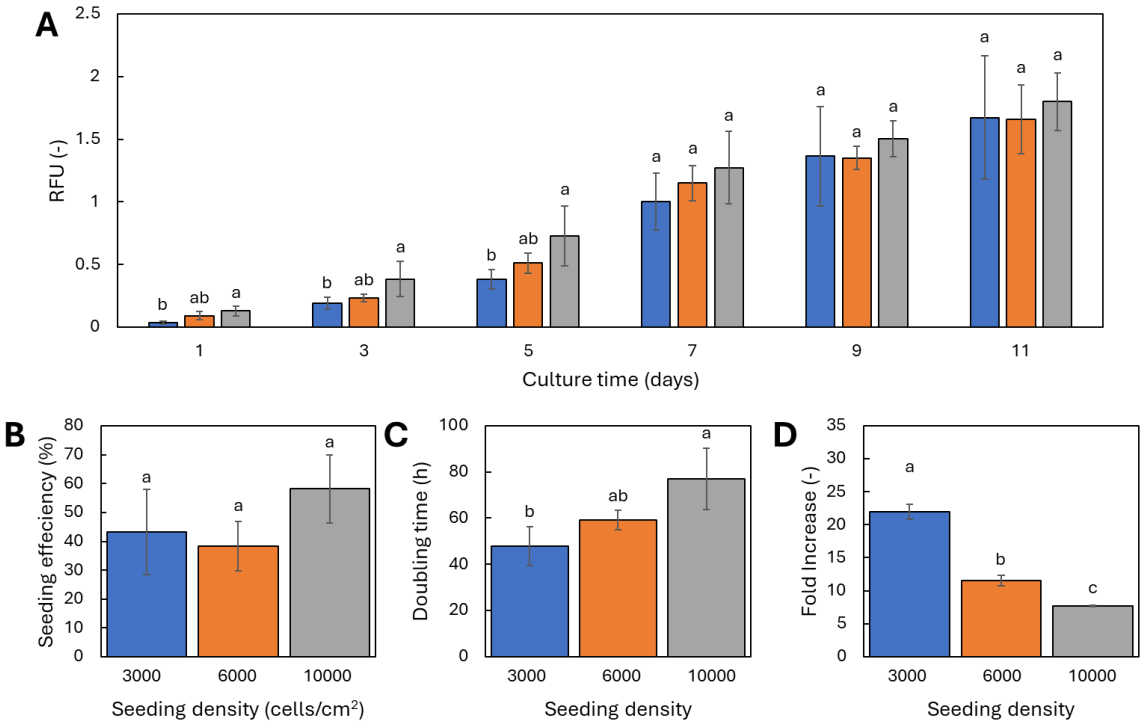

*Figure 40: (A) bMSC proliferation of NSF_{12}-E mats at different seeding densities: 3000 (blue), 6000 (orange), 10000 (grey) cells/cm^2. (B-D) Estimated growth kinetics of bMSC on NSF_{12}-E mats based on cell density results measured using the PrestoBlue™ assay calibration curve (**Appendix B, Figure S8**). (B) Seeding efficiency measured as the percentage of metabolically active cells attached to scaffolds on day 1, (B) bMSC doubling time in exponential growth stage (day 1-7), (C) Fold increase from days 1 to 11. Proliferation data displayed as mean ± SD (n=12), with lower-case letters indicating statistical differences between groups at each time point (p<0.05).*

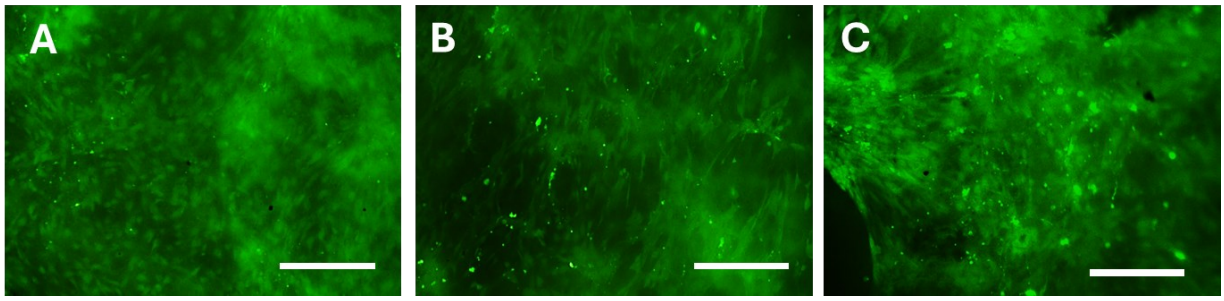

Figure 41: Fluorescent microscopy images of live/dead staining after 11 days of culture, with calcein AM staining live cells green and ethidium homodimer-1 staining the nuclei of dead cells red, on NSF_{12}-E mats seeded at (B) 3000, (C) 6000 or (D) 10000 cells/cm². Scale bar = 250 µm.

Like most mammalian cells, bMSCs are adherent and need to attach effectively to a surface to survive and proliferate. The probability of cell attachment to a biomaterial is influenced by the surface chemistry and physical characteristics of the substrate, including composition, surface charge, roughness, rigidity, stiffness, and wettability, the latter being determined using degrees of surface hydrophilicity (0–90°) and hydrophobicity (90–180°) through contact angle measurements. It has been shown that mesenchymal stem cells attach and proliferate on materials with moderately hydrophilic surfaces (40–90°; Bauer *et al*., 2008), with studies even suggesting that a 70° contact angle is ideal (Mohammadzadehmoghadam & Dong, 2019). The contact angle of EtOH-treated RSF_{12} films was measured as 55.5 ± 8.0° (n = 5; **Figure 33**), which fell within the optimal surface hydrophilicity levels reported for mesenchymal stem cell attachment. While contact angle alone may not be a perfect indicator of cell attachment due to the complexity of protein binding and other critical parameters, such as scaffold topography (Bauer *et al*., 2008), it could nevertheless contribute to the bMSCs attachment and growth on the otherwise inert surfaces provided by silk fibroin. Considering the absence of RGD-peptide motifs on silk fibroin and the lack of artificial functionalisation of the scaffolds, this amount of cell attachment was deemed acceptable. Blending silk fibroin with more functional materials (e.g. plant gums, ECM proteins and derivatives) or using the RGD-peptide-containing silk fibroin of certain wild silkworms (Kang *et al*., 2018) could potentially improve the seeding efficiency, at day 1, by increasing cell attachment (Duangpakdee *et al*., 2021).

3.4 Conclusion

Degumming and regeneration of silk fibroin fibres from *Bombyx mori* cocoons using 0.2% (w/v) Na_2CO_3 and Ajisawa's solution proved to be a reproducible and cost-effective process. FTIR spectroscopy showed that the regenerated silk fibroin was chemically identical to the commercial silk fibroin, yet the protein concentration was shown to be higher in regenerated silk fibroin resulting in higher insolubility, surface hydrophobicity and thicker fibres when non-woven mats were created by needle-electrospinning under identical conditions.

The direct current needleless Nanospider™ equipment produced mats which were free of defects, at a high production rate, approximately 2.5 g/h, more than 100 times faster than the laboratory needle-electrospinner setup. The Nanospider™ mats were also shown to be non-cytotoxic and to promote cell attachment, migration, and proliferation, with bMSCs achieving a doubling rate of 47.9 ± 8.5 h when seeded at 3000 cells/cm^2.

Although cells were able to grow on the electrospun scaffolds, the moderate seeding efficiency measured on the first day of culture, may indicate poor scaffold functionality possibly resulting in cell loss particularly at higher seeding concentrations. While bMSC were selected due to their multipotency and ability to differentiate into all the cells present in meat (muscle, fat, connective tissue and bone), mesenchymal stem cells have been shown to have a lower proliferation potential than myoblast and fibroblast cell lines *in vitro* (Ichim *et al*., 2018; Kindler *et al*., 2021). As such, simpler progenitor cell models with higher proliferation potential such as C2C12 myoblast or 3T3-L1 preadipocytes could be used to further biologically characterise the electrospun scaffolds. In addition, physical and chemical surface modifications could improve the functionality of the electrospun silk fibroin scaffolds.

Finally, AC electrospinning showed potential for tissue engineering scaffold design, due to the increased thickness of the fibres produced and, consequently, the creation of larger pores compared with DC electrospinning technologies. The relative alignment of larger fibres mixed with thinner randomly orientated ones could provide a suitable environment for specific stem cell differentiation and co-cultures. There is still a lot to learn from this recent and relatively untapped electrospinning technology, and future work is needed to elucidate its true potential.

The next chapter explores functionalisation strategies to enhance cell attachment and growth rate, with the aim of engineering novel non-spherical edible microcarriers.

CHAPTER IV

FUNCTIONALISATION OF SILK FIBROIN MATS AND CREATION OF IRREGULAR MICROCARRIERS

4.1 Introduction

One of the biggest challenges when facing scaled production of cultivated meat resides in the difficulty in efficiently expandind sufficient cell numbers to generate large amounts of meat tissue. From recent estimations, to assemble a single cultivated beef quarter pounder (120 g), approximately 10^{10} cells would be needed (Post *et al*., 2020), and impressively this could be achieved within 4 days, using bovine mesenchymal stem cells (bMSC) with optimal seeding conditions in stirred tank reactors (Hanga *et al*., 2020; Hanga *et* al., 2021; Moutsatsou *et al*., 2023).

To boost the yields of anchorage-dependant stem cells it is important to maximise scaffold attachment and reduce proliferation time. Efficient attachment greatly improves final cell yields and is dependent on several factors encompassing surface chemistry, topography and the presence of cell binding motifs (Derakhti *et al*., 2019). Biomaterial surface properties, such as hydrophilicity and surface charge, play a significant role in improving cell adhesion and can be easily modified with functionalisation strategies. For instance, blending materials can improve the surface chemistry of the composite by overcoming the factors that negatively affect cell adhesion in the main biomaterial or by displaying functional properties from the other. However, to securely attach cells, integrin-mediated binding to extracellular matrix binding motifs is desirable (Derakhti *et al*., 2019). In addition, chemical and physical modifications using crosslinking agents or UV-irradiation can purposefully alter the functional groups present on the scaffold surface to improve wettability and the adsorption of adhesive molecules during conditioning. Whatever the method, the chosen blending material or physical functionalisation procedure should also consider improving nutritional value, organoleptic properties and consumer perception without significantly impacting sustainability, cost or food safety.

To enhance proliferation, the surface available to cells should also be increased and the culture parameters controlled. To achieve this efficiently, cells should be expanded on 3-dimensional scaffolds

that can be integrated in bioreactor systems. One such method is using microcarriers, which provide a high surface-to-volume ratio and allow anchorage-dependent cells to grow in suspension in a controlled environment.

In this chapter, blend and physical functionalisation strategies are adopted to modify the surface chemistry of silk fibroin electrospun scaffolds in an attempt to improve cell attachment and proliferation. The scaffolds are then converted into non-spherical microcarriers and compared with commercial and prototype microcarriers in static conditions. This study provides the basis for future work on cell expansion in dynamic systems such as spinner flasks and stirred tank bioreactors.

4.2 Materials & Methods

4.2.1 Materials

Bovine adipose-derived mesenchymal stem cells (bMSCs) were purchased from Quest Meat Ltd (UK) at passage 1. Ethanol (99.8%), calcium chloride (97%), sodium carbonate (≥99.5%), paraformaldehyde in PBS (4%), formic acid (98+%) (Acros Organics), and zein anhydrous protein powder (Acros Organics) were purchased from Fisher Scientific (UK). Ground psyllium husk was purchased from Holland & Barrett (UK). Invitrogen™ LIVE/DEAD™ viability/cytotoxicity kit, Invitrogen™ PrestoBlue™ Cell Viability Reagent, Alpha-modified Eagle medium (α-MEM; Gibco™), ultraglutamine (Gibco™), Dulbecco's phosphate buffered saline (DPBS; Gibco™), penicillin-streptomycin (Gibco™), Trypan Blue solution 0.4% (Gibco™) were purchased from Thermo Fisher Scientific. Trypsin-EDTA and fetal bovine serum (FBS) were obtained from Merck Life Science (UK). *Bombyx mori* silkworm cocoons (brand TMISHION) were bought on Amazon (UK). Basic fibroblast growth factor (bFGF) was acquired from PeproTech (UK). Cytodex 3 was purchased from Cytiva (UK). Solohill® Plastic (P-221) microcarriers were obtained from Sartorius (UK). Hybrid X prototype microcarriers were gifted from Gelatex Technologies OÜ (Estonia). Deionised water was used in all experiments unless otherwise stated.

4.2.2 Degumming of silk fibroin

As in Chapter III, *section 3.2.2* silk fibroin was degummed from *B. mori* silk cocoons. After finely chopping the cocoons into small pieces and soaking them in diH_2O for 3h, they were soaked in 0.05% (w/v) Na_2CO_3 overnight. The pieces were then boiled three times in 0.2% (w/v) Na_2CO_3 and washed every time in diH_2O. Finally, the degummed fibres were dried under a laminar flow at room temperature overnight.

The degummed fibres were then dissolved in Ajisawa's solution and dialysed against diH_2O for 3 days. The final solution was then cast into petri dishes and oven-dried at 40 °C to produce regenerated silk fibroin (RSF) films.

4.2.3 Silk fibroin blends

Functionalisation was achieved by blending RSF films with psyllium husk or zein to produce an $SF_{\phi}PH_{\chi}$ or $SF_{\phi}Z_{\psi}$ electrospinning solution, where ϕ, χ, and ψ represent the weight percentage of silk fibroin, psyllium husk and zein, respectively. First, regenerated silk fibroin was dissolved in formic acid at a concentration of 6-10% (w/w) for SFPH or 0-12% (w/w) for SFZ, after which 1.5-3% (w/w) psyllium husk (**Table 6**) or 0-25% (w/w) zein (**Table 7**) was added progressively under constant stirring. The solutions were then left to dissolve for 24 h at room temperature under constant stirring. For SFPH, homogeneous solutions could not be achieved due to the presence of insoluble fractions in the psyllium husk composition that were not feasibly removable (Guo *et al*., 2008). The electrospinning solutions were then stored at 2 °C and used within 2 days.

Table 6: List of silk fibroin and psyllium husk blends used in this study.

Blends	Percentage of silk fibroin in formic acid (% (w/w))	Percentage of psyllium husk in formic acid (% (w/w))	Dry percentage of psyllium husk (%)
$SF_6PH_{1.5}$	6	1.5	20.0
SF_6PH_3	6	3	33.3
$SF_8PH_{1.5}$	8	1.5	15.3
SF_8PH_2	8	2	20.0
$SF_9PH_{1.5}$	9	1.5	14.3
SF_9PH_2	9	2	18.2
$SF_{10}PH_{1.5}$	10	1.5	13.0
SF_{12}	12	0	0.0
PH_2	0	2	100.0
PH_3	0	3	100.0

Table 7: List of silk fibroin and zein blends use in this study.

Blends	Percentage of silk fibroin in formic acid (% (w/w))	Percentage of zein in formic acid (% (w/w))	Dry percentage of zein (%)
Z_{25}	0	25	100.0
$SF_3Z_{18.75}$	3	18.75	86.2
$SF_6Z_{12.5}$	6	12.5	67.6
$SF_9Z_{6.25}$	9	6.25	41.0
SF_{12}	12	0	0.0
$SF_{12}Z_{6.25}$	12	6.25	34.2
$SF_{12}Z_{12.5}$	12	12.5	51.0

4.2.4 Electrospinning

As per Chapter III, *section 3.2.3*, a needle-electrospinner was used to electrospin silk fibroin SF_{12}, zein Z_{25}, $SF_\phi PH_\chi$ and $SF_\phi Z_\psi$ blends at 15 kV with a 10 cm collector distance. A variable flow rate of 0.1-1.0 mL/h was adapted according to the solvent evaporation time and jet formation rate. The resulting SF_{12}-U, Z_{25}-U, $SF_\phi PH_\chi$-U and $SF_\phi Z_\psi$-U mats were subsequently air dried for 24 h at room temperature and immersed in 98.8% EtOH for 20 min to produce stabilised SF_{12}-E, Z_{25}-E, $SF_\phi PH_\chi$-E and $SF_\phi Z_\psi$-E scaffolds. Electrospinning experiments were performed at 21 °C (± 2 °C) and 30% (± 5%) relative humidity.

4.2.5 UV functionalisation

Ultraviolet light (UV) functionalisation was attempted to induce surface modifications in silk fibroin electrospun mats. Research has shown that silk fibroin fibres absorb light strongly at around 270 nm in the UV-C range. Therefore, electrospun SF_{12}-U and SF_{12}-E mats were placed in a steel box, 3 cm directly below a 6W monochromatic 254 nm wavelength lamp for up to 480 min (**Figure 42**). To limit heat build-up, the box walls were covered in aluminium foil and a small hole was cut out. Mats were labelled as $SF_{12}UV_{\omega'}$-U when irradiated untreated, $SF_{12}UV_{\omega'}$-E when irradiated after EtOH-treatment, and $SF_{12}UV_\omega U \rightarrow E$ when irradiated first and then EtOH-treated, where ω' represents the UV exposure time in minutes.

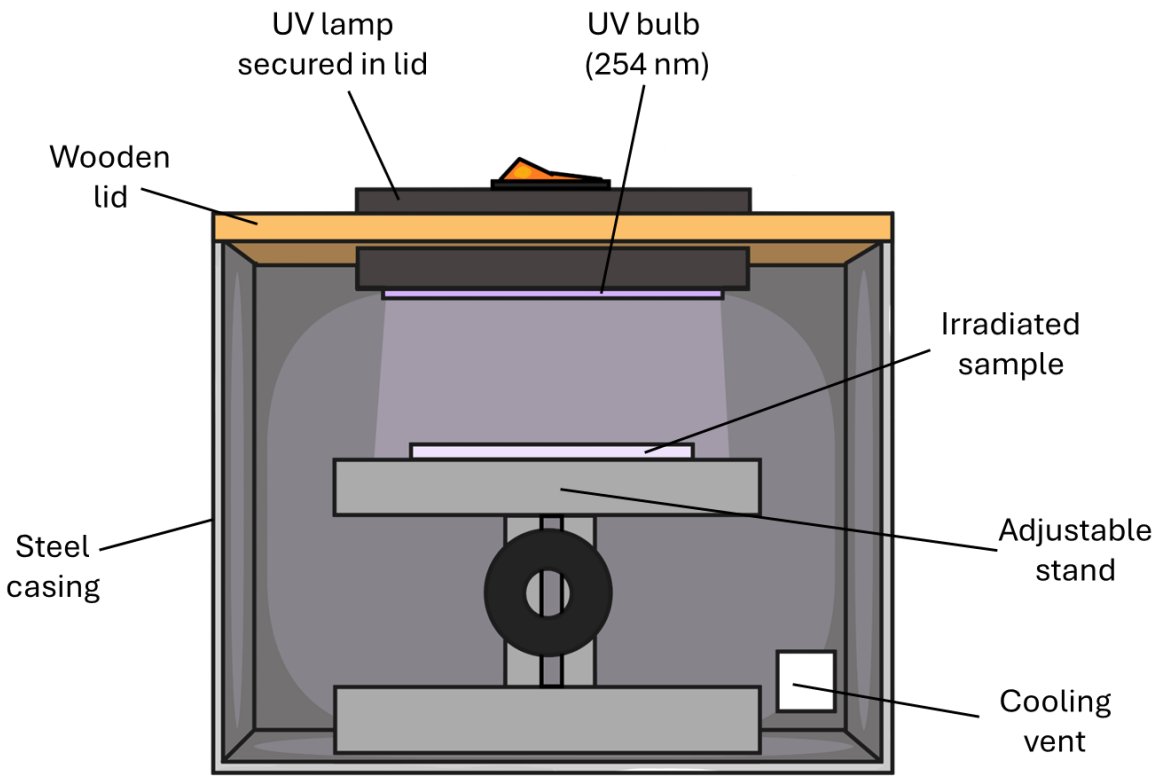

Figure 42: Cross-section of UV treatment box.

4.2.6 Engineering microcarriers

Non-spheroid nano-fibrous and micro-porous microcarriers were produced from electrospun mats in two ways: hand-sliced (hsMC) or cryomilled (cryoMC). The hand-sliced microcarriers were created from SF_{12}-E, $SF_{12}Z_{6.25}$-E and SF_9PH_2-E EtOH-treated electrospun scaffolds using a rotary blade (Sew Easy 45MM Rotary Cutter, Argos, UK) (**Figure 43**), and labelled as $hsMC_{SF}$, $hsMC_{SFZ}$ and $hsMC_{SFPH}$ respectively. Cryomilled microcarriers were produced from SF_9PH_2-E EtOH-treated electrospun mats only, using a CG-200 Freezer/Mill® cryomiller (Cole Parmer, UK), as a time efficient and reproducible alternative to hand-slicing, and labelled as $cryoMC_{SFPH}$. The milling cycle consisted of a 9 min sample precooling followed by a 2 min run time at a speed of 15 counts per second (cps) and 2 min cooling time. The cycle was repeated a total of 4 times. The dimensions and size distribution of the hsMC and cryoMC microcarriers were determined using SEM and ImageJ software.

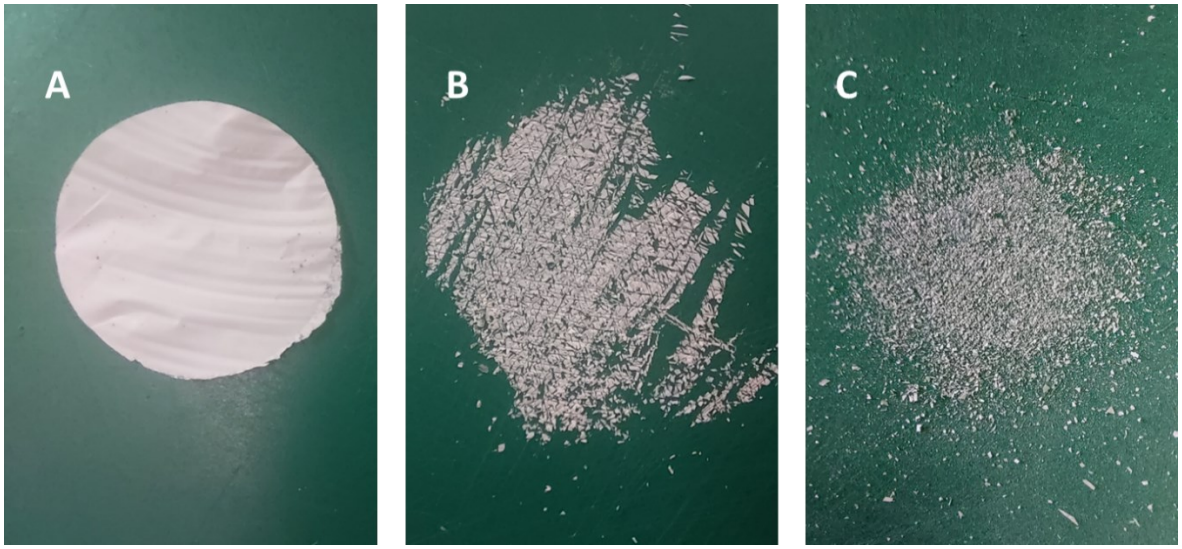

Figure 43: Process of hand cutting electrospun microcarriers. (A) A scaffold of known surface area is cut using a puncture tool. (B) The scaffold is sliced several times in multiple directions, (C) Using a paintbrush, the cut particles are swept into a pile and sliced again in multiple directions. This process is then repeated 3 more times.

The surface area available for culturing cells (SA_{hsMC}) and the specific surface area (SSA_{hsMC}) of hand-sliced microcarriers were determined based on two assumptions: (1) repeatedly hand-slicing scaffolds as a planar disc, reduces the size in the x- and y-directions but not significantly in the z-direction (height); and, (2) slicing scaffolds into smaller micro-scaffolds or microcarriers does not significantly affect the density of the fibrous material.

To calculate the area, hand-sliced microcarriers were first imaged using SEM, which displayed them as n-sided polygons. To then determine their average dimensions, the n-sided polygons were converted to the nearest fitting rectangle and the length (L), width (l) and height (h) were measured. As h matched the thickness of the electrospun scaffolds that were sliced, the first assumption could be validated. The surface area of hsMC for cell culture was approximated as the nominal surface area of the measured parallelepiped (**Equation 25**). This is reasonable because negligible distances in between fibres relative to the size of the cells largely prevented cell infiltration (Wu and Hong, 2016).

$$SA_{hsMC} = 2(Ll + lh + Lh) \tag{25}$$

In order to determine the specific surface area of the hand-sliced microcarriers (e.g. the total area of hsMCs per gram), the number of microcarriers per scaffold ($n_{hsMC/scaffold}$) was first calculated as the quotient of the volume of the scaffold disc and the volume of each microcarrier, where r represents the radius of the scaffold disc (**Equation 26**).

$$n_{hsMC/scaffold} = \frac{\pi r^2 h}{Llh} = \frac{\pi r^2}{Ll} \tag{26}$$

To then determine the amount of microcarriers per gram ($n_{hsMC/g}$), the number of microcarriers per scaffold was divided by the mass of a scaffold ($m_{scaffold}$) itself (**Equation 27**), measured as the product of the scaffold volume and the density of EtOH-treated electrospun silk fibroin (ρ_{SF-E} = 0.6330 g/cm^3).

$$n_{hsMC/g} = \frac{n_{hsMC/scaffold}}{m_{scaffold}} = \frac{\frac{\pi r^2}{Ll}}{\pi r^2 h \times \rho_{SF_{12}-E}} = \frac{1}{Llh\rho_{SF_{12}-E}} \quad (27)$$

Finally, the specific surface area was calculated as the number of microcarriers per gram, multiplied by the culturable area of a single microcarrier (**Equation 28**).

$$SSA_{hsMC} = A_{hsMC} \times n_{hsMC/g} = \frac{2(Ll + lh + Lh)}{Llh\rho_{SF_{12}-E}} \quad (28)$$

For cryomilled microcarriers, the irregular shapes created, combined with their altered fibrous structure would have likely changed the fibre density. As such, the specific surface area of cryoMCs could not be calculated. The culturable area (SA_{cryoMC}; **Equation 29**) was estimated as the average of the surface area calculated as a parallelepiped and as a sphere.

$$SA_{cryoMC} = \frac{2(Ll + lh + Lh) + 4\pi r^2}{2} = Ll + lh + Lh + 2\pi r^2 \quad (29)$$

The specific surface area (SSA) of the electrospun fibres was calculated as the ratio of the area (SA) and the mass (m) of the fibres (**Equations 30-32**), where r_f represents the radius of the fibres (which are considered infinitely long), and $\rho_{SF_{12}-E}$ is the fibre density.

$$SA = 2\pi r_f h \quad (30)$$

$$m = \pi r_f^2 h \rho_{SF_{12}-E} \quad (31)$$

$$SSA = \frac{SA}{m} = \frac{2}{r_f \rho_{SF_{12}-E}} \quad (32)$$

Finally, the fibrous area (a) was calculated as the specific surface area (SSA) divided by the number of microcarriers per gram ($n_{hsMC/g}$) (**Equation 33**).

$$a = \frac{SSA}{n_{hsMC/g}} \quad (33)$$

4.2.7 Physicochemical characterisation

4.2.7.1 FTIR

As per Chapter II, *section 2.2.4.1*, FTIR was used qualitatively to determine chemical and conformational changes in biomaterials and quantitatively to measure secondary structure contents in proteins.

FTIR spectra were adjusted by subtracting the absorbance baseline from 1900 cm^{-1} to 4000 cm^{-1} from the whole FTIR spectra values, so that at 4000 cm^{-1} and 900 cm^{-1} the absorbance reading would tend to 0. An offset was then performed by subtracting the average absorbance values of the region spanning 1900-1950 cm^{-1}. The data was then normalised using the integral absorbance of the region spanning 800-1800 cm^{-1} to compensate for signal intensity variations in the electrospun samples.

When normalisation was not possible due to predicted variance in most peaks as in the case of UV-functionalised mats, the ratio of the absorbance values at specific wavenumbers was used to compare peak intensities and conformation ratios between samples.

The $I_{amideI/II}$ ratio found in the literature as a marker for degradation analysis of silk fibroin provides information on the C=O to N-H and C-N by comparing the height of the amide I and amide II (Koperska *et al*., 2014; **Equation 34**).

$$I_{amide\ I/II} = \frac{A(amide\ I)}{A(amide\ II)} \tag{34}$$

To compare the ratio of β-sheets to random coils, the crystallinity index of the Amide I can be calculated as the quotient of the intensity of the values at 1620 cm^{-1} and 1652 cm^{-1} corresponding to β-sheets and random coils, respectively, in the Amide I (**Equation 35**).

$$I_{1620/1652} = \frac{A(1620\ cm^{-1})}{A(1652\ cm^{-1})} \tag{35}$$

Likewise, the crystallinity index of the amide II band can be calculated similarly by dividing the absorbance value at 1516 cm^{-1} (β-sheets) by that of 1540 cm^{-1} (random coils) in the amide II band (**Equation 36**).

$$I_{1516/1540} = \frac{A(1516\ cm^{-1})}{A(1540\ cm^{-1})} \tag{36}$$

All other intensity ratios were calculated similarly, by dividing the absorbance at a specific wavenumber (w) to that of the amide I maximum absorbance (**Equation 37**).

$$I_x = \frac{A(w)}{A(amide\ I)} \quad (37)$$

4.2.7.2 Scanning Electron Microscopy

As per Chapter II, *section 2.2.4.2*, SEM was used to analyse the shape and size of electrospun fibres and microcarriers.

4.2.7.3 Tensile testing

As per Chapter II, *section 2.2.4.5*, tensile testing was conducted to quantify the strength, elasticity and stiffness of $SF_{12}Z_{6.25}$ functionalised electrospun mats.

4.2.8 Biological characterisation

4.2.8.1 Cell proliferation on scaffolds

Electrospun scaffolds were autoclaved and conditioned in complete media in ultra-low attachment well plates for 1 h. Scaffolds were seeded with bovine mesenchymal stem cells (bMSCs) at 3000 cells/cm^2. A PrestoBlue™ proliferation assay and a full complete media exchange were carried out every two days from day 1 of culture (see Chapter III, *section 3.2.8.4*).

4.2.8.2 Cell proliferation on microcarriers

To compare the performance of the electrospun hand-sliced and cryomilled microcarriers with commercially available and prototype microcarriers, bMSCs were cultured in static conditions on hsMC, cryoMC, Cytodex 3 (C3), Solohill Plastic (SP), and Hybrid X (HX), all of which were prepared according to manufacturer's specifications.

Cytodex 3 microcarriers were briefly rinsed in DPBS (Ca^{2+} and Mg^{2+} free) and soaked in DPBS for at least 4 h before being autoclaved at 121 °C for 20 min. Solohill Plastic microcarriers were autoclaved in diH_2O at 121 °C for 20 min. Hybrid X microcarriers were sterilised using dry heat in a fan assisted high temperature oven (SQ Oven-80 HT; SciQuip, UK) at 170 °C for 1 h. The HX microcarriers were then soaked in DPBS for 1 h, after which the supernatant was removed. Finally, both hsMCs and cryoMCs were autoclaved in foil envelopes at 121 °C for 20 min. All microcarriers were then placed in cell strainers (70 µm mesh size; Falcon, FisherScientific, UK) in ultra-low attachment well plates (Corning, UK) and rinsed twice in DPBS before being conditioned for 1 h at 37 °C, 5% CO_2 in complete α-MEM growth media and seeded at 1500 cells/cm^2. A full media exchange was carried out every 2 days.

A PrestoBlue™ proliferation assay was performed every 2 days from day 1 of culture. Before and after every assay, the microcarriers were rinsed with DPBS twice. For each assay, the microcarriers were immersed in a 10% (v/v) PrestoBlue™ solution in α-MEM complete growth media, incubated at 37 °C, 5% CO_2 for 2 h, and then the fluorescence was read at 560/590 nm. A calibration curve was traced on

each day, using cells incubated in the same volume of PrestoBlue™ solution and treated under the same conditions as the cells in contact with the microcarriers (**Figure 44**).

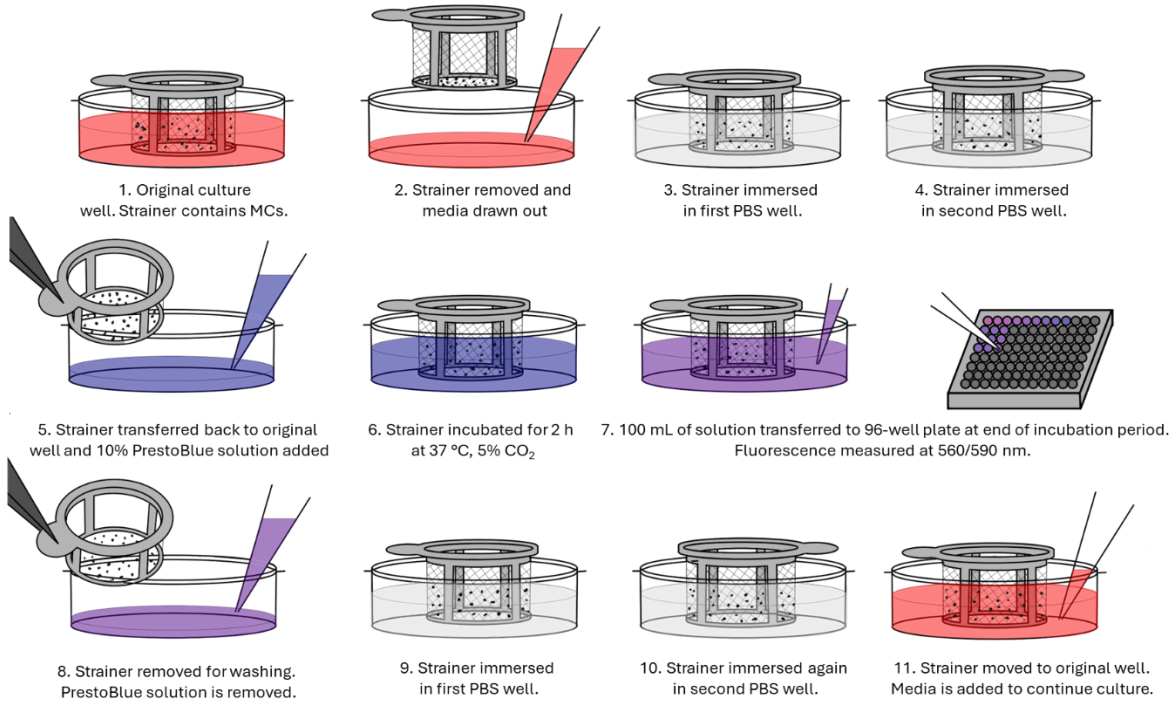

Figure 44: Flow chart showing bMSC proliferation assay on microcarriers.

4.2.8.3 Fluorescence imaging

To image bMSCs on scaffolds and microcarriers, the media was removed and the cells were rinsed twice in DPBS. The cells were then immersed in a 5 mM calcein-AM and 20 mM ethidium homodimer-1 staining solution (LIVE/DEAD™ viability/cytotoxicity assay) for 20 min at room temperature, after which the cells were rinsed twice with DPBS. Calcein-AM was used to stain the cytoplasm of live cells green, ethidium homodimer-1 was used to stain the nucleus of dead cells red. The cells were subsequently fixed in 4% paraformaldehyde and stored in DPBS at 4 °C.

4.2.9 Statistical analysis

Statistical analysis was carried out using Microsoft Excel version 2208 to determine the mean and standard deviation (SD), with a confidence interval of 95%. For biological characterisation, experiments were conducted in triplicates and other experiments were performed with 3 to 12 replicates. All results were displayed as mean $\pm\, SD$ ($n \geq 3$).

The statistical significance of the results was calculated using a one-way ANOVA followed by Tukey's Honestly Significant Difference test. Lower case letters were used to display groups that were statistically different from one another.

4.3 Results & Discussion

4.3.1 Functionalisation and characterisation of silk fibroin non-woven mats

As demonstrated in Chapter III, *section 3.3.3*, electrospun silk fibroin scaffolds could support bMSC attachment, migration and proliferation, but the inert protein fibres lacked strong adhesion, leading to a moderate seeding efficiency and lag phase. Therefore, to improve cell attachment and ultimately increase cell yields, the properties of silk fibroin were modified either by blending the protein with other more functional biomaterials, or physically, using UV-irradiation to induce chemical alterations on the surface of the electrospun fibres.

4.3.1.1 Electrospun blends

Blending biomaterials has the advantage of introducing functional properties to a carrier material affecting its mechanical, chemical and biological properties, while improving nutritional value and consumer acceptance (Sionkowska, 2011). Similarly to the carrier material, the blending material should be non-animal derived, abundant, renewable, easily extractable, food safe, compatible with processing techniques and commercially viable. Psyllium husk, a soluble fibre obtained from the seeds of *Plantago ovata* plants, is a versatile material commonly prescribed for the treatment for gastrointestinal disorders, high cholesterol and even chronic diseases such as colorectal cancer, all of which have been associated with the high consumption of red meat (de Bock *et al*., 2012; Alkandari *et al*., 2021). Psyllium husk is also commonly used in the food industry as a gelling and thickening agent due its high solubility and viscosity (Singh *et al*., 2021) and for landscaping as a low-cost and environmentally friendly natural binder (Guo *et al.*, 2008). Most of the benefits attributed to psyllium husk are owed to its high polysaccharide content, which constitutes 85-90% of its dry weight (Guo *et al*., 2008). Fabricating scaffolds from psyllium husk blends for cultivated meat production, could potentially provide a better microenvironment for cell attachment and proliferation in aqueous culture medium, as well as improve texture of the final product and boost consumer acceptance by making cultivated red meat potentially healthier than the slaughtered kind. The most abundant polysaccharides in psyllium husk are arabinoxylan and glucuronic acid, which represent 79% and 3.8% of its dry weight respectively (Guo *et al*., 2008). Although arabinoxylan is mostly composed of a (1→4)-β-linked xylose pyranose backbone, branched with α-linked arabinose furanose and β-linked xylose on C2 or C3, other carbohydrates such as galactose, mannose and rhamnose also occasionally branch the polysaccharide in psyllium husk (Ren *et al*., 2022).

FTIR was used to chemically characterise psyllium husk powder and silk fibroin-psyllium husk (SF_9PH_2) blends. The whole FTIR spectrum of psyllium husk (**Figure 45A**) displayed a broad band from 3670 cm^{-1}

to 2980 cm^{-1} corresponding to the O-H stretching vibration of bound water, probably caused by moisture in the fibre. The narrow band from 2930-2859 cm^{-1} was assigned to C-H stretching vibration. The peak at 1731 cm^{-1} was assigned to the C=O stretching vibrations of carboxyl groups in glucuronic acid (Singh *et al*., 2021; Ren *et al*., 2020). The absorbance in the band from 1600 cm^{-1} to 1700 cm^{-1} could be the amide I of protein (Singh *et al*., 2021), however the lack of amide II could result from the extremely low overall protein content in psyllium husk (<1%; Guo *et al*., 2008). The peak at 1411 cm^{-1} was assigned to C-H and -CH_2 bending deformation (Singh *et al*., 2021). The peaks at 1371 cm^{-1} and 1315 cm^{-1}, and 1245 cm^{-1} corresponded respectively to -CH_2 wagging and -CH_2 twisting out-of-plane deformations of the arabinose side chains (Wiercigroch *et al*., 2017). In the fingerprinting region (1200-800 cm^{-1}) a large sharp narrow band from roughly 1200 cm^{-1} to 900 cm^{-1}, expanded in **Figure 45B**, characterises the configurations of glycosidic linkages in the arabinoxylan polysaccharide. The peak at 1155 cm^{-1} was assigned to the C-OH stretching vibration of the pyranose rings of the xylose backbone. The peak at 1031 cm^{-1} was assigned to the C-O-C stretching vibrations of glycosidic bonds (Ren *et al*., 2020). A minor shoulder at 1097 cm^{-1} was linked to in-plane-bending of C-OH in arabinose (Wiercigroch *et al*., 2017), while the one at 1073 cm^{-1} was linked to the ring of xylose pyranose (Hong *et al*., 2021). The shoulders at 976 cm^{-1} and 953 cm^{-1} were assigned to the C-CH and C-C-O in-plane bending deformations in galactose (Wiercigroch *et al*., 2017) the third most common carbohydrate in psyllium husk (4.5% dry weight; Guo *et al*., 2008). Finally, the region spanning 900 cm^{-1} to 770 cm^{-1} identifies anomers of pyranose and furanose. The peak at 893 cm^{-1} corresponded to C-O ring stretching vibrations of the β-linkage of pyranoses in the β-linked xylose backbone of arabinoxylan (Wiercigroch *et al*., 2017; Hong *et al*., 2021; Ren *et al*., 2020). The shoulder at 843 cm^{-1} corresponding to C-O ring stretching vibration was assigned to the α-linkage of furanoses in α-linked arabinose side chains (Wiercigroch *et al*., 2017; Hong *et al*., 2021; Ren *et al*., 2020). The minor peaks at 809 cm^{-1} and 778 cm^{-1} have been linked to the CO stretching vibrations in the furanose rings of arabinose (Hong *et al*., 2021; Wiercigroch *et al*., 2017).

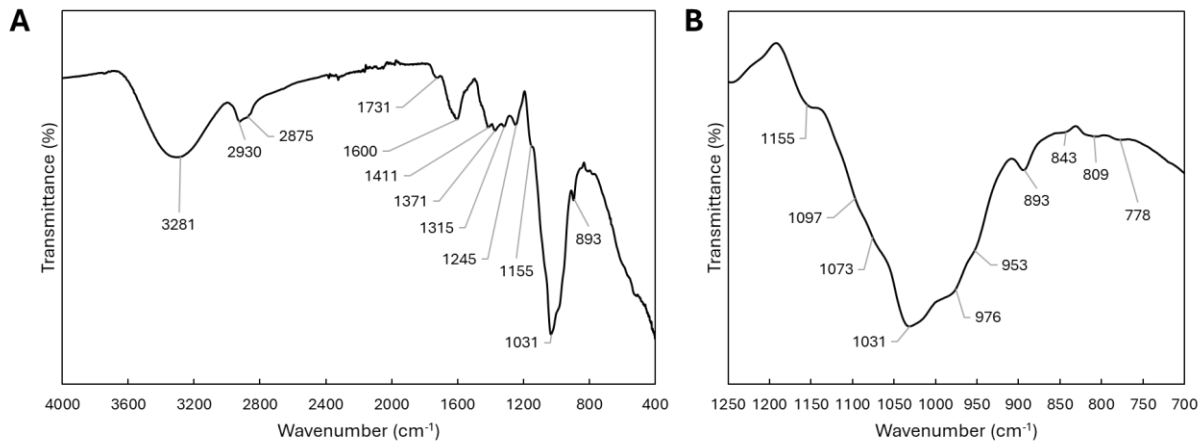

Figure 45: (A) Whole FTIR spectrum of psyllium husk powder, (B) Fingerprint region of the psyllium husk FTIR spectrum.

The FTIR spectra of electrospun SFPH-U blends, displayed in **Figure 46**, were characterised by a reduction in intensity in the amide I (1700-1600 cm^{-1}), II (1600-1500 cm^{-1}) and III (1300-1200 cm^{-1}) bands which correlated with a diminishing relative silk fibroin content in the electrospun blended mats. Likewise, an increase in intensity in the region spanning from 1216 cm^{-1} to 894 cm^{-1} showing an increase in polysaccharide content, correlated with an increase with the proportion of psyllium husk in the blended materials.

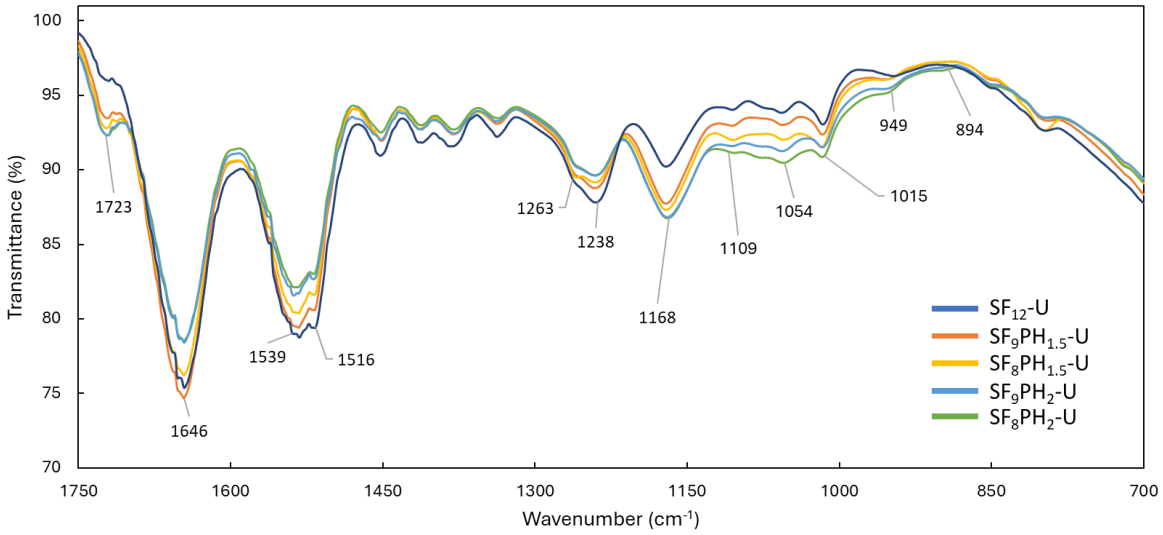

Figure 46: FTIR spectra of electrospun SFPH-U blends.

All preliminary attempts to electrospin psyllium husk alone (without silk fibroin) in water or formic acid were unsuccessful, although a Taylor cone could be observed at 2% (w/w) psyllium husk in formic acid. Despite the presence of the Taylor cone, only large unspun droplets were transferred with no indication of fibre formation on the collector. Increasing the psyllium husk concentration to 3% (w/w) was not feasible as the high viscosity of the polymer solution prevented continuous flow. No

improvement in the electrospinnability of psyllium husk alone was observed when modifying the voltage (10-20 kV), collector distance (7-15 cm) or flow rate (0.05-0.1 mL/h). It has been reported that many charged polysaccharides, while easily hydrated, do not dissolve completely and instead form a weak gelled structure, with a clear yield stress that prevents the sufficient build-up of a pulling force to maintain stable jets and results in the formation of droplets or complete absence of fibres despite the presence of a Taylor cone (Stijnman *et al.*, 2011). Therefore, the inability to electrospin psyllium husk in the present conditions is probably due to its high viscosity and negative electrical charge (Lee *et al*., 2009). When silk fibroin was blended with 1.5-3% (w/w) psyllium husk, electrospinning could be achieved at 15 kV with a 10 cm collector distance, however the percentage of silk fibroin in the polymer solution became a limiting factor in the electrospinnability of SFPH blends. When the silk fibroin concentration was too low (<8%), a Taylor cone formed but electrospraying occurred, and increasing the concentration of the polymer solution by adding psyllium husk did not improve fibre formation. By contrast, when the silk concentration was too high (>9%) the high viscosity of the polymer solution prevented continuous flow. However, continuous electrospinning was only possible when the concentration of silk fibroin was between 8-9% (w/w) and psyllium husk was between 1.5% and 2% (w/w). As shown in **Figure 47,** SFPH-U electrospun mats displayed a wide distribution of homogenous and randomly orientated smooth fibres, that increased in thickness with increasing silk fibroin and psyllium husk content within the limits of electrospinability (8-9% (w/w) silk fibroin and 1.5-2% (w/w) psyllium husk in formic acid; **Table 8**). SF_9PH_2-U (232 ± 79 nm) had the largest fibre diameter of all the SFPH blends approximately 54% larger than that of SF_{12}-U alone (150 ± 49 nm). As for SF_{12}-E mats, the fibre diameter of SF_9PH_2-E fibres increased with EtOH-treatment to 256 ± 70 nm (**Figure 48**).

Table 8: Average fibre diameter of electrospun SFPH-U blends ($n = 100$).

Blend	Average fibre diameter (nm)
$SF_9PH_{1.5}$-U	214.6 ± 58.2[a]
$SF_8PH_{1.5}$-U	127.6 ± 24.3[d]
SF_9PH_2-U	232.0 ± 78.7[a]
SF_8PH_2-U	177.1 ± 48.7[b]
SF_{12}-U	150.2 ± 48.7[c]

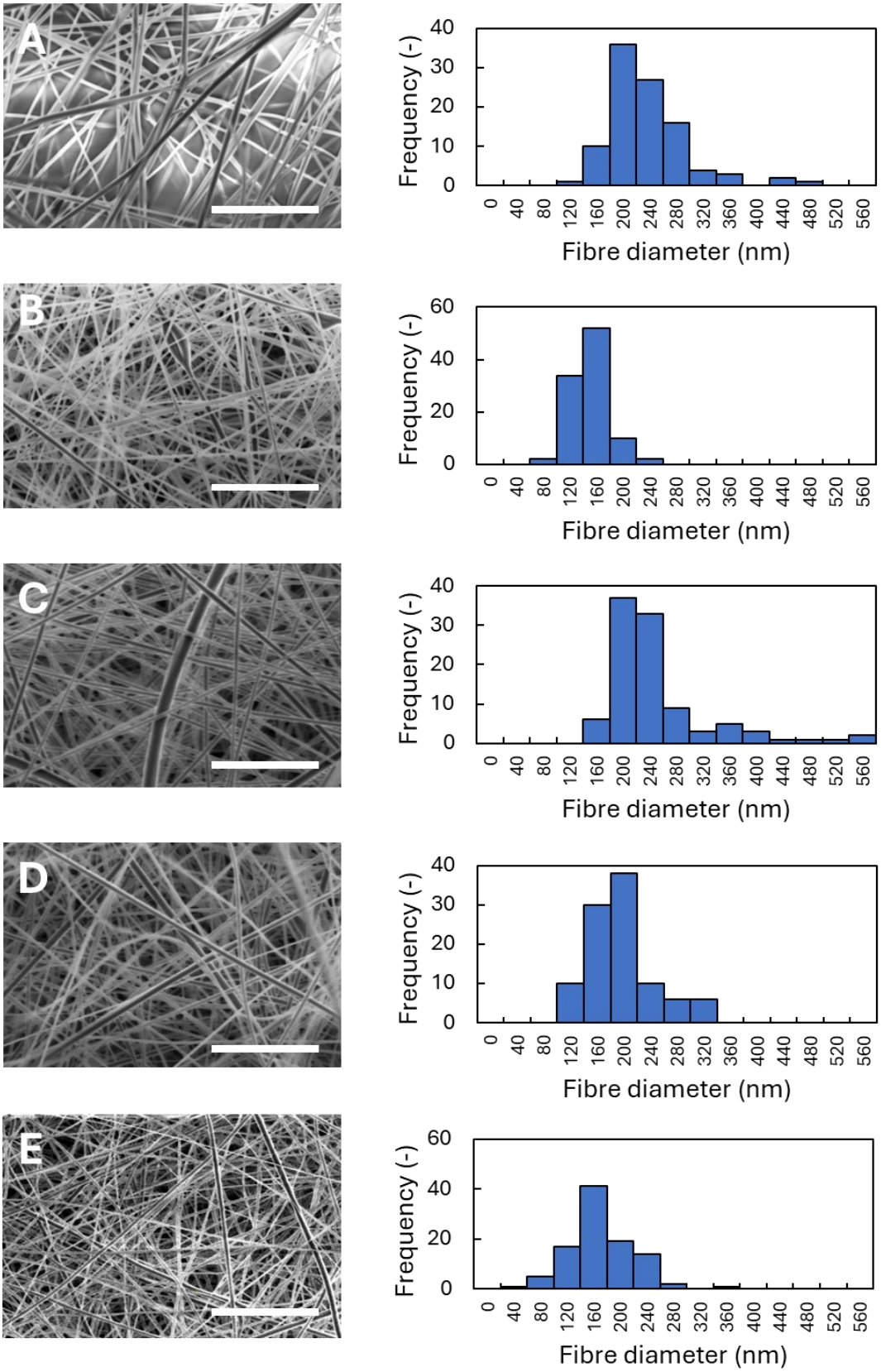

Figure 47: SEMs of untreated silk fibroin/psyllium husk blends (left) and fibre distribution (right; n=100). (A) $SF_9PH_{1.5}$-U, (B) $SF_8PH_{1.5}$-U, (C) SF_9PH_2-U, (D) SF_8PH_2-U, and (E) SF_{12}-U . Scale bar=5 µm.

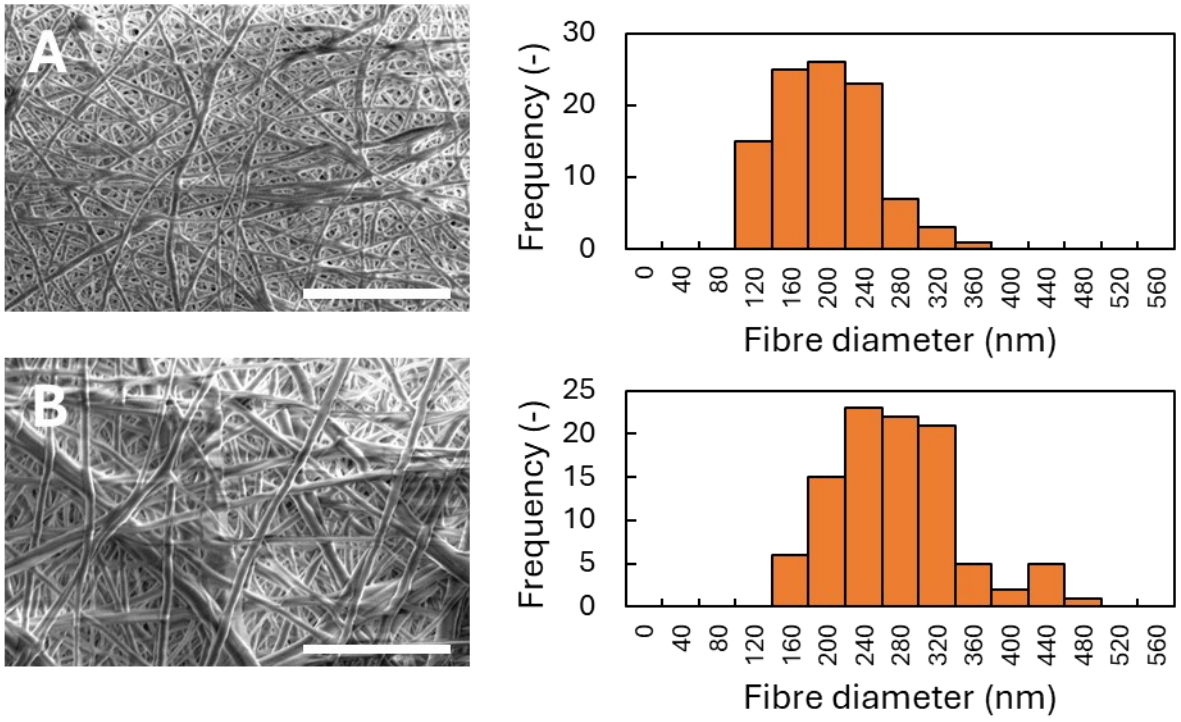

Figure 48: SEMs (left) and fibre distribution (right; n=100) of EtOH-treated (A) SF_{12}-E and (B) SF_9PH_2-E. Scale bar=5 µm.

Zein is a globular protein often used in scaffolds for tissue engineering and cultivated meat research due to its renewability, biodegradibility, electrospinnability, desirable mechanical properties, excellent cytocompatibility and high consummer acceptance (Li *et al*., 2016; Melzener *et al*., 2023; Jeong *et al*., 2024). As a prolamin, serving as storage protein in maize (*Zea mays*), zein is typically extracted from distiller's dry grain, a cheap by-product of the starch and EtOH industry making it extremely abundant and readily available (Keshanidokht *et al*., 2022). Zein is an amphiphilic protein with over half of its amino acids being either hydrophobic or of low polarity, making zein insoluble in water and absolute EtOH, but soluble in formic acid and aqueous ethanol (50-85% w/v; Lawton, 2006; Yao *et al*., 2009; Li *et al*., 2012b; Nonthanum *et al*., 2013). Because of its hydrophilic domains, zein is able to swell in water (Rahman *et al*., 2023). Zein also possesses several beneficial biological features such as its high biocompatibility, ability to promote cell attachment and proliferation via interactions with ECM components (Cui *et al*., 2016; Cardenas Turner *et al*., 2019; Plath *et al*., 2021), and possession of antibacterial properties which could improve the shelf life of zein-containing products (Lu *et* al., 2016; Ghalei *et al*., 2022). On paper, zein appears as a strong contender to silk fibroin as a plant-derived biomaterial for electrospun edible scaffold fabrication, but in fact it suffers from one major drawback: its poor hydrolytic stability. While stabilisation is possible through crosslinking, most agents used (i.e., glutaraldehyde, N-(3-Dimethylaminopropyl)-N'-ethylcarbodiimide or genipin) are

either cytotoxic, unsafe for consumption or detrimental to fibrous structures in electrospun mats (Huang *et al*., 2015). Blending zein and silk fibroin (SFZ blends), with silk fibroin acting as a carrier material, could allow stabilisation of the fibres with 99.8% EtOH, while improving the surface wettability and creating a more suitable microenvironment for cell attachment and proliferation (Plath *et al*., 2021). In addition, zein could enhance consumer perception as non-animal-derived additive with GRAS status, which could also ease regulatory approval as a scaffold material for cultivated meat production (Falsafi *et al*., 2023). Finally, SFZ blends could provide some protection against common food-borne contaminants, such as *Escherichia coli* or *Staphylococcus aureus* (Zhou *et al*., 2014; Lenzuni *et al*., 2024).

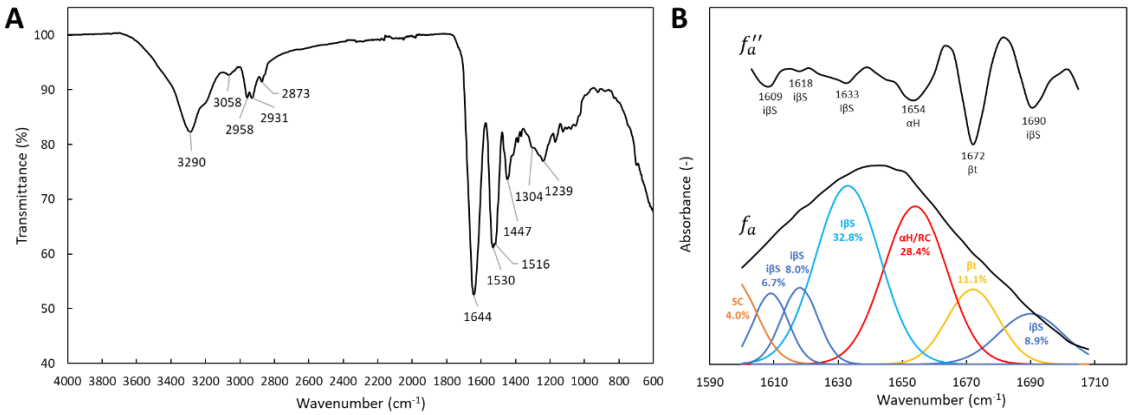

Figure 49:(A) Whole FTIR spectrum of zein protein powder, (B) second derivative (top) and spectral decomposition (bottom) of the amide I (1600-1710 cm-1) of zein protein powder.

FTIR was used qualitatively and quantitatively to characterise the secondary structure of zein protein powder. As shown in **Figure 49A**, a large sharp peak at 3290 cm^{-1} followed by smaller peaks at 3058 cm^{-1} were assigned to N-H stretching vibrations in the amide A and B respectively. The peaks at 2958 cm^{-1}, 2931 cm^{-1} and 2873 cm^{-1} were assigned to C-H stretching vibrations in aliphatic compounds. For the amide I (C=O stretching vibrations), II and III (C-N stretching vibrations and N-H in-plane bending deformations) bands, the peaks at 1644 cm^{-1}, 1530 cm^{-1} and 1239 cm^{-1} were characteristic of zein's α-helix and random coil conformations (Erickson *et al.*, 2020; Sadat *et al*., 2022). Finally, a relatively narrow peak at 1447 cm^{-1} was assigned to N-H in-plane bending deformations (Cardenas Turner *et al*., 2019). As shown in **Figure 49B**, second derivative analysis and curve fitting was used to measure the relative conformations in the secondary structure of zein protein revealing a mostly crystalline structure formed of α-helices and intramolecular β-sheets.

Electrospinning zein on its own (Z_{25}) led to a shift from 1644 cm^{-1} to 1652 cm^{-1} in the amide I and from 1530 cm^{-1} to 1541 cm^{-1} in the amide II bands indicating a reduction in β-sheets and increase in α-helix and random coil conformations (**Figure 50A**). This conformational shift was caused by formic acid

cleaving hydrogen bonds in the intra-molecular and inter-molecular β-sheets of the globular protein, allowing its molecular chains to dissolve and entangle for successful electrospinning. After EtOH-treatment, peaks in the amide I and II shifted back to 1645 and 1530 respectively, indicating a conformational shift back to zein's crystalline β-sheet- and α-helix-dominant structure (**Figure 50B**).

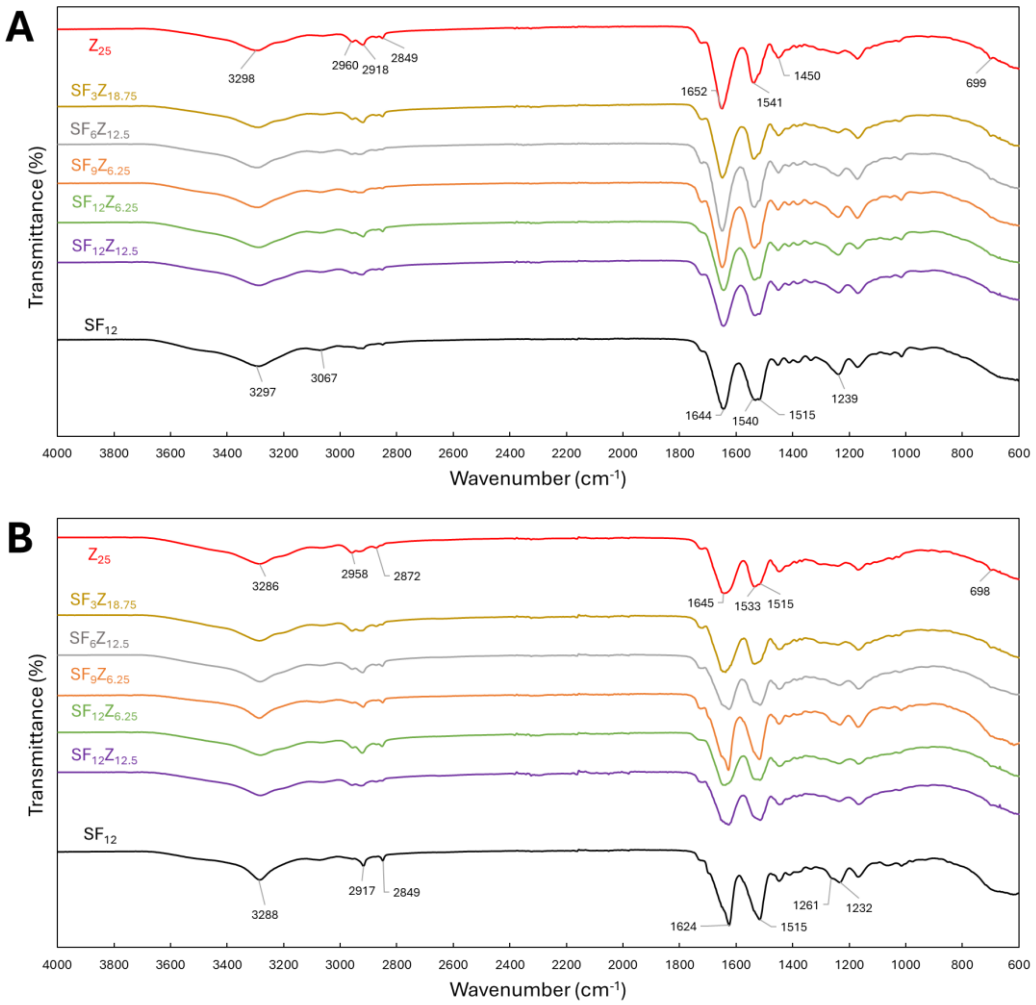

Figure 50: Whole normalised FTIR spectra of SFZ blends before (A) and after (B) EtOH-treatment.

An increase in β-sheet crystallinity was observed after EtOH-treatment for all SFZ electrospun blends (**Figure 51**), marked by a strong increase in inter-molecular β-sheets. This was further observed by an increase in brittleness of the EtOH-treated SFZ samples (with a Young's modulus of 671.1 ± 83.4 MPa and ultimate tensile strength of 7.6 ± 1.3 MPa for $SF_{12}Z_{6.25}$-E, see ***Appendix C, Figure S12***). Although silk fibroin displayed a similar level of crystallinity to zein, in terms of total β-sheets, the proportion of inter-molecular β-sheet (of the total β-sheet content) was considerably higher in SF_{12}-U (36%) and SF_{12}-E (57%) than in Z_{25}-U (11%) and Z_{25}-E (23%). Despite this, no trend was observed between the crystallinity levels or composition of SFZ blends in relation to their silk fibroin to zein ratio.

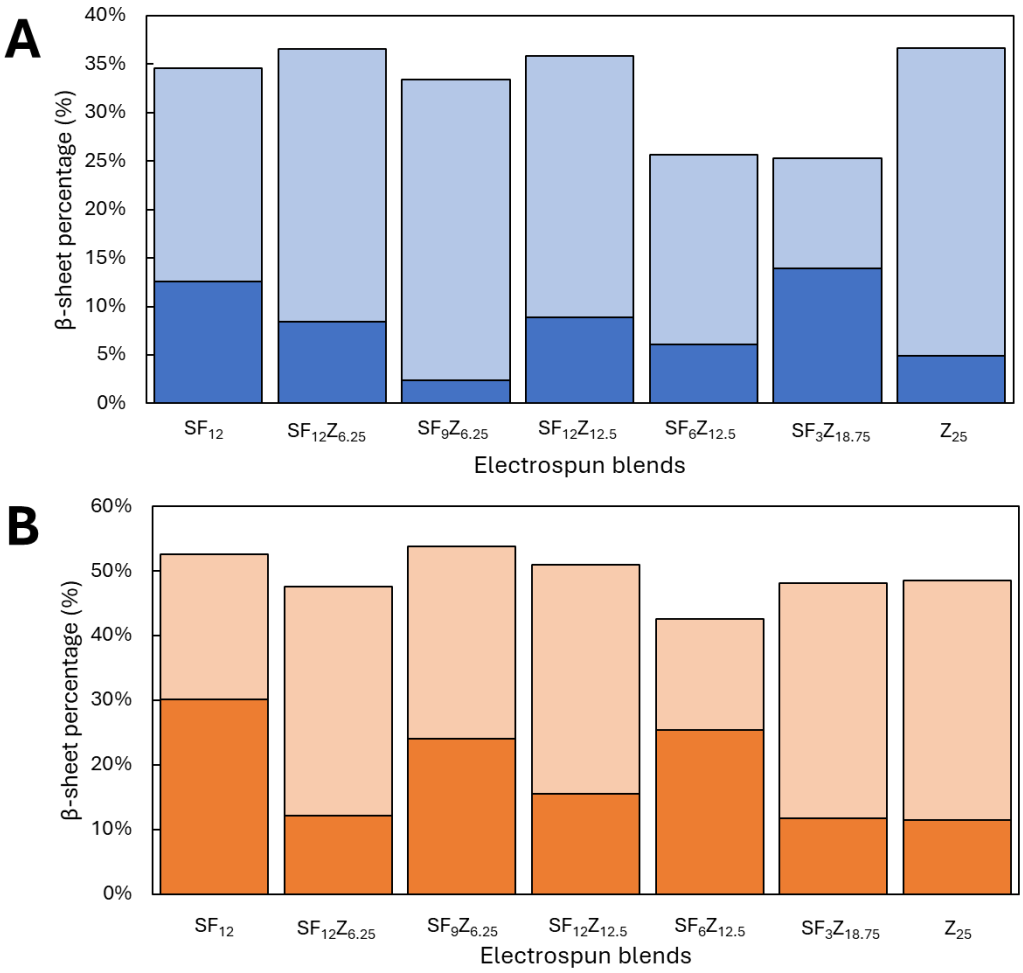

*Figure 51: Effects of zein blending with silk fibroin on β-sheet crystallinity (whole bar, with inter-molecular β-sheets (dark) and intra-molecular β-sheets (light)) in (A) untreated and (B) EtOH-treated electrospun mats. Blends were ordered from left to right by increasing overall zein content. For detailed results see **Appendix C, Figures S10** and **S11**).*

On its own, zein (Z25) was easy to electrospin and no optimisation was needed to obtain thick, uniform, and bead-free randomly orientated fibres at voltages around 15-20 kV and 10-15 cm collector distance. Therefore a 15 kV and 10 cm collector distance were chosen for all SFZ blends to match the silk fibroin electrospinning parameters (**Figure 52**). Zein produced significantly thicker fibres than silk fibroin, with a diameter of 259 ± 44 nm compared to 160 ± 48 nm, respectively. The SF3Z18.75-U blend displayed a bimodal distribution of fibres with larger fibres (>170 nm; n=24) and thinner fibres (<169; n=76), averaging 248 ± 60 nm and 67 ± 33 nm, respectively. The larger fibres of the SF3Z18.75-U blend were similar in size to those of Z25 which could indicate a lack of miscibility in between silk fibroin and zein at those ratios. In addition, the smaller fibres could be caused by silk fibroin producing its own fibres off the zein polymer jets, in which case zein would be acting as the carrier material for silk fibroin. When increasing the silk fibroin concentration and further lowering the zein concentration, the fibre size distribution narrowed significantly, and a normal distribution was observed. However, when adding zein to 12% silk fibroin to form SF12Z6.25-U and SF12Z12.5-U blends, the average fibre

diameter and distribution increased considerably reaching 416 ± 141 nm and 687 ± 122 nm, respectively. No obvious correlation between the silk fibroin to zein ratio and fibre diameter could be identified. Yao et al. (2009) showed a fibre diameter reduction in zein blends with silk fibroin at 2:1, 1:1 and 1:2 ratios, although their results seemed to correlate with a strong reduction in the overall polymer concentration used for each blend which would naturally decrease fibre diameter independently of the silk fibroin or zein ratio (Yao et al., 2009; Haider et al., 2018).

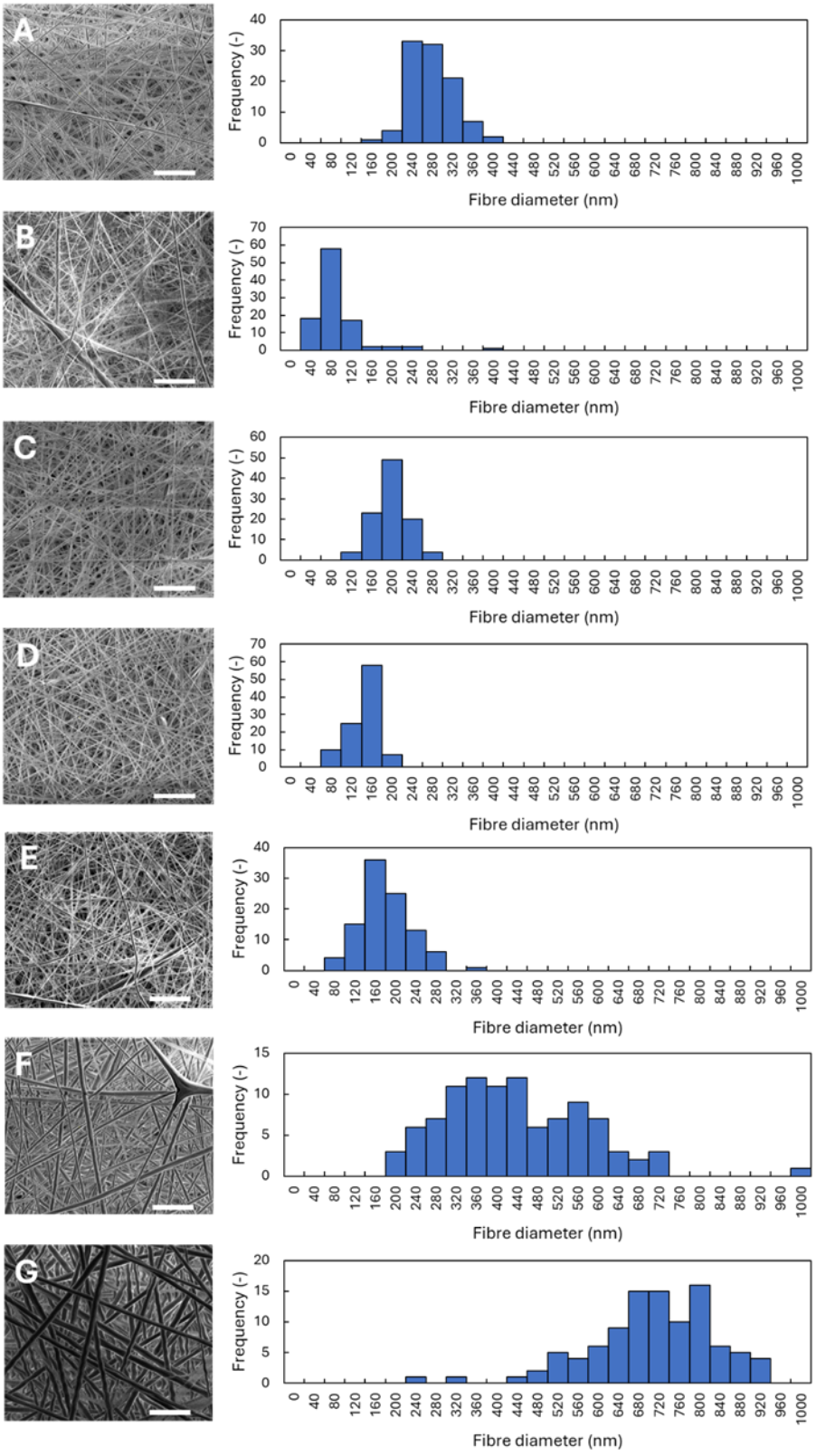

Figure 52: SEM images (left) and fibre size distribution (right; n=100) of untreated silk fibroin/zein (SFZ) needle electrospun blends. (A) Z_{25}-U, (B) $SF_3Z_{18.75}$-U, (C) $SF_6Z_{12.5}$-U, (D) $SF_9Z_{6.25}$-U, (E) SF_{12}-U, (F) $SF_{12}Z_{6.25}$-U and (G) $SF_{12}Z_{12.5}$-U. Scale bar = 5 µm.

Immersing electrospun Z_{25}-U mats in 99.8% (v/v) EtOH immediately caused them to visibly shrink, harden and become very brittle after drying, making them unsuitable for handling and tissue

engineering applications. SEM results (**Figure 53A**) showed a total disappearance of the nanofibrous structure of Z_{25}-E and instead displayed a film-like surface. While zein does not dissolve in 100% EtOH, self-assembly occurs, causing a conformational shift and transition from fibrous structures to other complex spatial states (Erickson *et al*., 2022). Increasing the silk fibroin content in SFZ blends caused patchiness in the EtOH-treated samples where some intact fibres were seen engulfed in a swollen and film-like substance (**Figure 53B,C**). This was most evident in $SF_6Z_{12.5}$-E (**Figure 53C**) where patches occupied approximately half of the mat surface. In samples with higher silk fibroin content (>9% (w/w); **Figure 53D-G**) the fibres appeared swollen but distinctly visible, as is characteristic of stabilised silk fibroin. These results demonstrate the reliance on carrier materials when electrospinning zein blends, with zein acting as a hydrogel-like material, absorbing water and swelling to the point of affecting fibre morphology and even damaging the fibrous network in highly concentrated blends. Therefore, a sufficient concentration of silk fibroin is required in the polymer solution to form stronger bonds between silk fibroin and zein, allowing the blended polymer solution to produce uniform jets during electrospinning and displaying composite fibres that exhibit large randomly aligned nanofibers.

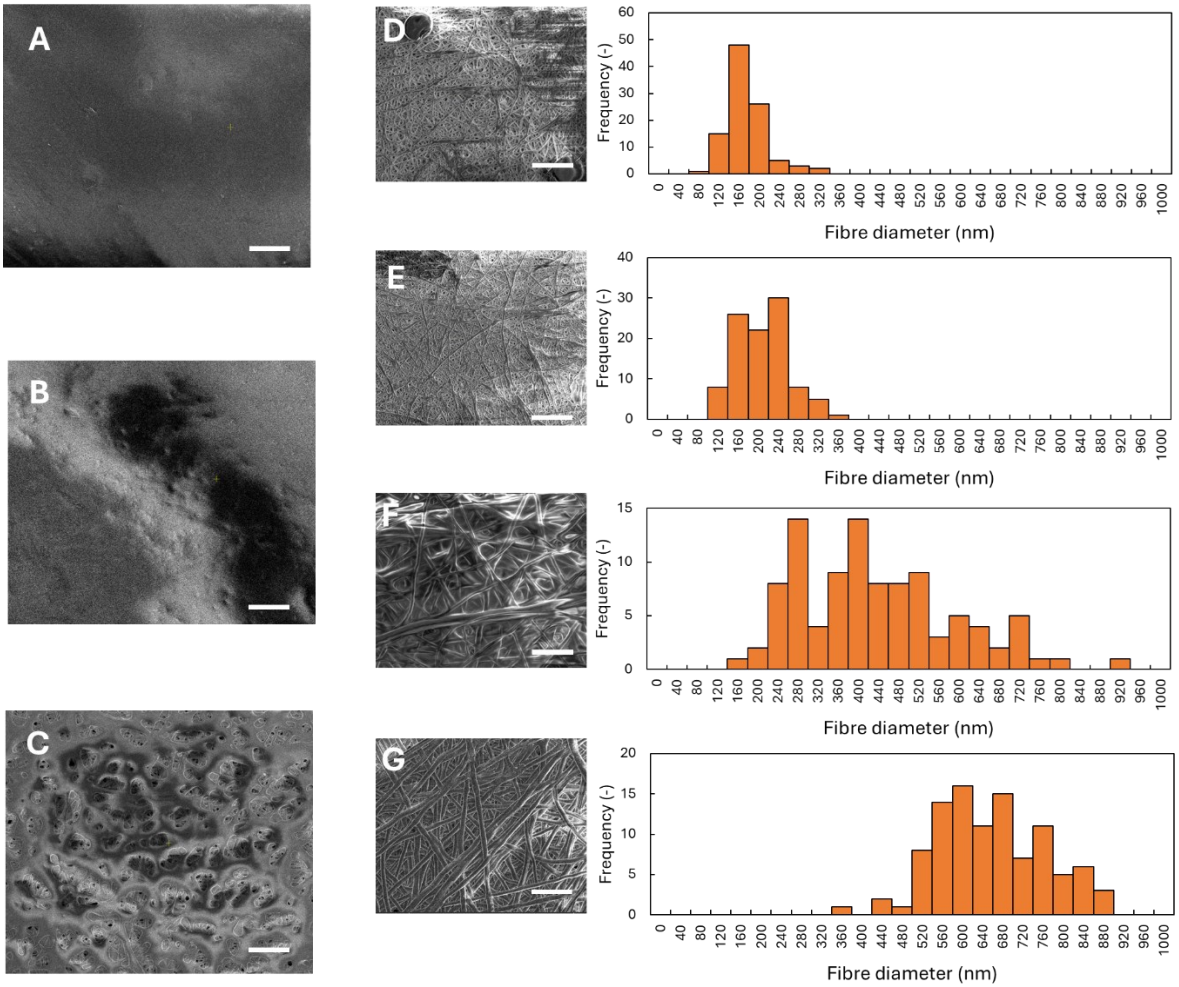

Figure 53: SEM images (left) and fibre distribution (right; n=100) of EtOH-treated silk fibroin/zein (SFZ) needle electrospun blends. (A) Z_{25}-E, (B) $SF_3Z_{18.75}$-E, (C) $SF_6Z_{12.5}$-E, (D) $SF_9Z_{6.25}$-E, (E) SF_{12}-E, (F) $SF_{12}Z_{6.25}$-E and (G) $SF_{12}Z_{12.5}$-E. Scale bar =5 µm.

As shown in **Figure 54**, a significant increase (p<0.05) in fibre diameter was observed following EtOH-treatment in $SF_9Z_{6.25}$-E and in SF_{12}-E from 125 ± 29 nm and 160 ± 46 nm to 157 ± 39 nm and 179 ± 51 nm, respectively. In $SF_{12}Z_{6.25}$-E fibre diameter was unaffected and in $SF_{12}Z_{12.5}$-E it even decreased slightly from 417 ± 141 nm and 687 ± 121 nm to 424 ± 164 nm and 637 ± 105 nm, respectively. All further characterisation experiments were carried out on $SF_9Z_{6.25}$-E, $SF_{12}Z_{6.25}$-E and $SF_{12}Z_{12.5}$-E as these were the only mats that remained intact following EtOH-treatment.

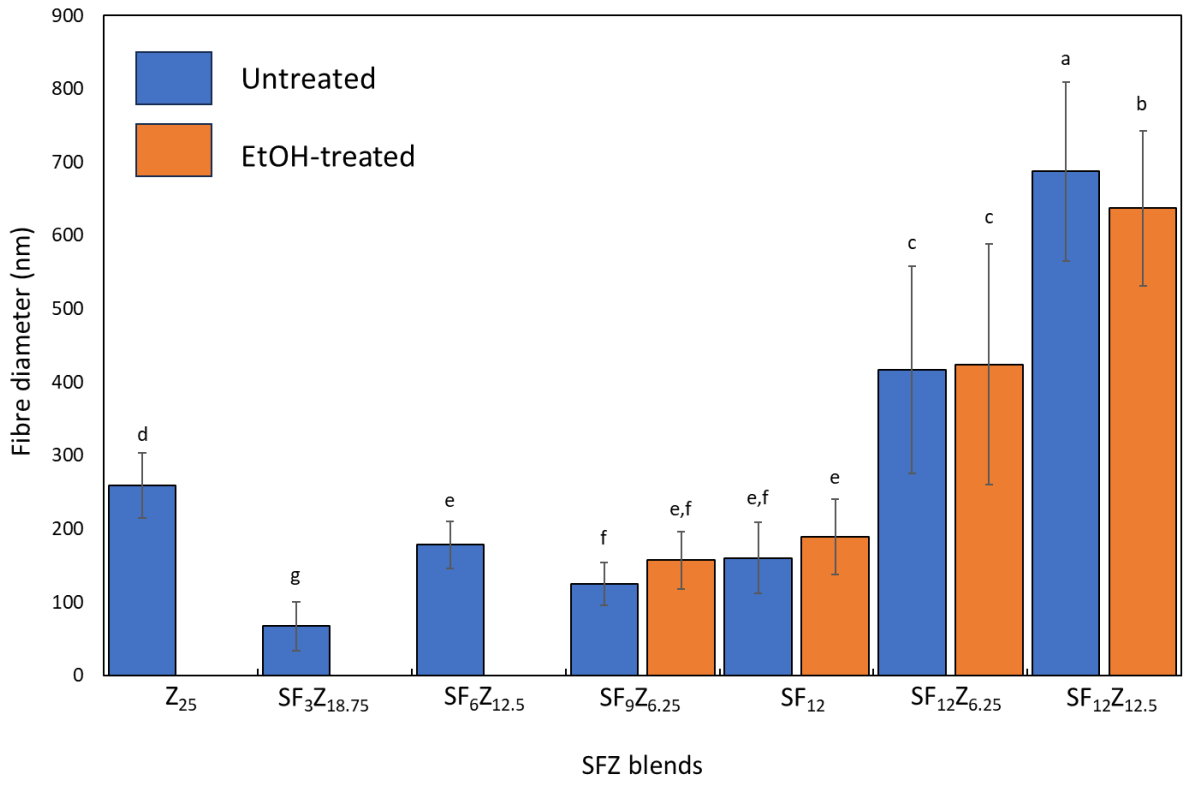

Figure 54: Average fibre diameter before (b*lue bars*) and after (*orange bars*) EtOH-treatment *of electrospun mats created from silk fibroin and zein blends*. Results displayed as mean ± SD (n = 100 fibres)*, with different lower-case letters indicating statistical differences ($p<0.05$). For Z_{25}, $SF_3Z_{18.75}$ and $SF_6Z_{12.5}$ no results were produced for EtOH-treated samples.*

4.3.1.2 UV-functionalisation

Moving away from the blending strategies, silk fibroin electrospun mats were also functionalised post-processing using UV-irradiation, a common method for modifying the surface properties of electrospun proteins (Sionkowska and Planeka, 2011; Li *et al*., 2012a; Sionkowska *et al*., 2014; Girao *et al*., 2019). In addition, UV functionalisation is generally considered as a cheap and environmentally friendly alternative to chemical crosslinking agents (Girao *et al*., 2019), and UV radiation is commonly used in food processing systems (Gomez-Lopez *et al*., 2021; Levi *et al*., 2022). By emitting an intense monochromatic light in the material's UV absorption range (10-400 nm), high energy photons can induce photochemical reactions on the material's surface, improving wettability without significantly affecting bulk properties (Li *et al*., 2012a; Duque Sanchez *et al*., 2016). UV radiation has been widely used in the textiles industry for coloration and filtration purposes (Rastogi *et al*., 2019; Hu *et al*., 2020) and more recently in tissue engineering for scaffold functionalisation (Uchiyama *et al*., 2014; Girao *et al*., 2019; Porras Hernández *et al*., 2020). Silk fibroin has been shown to have a strong absorption peak around 270-275 nm in the UV-C range (100-280 nm) (Sionkowska and Planeka, 2011; Girao *et al*., 2019). While the effects of UV-C on silk fibroin have been investigated on films and untreated

electrospun fibres (Sionkowska *et* al., 2014; Girao *et al*., 2019), its effects on cell attachment on EtOH-treated electrospun silk fibroin scaffolds have not.

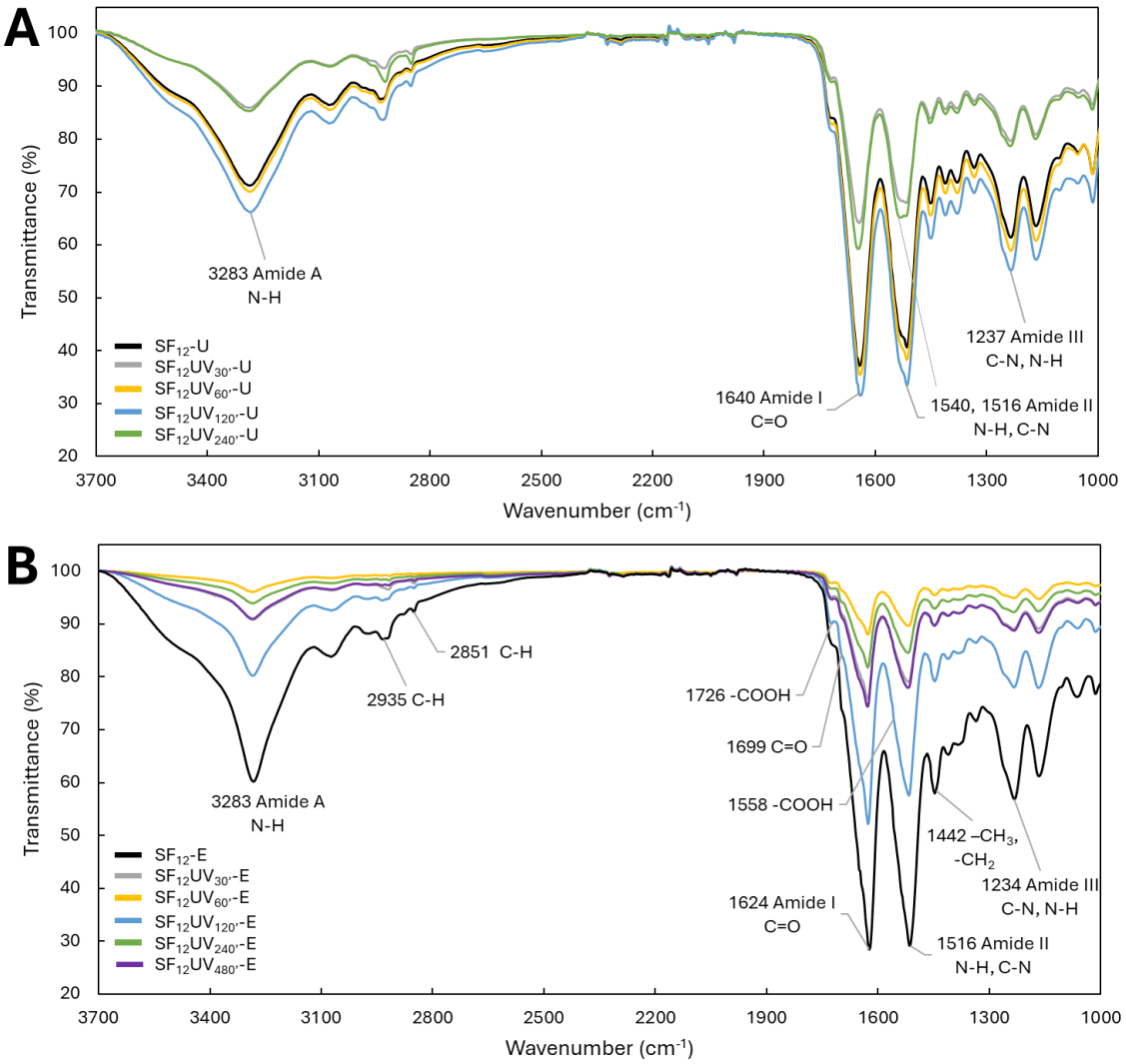

Figure 55: Baseline corrected, non-normalised, FTIR spectra of (A) SF_{12}UV-U and (B) SF_{12}UV-E following a 0 to 480 min UV-irradiation time ($\lambda = 254$ nm). No spectrum was presented for $SF_{12}UV_{480'}$-U as samples disintegrated preventing FTIR analysis.

FTIR was used to characterise UV-irradiation photochemical modifications to the molecular and secondary structure of SF_{12}UV-U (**Figure 55A**) and SF_{12}UV-E (**Figure 55B**). The spectra of the UV-irradiated samples were characteristic of electrospun SF_{12}-U and SF_{12}-E with only minor occasional band shifts (≤3 cm^{-1}). Both SF_{12}UV-U and SF_{12}UV-E presented broad bands at 3283 cm^{-1} corresponding to N-H bending (Amide A) trailed by minor peaks at 2935 cm^{-1} and 2581 cm^{-1} relating to the C-H stretching of aromatic rings. Similarly, there were small shifts for the Amide I (C=O stretching), Amide II (N-H bending and C-N stretching) and Amide III (C-N stretching and N-H bending) peaks for SF_{12}UV-U

(at 1640 cm^{-1}, 1540 cm^{-1} and 1516 cm^{-1}, and 1237 cm^{-1}, respectively; **Figure 55A**), and for SF_{12}UV-E (at 1627 cm^{-1}, 1516 cm^{-1}, and 1234 cm^{-1}, respectively; **Figure 55B**).

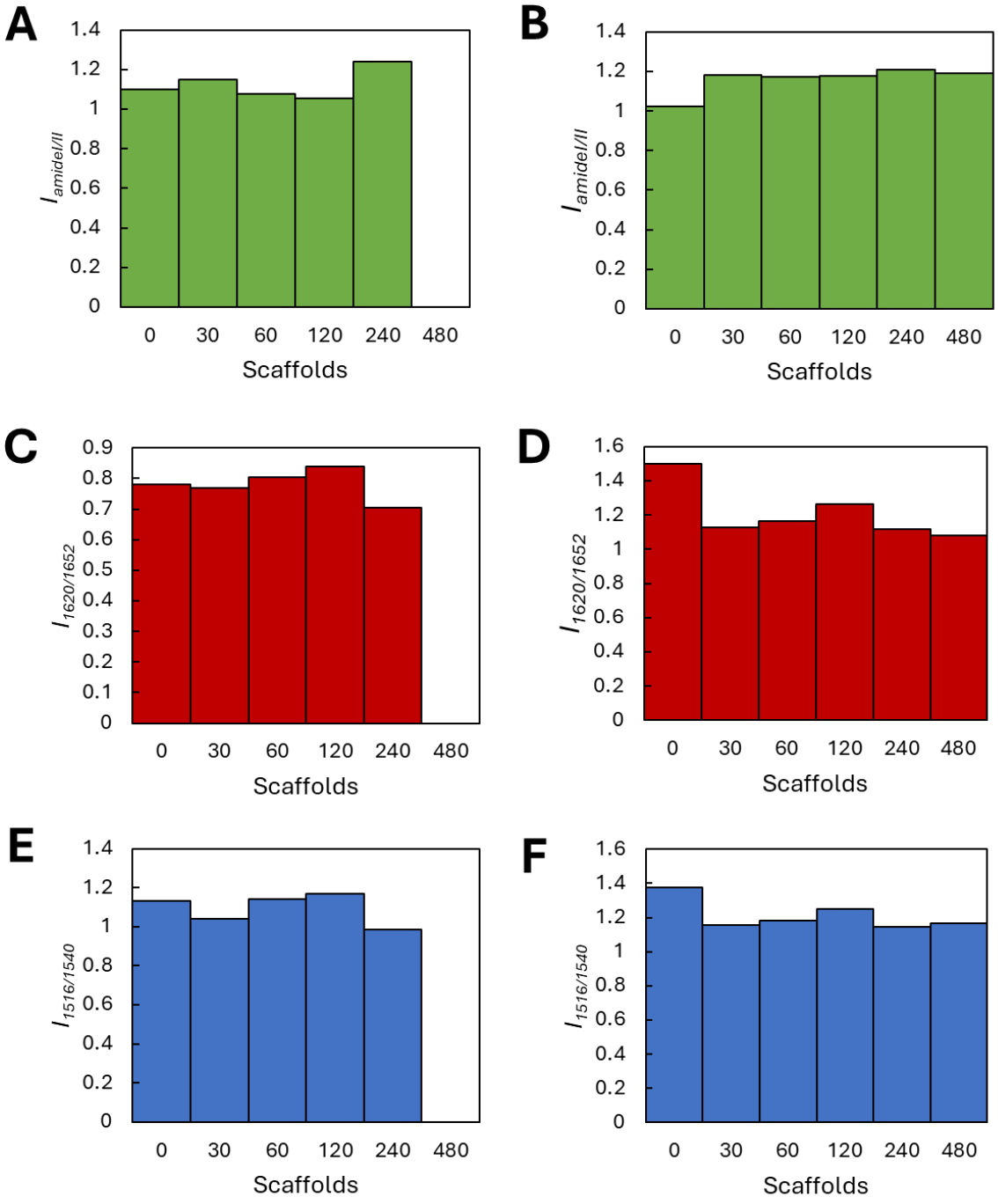

Figure 56: Chemical changes of silk fibroin electropsun mats following exposure to UV for up to 480 min. Estimated degradation of amide I (C=O stretching) to amide II (N-H bending and C-N stretching) for (A) untreated mats SF_{12}UV-U and (B) following EtOH treatment SF_{12}UV-E. Crystallinity indexes of the amide I in (C) SF_{12}UV-U and (D) SF_{12}UV-E, and for the amide II for (E) SF_{12}UV-U and (F) SF_{12}UV-E. No results were collected for $SF_{12}UV_{480'}$-U as samples disintegrated preventing FTIR analysis.

Due to the ability of UV-C to degrade O-H, C-H, C-N, N-H, C-C and S-S covalent bonds, normalisation was not possible and quantitative analysis of the spectra had to be done using absorbance intensity ratios (Kumar *et al*., 2021; Koperska *et al*., 2014). The ratio $I_{amide\ I/II}$ of the maximum intensity of the Amide I (~1640 cm^{-1} for SF_{12}UV-U or ~1627 cm^{-1} for SF_{12}UV-E) and the Amide II (1516 cm^{-1} in both SF_{12}UV-U and SF_{12}UV-E) bands, provides some useful information when studying the degradation of silk fibroin (Koperska *et al*., 2014). In SF_{12}UV-U, the $I_{amide\ I/II}$ remained constant until 240 min of UV exposure (**Figure 56A**) at which point a small increase of the amide I (C=O) was observed. In addition, the crystallinity indexes $I_{1620/1652}$ comparing the ratio of β-sheets to random coils in the amide I showed a reduction in β-sheets from 240 min of irradiation (**Figure 56C**). In contrast, in SF_{12}UV-E, UV-irradiation caused a slight increase in $I_{amide\ I/II}$ within the first 30 min of exposure, which remained constant up to 240 min (**Figure 56B**). This also resulted in a reduction of the crystallinity index $I_{1627/1640}$ of the amide I band (**Figure 56D**). These results therefore suggest that UV irradiation damages β-sheets with prolonged exposure time leading to reorganisation into random coils. As such extending the UV irradiation time led to a reduction in crystallinity even though no major shift was observed on the FTIR spectra of SF_{12}UV-U and SF_{12}UV-E. The reduction in crystallinity is thought to result from cleavage of the hydrogen bonds linking polypeptide chains resulting from extended UV-irradiation time (Gong *et al*., 2024).

As shown in **Figure 57**, the relative absorbance at specific wavenumbers gave information on the degradation and creation of functional groups from increased UV-C exposure to SF_{12}UV-E mats. The relative absorbance at 3283 cm^{-1} and 1442 cm^{-1} (**Figure 57A,F**) corresponded to a progressive reduction of N-H, $-CH_3$ and $-CH_2$ bonds, indicating damage to the primary structure of silk fibroin with increased UV-irradiation time (Matreveli *et al*., 2010). In contrast, the relative absorbance at 1726 cm^{-1} and 1699 cm^{-1} (**Figure 57D,E**) showed a progressive increase in C=O bonds resulting from the creation of carboxyl (-COOH) photoproducts with increased UV-irradiation time (Sionkowska *et al.,* 2011). Interestingly, the relative absorbance at 2935 cm^{-1} and 2851 cm^{-1} (**Figure 57B,C**) slightly increased within the first 30 minutes of UV exposure but then dropped at around 60 minutes, after which it increased slowly with UV-irradiation time. This could indicate damage to hydrogen bonds and the subsequent creation of -COOH photoproducts (Koperska *et al*., 2014).

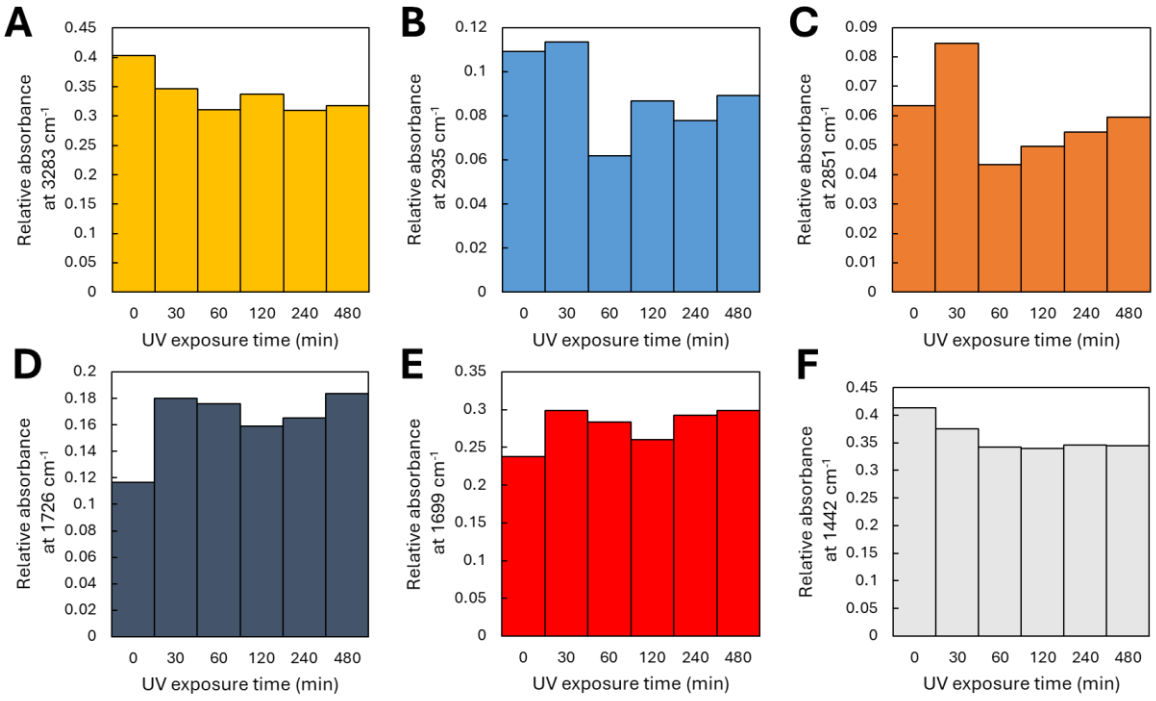

Figure 57: Relative absorbance at (A) 3283 cm^{-1}, (B) 2935 cm^{-1}, (C) 2851 cm^{-1}, (D) 1726 cm^{-1}, (E) 1699 cm^{-1}, (F) 1558 cm^{-1}, (G) 1442 cm^{-1} following increasing UV irradiation exposure in SF_{12}UV-E mats.

The formation of new C=O and -COOH groups by photooxidation has been confirmed in the literature by multiple studies (Koperska *et al.,* 2014; Lee *et al*., 2021; Gong *et al*., 2024). In contrast to the results obtained with SF_{12}UV-U, which showed no significant change from UV-irradiation before 240 min, Sionkowska and Planeka (2011) showed significant reductions for all amide bands from 30 min of UV exposure that continued to decrease with extended UV exposure time (λ=254 nm) in Silk I dominant films. It is worth noting however, that the FTIR spectra in the study was not showing any change in other expected areas translating to the presence of photoproducts, and therefore the apparent reduction in all amide bands could have been the result of inappropriate normalisation (Sionkowska and Planeka, 2011).

Due to the absence of shift from Silk I to Silk II in SF_{12}UV-U, further EtOH-treatment was required to stabilise the electrospun scaffolds. To investigate the effects of EtOH-treatment on previously UV-irradiated electrospun samples, FTIR was carried out on $SF_{12}UV_{240'}$-U, after which the sample was treated in EtOH for 20 min ($SF_{12}UV_{240'}$-U→E) and analysed using FTIR once again. The results presented in **Figure 58A** showed an expected shift from 1649 cm^{-1} to 1627 cm^{-1} in the Amide I band corresponding to a transition from Silk I to Silk II conformations. This is further confirmed by a reduction in the intensity of the peaks at 1540 cm^{-1} and 1230 cm^{-1} indicating a reduction in random coils. However, quantitative analysis of the relative intensity ratios (**Figure 58B-D**) showed a closer similarity between $SF_{12}UV_{240'}$-U→E and SF_{12}-E than between $SF_{12}UV_{240'}$-U→E and $SF_{12}UV_{240'}$-E, as $SF_{12}UV_{240'}$-U→E and

SF_{12}-E shared similar crystallinity indexes in both the amides I and II bands and $I_{Amide\ I/II}$ ratios. This may have been due to the dehydrative effect of EtOH, absorbing water molecules from the newly formed functional groups and hydrophobic amino acids, repairing broken covalent bonds in tyrosine, phenylalanine, alanine and glycine and enhancing crystalline domains and β-sheet formation (Johari *et al*., 2020; Kaewpirom and Boonsang, 2020). Consenquently, UV functionalisation should always be performed after EtOH-treatment.

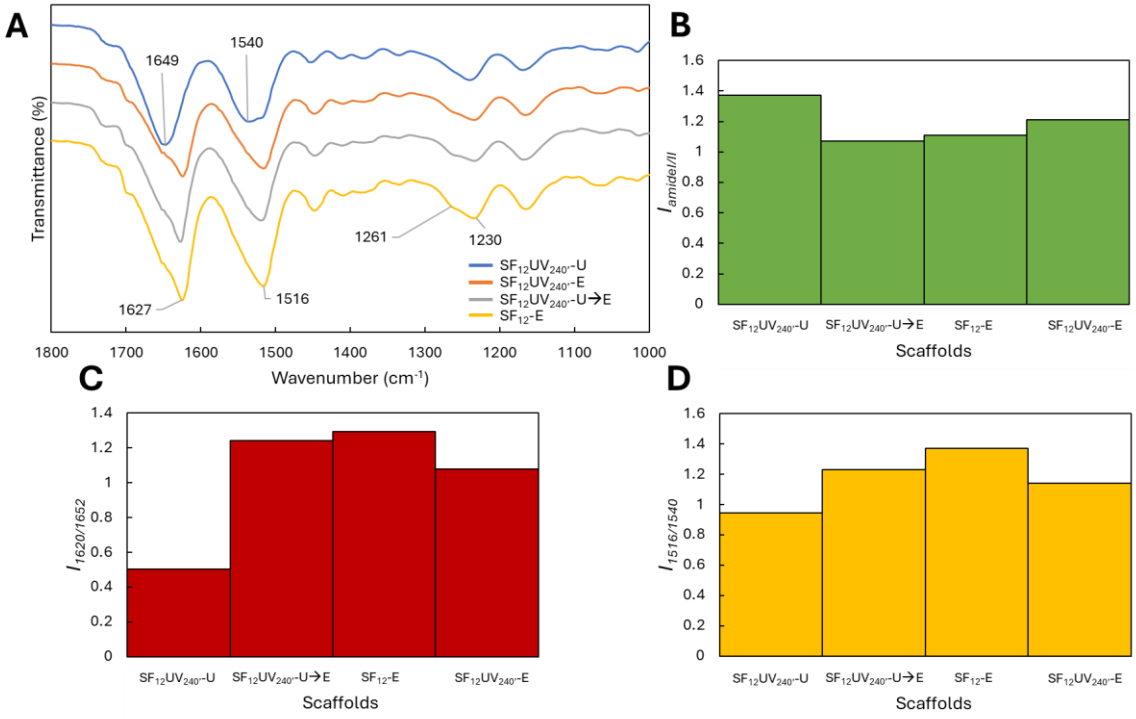

Figure 58: Comparison of the effects of EtOH-treatment on electrospun silk fibroin before and after UV-irradiation. (A) Baseline adjusted non-normalised FTIR spectra of EtOH-treated SF_{12}-E without UV irradiation, UV-irradiated untreated $SF_{12}UV_{240'}$-U and EtOH-treated $SF_{12}UV_{240'}$-E mats, and UV-irradiated untreated silk fibroin subsequently treated with EtOH $SF_{12}UV_{240'}$-U→E. (B) Degradation indicator $I_{Amide\ I/II}$, (C) crystallinity index of the amide I $I_{1620/1652}$ and (D) crystallinity index of the amide II $I_{1516/1540}$.

4.3.2 Cell culture on functionalised scaffolds

To measure the impact of blending and physical functionalisation strategies on electrospun silk fibroin scaffolds, PrestoBlue™ assays were conducted to monitor bMSC attachment and proliferation on SF_9PH_2, various SFZ blends and SF_{12}UV scaffolds over a 7-day period to encompass the whole exponential growth phase (**Figure 59**). Blending silk fibroin with psyllium husk (**Figure 59A**) resulted in a reduction in bMSC proliferation growth rate reduction and an increased doubling time compared to the SF_{12}-E control, from 42.3 ± 1.8 h to 50.5 ± 4.8 h (**Figure 60B**) with no change in apparent cell attachment or seeding efficiency. In contrast, zein blends had a neutral to positive effect on bMSC proliferation which appeared to associate with the fibre diameter of the scaffolds (**Figure 59B**). Indeed,

the zein blends with the largest fibres, $SF_{12}Z_{6.25}$-E (424 ± 164 nm) and $SF_{12}Z_{12.5}$-E (637 ± 105 nm), significantly outperformed those with smaller fibres $SF_9Z_{6.25}$-E (157 ± 39 nm) and SF_{12}-E (179 ± 51 nm) in terms of bMSC growth rate and proliferation. In addition, no significant difference in cell proliferation was measured on day 7 between $SF_{12}Z_{6.25}$-E and $SF_{12}Z_{12.5}$-E, nor between $SF_9Z_{6.25}$-E and SF_{12}-E, supporting this theory. An increase in scaffold porosity may have stemmed from increased fibre diameter, facilitating O_2 and nutrient diffusion and roughness, thereby increasing cell attachment for $SF_{12}Z_{6.25}$-E and $SF_{12}Z_{12.5}$-E (Milleret *et al*., 2012). In addition, the $SF_{12}Z_{6.25}$-E blend displayed on day 1 a seeding efficiency above 100% indicating that the blend significantly promoted cell attachment and proliferation. As a result on day 7, bMSCs grown on $SF_{12}Z_{6.25}$-E electrospun scaffolds demonstrated 31.3 ± 7.4 fold increase, almost double that of bMSC grown on SF_{12}-E at 15.8 ± 1.9 (**Figure 60D**). Finally, UV-functionalisation had a detrimental effect on bMSC proliferation on SF_{12}UV scaffolds that was significantly worsened with increasing UV exposure time (p<0.05), although the considerable reduction for $SF_{12}UV_{240'}$-E was not statistically significant (p>0.05). Surprisingly, UV functionalisation had the opposite effect of what was expected as the increase in -COOH functional groups has been shown to promote cell attachment and proliferation (Li *et al*., 2005; Koperska *et al*., 2014). This deteriorating effect may be subject to the overabundance of negatively charged functional groups repulsing negatively charged cells, and hindering cell attachment and proliferation. Indeed, Yuan *et al*. (2015) showed charge repulsion on carboxylated PCL microcarriers which was attributed to the anionically charged -COOH and led to reduction in endothelial cell attachment (Yuan *et al*., 2015).

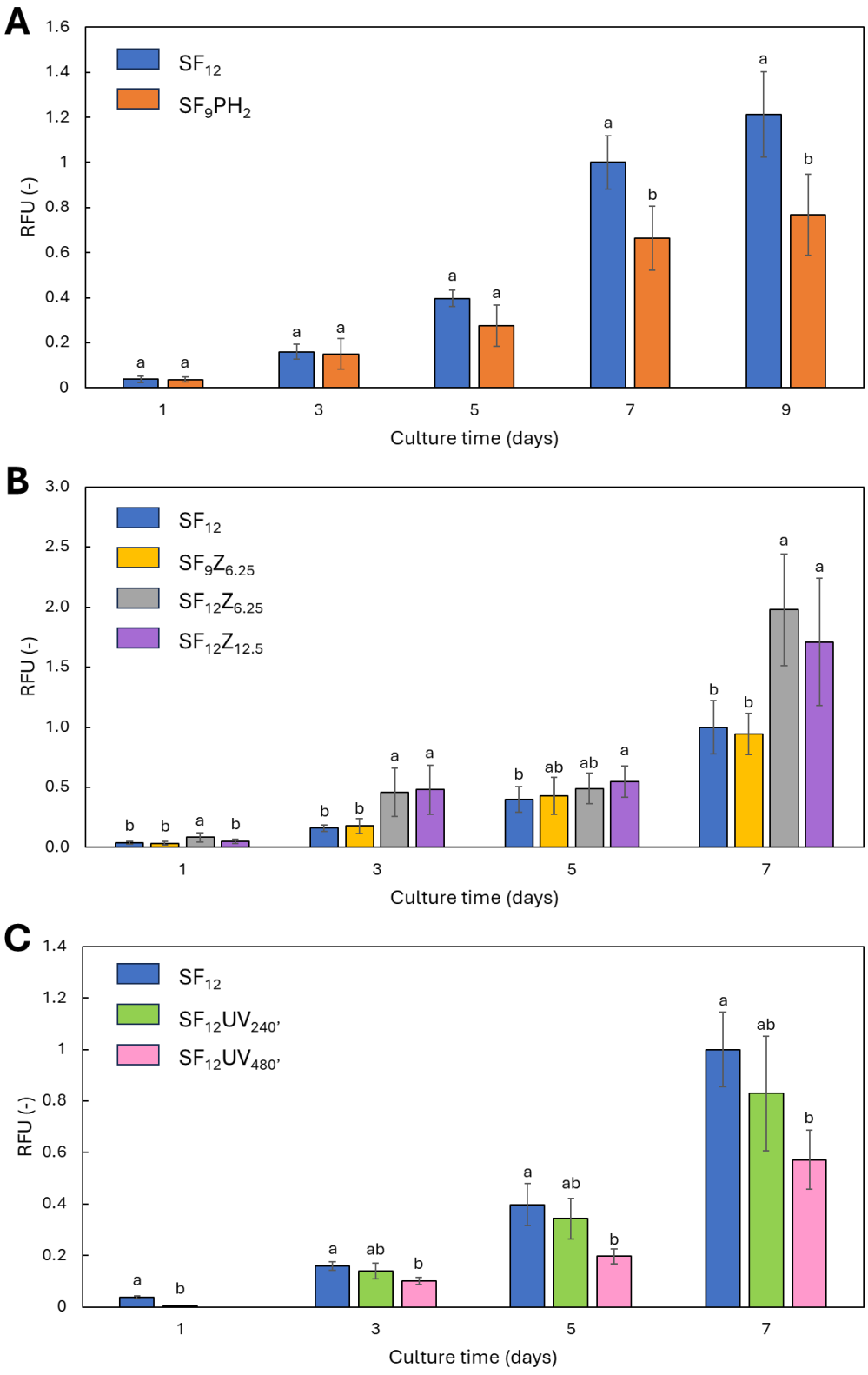

Figure 59: Relative bMSC proliferation on electrospun (A) silk fibroin and SFPH blends (SF_{12}-E and SF_9PH_2-E), (B) silk fibroin and SFZ blends (SF_{12}-E, $SF_9Z_{6.25}$-E, $SF_{12}Z_{6.25}$-E and $SF_{12}Z_{12.5}$-E), (C) silk fibroin and UV-functionalised scaffolds (SF_{12}-E, $SF_{12}UV_{240'}$-E and $SF_{12}UV_{480'}$-E). Results displayed as mean ± SD (n>6), with different lower-case letters indicating significant differences at each time point.

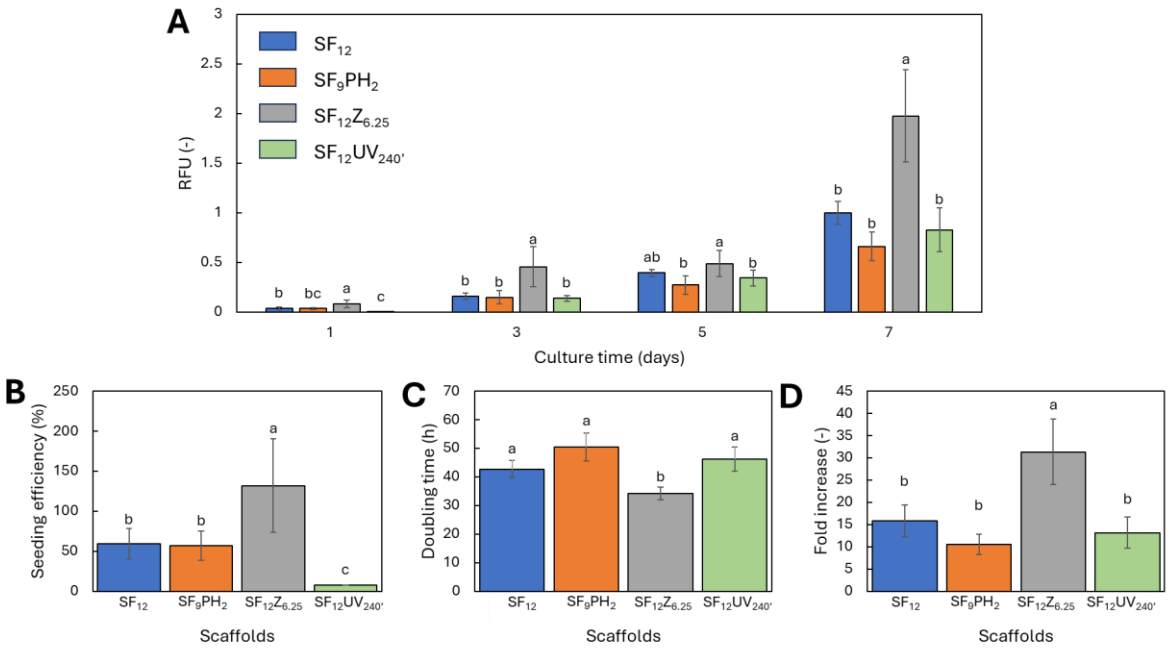

*Figure 60: Comparative proliferation of electrospun silk fibroin, zein and psyllium husk blends and UV-functionalised scaffolds. (A) Prestoblue proliferation assay, (B-D) Growth kinetics based on cell density results obtained from calibration curve (**Appendix B, Figure S8**), with (B) Seeding efficiency, (C) Doubling time during exponential growth phase and (D) Fold increase during exponential growth phase. Results shown as mean ± SD ($n > 6$), with different lower-case letters showing significant differences between means ($p<0.05$).*

As shown in **Figure 60**, electrospun $SF_{12}Z_{6.25}$-E scaffolds showed the greatest increase in cell attachment (**Figure 60B**) and fold increase (**Figure 60D**), and largest decrease in doubling time (**Figure 60C**), thereby considerably increasing the scalability of bMSC expansion. Although SF_9PH_2-E performed slightly worse than the SF_{12}-E control, its health, digestive and antimicrobial properties could still benefit electrospun scaffolds if these properties were transferred to the final meat product. In contrast, $SF_{12}UV_{240'}$-E had a comparable doubling time (46.2 ± 4.3 h) and fold increase (13.1 ± 3.5) to SF_9PH_2-E, but has no other functional benefits. As such only the $SF_{12}Z_{6.25}$-E and SF_9PH_2-E blends were investigated further.

4.3.3 Cell culture on functionalised microcarriers

For the electrospun materials to be fit-for-purpose and become integrated into large scale cell expansion systems such as stirred tank bioreactors, they must be converted into microcarriers. Initial experiments relied on manual cutting of the scaffolds to create irregularly shaped microstructures (**Figure 43**). Hand-slicing the microcarriers predictably led to some batch-to-batch variation, with particles appearing as irregular n-sided polygons that varied in size but matched the thickness of the electrospun scaffold that they were crafted from (**Figure 61**). Overall, measuring the dimensions of

over 400 hand-sliced electrospun silk fibroin microcarriers ($hsMC_{SF}$) over four separate experiments led to an average length of 115 ± 29 µm and thickness of 20 ± 2 µm (results shown as mean ± SD). SEM analysis confirmed that the hand-sliced microcarriers retained their nanofibrous and microporous architecture, with the cross-section along the sliced edge showing truncated fibres with no visible deformation from blade compression (**Figure 61C**). As such, the hand-sliced microcarriers can be considered as micro-sized electrospun scaffolds that would logically share the same physical properties in relation to fibre density and porosity, as the regular sized electrospun scaffolds. Despite these structural similarities, the higher surface-to-volume ratio of hand-sliced microcarriers is a major difference with the electrospun scaffolds. Indeed, the total growth area of all microcarriers cut out from a single scaffold, exceeds the growth surface area of that scaffold. As shown in **Figure 61**, the hand sliced microcarriers had an average growth area of 0.00041 ± 0.00012 cm^2, regardless of the material or blend type ($hsMC_{SF,}$ $hsMC_{SFZ}$, $hsMC_{SFPH}$), which was smaller but within the same order of magnitude as commercially available Cytodex-3 (C3; 0.00071 cm^2) and Solohill Plastic (SP; 0.00090 cm^2) microcarriers (**Table 9**). Any variance regarding the dimensions, and by extension the growth surface area, of the hand sliced microcarriers was deemed to result from the effects of manual slicing. It should be noted that, at a nano-scale, there was a considerable difference between the fibrous area of the hand sliced microcarriers of different blends, which decreased with increased fibre diameter (a_{SF} = 0.091 cm^2; a_{SFPH} = 0.051 cm^2; a_{SFZ} = 0.030 cm^2) although the size of the fibrous area would have a negligeable impact on cell proliferation as bMSCs cannot infiltrate the electrospun microcarrier nano-sized pores (Ge *et al*., 2021). The total culturable surface of the hand sliced microcarriers should therefore be regarded as 2-dimensional (Wu and Hong, 2016).

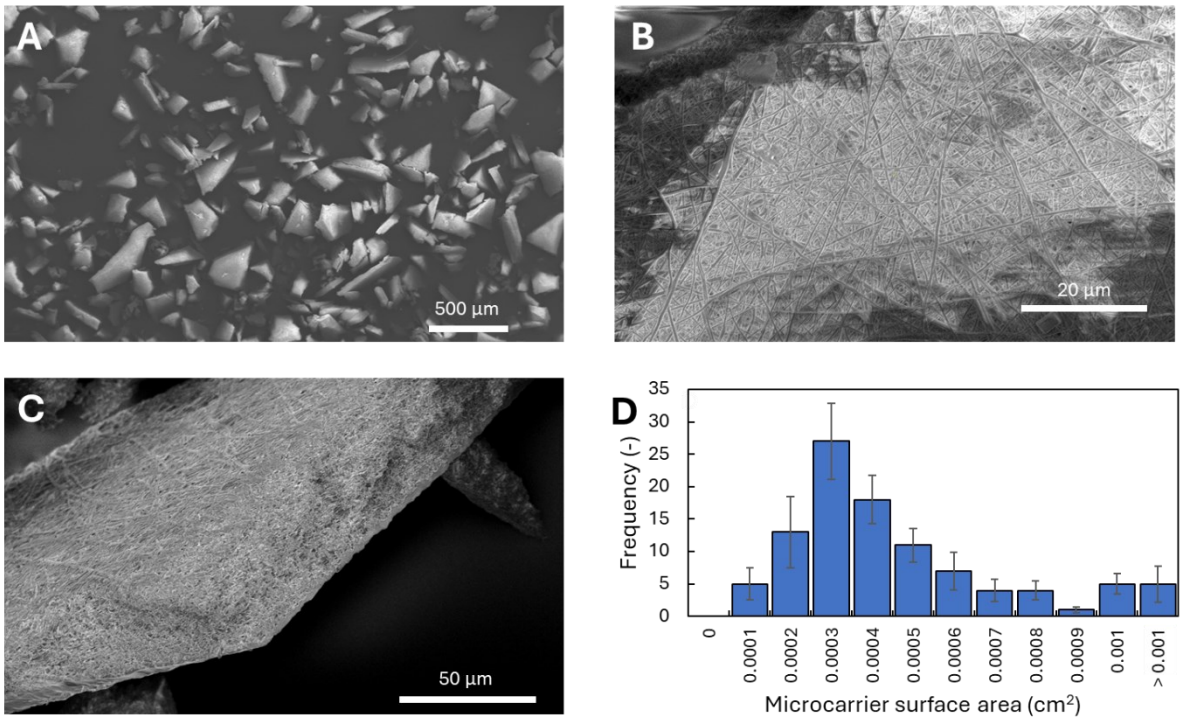

Figure 61: Scanning Electron Microscopy images of (A) irregularly shaped hand sliced electrospun $hsMC_{SF}$ microcarriers, (B) top view of a single $hsMC_{SF}$, (C) side view of a single $hsMC_{SF}$; (D) surface area distribution of $hsMC_{SF}$. Area distribultion results displayed as mean $\pm$ SD (n = 100; 4 repeats).

Table 9: Types of microcarriers used in this study.

Microcarrier	Materials	Shape	SA ($x10^{-5}$ cm^2)	Number of microcarriers per gram (dry)	Density (g/cm^3)	SSA (cm^2/g)	Comments
Electrospun hand-sliced ($hsMC_{SF}$)	Silk fibroin (100%)	Polygonal L=115 µm h=20 µm	4.37	4.9×10^6	0.64	2000	Highly porous, edible, irregular, non-scalable
Electrospun hand-sliced ($hsMC_{SFPH}$)	MC_{SFPH} Silk fibroin (81.8%) Psyllium husk (18.2%)	Polygonal L=115 µm h=20 µm	4.37	4.9×10^6	0.64	2000	Highly porous, edible, irregular, non-scalable, improved functionality
Electrospun hand-sliced (MC_{SFZ})	Silk fibroin (65.8%) Zein protein (34.2%)	Polygonal L=115 µm h=20 µm	4.37	4.9×10^6	0.64	2000	Highly porous, edible, irregular, non-scalable, improved functionality
Electrospun Cryomilled (cryoMC)	Silk fibroin (81.8%), psyllium husk (18.2%)	Irregular polyhydron Ø=120.5 µm	4.41	5.6×10^6	N/A	N/A	Irregular, scalable and reproducible
Cytodex 3 (C3)	Cross-linked dextran coated with thin layer of denatured collagen	Spherical Ø=150.0 µm*	7.07	$3.0 \times 10^{6*}$	1.04*	2700* (wet)	Gold standard, non-edible, functionalised with ECM proteins
Solohill Plastic (SP)	Cross-linked polystyrene	Spherical Ø=168.5 µm*	8.94	$4.6 \times 10^{5*}$	1.03*	360*	Plastic, non-edible
Hybrid X (HX)	Zein protein (91%), gelatin (8%), monosaccharide	Spheroid Ø=358.5 µm*	40.36	$4.1 \times 10^{4*}$	1.17*	165* (dry)	Edible, non-commercial prototype, functionalised with ECM proteins

*As quoted by manufacturer.

The morphology (**Figure 62A,C,E,G**) and structural characteristics (**Figure 62B,D,F,H**) of each microcarrier used in this study, showed some similarities between microcarrier types as well as some limitations that may partially impact the validity of the study. Firstly, the hsMCs are the only non-spheroid microcarriers (**Figure 62A**). Secondly, the fibre diameter and porosity, which has been shown to promote cell attachment and proliferation by providing increased focal adhesion sites and facilitating nutrient and O_2 diffusion (Molina *et al.*, 2021; Rahmati *et al*., 2021), differ significantly between the nanofibrous hsMC and Cytodex-3 and microfibrous Hybrid X microcarriers. In addition, while it is known that Cytodex-3 microcarriers are only fibrous on their exterior (collagen coating), no information is available on the interior of Hybrid X microcarriers (**Figure 62B,D,H**). Therefore, it may be that hsMCs were the only microcarriers with interconnected pores considered in this study. Thirdly, differences in density between the commercial Cytodex-3 (1.04 g/cm^3) and Solohill Plastic (1.03 g/cm^3) are very different to the heavy Hybrid X (1.17 g/cm^3) and light hsMCs (0.64 g/cm^3). With a density lower than culture medium (∼1 g/cm^3) the hsMCs float in static conditions, making cell attachment suboptimal. Although this was also the case for larger electrospun scaffolds, these could be sunk by sufficiently wetting the scaffolds and dunking them using a pipette tip. Fourthly, the microcarriers have different degrees of functionality as both Cytodex-3 and Hybrid X are coated with ECM proteins. As such, these microcarriers carry adhesion motifs that are expected to enhance cell attachment and proliferation. Fifthly and possibly most importantly, the specific surface area of each microcarrier is calculated differently by each manufacturer with Solohill Plastic, Hybrid X and hsMC measured using the nominal surface area and Cytodex-3 seemingly including the outer fibrous area. While the nominal surface area of hsMC and Solohill Plastic microcarriers may not differ too significantly from their culturable surface area, the large and protruding macrofibres constituting Hybrid X microcarriers should logically play an important role in increasing its available surface area (**Figure 62H**).

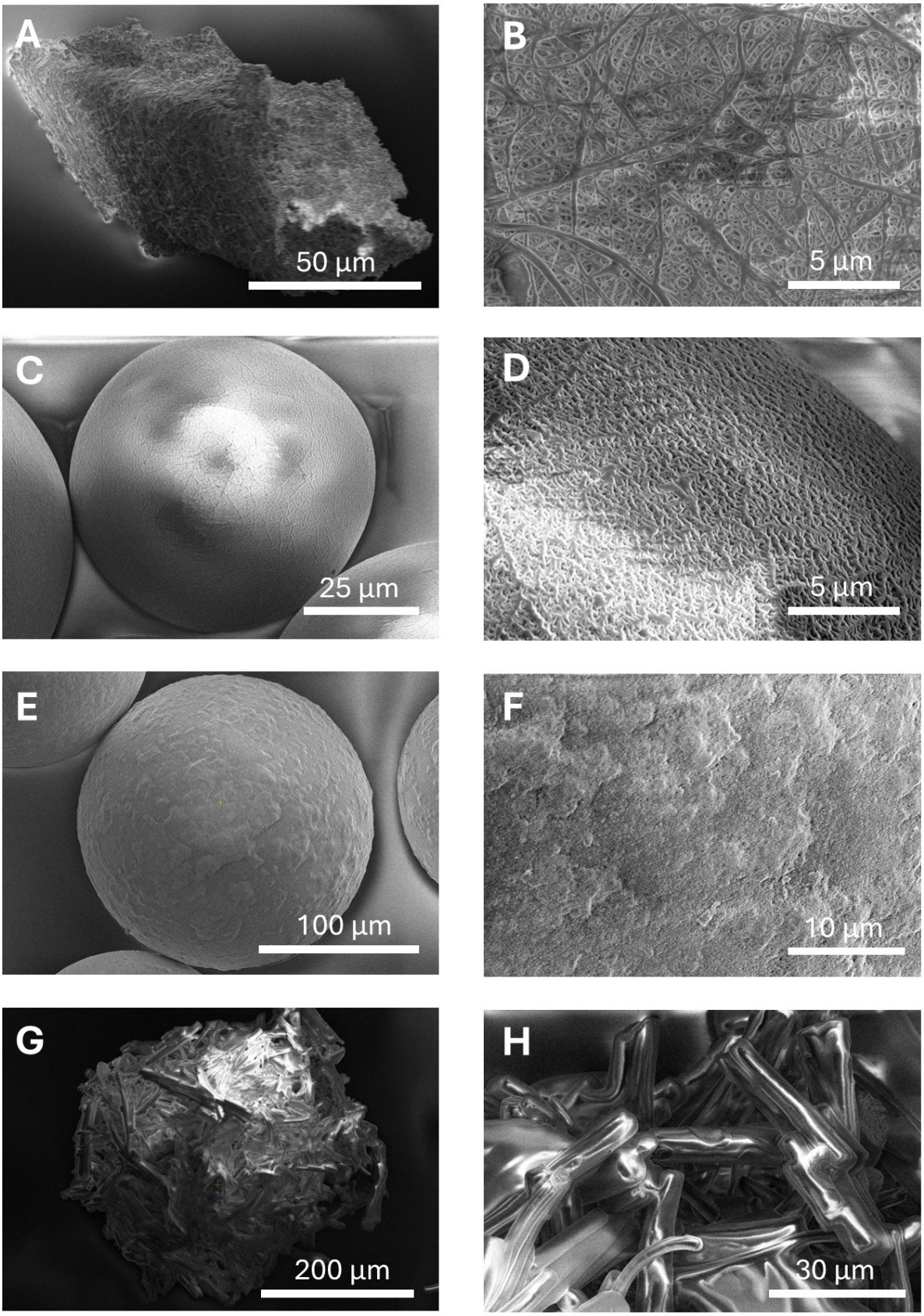

Figure 62: SEM images of dry microcarriersand their surface topology. (A) hsMC, (B) nanofibrous surface of hsMC, (C) Cytodex-3, (D) fibrous collagen coating of Cytodex-3, (E) Solohill Plastic, (F) relatively smooth surface of Solohill Plastic, (G) Hybrid X, (H) macrofibrous surface of Hybrid X.

As shown in **Figure 63**, the comparative results of bMSC proliferation on $hsMC_{SF}$, $hsMC_{SFPH}$ and $hsMC_{SFZ}$ were similar to those on electrospun SF_{12}-E, SF_9PH_2-E and $SF_{12}Z_{6.25}$-E scaffolds (**Figure 60**). As expected, this was marked by greater bMSC proliferation on $hsMC_{SFZ}$ than proliferation on $hsMC_{SF}$ and $hsMC_{SFPH}$ which performed similarly (p>0.05). Interestingly, the electrospun hsMCs performed on par with commercial and experimental ones when seeded at 1500 cells/cm^2 in static conditions (**Figure 63**). All microcarrier types displayed a relatively poor seeding efficiency, with the more efficient ones being 29.9 ± 3.6% for $hsMC_{SFZ}$ and 29.2 ± 3.6% for Hybrid X and the less efficient ones being 17.5 ± 7.5% for Cytodex-3 and 8.9 ± 6.1% on Solohill Plastic microcarriers. These results were far lower than the seeding efficiency results on scaffolds (40-137% for SF_{12}-E and $SF_{12}Z_{6.25}$-E, see *section 4.3.2*), and could therefore be due to the experiment design as well as the time needed for cells to adapt to the microcarrier surface. To ensure that the PrestoBlue™ assay could be carried out over multiple days and prevent microcarrier loss from frequent washing steps, the microcarriers were held in an inert 70 µm cell strainer which allowed non-adhered cells to pass through but retained microcarriers (**Figure 44**). It is possible that many cells seeded on day 0 did not attach to any microcarriers and were subsequently lost on day 1 at the start of the proliferation assay. In addition, the lower density of the electrospun hsMCs, causing some to float, also prevented many microcarriers from coming into prolonged contact with cells. Despite this, bMSC proliferation rate was comparable between the microcarrier types and increasing at an exponential rate up to day 7 and then slowing down up to day 11 when cells entered the stationary phase. Interestingly, bMSC grown on Solohill Plastic microcarriers reached a maximum proliferation on day 9 (with a 29.9 ± 5.7 fold increase) after which the fluorescence started decreasing steadily. This can be explained by cell detachment on the plastic microcarriers occurring after reaching confluency. As cells cease to divide and become senescent, their metabolic activity is diminished leading to a reduction in resazurin and leading to a lower fluorescence (Sonnaert *et al.*, 2015; Weng *et al.*, 2022). In addition, the detaching cells that did not migrate to empty microcarriers contributed to a continuous decrease in cell population.

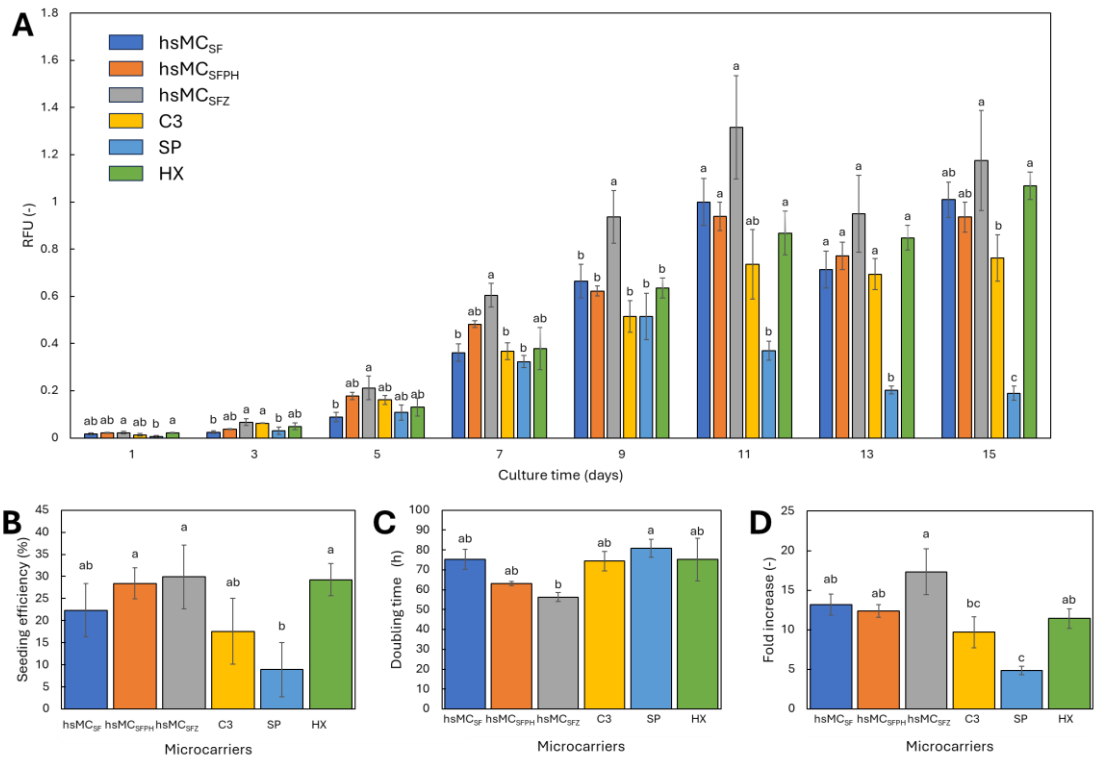

*Figure 63: (A) bMSC proliferation on electrospun hand-sliced (MC_{SF}, MC_{SFPH} and MC_{SFZ}), Cytodex-3 (C3), Solohill Plastic (SP) and Hybrid X (HX) microcarriers; (B-D) bMSC growth kinetics on the microcarrier types, with (B) displaying the seeding efficiency, (C) the doubling time in the first 7 days, and (D) the fold increase at day 11 (day 9 for SP). Results shown as mean ± SD (n=3), with different lower-case letters showing significant differences between means (p<0.05). Cell density was estimated based on calibration curve (**Appendix C, Figure S13**).*

Fluorescent microscopy was used as a qualitative tool to study the proliferation of bMSCs on electrospun hsMCs, Cytodex-3, Solohill Plastic and Hybrid X microcarriers (**Figure 64**). However, it was difficult to detect any cells on electrospun hsMCs and Hybrid X microcarriers, due to their strong autofluorescence (**Figure 64A-C,F**). This is because silk fibroin and zein (the main component of Hybrid X microcarriers) contain aromatic amino acids, namely tyrosine and phenylalanine, that absorb photons in the UV range and emit light in the blue to green range (Amirikia *et al*., 2018). Consequently, this autofluorescence interferes with the emission of fluorescent dyes such as calcein AM. In addition, the low intensity of the autofluorescence prevents effective visualisation of the microcarrier fibrous morphology (Bucciarelli *et al*., 2023). In contrast, the Cytodex-3 and Solohill Plastic microcarriers imaged well due to their relative transparency. As expected, the Cytodex-3 microcarriers were mostly covered in cells, but surprisingly the Solohill plastic ones were mostly devoid of cells altogether. This would suggest that cells were in fact detached, and lost, from the Solohill Plastic microcarriers. This likely resulted from the absence of functional properties of the polysterene microcarriers which may have only provided weak adhesion to the bMSCs due to is mostly smooth surface and neutral electric charge. To better study the attachment of bMSC on the different microcarriers it is important to

address the autofluorescence of hsMC and Hybrid X microcarriers in the blue and green range (400 – 550 nm). As such dyes with emissions in the far red or infrared should be prioritised. For instance, as an alternative to calcein AM which emits within the autofluorescence range (~ 515 nm), Calcein Deep Red AM, which emits light in the far red (~ 660 nm), can stain live cells red. In contrast ethidium homodimer-1 could be replaced with Live/Dead Fixable Yellow stain or SYTOX Green (Taborda *et al.*, 2023) which emit at 575 and 523 nm, respectively. As an alternative to Live/Dead staining, phalloidin stains such as rhodmanine-phalloidin have commonly been used to dye the F-actin cytoskeleton of mesenchymal stem cells red (Kumar *et al.*, 2011; Plath *et al.*, 2021; Bai *et al.*, 2023; Yang *et al.*, 2023).

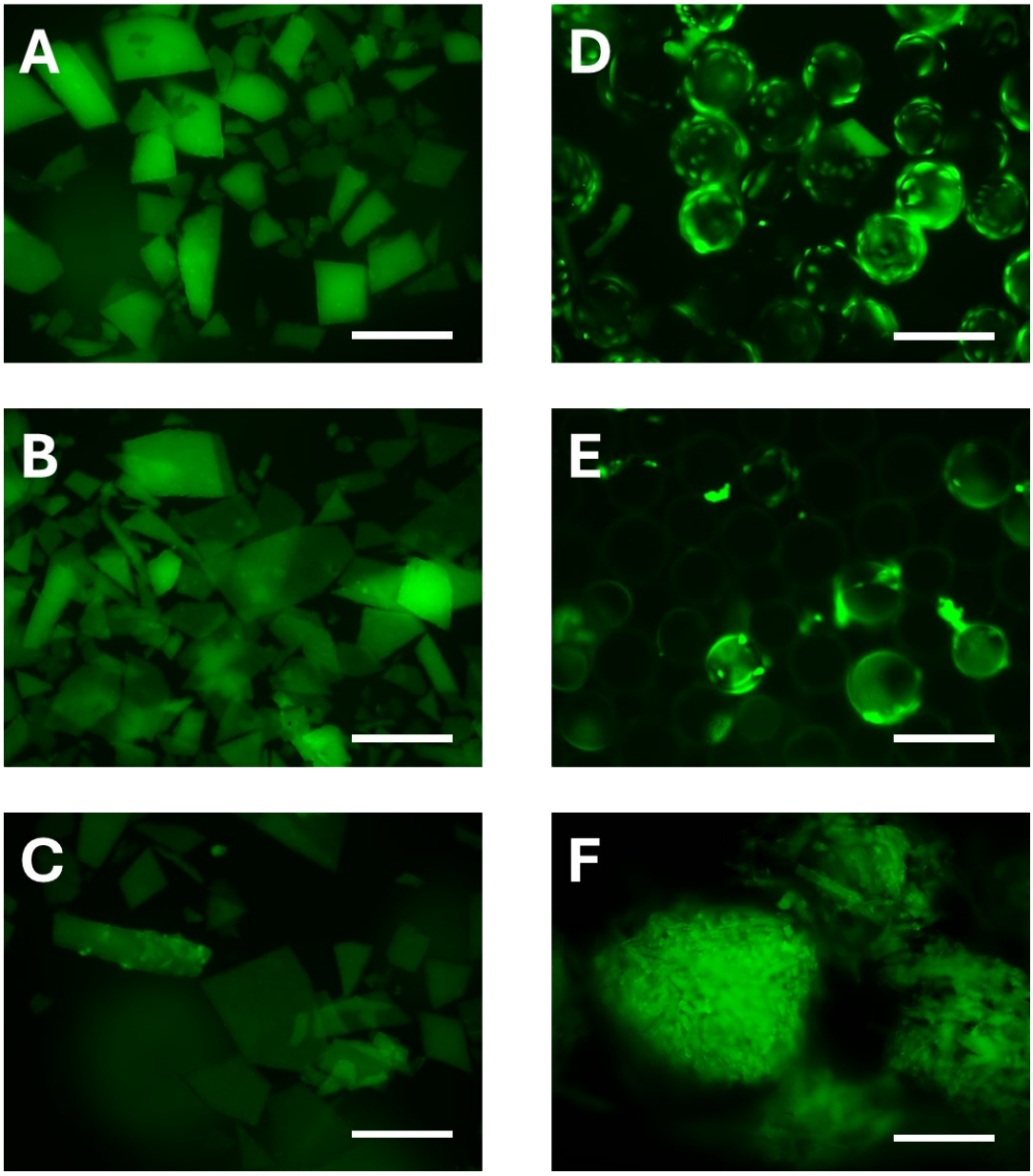

Figure 64: bMSC stained with calcein AM after 11 days of culture on (A) MC_{SF}, (B) MC_{SFPH}, (C) MC_{SFZ}, (D) Cytodex 3, (E) Solohill Plastic and (F) Hybrid X. Scale bar = 250 µm. A, B, C and F display significant autofluorescence.

While the electrospun microcarriers were shown to act as capable contenders to commercial microcarriers in static conditions, cell expansion in static environments is neither efficient nor financially feasible for cultivated meat production (Post *et al*., 2020; Bodiou *et al*., 2020). Therefore, it is important that microcarriers can be used in large scale bioreactors and be fabricated with low batch-to-batch variability, as quality control is a critical step towards cultivated meat regulatory approval (Lanzoni *et al*., 2024). To remediate this and attempt to replace the hand slicing method with a more industrially relevant and reproducible way to generate microcarriers, electrospun SF_9PH_2-E mats were cryomilled into cryoMC_{SFPH}. Cryomilling is considered an environmentally friendly technology for the fast production of millimetre-to-nanometre particles. Unlike traditional ball milling, cryomilling is performed at very low temperatures (<150 °C) and often cooled in liquid nitrogen, preventing heat build-up and degradation of the milled material (Shamshina *et al*., 2021). Cryomilled particles also have smoother edges and conserve material morphology, crystallinity and mechanical properties better than those produced under conventional milling methods (Katiyar *et al*., 2020). Cryomilling is also very versatile and has been used for a variety of foods and spices, metals, ceramics and alloys, explosives and tissue engineering scaffolds (Jonnalagadda *et al*., 2014; Lim *et al*., 2014; Fernandez-Perez and Ahearne, 2019). Furthermore, it is scalable from laboratory to industrial systems capable of producing up to 4000 kg of particles per hour (Katiyar *et al*., 2020).

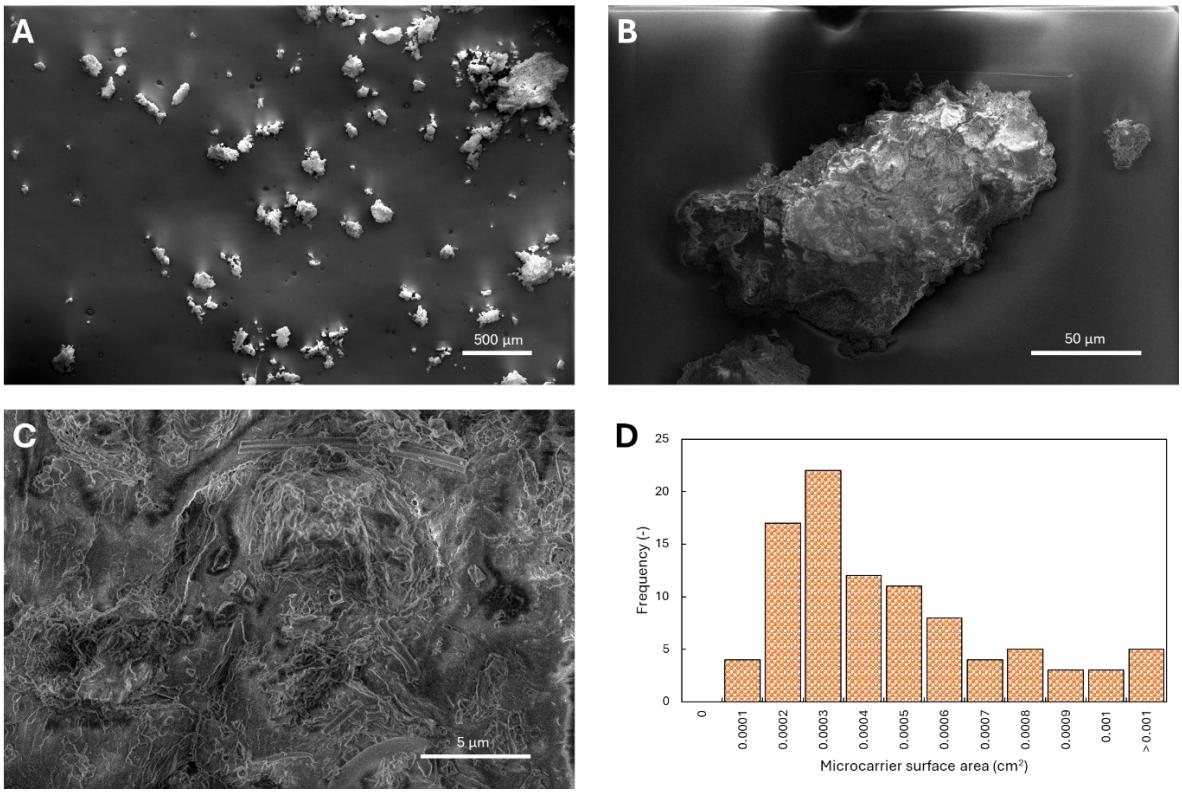

Figure 65: (A-C) SEM images and (D) Surface area distribution of cryoMC_{SFPH} microcarriers.

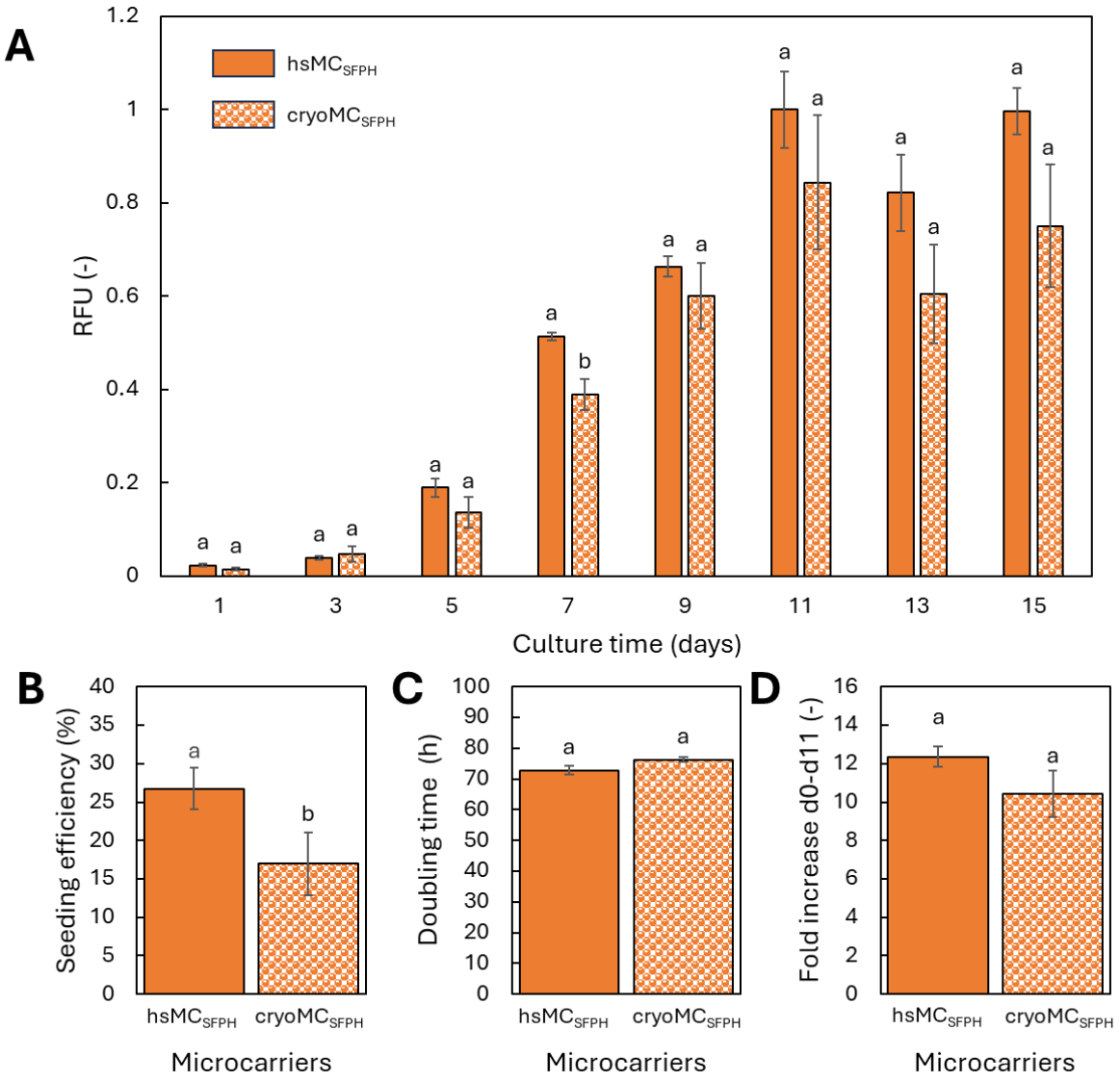

*Figure 66: (A) Proliferation and (B) doubling times of bMSC grown on MC$_{SFPH}$ and cryoMC$_{SFPH}$. Cells were seeded at 3000 cells/mg. Results displayed as mean ±SD (n=3) with different lower-case letters indicating significant differences between the means. Cell density was estimated based on calibration curve (**Appendix C, Figure S13**).*

Due to time and material constraints only one batch of cryoMC$_{SFPH}$ was produced, characterised and tested with bMSCs. Unlike the hand-sliced electrospun microcarriers, the cryomilled microcarriers appeared as broken 3-dimensional shapes with no defined edges or common dimensions (**Figure 65**). There was a high variability in microcarrier sizes with an average diameter of 121 ± 65 µm and growth area around 0.00049 ± 0.00074 cm^2, although the size distribution could be narrowed in future experiments by optimising particle size on the cryomiller settings or sieving to retain microcarriers of desired sizes (Shamshina *et al.*, 2021). Cryomilled electrospun microcarriers did not retain their nanofibrous and microporous architecture and instead appeared as a dense amalgamation of sheared fibres (**Figure 65C**) which made estimations of density measurement impossible. Therefore,

bMSC proliferation on $hsMC_{SFPH}$ and $cryoMC_{SFPH}$ was compared by weight after seeding cells at 3000 cells/mg, a cell density close to 1500 cells/cm^2 for $hsMC_{SFPH}$. Despite major morphological differences, $hsMC_{SFPH}$ and $cryoMC_{SFPH}$ performed similarly, albeit with a slightly slower doubling time on $cryoMC_{SFPH}$ of 76.3 ± 4.0 h compared to 72.9 ± 1.9 h for $hsMC_{SFPH}$ and slightly lower fold increase, at day 11, of 10.4 ± 1.4 compared to 12.4 ± 0.8 (p>0.05). This may result from a comparatively rough surface resulting from tightly interspaced smooth fibres in the case of $hsMC_{SFPH}$ and tightly packed sheared fibres for $cryoMC_{SFPH}$. It is also worth noting that $hsMC_{SFPH}$ and $cryoMC_{SFPH}$ behaved differently in suspension with the cryomilled microcarriers sinking to the bottom of the cell culture wells, highlighting the higher density of the milled particles, which may be sufficient for culture in bioreactors.

4.4 Conclusion

Silk fibroin was successfully blended with abundant plant-derived biopolymers (psyllium husk or zein) to produce functionalised electrospun scaffolds with increased fibre diameter and potential antimicrobial and health benefits. Cell proliferation was similar between blended silk fibroin and psyllium husk and non-blended silk fibroin scaffolds. In contrast the silk fibroin and zein ($SF_{12}Z_{6.25}$-E) scaffolds had a significantly greater cell attachment, doubling times and yields. This was attributed to the much larger nanofibres of $SF_{12}Z_{6.25}$-E (417 ± 121 nm) which may have provided a better surface for cell attachment.

Silk fibroin electrospun scaffolds were also functionalised with UV irradiation, which demonstrated an increase in -COOH photoproducts with increasing UV exposure times. However, unexpectedly, this had a detrimental effect on cell attachment and proliferation, possibly caused by charge repulsion of the excessive negatively charged functional groups on the scaffold surface after long UV exposure times (>240 min). To investigate this further contact angle testing could be used to measure the surface wettability and energy (Idaszek *et al*., 2014).

To increase the scalability of the bioprocess, electrospun scaffolds were converted into electrospun hand-sliced (hsMCs) and cryomilled (cryoMCs) non-spherical microcarriers, a first of their kind. The hsMC were characterised and a cell proliferation assay revealed that bMSC proliferation on hsMCs was comparable to commercially available (Cytodex-3 and Solohill Plastic) and experimental (Hybrid X) microcarriers. In addition, the hsMCs produced from $SF_{12}Z_{6.25}$-E outperformed all other microcarriers tested, highlighting the biocompatibility of the silk fibroin and zein composite. Finally, cryomilling proved to be an efficient and scalable method for microcarrier production, as cryoMCs

performed on a par with hsMCs when comparing bMSC growth by microcarrier weight. However, it is too soon to draw firm conclusions as there was no time to repeat any experiments with microcarriers.

CHAPTER V

MECHANICAL AND TEXTURAL PROPERTIES OF BEEF BURGERS AND THEIR PLANT-BASED ANALOGUES

5.1 Introduction

Texture plays an important role in how consumers perceive food, with mouthfeel experiences trumping taste when determining product quality (Isutzu and Wani, 1985; Chow *et al*., 2024). In addition, several studies have reported that familiarity with existing products, especially their organoleptic properties, drives consumers to try and repeat-buy alternative products and novel foods (Imtiyaz *et* al., 2021; Pakseresht *et al*., 2022; Kamei *et al*., 2024). For cultivated meat products to be widely adopted, it is therefore highly desirable that they should have sensory and textural properties which match the consumer expectation of farmed meat (Verbeke *et al*., 2015; Pakseresht *et al*., 2022). The texture of farmed meat is influenced by several evolutionary, biological, physiological and environmental factors as well as post-mortem maturation that cannot be replicated in plant-based alternatives (Starkey *et al*., 2016). Instead, commercially available alternative protein products must rely on the heavy use of secondary ingredients such as meat extenders and fillers to improve organoleptic properties and texture. Despite many plant-based analogues (PBAs) looking, cooking and tasting just like real meat, there are still palpable differences in product texture compared with farmed meat (Goldschalk-Broers *et al*., 2022). While cultivated meat production could theoretically replicate many of the biological and physiological factors affecting meat texture, the precise impact of each factor on texture is not well understood. A more feasible approach might be to engineer scaffolds and hydrogels, which when combined with the cultivated tissue growing on them, complete the textural profile of the final product to replicate that of traditional meat (Ben-Arye *et* al., 2020; Bonkamp *et al*., 2022). However, for this to occur, the desired textural properties of the cultivated meat must be ascertained and quantified.

Food texture can be assessed either descriptively, by trained human testers evaluating mouthfeel characteristics based on their sensory perception, or instrumentally, using methods that replicate

mouthfeel through mechanical forces (Murray *et* al., 2001; Shreuders *et al*., 2021; Nasrollahdazeh *et al.,* 2024). Texture profile analysis (TPA) is widely recognised as the most useful instrumental method for determining the textural properties (hardness, adhesiveness, cohesiveness, springiness, resilience and chewiness) of raw and cooked meat products (de Huidobro *et* al., 2005; Bonkamp *et al*., 2022; Paredes *et al*., 2022). However, the lack of a standard protocol for TPA is a limitation for direct comparison between studies (Shreuders *et al.,* 2021). The mechanical tests of the International Organization for Standardization (ISO) standardised protocols have also been used to quantify meat, with tensile testing becoming increasingly popular (Paredes *et* al., 2022; Ko *et* al., 2023; Nasrollahdazeh *et al*., 2024). However, the ISO protocols were designed for plastics and semi-rigid plastic composites rather than food (International Organization for Standardization, 2002; International Organization for Standardization, 2019a; International Organization for Standardization, 2019b) and the resulting values have yet to be characterised as mouthfeel properties which differentiate between products of a similar food type (*e.g.* beef burgers).

This chapter aims to characterise the mechanical and textural properties of beef and plant-based analogue burgers, using a battery of robust mechanical tests and TPA, to identify and present relevant mechanical and textural values as a guide for cultivated meat production to develop and replicate the mouthfeel expectations of traditional meat in order to appeal to consumers.

Disclaimer: The work presented in this chapter was a team effort. I conducted the pilot study on the characterisation of the mechanical properties of beef burgers with the aim of informing cultivated meat production. For this initial study burgers B1-B3 were selected based on customer reviews and were characterised in flexion, tension, compression and cutting following ISO standards (2002; 2019a; 2019b) in both raw and cooked states. The results of the pilot study provided a case to expand the testing parameters and extend the range of tested burgers (B4-B7). Although I was still associated with this research, I neither collected nor processed the data for the mechanical results for burgers B4-B7 (although I tested B6 in tension and flexion in alternative conditions) and provided the TPA results for all types of burger (B1-B7). I was, however, involved in the supervision of the undergraduate students who did part of this project, and contributed to the paper introduction, methods, results and discussion that encompasses the whole study presented here (Souppez et al., 2025).

5.2 Materials & Methods

5.2.1 Burgers tested

To obtain a representative characterisation of the mechanical and textural properties of burgers across the breadth of commercially available products, five beef burgers of varying beef content (high beef content > 95%; low beef content < 85%), fat content (high fat > 19%; low fat < 5%) and price points (high price > 10 £/kg; low price < 10 £/kg) were tested, along with two plant-based analogues

(PBA) – pea and soy protein. All tested burgers, labelled B1-B7, were purchased fresh (*i.e.* not frozen) and their details and full ingredients composition are displayed in **Table 10**.

5.2.2 Burger preparation

All burgers were tested in raw (straight from the package) and cooked (well-done) states. The mechanical and textural properties of burgers in the raw state were particularly relevant to manufacturing and handling, while those in the cooked state were most relevant to mouthfeel and potential consumer acceptance.

All experiments were conducted at room temperature (15.8-24.2 °C) and ambient humidity (26-41 %RH). All burgers were tested within the shelf life of the product (*i.e*. before the *best before* date). Raw burgers were tested on the day that the package was opened, whereas cooked burgers were tested within 24 h of cooking. In line with previous work (Hautrive *et al*., 2019; Cho and Ryu, 2022), a pre-heated oven at 200 °C was used to cook the burgers for 8 min (4 min of each side). The cooked burgers were then cooled at room temperature for at least 4 h and placed in an air-sealed container until further use.

*Table 10: Summary of the burgers tested, based on manufacturer's packaging information. *Prices as of April 2023.*

Label	Protein Source	Commercial description	Fat (%)	Price* (£/kg)	Ingredients list
B1	Beef	Morrisons 4 Beef Burgers 5% Fat	4.7	8.81	Beef (96%), rice flour, black pepper, salt, preservative (sodium sulphite), antioxidant (sodium ascorbate).
B2	Beef	Marks & Spencer 4 Aberdeen Angus Beef Burgers	19.4	10.46	British beef (95%), water, dried potatoes, rice flour, sea salt, cracked black pepper, preservative (E223 (sulphites), salt, dextrose).
B3	Beef	Haji Baba Halal Beef Burger	3.8	17.57	Beef (82%), chilli burger seasoning (8%) (rusk (wheat flour (calcium carbonate, iron, niacin, thiamine), salt), spices (chilli, paprika, cumin, chipotle chilli) (13.34%), salt, red peppers, demerara sugar, stabilisers (E450), preservative (E223) (1.13%) (sulphite), spice extracts (pepper, chilli), antioxidant (E300)), chilli, coriander.
B4	Beef	Marks & Spencer Select Farms 4 Beef Burgers 3% Fat	2.8	12.5	Beef (81%), water, roast beef stock (water, beef bones, tomato purée, mushrooms, seaweed, onions, carrots, white wine vinegar), dried potatoes, onions, broad bean flour, rice flour, sea salt, salt, preservative: E223 (sulphites), cracked black pepper, dextrose.
B5	Beef	Morrisons 4 British Beef Quarter Pounders	19.2	5.93	Beef (76%), pea flakes, water, cracked black pepper, salt, sea salt, preservative (sodium metabisulphite), coarse tellicherry pepper, antioxidant (ascorbic acid), rapeseed oil.
B6	Soy	Tesco Plant Chef 2 Meat Free Burgers	12.1	6.86	Reconstituted soya protein (47%), water, rapeseed oil, rice flour, shea fat, maize flour, soya protein concentrate, pea fibre, stabiliser (methyl cellulose), coconut oil, colours (plain caramel, beetroot red), salt, yeast extract, flavouring, smoked rice flour, black pepper, maize starch, maltodextrin, modified tapioca starch, sugar, dextrose, onion.
B7	Pea	Beyond Meat 2 Plant Based Burgers	19.0	17.70	Water, pea protein (16%), canola oil, coconut oil, rice protein, flavouring, stabilizer (methylcellulose), potato starch, apple extract, colour (beetroot red), maltodextrin, pomegranate extract, salt, potassium salt, concentrated lemon juice, maize vinegar, carrot powder, emulsifier (sunflower lecithin).

The cooking yield by mass Y_M (**Equation 38**) and by volume Y_V (**Equation 39**) are respectively calculated as:

$$Y_M = \frac{M_{cooked}}{M_{raw}} \tag{38}$$

and

$$Y_V = \frac{V_{cooked}}{V_{raw}} \tag{39}$$

where: M_{cooked} is the cooked mass, M_{raw} is the raw mass, V_{cooked} is the cooked volume, and V_{raw} is the raw volume.

5.2.3 Mechanical testing

Mechanical testing refers to tests conducted to determine and characterise the properties of meat as an engineering material, when subjected to a load. The tests, namely flexion, tension, compression and cutting (blade-compression), were performed on a TA ElectroForce 3200 Series III (TA Instruments, USA) using a 10 N load cell (LC1) for the raw burgers and a 450 N load cell (LC2) for the cooked ones. Measurements were recorded at 100 Hz with a displacement rate of 2 mm/min, with both load cells employing a 0.1 N pre-load applied at 2 mm/min. Samples were prepared from single burgers using a precision cutting knife. The dimensions for each test were measured using a calliper and were defined by standards ISO 178 (International Organization for Standardization, 2019a), ISO 527 (International Organization for Standardization, 2019b) and ISO 604 (International Organization for Standardization, 2002) for the determination of flexural, tensile and compressive properties of plastics, respectively.

5.2.3.1 Flexion

Flexural tests were undertaken in accordance with the ISO 178 (International Organization for Standardization, 2019a) using a 3-point bending setup (**Figure 67A**), where the contact points were 4 mm diameter cylinders 40 mm apart.

The flexural strain (ε_f; **Equation 40**) was defined as:

$$\varepsilon_f = \frac{6\omega h}{s^2} \tag{40}$$

where: ω is the measured deflection, h is the thickness and s is the span between support points (s = 40 mm).

The flexural stress (σ_f; **Equation 41**) was given as:

$$\sigma_f = \frac{3Fs}{2lh^2} \tag{41}$$

where: F is the measured force and l is the sample width.

Finally, the flexural modulus (E_f; **Equation 42**) was calculated using the linear least square method for 0.005 ≤ ε_f ≤ 0.025, provided that the coefficient of determination R^2 ≥ 0.995, such that:

$$E_f = \frac{\sigma_f}{\varepsilon_f} \tag{42}$$

When R^2 < 0.995 then the upper bound of ε_f was reduced from the ISO recommendation of 0.005 ≤ ε_f ≤ 0.025 by the minimum amount to yield R^2 ≥ 0.995. This was necessary due to the varying failure behaviours and yield strains obtained from the different burgers.

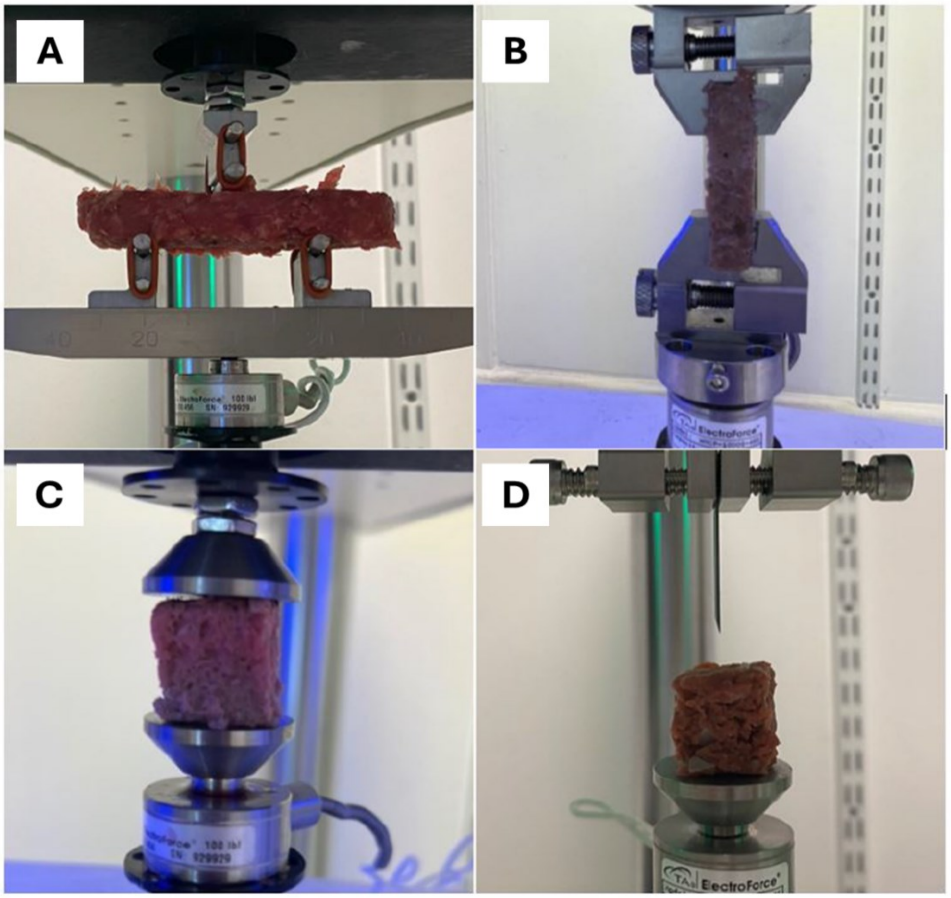

Figure 67: TA ElectroForce 3200 Series III experimental setup for (A) flexion, (B) tension, (C) compression and (D) cutting

5.2.3.2 Tension, Compression and Cutting

Tensile tests were performed in accordance with ISO 527 (International Organization for Standardization, 2019b) with serrated grips, 15 mm wide and 10 mm long (**Figure 67B**). The compressive tests were measured following the ISO 604 (International Organization for

Standardization, 2002) using 20 mm diameter compression plates (**Figure 67C**). The cutting tests, while not directly following any specialised ISO protocol, were conducted similarly to the compressive tests, replacing the upper compression plate with an 11 mm square blade of 1 mm thickness and 30 ° bevel (**Figure 67D**).

For tension, compression and cutting, the strain (ε; **Equation 43**) was defined as:

$$\varepsilon = \frac{\Delta L}{L} \tag{43}$$

where: ΔL is the measured changed length (elongation in tension, contraction in compression and cutting) and L is the original length of the sample. For tension L is equivalent to the gauge length L_0, while in compression and cutting it represents the distance between the bottom plate and upper plate or blade respectively.

The stress (σ; **Equation 44**) was calculated as:

$$\sigma = \frac{F}{lh} \tag{44}$$

with lh representing the cross-sectional area perpendicular to the load direction. For cutting, lh is also the projected area of the blade during compression.

5.2.4 Texture profiling using Texture Profile Analysis (TPA)

Texture Profile Analysis (TPA) is a test which characterises the properties of a food by quantifying its mouthfeel. TPA was performed on an Instron 5965 Series (Instron, USA) fitted with a 500 N load cell (LC3). Measurements were recorded at a frequency of 1000 Hz and a displacement rate of 1 mm/s. The test consisted of two loading cycles (where a cycle is defined as a compression followed by a withdrawal), each to a strain of ε = 0.50, and with a 1 s pause between the first and second compression cycles. The resulting force-time curve, as shown in **Figure 5.2**, provides information on the following values:

- F_1, the peak force of the 1st compression cycle.
- $t_1$and t_2, the times required for the sample to reach maximum load from initial deformation for the 1st and 2nd compression cycle respectively.
- A_a, the area under the force-time curve during the 1st compression (downstroke).
- A_b, the area under the force-time curve during the 1st withdrawal (upstroke) while $F \geq 0$.
- A_c, the area under the force-time curve 1st withdrawal (upstroke) and for $F \leq 0$.
- A_d, the area under the force-time curve during the 2nd compression (downstroke).
- A_e, the area under the force-time curve during the 2nd *w*ithdrawal (upstroke) and for $F \geq 0$.

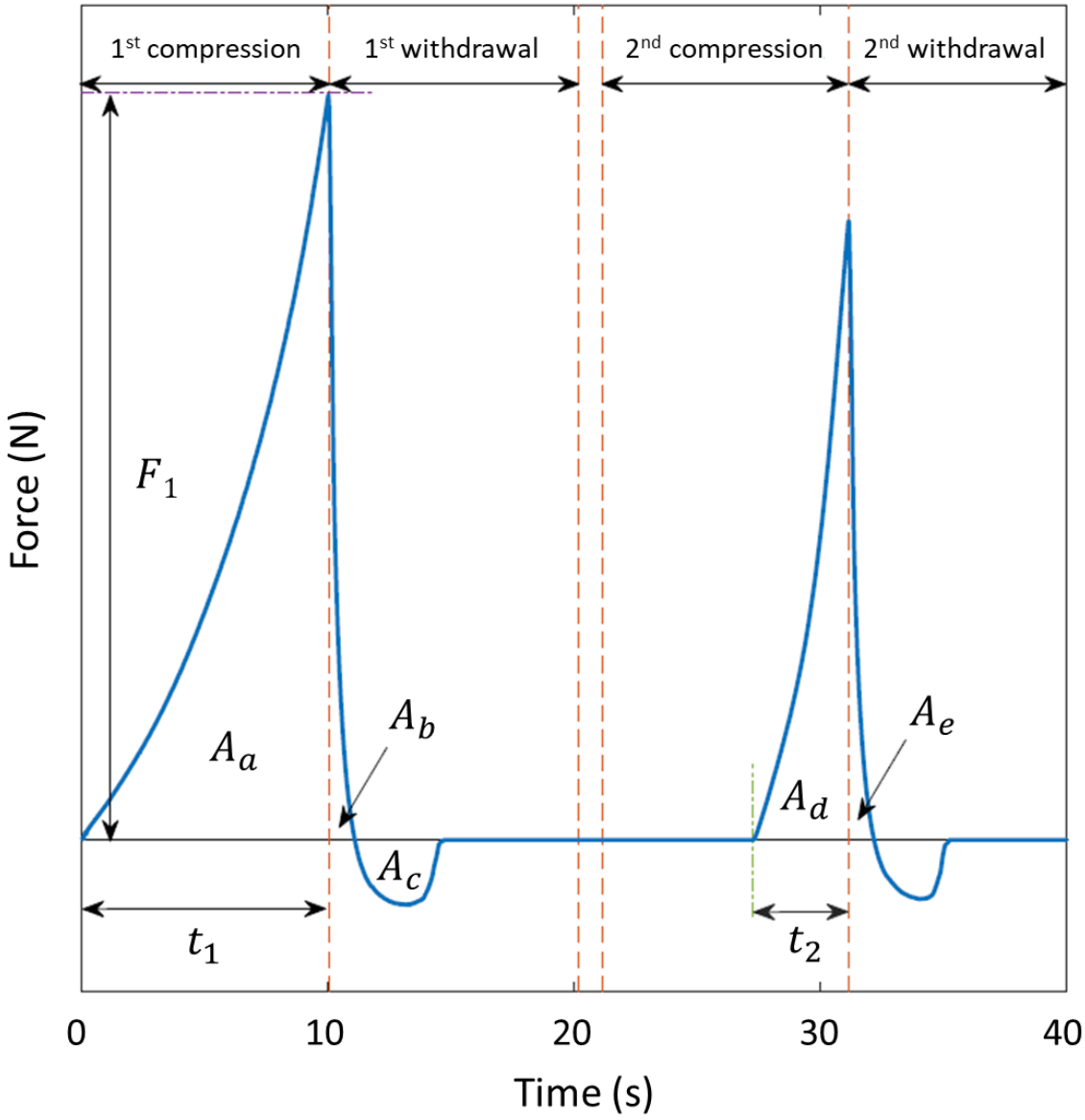

Figure 68: Sample force-time curve resulting from TPA, displaying the two compression and withdrawal cycles separated by a 1 s pause, and definition of the hardness F_1, times t_1 and t_2, and areas A_a, A_b, A_c, A_d and A_e.

From these values, the following textural properties can be ascertained:

- The hardness H (**Equation 45**), relates to the stiffness of the burger and directly influences the mouthfeel of the first bite.

$$H = F_1 \tag{45}$$

- The adhesiveness A_h (**Equation 46**) corresponds to a negative force being generated due to the stickiness of the burger.

$$A_h = A_c \tag{46}$$

- The cohesiveness C_o (**Equation 47**), relates to the consistency of the burger, a lower value being characteristic of disintegration. It is defined as the ratio of the area under the force-time

curve of the second compression cycle (downstroke and withdrawal), compared to the first cycle.

$$C_o = \frac{A_d + A_e}{A_a + A_b} \tag{47}$$

- The springiness S (**Equation 48**), relates to the ability of the burger to recover its original geometrical shape between the two compression cycles, and is computed as the ratio of the time needed to reach maximum force for the 2nd downstroke compared to the first.

$$S = \frac{t_2}{t_1} \tag{48}$$

- The resilience R (**Equation 49**), quantifies the recovery from deformation during the first compression cycle. It is defined as the ratio of the area under the curve of the first withdrawal compared to the first compression.

$$R = \frac{A_b}{A_a} \tag{49}$$

- The chewiness C_h (**Equation 50**) relates to the ease of biting and energy needed to chew to swallow. It is calculated as the product of hardness, springiness and cohesiveness.

$$C_h = HSC_o \tag{50}$$

5.2.5 Uncertainty and Statistical analysis

The uncertainty U (**Equation 51**) of the results is expressed as the root sum of the bias B and the precision P, such that:

$$U = \sqrt{(B^2 + P^2)} \tag{51}$$

The bias (**Equation 52**) of a given quantity X, computed using a number N of independent measured variables x_i, is given as:

$$B(X) = \sqrt{\sum_{i=1}^{N} \left(\frac{\partial X}{\partial x_i} B(x_i) \right)^2} \tag{52}$$

where the bias limits $B(x_i)$ associated with the measured quantities and load cells employed are detailed in **Table 11**.

The precision (**Equation 53**) is computed as the 95% confidence level such that:

$$P = \frac{t_{95}\sigma_{dev}}{\sqrt{n}} \tag{53}$$

Where t_{95} = 2.201 is the critical value at 95% confidence for the number of samples tested n = 12 and σ_{dev} is the standard deviation.

The results were analysed using a one-way analysis of variance (ANOVA) followed by a Tukey's Honestly Significant Difference (HSD) test (see Chapter II, *section 2.2.5*). The bar charts presented in this chapter show the means for each type of burger (n = 12), with error bars representing the uncertainty associated with the mechanical properties quantified. The different letters above each bar indicate statistical difference ($p<0.05$). Burger types with the same letter have means that are not significantly different from each other.

Table 11: Summary of bias limits for the three load cells used for testing.

Bias	TA ElectroForce		Instron
	LC1 (10 N)	LC2 (450 N)	LC3 (500 N)
Force, $B(F)$ (N)	0.00013	0.00020	0.0005
Width, $B(l)$ (mm)	0.005	0.005	0.005
Thickness, $B(h)$ (mm)	0.005	0.005	0.005
Length, $B(L)$ (mm)	0.005	0.005	0.005
Elongation, $B(\Delta L)$ (mm)	0.00073	0.00233	0.0005
Span, $B(s)$ (mm)	0.005	0.005	0.005
Deflection, $B(\omega)$ (mm)	0.00073	0.00233	0.0005
Sampling time, t_s (s)	0.005	0.005	0.0005

5.3 Results & Discussion

5.3.1 Burger selection

Food quality is subjective and therefore choosing burgers that represent the ideal meat texture can be difficult without extensive consumer studies. However, it is well known that human senses directly influence the perception of taste and the likelihood that a consumer would buy a product again (Imtiyaz *et al*., 2021; Pakseresht *et al*., 2022). Moreover, properties such as visual aspect, smell, flavour, texture and mouthfeel, influence the perception of quality (Akdeniz *et al*., 2013). To determine the textural properties that make meat products unquestionably *meat-like*, burgers were selected based on attributes that drive quality perception, notably the price, branding, degrees of naturalness and processing. When possible, high (≥ 19%) and low (≤ 5%) fat burgers of the same brand were compared to elicit the role of fat on texture. In addition, two PBA burgers were selected based on the same marketing concepts to compare the texture of existing alternative protein products with

their traditionally farmed beef counterparts. A summary of the burgers used in this study as well as their composition and marketable attributes were presented in **Table 10**.

The B2 and B4 burgers were purchased from Marks & Spencer, a brand that has long been associated with food quality and excellent service (Freear, 2015) and has for the third consecutive year won the annual "Which? UK Supermarket Satisfaction Survey" (Walsh and Simmonds, 2024). On the other hand, the B1 and B5 were purchased from Morrisons which came in last position in that same survey, scoring especially low on the perception of their own brand of products. Although, product quality cannot be ascertained from perception of the retailer, and the higher prices of B2 and B4 cannot stand as scientific proof of better burger quality than the lower priced B1 and B5, it has been shown that consumers are heavily influenced by marketing when choosing a product and determining its quality (Kurz *et al*., 2023). Known as the price-quality heuristic, consumers tend to associate higher prices with better food quality and thereby create higher expectations of more expensive products. This in turn can trigger the marketing placebo effect where products taste better when they are either labelled with higher price tags (Plassmann and Weber, 2015) or presented in nicer environments (Freear, 2015; Seo, 2015). Burger B3, being the only handmade burger could also be perceived as of better quality, since consumers are generally concerned about industrial food processing techniques, resulting in a perceived loss of flavour (Abouab and Gomez, 2015). In fact, it has been shown that that consumers tend to view handmade foods as unique products of higher value crafted with care (Rivaroli *et al*., 2020). It is worth noting that while the higher cost of B3 may partially reflect the handmade assembly of the burger, its inflated cost is also likely associated to halal branding. The composition of the various meat burgers (**Table 10**) also revealed important differences in terms of meat content that could influence the perceived quality of the products. B1 and B2 had the highest meat contents (≥ 95%) compared to B3, B4 and B5 (≤ 82%), which were composed of more additives as meat extenders. While additives in the meat burgers were mostly natural (*e.g.* water, spices), some antioxidants and preservatives could also be present. The naturalness of a product has been shown to boost consumer perception of quality, with reports of consumers willing to pay more for additive-free foods (Rivaroli *et al*., 2020). Products with fewer and more natural ingredients were shown to be associated with higher food quality by consumers (Siegriest and Sütterlin, 2017).

For the PBA burgers, Tesco own brand Plant Chef B6 burgers were compared to the highly promoted Beyond Meat B7. While the higher price of the latter might indicate a higher quality product, part of the burger's high price can be attributed to the costs of research and development and marketing of novel foods (GFI, 2021). By contrast, supermarket giants tend to operate on a low-margin/high-volume model which enables price parity with traditional meat products (GFI, 2021).

The cooking yields, both by mass and volume, for the seven burgers under investigation were measured and presented in **Table 12**. The cooking yield by mass was lower for B2 and B5, possibly resulting from some fat loss during cooking, although no correlation was observed between fat content and cooking yield by volume. B1, which had just under a quarter of the fat of B2 and B5 and, unlike these, an absence of water in the ingredients, had the highest cooking yield by mass and volume. This would suggest that the mass and volume lost during cooking resulted from the melting of fats and evaporation of water. As for the PBA burgers, the yield by volume and mass remained high due to the presence of oils designed to keep the burgers moist and voluminous during the cooking process (Kyriakopoulou *et al*., 2021).

Table 12: Cooking yield by mass $\boldsymbol{Y_M}$ and volume $\boldsymbol{Y_V}$ ($n \geq 4$).

Label	$\boldsymbol{Y_M}$	$\boldsymbol{Y_V}$
B1	0.755 ± 0.15	0.953 ± 0.07
B2	0.522 ± 0.10	0.849 ± 0.13
B3	0.599 ± 0.09	0.882 ± 0.03
B4	0.655 ± 0.07	0.876 ± 0.12
B5	0.537 ± 0.08	0.871 ± 0.06
B6	0.623 ± 0.10	0.946 ± 0.05
B7	0.612 ± 0.09	0.890 ± 0.14

5.3.2 Mechanical properties

5.3.2.1 Flexion

Flexion is a measure of how resistant a material is to being bent. It can be compared to the forces applied by the tongue when firmly biting or chewing on a food, thereby directly relating to mouthfeel. Results are shown in **Figure 69** for all samples except raw B7 which lacked sufficient integrity to be handled in its uncooked state at room temperature.

The cooking process led to an increase in flexural modulus of about one order of magnitude. Yield strains (ε_{yf}), on the other hand, remained comparable between the raw and cooked burgers, although a slight increase in meat products contrasted with a reduction in the plant-based B6. The values of $\varepsilon_{yf,cooked}$ were of particular interest and exhibited a relevant pattern which could be a first step towards characterising the desirable mechanical properties for cultivated meat products.

The three highest values were achieved by the handmade (B3) and high-beef content products (B1 and B2, 96% and 95% beef, respectively), with $\varepsilon_{yf,cooked} \geq 0.190$, followed by the low-beef content

products (B4 and B5, 81% and 76%, respectively) which exhibited a similar values $\varepsilon_{yf,cooked} \approx 0.148$, and the plant-based burgers (B6 and B7) $\varepsilon_{yf,cooked} \leq 0.115$ had the lowest values.

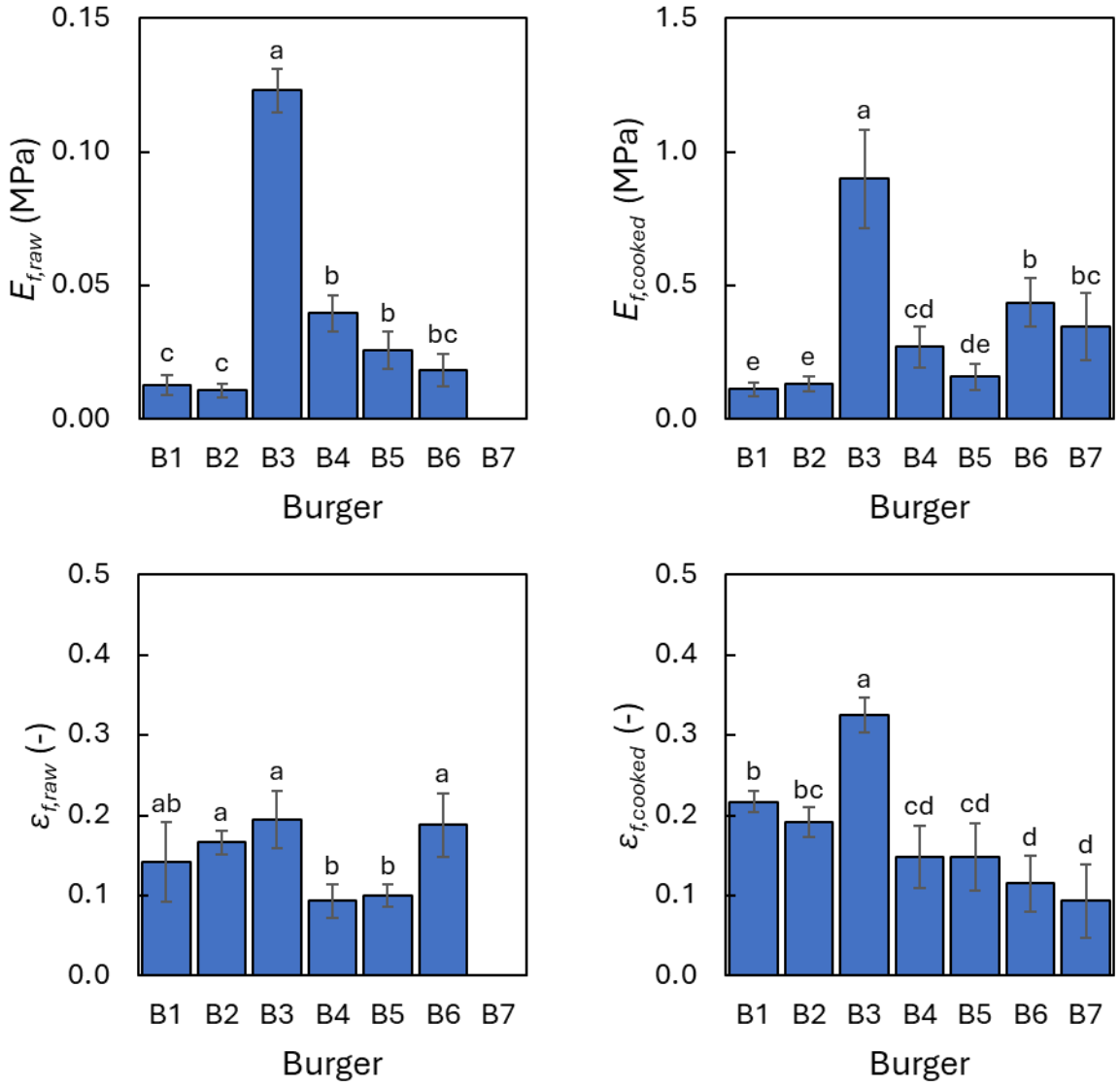

Figure 69: Flexural results for (A) the raw burger modulus $E_{f,raw}$, (B) the cooked burger modulus $E_{f,cooked}$, (C) the raw yield strain $\varepsilon_{f,raw}$ and (D) the cooked yield strain $\varepsilon_{f,cooked}$ (n = 12). Note: no results are presented for B6 in subfigures (A) and (C) as the B6 burger did not have sufficient structural integrity to undergo the tests when raw. The letters above each bar indicate statistical difference ($p<0.05$). Burger types with the same letter have means that are not significantly different from each other.

It is also notable that the B3 burger stood out with higher moduli (raw and cooked) and yield strain (cooked) than all other burgers (**Figure 69A,B,D**). This could be attributed to the unique manufacturing process of the product. As the only handmade burger, it is possible that the meat was ground more coarsely, leading to larger meat chunks in the final product (Witte *et al.*, 2022), which would affect the mechanical properties of B3 in flexion (Gurikar *et al.*, 2014). Another factor that would influence the mechanical properties of B3 was its high composition of wheat flour (**Table 10**) used as a cheap natural

binder in reconstructed meats. Wheat flour is composed of 70-75% starch and 2-4% arabinoxylans (Moiraghi *et al*., 2019) that act by absorbing, entrapping, and emulsifying water and fat (Sharma *et al*., 2014; Ahmad *et al*., 2022), providing a gelling and thickening effect in raw products and preventing fluids from leaking during cooking (Kyriakopoulou *et al*., 2021). The addition of natural binders plays a big role in improving meat texture and consumer acceptance in reconstructed meats (Boles and Shand, 1999). However, while nearly all the burgers use binders such as rice flour (B1, B2, B4, B6), broad bean flour (B4), potato starch (B7) and maize and tapioca starch (B6), the relative concentration by weight of binders in other beef burgers was lower (< 5%, for B1 and B2; and listed as final ingredients before salt and pepper, for B4) than that of wheat flour in B3 (~ 8%).

B7 has a very high liquid content with water listed as the first ingredient and rapeseed oil as the third, and this is probably the reason for the lack of ability of the raw B7 to maintain its integrity under the standard testing conditions. No flexural tests **(Figure 69A,C**) could be performed in its raw state, even by reducing the span from s = 4 mm to s = 2 mm to improve sample stability However, when the sample temperature was also lowered (9-15 °C) the B7 burgers exhibited sufficient integrity to be tested but, due to a lack of clear sample fracture, only the flexural modulus could be measured $E_{f,raw}$ = 0.0020 MPa, which was comparable to the B6 burger at $E_{f,raw}$ = 0.0019 MPa under the standard conditions. While the increased integrity of raw B7 in the new testing conditions may have resulted from the increased solidity of coconut oil at lower temperatures, it could also have been caused by the stiffening from chilling of other components, as mechanical properties of foods are temperature dependent (Polachini *et al*., 2023). It should be noted that as both beef and PBA burgers are intended to be stored in a fridge until they are cooked, the handling of B6 and B7 burgers should be similar to that of traditional meats in a normal food preparation setting.

Vegetable oils are often used in PBAs as replacement product for animal fat (Lee et al., 2023). Just like meat fat, the low melting temperature of many vegetable oils allows the fluids to seep out of the plant-based burger during cooking, improving the flavour, juiciness and tenderness of the patty (Lee et al., 2023). Some vegetable oils, such as coconut oil, are rich in saturated fats and semi-solid at room temperature ($T_{m,coconut\ oil}$ = 25 °C; Srivastava et al., 2017) and are used in PBAs to mimic the appearance and texture of animal fat. However, it has been shown that diets with too much saturated fat raise cholesterol and incidence of cardiovascular disease (Maki et al., 2021; Wang et al., 2023). To counter this and improve cooking properties, other vegetable oils which are rich in unsaturated fats, such as rapeseed oil, are widely used in food processing but are completely liquid at room temperature due to their low melting point ($T_{m,rapeseed\ oil}$ =- 10 °C; Fasina et al., 2008). Both B6 and B7 contain rapeseed and coconut oils, however B6 had more vegetable oil and that was predominantly rapeseed

oil. Studies have also shown that the amount of vegetable oils present in PBA products positively correlated with lower product elasticity (de Santos-Paglarini et al., 2019).

5.3.2.2 Tension

Tension is a measure of how resistant a material is to being torn. Unlike flexion and compression, this process has no direct analogy to eating and mouthfeel. The results of tensile testing are shown in **Figure 70**.

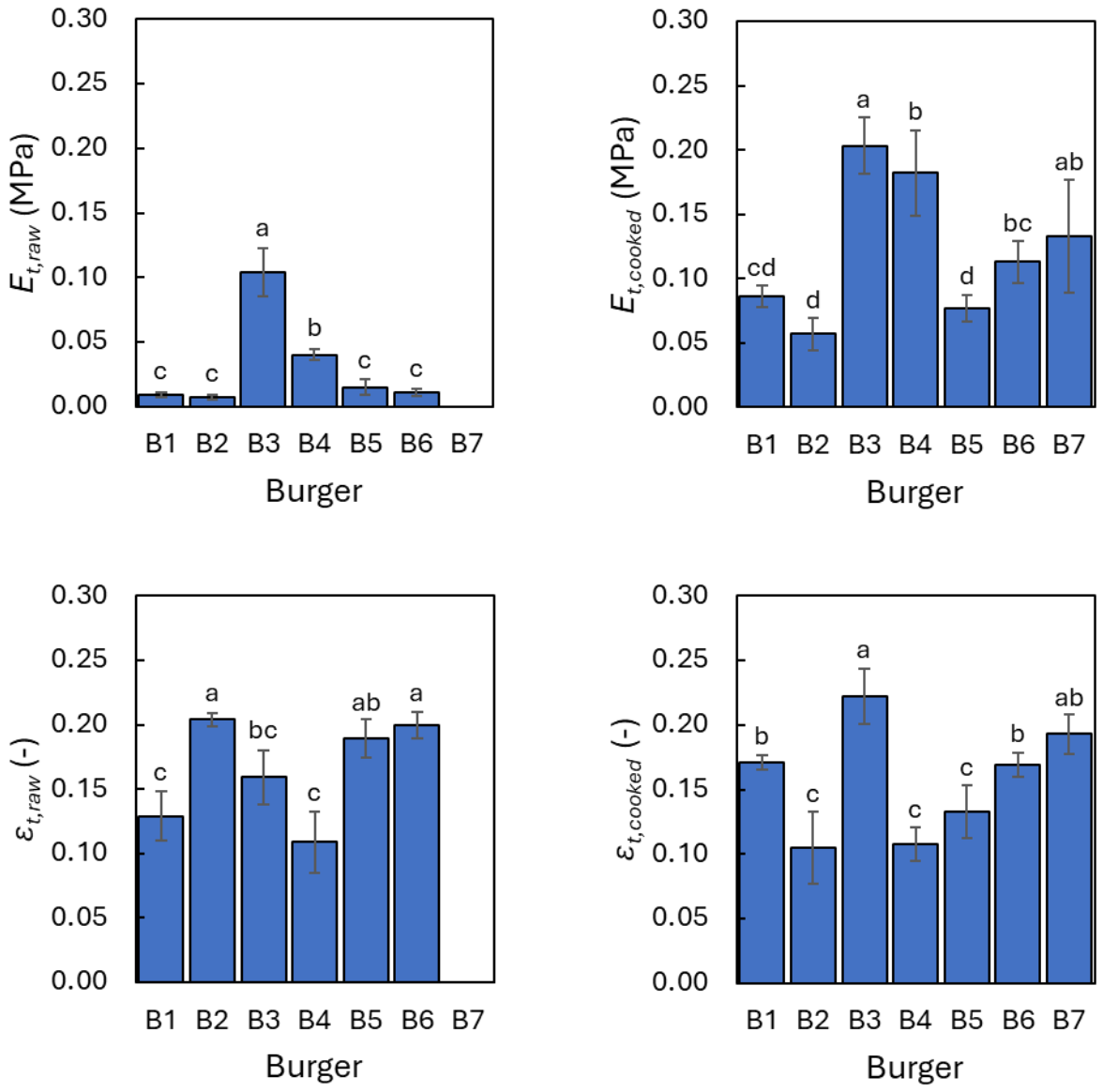

Figure 70: Tensile results for (A) the raw burger modulus $E_{t,raw}$, (B) the cooked burger modulus $E_{t,raw}$, (C) the raw yield strain $\varepsilon_{t,raw}$ and (D) the cooked yield strain $\varepsilon_{t,cooked}$(n = 12). Note: no results are presented for B6 in subfigures (A) and (C) as the B6 burger did not have sufficient structural integrity to undergo the tests when raw. The letters above each bar indicate statistical difference ($p<0.05$). Burger types with the same letter have means that are not significantly different from each other.

As for flexion testing (*section 5.3.2.1*), burger B7, with its high content of fluids, notably water and rapeseed oil, exhibited poor structural integrity and could not be tested raw. Thus, no data are

displayed for B7 in **Figure 70A** and **Figure 70C**. Subsequent testing showed that reducing the gauge length to L_0 = 1.5 mm and lowering the testing temperature allowed sufficient integrity for the raw testing of B7. The modulus of the chilled B7 ($E_{t,raw}$ = 0.026 MPa) was significantly higher than that of B6 tested under the original conditions ($E_{t,raw}$ = 0.011 MPa), and lay within the range of measurements of the beef burgers, tested in the original conditions (0.007 MPa ≤ $E_{t,raw}$≤ 0.104 MPa).

As in flexural testing (*section 5.3.2.1*) the B3 burger stood out with higher moduli (raw and cooked) and yield strain (cooked) than all other burgers. The burgers with the highest meat content (B1 and B2, 96% and 95%, respectively) had raw tensile moduli of $E_{t,raw}$ ≈ 0.008 MPa, whereas burgers with lower meat content (B3, B4 and B5, 82%, 81% and 76% respectively) had raw tensile moduli of considerably higher levels, 0.015 MPa ≤ $E_{t,raw}$ ≤ 0.104 MPa. Although cooking increased the tensile modulus of all burgers, the absence of any pattern in the results could be due to the presence and cooking of different additives in the burger composition of each sample. No other pattern distinguishing different types of burgers was easily discerned from either the moduli or the yield strains (raw and cooked), which suggests that tensile properties, despite having a well-established ISO test protocol ISO (2019b), may be poor indicators for quantifying a burger's sensory profile.

Nevertheless, increasing numbers of studies have used tensile testing either with, or as an alternative to, textural profiling methods in foods and especially for meat and meat-replacement products (de Avila et al., 2014; Ko *et* al., 2023; Shlangen *et al*, 2023). Interestingly, tensile testing is also commonly used in tissue engineering for biomechanical characterisation, assessing soft tissue integrity (Griffin *et al*., 2016; Sholze *et* al., 2020; Wale *et al*., 2024), and optimising substrate stiffness for cell differentiation (Yi *et al*., 2022) which is particularly relevant to cultivated meat production and textural properties (Lee *et al*., 2024. *Lv et al.*, 2015).

5.3.2.3 Compression

Compression is a measure of how resistant a material is to being crushed. It is comparable to the forces applied by the jaw when firmly biting into a food at the back of the mouth (molar teeth), thereby directly relating to mouthfeel. The compression testing results, displayed in **Figure 71** showed striking differences between both the raw and cooked moduli (**Figure 71A,B**) and the cooked yield strains (**Figure 71D**) of meat and plant-based burgers. The raw compressive modulus of beef burgers $E_{c,raw}$ ≥ 0.09 MPa was significantly higher than that of PBA burgers at $E_{c,raw}$ ≤ 0.03 MPa. In addition, the cooking stiffened all burgers by approximately one order of magnitude, bringing the compressive modulus of cooked beef burgers to $E_{c,cooked}$ ≥ 0.94 MPa and that of PBA burgers to $E_{c,cooked}$ ≤ 0.42 MPa. In contrast, in the compressive yield strains, higher values were achieved by PBA burgers $\varepsilon_{c,cooked}$ ≥ 0.210, compared to the high-beef-content and handmade burgers (B1, B2, and B3) scoring

intermediate values 0.084 ≥ $\varepsilon_{c,cooked}$ ≥ 0.149, and the low-beef-content burgers (B4 and B5) having the lowest values at around $\varepsilon_{c,cooked}$ ≈ 0.048. In summary, cooked beef products were characterised by a high compressive modulus and low compressive yield strain, whereas the cooked PBA products featured a low compressive modulus and high compressive yield strain. This represents a clear distinction, which could inform efforts to develop properties in cultivated meat that would meet consumer expectations, while being governed by an established test protocol (International Organization for Standardization, 2002) to ensure reproducibility.

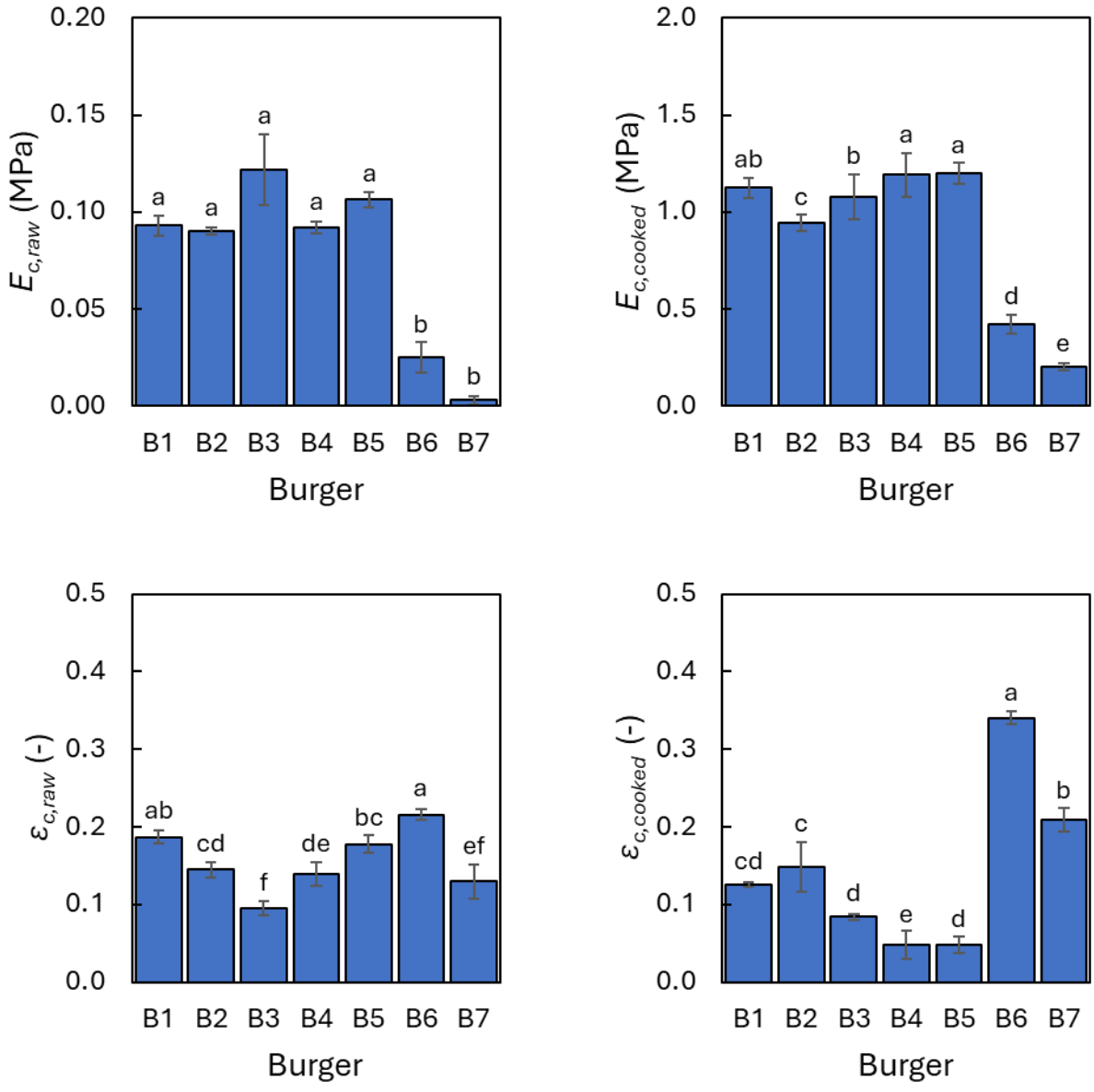

Figure 71: Compressive results for (A) the raw burger modulus $E_{c,raw}$, (B) the cooked burger modulus $E_{c,cooked}$, (C) the raw yield strain $\varepsilon_{c,raw}$ and (D) the cooked yield strain $\varepsilon_{c,cooked}$ (n = 12). The letters above each bar indicate statistical difference ($p<0.05$). Burger types with the same letter have means that are not significantly different from each other.

5.3.2.4 Cutting

Cutting is a measure of how resistant a material is to being chopped. In essence, cutting is a measurement of compression applied to a much thinner area within the sample and employs a blade that descends vertically into a material. This is comparable to the forces applied by the jaw when firmly biting into a food at the front of the mouth (incisor teeth), thereby directly relating to mouthfeel.

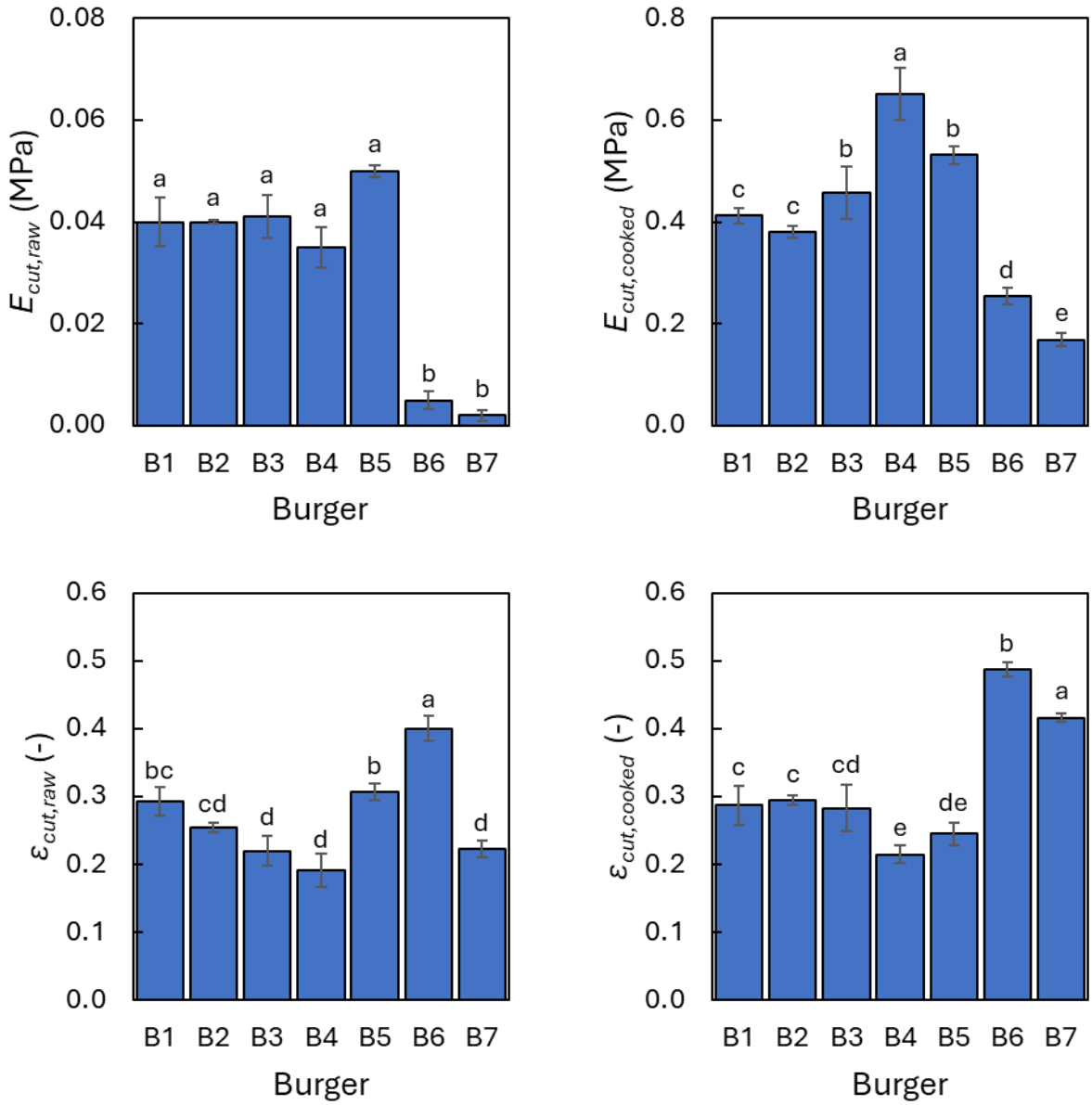

Figure 72: Cutting results for (A) the raw burger modulus $E_{cut,raw}$, (B) the cooked burger modulus $E_{cut,cooked}$, (C) the raw yield strain $\varepsilon_{cut,raw}$, and (D) the cooked yield strain $\varepsilon_{cut,cooked}$ (n = 12). The letters above each bar indicate statistical difference (p<0.05). Burger types with the same letter have means that are not significantly different from each other.

The cutting results for the raw and cooked modulus $E_{cut,raw}$ and $E_{cut,cooked}$ and the raw and cooked yield strain $\varepsilon_{ycut,raw}$ and $\varepsilon_{ycut,cooked}$ are presented in **Figure 72** which shows that similarly to the compressive results (*section 5.3.2.3*), there were clear distinctions between the beef and PBA burgers with regards to raw and cooked moduli (**Figure 72A,B**) and cooked strains (**Figure 72D**). Again, the

beef burgers had significantly higher cutting moduli than PBA burgers, however a stronger distinction could be made between cutting moduli of the cooked higher-beef-content burgers and handmade burger (B1, B2, and B3) $0.38 \leq E_{cut,cooked} \leq 0.41$ MPa, lower-beef-content burgers (B4 and B5) $E_{cut,cooke} \geq 0.53$ MPa and PBA $E_{cut,cooked} \leq 0.25$ MPa (**Figure 72B**). Likewise, the cooked yield strain, PBA burgers $\varepsilon_{cut,cooked} \geq 0.416$, had the highest values, followed by higher-beef-content and handmade burgers, around $\varepsilon_{cut,cooked} \approx 0.288$, and lastly beef burgers with lower beef content, $\varepsilon_{cut,cooked} \leq 0.245$.

These results quantify another sensory aspect of the burgers, clearly establishing trends between various types. However, the lack of an ISO protocol dedicated purely to cutting could limit the reproducibility of these tests.

To summarise, the mechanical properties obtained from reproducible ISO standardised single cycle uniaxial tests, namely flexion, tension, compression and cutting (using the modified compression ISO protocol) on a range of burgers, provided key aspects and indicators of burger quality and ingredient compositions. Compression, cutting and flexion tests also showed trends that highlighted differences between the higher-beef-content, lower-beef-content and PBA burgers, all of which could inform the development of cultivated meat with a view to improving mouthfeel properties and thus increasing consumer acceptance. Conversely, despite its use in tissue culture, no clear patterns were observed within tensile properties to differentiate between the various burger types.

5.3.3 Textural properties

Textural profiling analysis (TPA), focussing directly on texture, may yield properties more relevant for food products than ISO standards for mechanical testing, even though there are no established standards for TPA. The results for six properties yielded by the TPA double compression cycle test are examined in this section.

5.3.3.1 Hardness

Hardness is the resistance of a material to plastic deformation and corresponds to the maximum force applied during the first compression (downstroke) taken to the same strain for all samples. In short, hardness gives information on how easy it is to bite into a material.

As expected, the hardness results shown in **Figure 73** for both raw and cooked burgers were consistent with the compressive moduli of raw and cooked burgers (*section 5.3.2.3*). PBA burgers continued to exhibit lower values $H_{cooked} \leq 24.845$ N compared to beef burgers $34.487 \leq H_{cooked} \leq 43.863$ N. A further distinction could also be made between the higher-beef-content and handmade burgers (B1, B2 and B3) $41.177 \leq H_{cooked} \leq 43.863$ N and the lower-beef-content burgers (B4 and B5)

34.487 ≤ H_{cooked} ≤ 37.814 N. These results confirmed the results of the compression and cutting mechanical tests, which showed that the beef burgers had a greater resistance to deformation than PBAs.

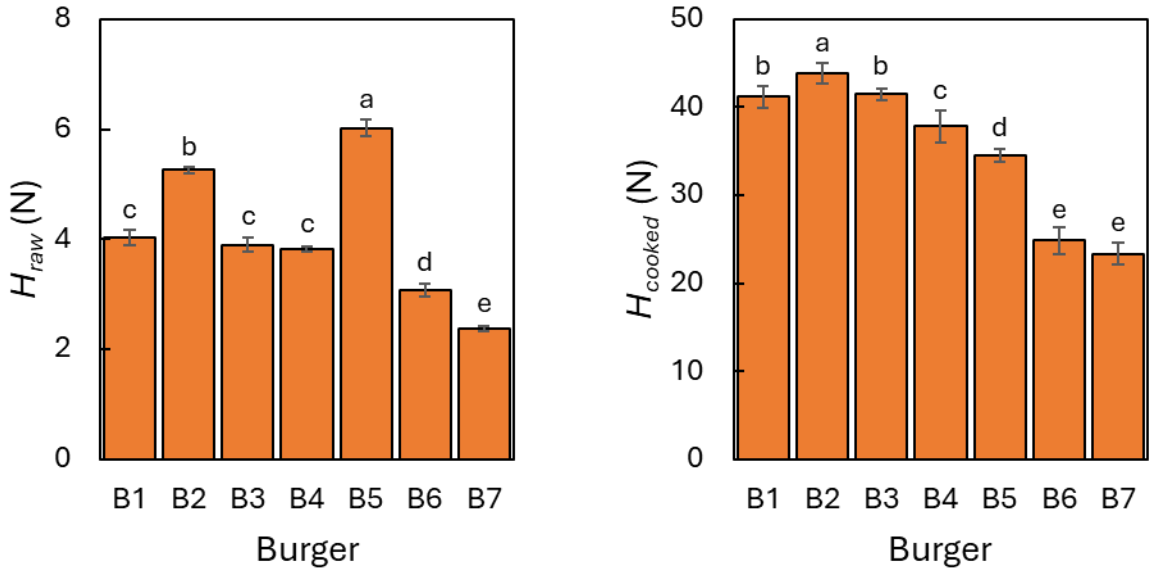

Figure 73: Hardness results for (A) raw burgers and (B) cooked burgers (n = 12). The letters above each bar indicate statistical difference (p<0.05). Burger types with the same letter have means that are not significantly different from each other.

5.3.3.2 Adhesiveness

Adhesiveness is a measure of material stickiness and can relate to the likelihood of foods attaching to the mouth, mainly the palate and teeth. While adhesiveness was measured on both raw and cooked burgers, no adhesiveness was observed in any of the burgers. Consequently, only the raw results were presented in **Figure 74.**

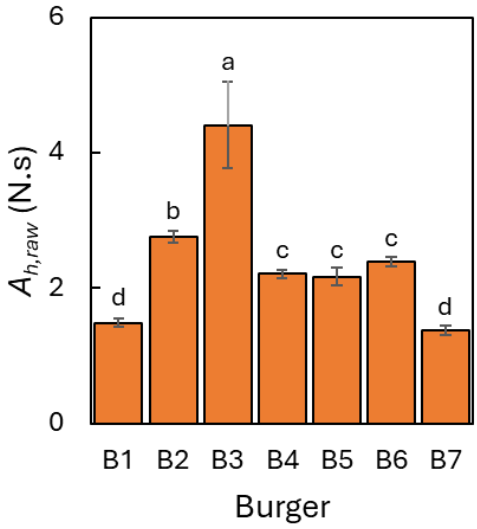

Figure 74: Adhesiveness results for raw burgers (n = 12). The letters above each bar indicate statistical difference (p<0.05). Burger types with the same letter have means that are not significantly different from each other.

No clear trend was evidenced in the results shown although the values may be relevant to the manufacturing process, where the adhesiveness of raw burgers could have a non-negligeable impact for machinery (*e.g.* conveyor belts). In a niche setting, these results could also serve as a guide for producing cultivated meats aimed at being served raw (*e.g*. steak tartare).

5.3.3.3 Cohesiveness

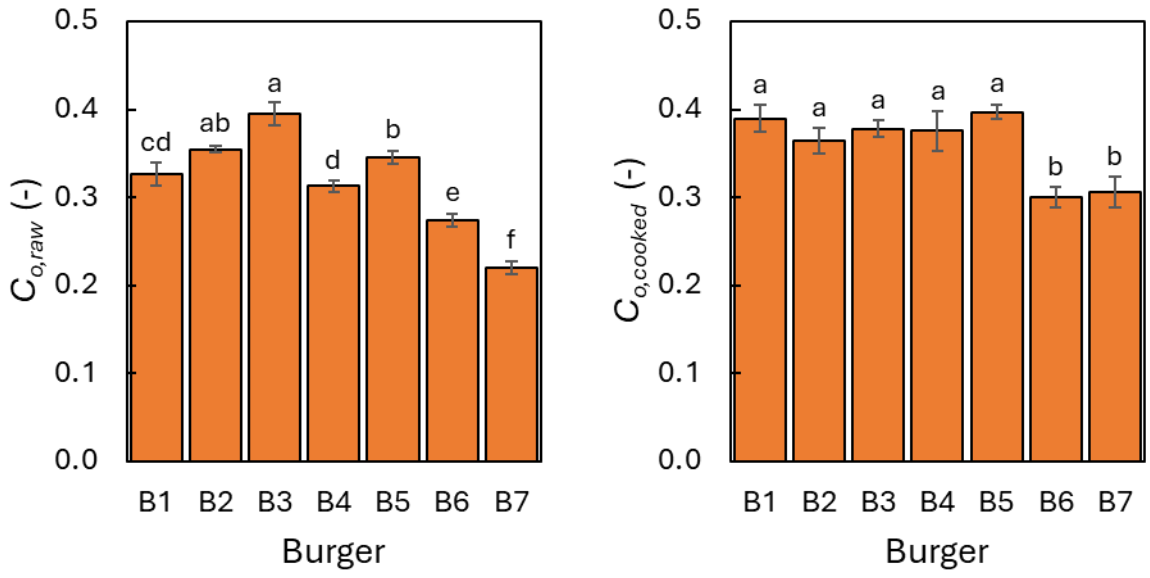

Figure 75: Cohesiveness results for (A) raw burgers and (B) cooked burgers (n = 12). The letters above each bar indicate statistical difference (p<0.05). Burger types with the same letter have means that are not significantly different from each other.

Cohesiveness relates to the strength of bonds within the body of a food and therefore represents the main determinant of food integrity, with lower values indicating food disintegrating more easily. As shown in **Figure 75**, minimal changes were observed between the cohesiveness results in raw and cooked states, however, the cohesiveness of beef burgers (0.376 ≤ $C_{o,cooked}$ ≤ 0.397) was significantly higher than that of PBA burgers ($C_{o,cooked}$ ≈ 0.3). These results highlight textural differences between the *firmness* of beef burgers and *mushiness* of PBAs.

5.3.3.4 Springiness

Springiness is a measure of the recovery and the viscoelastic properties of a food and is therefore dependent on cohesiveness. In essence, this corresponds to how quickly a food recovers its shape between successive bites. **Figure 76** shows that in the raw state there is a clear distinction between high-beef-content (0.684 ≤ S_{raw} ≤ 0.812), low-beef-content (0.500 ≤ S_{raw} ≤ 0.585) and PBA burgers (0.359 ≤ S_{raw} ≤ 0.464). However, the cooked results for all the burgers were similar, indicating the success of the PBA burgers in achieving this meat-like property. Nevertheless, high-beef-content burgers (B1, B2) exhibited the highest springiness of all (0.85 ≤ S_{cooked} ≤ 0.88) although the

differences in values within the high-beef and low-beef content groups were not statistically significant.

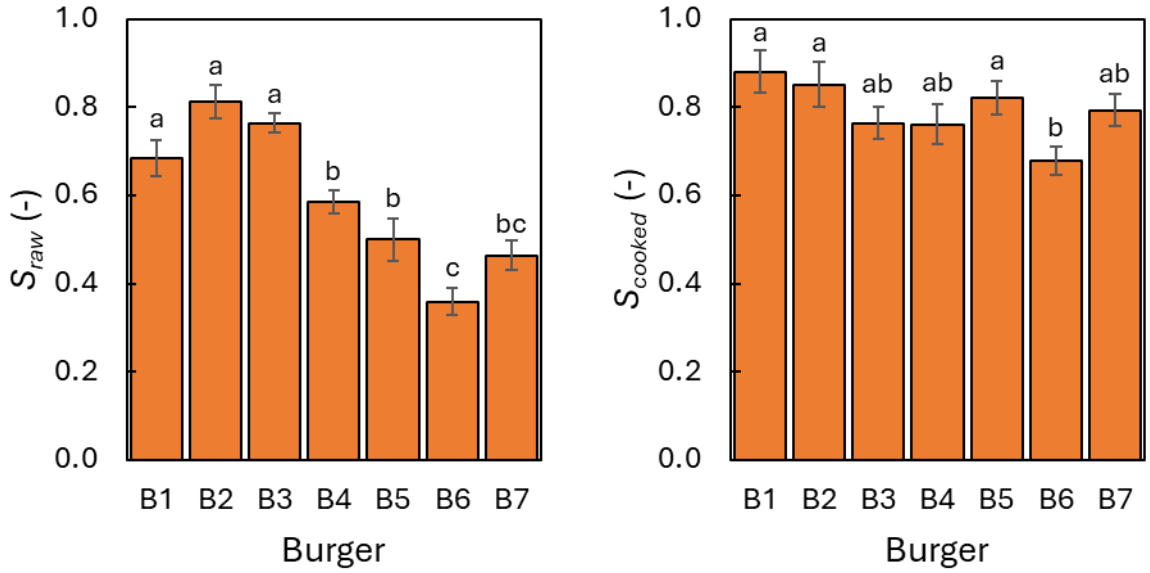

Figure 76: Springiness results for (A) raw burgers and (B) cooked burgers (n = 12). The letters above each bar indicate statistical difference ($p<0.05$). Burger types with the same letter have means that are not significantly different from each other.

5.3.3.5. Resilience

Resilience is another measure of the recovery, but unlike springiness, it quantifies how well a material regains its original height following plastic deformation. This corresponds to how well foods retain their shape after successive biting. Highly resilient foods will require longer chewing before they can be swallowed. The resilience of all burgers was significantly increased by cooking, as shown in **Figure 77**:. In their raw state the beef burgers showed slightly more resilience (0.056 ≤ R_{raw} ≤ 0.069) than PBAs (0.045 ≤ R_{raw} ≤ 0.049), and the difference was significantly accentuated in the cooked samples to 0.139 ≤ R_{cooked} ≤ 0.159 for beef burgers and 0.106 ≤ R_{cooked} ≤ 0.107. These results continue to highlight differences in firmness of beef and PBA burgers.

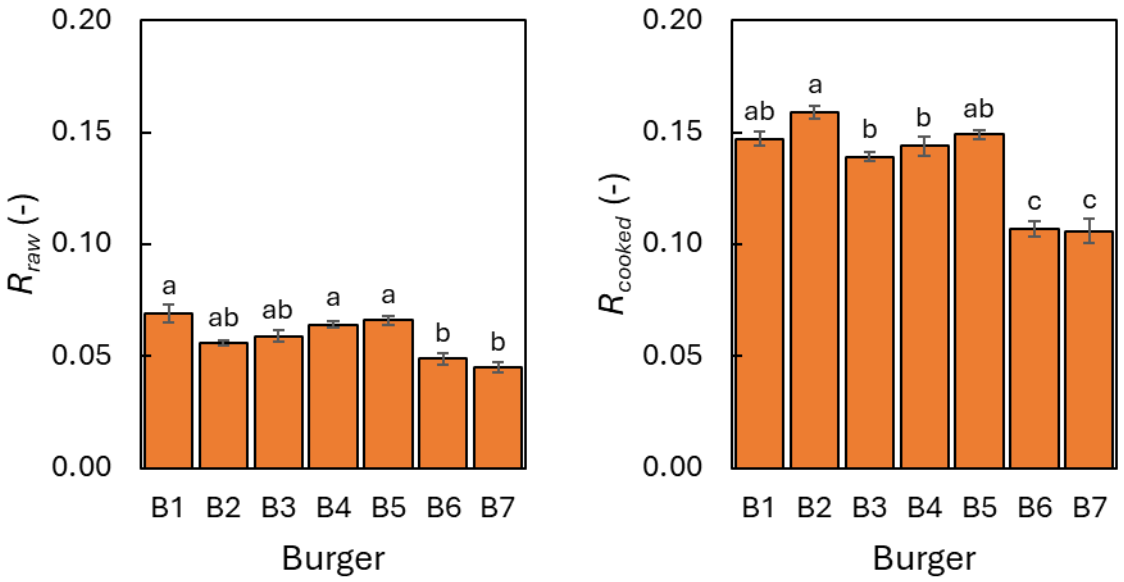

Figure 77: Resilience results for (A) raw burgers and (B) cooked burgers (n = 12). The letters above each bar indicate statistical difference (p<0.05). Burger types with the same letter have means that are not significantly different from each other.

5.3.3.6 Chewiness

Chewiness, the product of hardness, springiness and cohesiveness is an aggregated indicator of mouthfeel. In essence, chewiness quantifies how much a food needs chewing for it to be swallowed efficiently. Optimising chewiness is therefore fundamental when designing new foods with consumer acceptance in mind. Results for chewiness are presented in **Figure 78**. No clear pattern can be identified from the beef burgers in their raw state (**Figure 78A**) due to the lack of pattern in the raw hardness (*section 5.3.3.1*) and raw cohesiveness (*section 5.3.3.3*) in these burger types. However, there was a significant difference between the chewiness of beef burgers (0.701 ≤ $C_{h,raw}$ ≤ 1.516 N) and PBA burgers (0.242 ≤ $C_{h,raw}$ ≤ 0.302 N). Moreover, the cooking process significantly increased the chewiness of all burger types by one order of magnitude and revealed a clear distinction between the higher-beef-content and handmade (B1, B2 and B3; 13.544 ≤ $C_{h,cooked}$ ≤ 14.143 N), the lower-beef-content(B4 and B5; 10.82 ≤ $C_{h,cooked}$ ≤ 211.254 N) and PBA (4.469 ≤ $C_{h,cooked}$ ≤ 5.054 N) burgers. The chewiness range within the burger types was also very narrow, only 4.4% for the higher-beef-content and homemade burgers and 4.0% for the lower-beef content burgers. This is particularly important because it provides defined ranges for texture optimisation that may clearly correlate to consumer expectations and acceptance. On the other hand, the range of the PBA burgers (11.5%) was wider and can be explained by the great differences in the main protein type and composition of secondary ingredients.

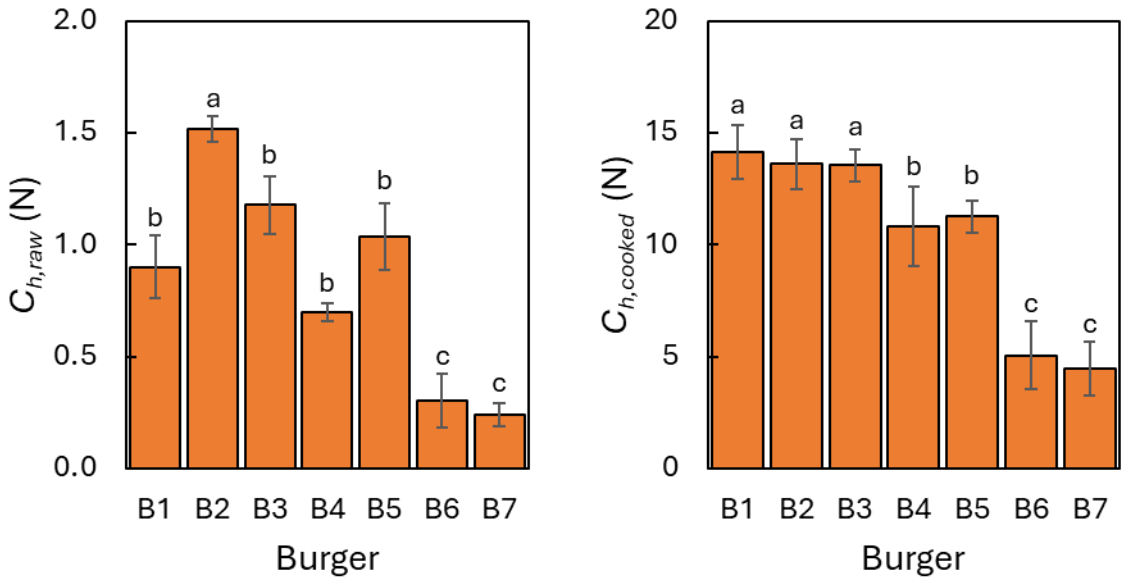

Figure 78: Chewiness results for (A) raw burgers and (B) cooked burgers (n = 12). The letters above each bar indicate statistical difference ($p<0.05$). Burger types with the same letter have means that are not significantly different from each other.

Overall, the TPA results for the cooked burgers showed clear similarities between all the beef burgers and a stark contrast between beef and PBA burgers. In the case, of chewiness, which is a composite indicator (the product of hardness, springiness and cohesiveness) there was also a clear distinction between high and low beef content burgers, as in the earlier flexural and cutting mechanical tests, and the handmade burger had similar results to the high beef content burgers. The results for the raw burgers also showed that PBAs generally had much lower values than the beef products but proved to be less useful in identifying common characteristics across the beef burgers.

5.3.4 Textural optimisation for cultivated meat production

Both the mechanical and textural tests identified relevant tests to be undertaken as well as key properties to be targeted to improve mouthfeel and increase consumer satisfaction when designing new alternatives to traditional meat. In the mechanical tests PBA burgers were characterised as having lower moduli and higher yield strains in compression and cutting compared with beef burgers. In flexion, however, the PBAs had the lowest yield strains. These results indicated that yield strain, whether in flexion, compression or cutting, can be used as the most relevant metric to distinguish between burger types. In addition, as a measure of plastic deformation, yield strain was the most relevant mechanical value to mouthfeel. PBAs were also shown to have lower textural values than the beef burgers in most of the TPA assessed properties. The difference between PBA and beef burgers was clearest in terms of chewiness which was the best single differentiator of mouthfeel and indicator of burger quality.

The ingredient composition of burgers played an important role in both mechanical and textural properties. While the effect of each individual ingredient could not be undertaken and, in any case, would yield poor conclusions due to their unspecified quantities, some secondary ingredients could be grouped by their function and compared by their relative concentration (as determined by their position on the ingredients list compared to the meat percentage). Here, three ingredient classes are investigated – bulking agents (water), binders and meat extenders (flours, starches, flakes), and fat replacers. All burgers, except for B1 had some water added to the products during manufacturing. While water is generally incorporated into meat to improve the cooking experience and increase juiciness (Zhang *et al*., 2024), it is also a bulking agent that increases the product volume and weight and, subsequently, profit margins. As the only burger without added water, the cooking yield by volume and by mass was highest in B1, although there were no apparent correlations between water content and mechanical and textural properties. Binding agents were used in all burgers, to improve meat consistency by binding and containing water and fat in the restructured product. The B3 burger had high values for its mechanical and textural properties, which could be attributed to the greater presence of natural binders, namely wheat flour, which represented around 8% of its composition. Additionally, B3 also differed from the rest of the burgers tested by its manufacturing method. The burger was handmade as opposed to factory ground, which would have likely affected the meat chunk size, and consequently its properties.

Fat replacers, such as substitutes (rapeseed and coconut oils) and mimetics (maltodextrin), were used to increase the fat content and visual aspect of the PBA burgers (Owusu-Ansah *et al*., 2022). Like animal fats, fat substitutes influence the juiciness and taste of foods, however their low melting points can negatively affect the integrity of products, as seen with B7 which could not be handled effectively when raw (*sections 5.3.2.1* and *5.3.2.2*). Interestingly, the animal fat percentage of beef burgers did not appear to contribute to any measured mechanical or textural property. Although it is undeniable that fat plays a major role in consumer acceptance by improving flavour, juiciness and visual appearance (Fish *et al*., 2020), studies have shown contradicting evidence on its role in food texture. While some studies have demonstrated that fat increased shear force, tensile strength and textural properties such as adhesiveness and cohesiveness (Okeudo and Moss, 2005; de Avila *et al*., 2014; Starkey *et al*., 2016), others have shown either a negative correlation (Fiems *et al*., 2000) or no correlation at all (Zhang *et al*., 2022). The two beef burgers with the highest fat content (B2 and B5) did however exhibit the lowest cooking yield by mass and volume. As the melting temperature of beef fat is reached during cooking (25 °C < $T_{M,beeffat}$< 50 °C; Lloyd *et al*., 2014; Huang and Joo, 2017), a large portion of the fat content is lost, which could contribute to the lack of an obvious pattern in the cooked burgers. In addition, the differences between higher- and lower- fat-containing meat burgers

could have been overlooked due to the load cells used, and with a tensile modulus of $E_{t,fat}$ = 0.0001 MPa, minor differences in mechanical and textural properties may not have been recorded. Furthermore, physiological factors, such as post-mortem ageing and muscle-shortening which have been shown to play an important role in texture (Starkey *et al*., 2016), could have also obscured the role of fat. Due to the lack of standardisation of TPA and limited role of tensile testing, the quantitative comparison of textural properties across the literature has been limited.

No correlation between the mechanical and textural properties of burgers and their price was apparent either. While it has been shown that consumers are willing to pay more for foods of seemingly higher quality (Kurz *et al*., 2023), it has also been demonstrated that once consumers had associated a food product with an outcome (expected liking) they pay little attention to the experience of consuming it (Oxoby and Finnigan, 2007; Kurz *et al*., 2023). Consequently, prices may be more influenced by marketing strategies than actual mouthfeel qualities.

The meat content of beef burgers played the biggest role in differentiating between burger types. Those with increased beef content (B1 and B2) had significantly higher cooked flexural, compressive and cutting yield strains and higher hardness, and chewiness than the ones with lower beef content (B4 and B5), indicating that beef content must play a definitive role in the sensory properties of cooked products. As such, to appeal to consumer sensory expectations, alternative protein and cultivated meat burgers should aim to match the mechanical and textural properties of traditionally farmed meat, distancing themselves from existing PBA products. The mechanical and textural ranges for farmed beef and PBA burgers established in this study are presented in **Table 13**.

Despite being essentially meat at a cellular level, cultivated meat may not exhibit the same mechanical and textural properties as traditional meat as the cells are not grown *in vivo* under normal biological conditions. Using TPA and tensile testing, Paredes *et al*., (2022) showed that cultivated Frankfurter sausages were texturally significantly different to traditional Frankfurter sausages, although there were similarities between the cultivated Frankfurter sausages and other existing processed and non-processed meat products.

Depending on how meat is cultivated, it could contain edible scaffolds, hydrogels or microcarriers that aim to biologically and mechanically mimic the function of the extracellular matrix (ECM). *In vivo*, the ECM stiffens allowing stem cells to differentiate towards fat ($E_{t,ECMfat}$ = 0.0001 MPa), muscle ($E_{t,ECMmuscle}$ = 0.01 MPa) or bone ($E_{t,ECMbone}$ = 0.03-0.05 MPa; Lee *et al*., 2022). Emulating the specific stiffness of ECM in scaffolds could promote better cell differentiation (Engler *et al*., 2006) contributing directly to mouthfeel (Bonkamp *et* al., 2023; Lee *et al*., 2024). On the other hand, cultivated meats grown by self-aggregation may lack the sufficient cellular alignment to replicate

intramuscular cohesiveness, despite being *purer* on a biological and nutritional level. By combining the mechanical and textural properties of cultivated tissues and their respective carrier materials (scaffolds or hydrogels) the range of properties presented in this study could be achieved, ensuring that products meet consumer expectations of mouthfeel and quality.

Table 13: Range of values for the mechanical and textural properties of beef burgers and plant-based alternatives. Note: cohesiveness, springiness and resilience did not yield any distinction between high and low beef content

Property		Meat		PBA
		High beef content	Low beef content	
Mechanical	Flexural yield strain (-)	0.19 - 0.33	0.15	0.09 - 0.12
	Compressive yield strain (-)	0.08 - 0.15	0.05	0.21 - 0.34
	Cutting yield strain (-)	0.28 - 0.30	0.22 - 0.25	0.42 - 0.49
Textural	Hardness (N)	41.2 - 43.9	34.5 - 37.8	23.2 - 24.9
	Cohesiveness (-)	0.38 - 0.40		0.30 - 0.31
	Springiness (-)	0.76 - 0.88		0.63 - 0.68
	Resilience (-)	0.14 - 0.15		0.11
	Chewiness (N)	13.5 - 14.1	10.9 - 11.3	4.5 - 5.1

In addition, the PBA burgers tested in this study failed to exhibit the textural properties of beef burgers, which suggests that cultivated meat may not be able to rely on additives to mimic the texture of meat. There is an increased trend towards the design of hybrid plant and cultivated meat products and several studies have shown that replacing vegetable oils in PBA products with animal fat enhanced their textural properties and led to positive consumer perceptions (Fish *et al*., 2020; Grasso and Goksen, 2023).

5.4 Conclusion

To help design cultivated meat products that match the organoleptic properties of traditional meat, the mechanical and textural properties of raw and cooked beef and PBA burgers were measured using ISO standardised mechanical testing and TPA. The mechanical flexion, compression and cutting tests were selected as the most relevant mechanical tests for describing burger quality, as each test could replicate an action incurred during chewing. Despite its common use in meat texture analysis, tensile testing was shown to be a poor indicator of burger quality as no pattern could be identified to

differentiate between burger types. This may suggest that tensile testing may differentiate well between group types (*e.g.* burgers, sausages, fillets), but not when comparing products within the same group (*e.g.* burgers only).

The cooking process appeared to significantly increase the stiffness (modulus), hardness, cohesiveness, resilience and chewiness of all the tested burgers, and the results obtained from cooked samples were the most relevant to mouthfeel.

The composition of burgers played a major role in their mechanical and textural properties, with beef content being the highest differentiator. Beef burgers with higher meat content had higher strains in the standardised ISO flexion, compression and cutting mechanical tests, compared to those with lower meat content. PBA burgers had the highest strains of all burger types, exemplifying their softer texture. This pattern was also recurrent in the TPA results, this time with PBA properties being lowest for hardness and chewiness, which was shown to be the best descriptor of mouthfeel due to the clear distinction and low variance between beef and PBA burger types.

The plant-based burgers in this study systematically exhibited different mechanical and textural characteristics from traditional beef burgers, highlighting the fact that meat extenders and fat replacers do not accurately replicate meat texture. This is a key point for cultivated meat production, as while meat extenders are not essential, manufacturers may want to include them in order to reduce the high costs of cultivated products. Instead, it may be best to mimic traditional meat texture through scaffold optimisation, moving away from the low expectations associated with plant-based burgers towards improved consumer satisfaction in a more traditional *meat-like* product.

Moreover, as consumers are drawn to similarities with existing and familiar products when determining the quality of new products, it can be deduced that the mechanical and textural properties associated with meat organoleptic properties, should be considered when designing cultivated meat products. While these metrics do not guarantee that all properties will be identical at all levels, other measures such as contractile stress, intramuscular cohesion or shear, and tensile modulus may be more useful for comparing meats at a cellular level. That said, as organoleptic properties are perceived at a macroscopic level, the descriptors of burger quality identified in this study, namely flexural, compressive and cutting strains, hardness and chewiness should be prioritised.

The results laid out in **Table 13** show novel insights into the characterisation of the mechanical and textural properties of both beef and plant-based burgers. However, to effectively compare results within the wider literature, method standardisation is needed. Therefore, future work should investigate the effects of TPA variables (*e.g*. maximum strain or displacement rate), storage effects

(*e.g.* fresh or frozen), cooking parameters (*e.g.* rare to well-done, convection to conduction) and sample selection (*e.g.* mycoprotein) on the resulting properties of meat and propose a new set of ISO protocols for the characterisation of meat products that includes cutting and TPA. Finally, to establish a clearer link between the effects of perceived meat quality and the results obtained in this study, the psychology of consumer acceptance should be investigated by descriptive sensory analysis. This would, in turn, help advance the development of all alternative protein products to ensure consumer acceptance by design.

CHAPTER VI

CONCLUSION AND FUTURE WORK

6.1 Conclusion

The work presented in this thesis set out to design novel edible electrospun microcarriers that efficiently promote bovine mesenchymal expansion, with the future goal of scaling unstructured cultivated beef production. By developing edible microcarriers which can remain in the final product as supports for cell expansion, differentiation and tissue maturation, the need for cell dissociation is eliminated whilst opportunities of improving the nutritional and organoleptic properties of cultivated ground beef through scaffold engineering are opened up.

Silk fibroin, extracted from the silk cocoons of *Bombyx mori* silkworms, is an abundant, low environmental impact and versatile fibrous protein with extensive applications in tissue engineering where it is used as scaffolds for regenerative medicine and as a preservative and sustainable packaging in the food industry. In addition, with its GRAS status, food-safe solvents and cross-linkers, and reported excellent cytocompatibility, mechanical properties, and electrospinnability, silk fibroin was chosen as a promising biomaterial for scaffold design.

Non-woven silk fibroin mats were successfully electrospun using a benchtop needle-electrospinning setup for research and characterisation purposes. Optimising the polymer solution concentration and electrospinning parameters allowed the fabrication of randomly orientated, continuous, homogenous and defect-free nanofibers (98 – 160 nm in diameter) using a 12% (w/w) silk fibroin in formic acid polymer solution electrospun at 15 kV and 10 cm collector distance. The electrospun mats were subsequently stabilised by immersion in monohydric alcohols: ethanol (EtOH) or methanol (MeOH). Stabilisation was shown to induce a conformational shift in the protein secondary structure, converting Silk I irregular structures (mainly random coils) into Silk II highly ordered and stable anti-parallel inter-molecular β-sheets. No differences were observed between the effects of EtOH and MeOH on β-sheet crystallinity. When immersing silk fibroin nanofibers in EtOH, the conformational shift from silk I to Silk II occurred almost instantly (within 1 min of immersion). No change to β-sheet crystallinity was measured thereafter, even up to 1 hour of immersion. Given the similar performances of EtOH and MeOH, EtOH was chosen for further work as MeOH is toxic when ingested. Therefore, the default stabilisation method was chosen as 20 min immersion in 99.8% EtOH.

As a result of stabilisation, the aggregation of hydrophobic amino acids forming β-sheets (alanine, glycine and serine) made silk fibroin almost entirely insoluble in water, and after long immersion times (> 72h) water annealing appeared to improve hydrolytic stability of silk fibroin mats, making these alcohol-treated supports suitable for tissue culture in aqueous environments for at least 2 weeks, which is sufficient time to grow muscle tissue. Alcohol treatment also caused the nanofibres to swell, significantly increasing in diameter (160-180 nm), but halving the porosity and thickness of the electrospun mats. Moreover, the conformational shift, significantly increased the stiffness (350-450 MPa) and brittleness of the previously ductile electrospun mats (100 MPa). It should be noted that the extremely high stiffness in both untreated and alcohol-treated electrospun mats far exceeded the stiffness of skeletal muscle extracellular matrix (ECM) which may affect its mechanotransductive effects on cell differentiation to soft tissues (muscle and fat). Despite this, the shear modulus proved more than sufficient to support the shear stresses encountered in bioreactors of any existing scale and impellor speed.

To improve the cost effectiveness of electrospinning silk fibroin, silk fibroin was degummed from the raw silk of domesticated *Bombyx mori* silkworms using aqueous sodium carbonate (Na_2CO_3), a highly efficient and food safe method at low concentrations. The degumming ratio was lowest, around 30%, when using highly diluted Na_2CO_3 (0.2% (w/v)) indicating complete removal of silk sericin with very little silk fibroin loss. To become electrospinnable, the silk fibroin was then dissolved with calcium chloride ($CaCl_2$) in a solution of $CaCl_2$:EtOH:H_2O in a 1:8:2 molar ratio, referred to as Ajisawa's solution, a more sustainable and food safe alternative to the traditional method of dissolution in concentrated lithium bromide (LiBr), before being dialysed against water. The regeneration ratio was also lowest when using 0.2% (w/v) Na_2CO_3 indicating that sodium carbonate damaged molecular chains of degummed silk fibroin, reducing its molecular weight and resulting in protein loss during dialysis, an effect that increased with sodium carbonate concentration. As such, using 0.2% Na_2CO_3 significantly increased regenerated silk fibroin yields and reduced cost of production. Bulk purchase of raw silk could also reduce the cost of silk fibroin in production at scale. For the purpose of illustration, a notional price of 0.12 £/g silk fibroin was estimated based on the global market index price of raw silk cocoons and the regeneration ratio (this does not take account of the inhouse costs of the process of regeneration).

The productivity of nanofibre production could also be improved considerably using needleless-electrospinning methods. Using the Nanospider^{TM} NS1S500U semi-industrial DC needleless-electrospinner, nanofibres were produced at 40 kV at 10 cm at more than 100 times the speed of the benchtop needle-electrospinner. In addition, the integrated climate control improved the quality of the fibres, allowing better evaporation of formic acid and creating flawless nanofibres (150 nm

untreated to 170 nm EtOH-treated). With industrial-scale DC electropsinners able to produce fibres up to 1 kg/h (approximately 50000 times faster than the single needle benchtop electrospinner), this highly efficient method could enable the mass production of fibres needed for a scalable production of cultivated meat, without compromising on fibre quality. In addition, silk fibroin was also successfully electrospun using AC needleless electrospinning, at 35 kV and 50 Hz, producing a thick plume of widely distributed large and partially orientated nanofibres (500 nm untreated). However, due to time constraints and the fact that this method is still in development, no further work could be carried out on this high potential electrospinning technique.

Heat proved to be an efficient, easy and quick method for the sterilisation of electrospun silk fibroin due to its stability at high temperature (260-280 °C). Moreover, autoclaving at 121 °C for 20 min decreased the amount of formic acid traces bound to the nanofibres making the electrospun fibres less acidic and improving food safety. Bovine mesenchymal stem cells (bMSCs) seeded onto electrospun scaffolds were shown to attach and proliferate efficiently. The highest yields were obtained at the lowest seeding density (3000 cells/cm^2), achieving a 48 h doubling time from day 1 to day 7 and a 22-fold increase at the end of the exponential growth stage (on the 7^{th} day of culture). In addition, live/dead staining showed only live cells on the electrospun scaffolds after 8 days of culture, demonstrating the excellent cytocompatibility of silk fibroin. Although, cellular infiltration was likely minimal due to the micropores being much smaller than the cells, cell migration was effective and fluorescent microscopy images performed on day 13 of culture showed scaffolds covered in bMSCs as they reached confluency. It was assumed that cell attachment and proliferation was possible on the inert fibres due to favourable surface chemistry properties and in particular its mild hydrophilicity (56 °) which is ideal for mesenchymal stem cell attachment.

Further investigation of functionalisation of electrospun scaffolds to improve cell attachment and proliferation was carried out by testing blends of silk fibroin with psyllium husk (SFPH) and with zein (SFZ), in the polymer solution, and by UV-irradiating silk fibroin electrospun mats for up to 480 min. However, while no significant change to bMSC attachment or proliferation was measured on SFPH scaffolds, the dietary, health and antimicrobial properties of psyllium husk could be beneficial if these are conserved in the scaffolds or indeed in the final cultivated meat product. As such, it may be possible to reduce the incidence of red meat-associated diseases such as type-II diabetes, high cholesterol or even colorectal cancer, by consuming psyllium husk as part of the cultivated meat product. In contrast, SFZ was shown to significantly promote attachment, doubling times and yields when prepared with high percentages of silk fibroin (12% (w/w) in formic acid) and zein (≥ 6.25% (w/w) in formic acid) probably as a result of larger fibre diameters (424 – 637 nm) in the SFZ electrospun

scaffolds. Zein also possesses antimicrobial properties and, therefore, SFZ scaffolds may prevent bacterial contamination and improve the food safety of the cultivated meat product.

UV-irradiation (at 254 nm) caused minor conformational changes from Silk II to Silk I that increased with exposure time. In addition, an increase in carboxyl functional groups were detected which increased with irradiation time, indicating the formation of negatively charged soluble photoproducts on the surface of the fibres. The effect of UV-functionalisation (≥ 240 min) proved to be detrimental on bMSC attachment and proliferation which were significantly worsened with longer exposure times (480 min), making this method unsuitable for functionalisation.

To increase the scalability of bMSC expansion, the electrospun silk fibroin, SFPH and SFZ scaffolds were converted into novel electrospun non-spherical microcarriers. As a first proof-of-concept the electrospun microcarriers were engineered by manually slicing electrospun mats into micro-sized scaffolds with identical chemical, mechanical and structural properties as the macro-sized scaffolds (from which they were made). The hand-sliced microcarriers (hsMCs) appeared as irregular n-sided polygons with a constant height (matching the thickness of the original electrospun mat). Although they were slightly smaller than commercially available (Cytodex-3 and Solohill Plastic) microcarriers their surface area was within the same order of magnitude. Seeding the hand-sliced microcarriers was particularly inefficient due to the low density of the highly porous hsMCs, which caused many to float and prevented the sustained contact required for cell attachment. Moreover, experimental design limitations allowed cell loss through the cell strainers which held the microcarriers. Nevertheless, bMSCs were able to proliferate on hsMCs with an average 75 h doubling time during the exponential growth stage, matching bMSC growth on the functionalised Cytodex-3 and experimental Hybrid X microcarriers. In addition, by day 11, the hsMCs performed as well as the commercial microcarriers despite the fact that commercial microcarriers are functionalised with ECM proteins (in fact the measured yields were higher in hsMCs but this difference was not statistically significant). As with growth on SFZ scaffolds, bMSC growth on hsMCs made from zein and silk fibroin outperformed all microcarrier types with increased attachment (30% seeding efficiency), proliferation (56 h doubling time) and yields (17-fold increase), confirming the efficacy of the blends. To then explore the scalability of electrospun microcarrier fabrication, electrospun SFPH blended mats were cryomilled to form cryoMCs which appeared similar in surface area to hsMCs but lost their defined fibrous structure. Still bMSC growth on cryoMCs was not significantly different to growth on hsMCs, likely resulting from the higher density of cryoMCs which sunk in growth medium, and it is possible that roughness caused by shearing of the nanofibres on the surface of the cryoMCs improved cell adherence.

Relevant mechanical and textural properties of raw and cooked beef and plant-based analogue burgers (PBAs) were quantified and characterised to determine specific values directly relating to mouthfeel. Mechanical tests that mimicked chewing actions (flexion, compression and cutting) were shown to be most relevant to quantify the organoleptic properties of meat, with the yield strains being the best descriptors of quality. Likewise, differentiation between beef and PBA burgers was best achieved by measuring hardness and chewiness. Ingredient composition played a major role on the mechanical and textural properties of burgers, with beef and PBAs showing systematically different values. No clear relationship was observed between the textural and mechanical properties of meat burgers when compared by price or fat percentage, however a clear divide was shown when comparing burgers by meat content. As such, high meat content burgers (> 95%) displayed higher flexural strength, compressiveness, hardness and chewiness than lower meat content (76-82%) burgers and both had significantly higher values in these variables than the PBAs. The mushiness of PBAs was explained by their high yield strains and low chewiness, probably resulting from the excessive use of meat extenders and fat replacers that do not accurately replicate meat texture. While cultivated meat are still in development, the mechanical and textural properties of PBAs provide a lesson regarding consumer satisfaction. Cultivated meat products should not rely on meat extenders to bulk up the products, instead research could focus on developing edible supports that are designed to improve texture and are integrated into the cultivated meat product from the start. Finally, the values obtained could provide targets for cultivated meat production, however it should be noted that the lack of specific ISO testing standards for mechanical and textural testing of meat products limits comparisons between studies.

6.2 Future work

The work presented in this thesis provides the groundwork for future experiments on electrospun silk fibroin microcarriers for cultivated meat production. Had more time been available, four future work avenues could have been explored and are discussed here.

6.2.1 Overcoming experimental limitations and reproducibility

Although most of the work presented in this thesis has been statistically analysed for significance using one-way ANOVA and Tukey's Honestly Significant Difference test, some experiments such as FTIR and SEM analysis of fibre morphology and size, consisted of measurements of single samples. As such, no standard deviation or formal statistics could be calculated. Moreover, bMSC proliferation on microcarriers was performed only once in triplicate which could not allow for experimental bias.

Rather than relying entirely on the literature to interpret and quantify protein secondary structures, complementary spectroscopic methods such as Raman spectroscopy (Lefèvre *et al*., 2017), X-ray crystallography (Narita *et al*., 2020) or even nuclear magnetic resonance (Asakura *et al*., 1999) could be used to validate the methodology for protein conformation quantification, thereby improving the accuracy of secondary structure content estimations (Belton *et al*., 2018).

In addition, to avoid relying on indirect estimations of metabolically active cells and directly quantify live cell densities on scaffolds and microcarriers, all bMSC proliferation experiments could be repeated, this time by detaching cells with Trypsin-EDTA, and counting cells using a haemocytometer. Alternatively, the cells could be directly counted using fluorescent microscopy at defined time points or using live cell monitoring techniques to precisely measure bMSC attachment and growth kinetics on various substrates.

Finally, measuring the density of cryomilled microcarriers (cryoMCs) could enable more accurate seeding on cryoMCs, enabling comparison with other microcarrier types. The density of cryoMCs could be measured by weighing packed cryoMCs in a known volume and then dividing the mass by the volume. Alternatively, the density of the cryoMCs could be measured in suspension using a hydrometer by measuring the buoyancy of the microparticles.

6.2.2 Improving functionality

To continue the functionalisation work explored in and characterised in Chapter IV, electrospun silk fibroin could be functionalised with cell adhesion motifs. This could be achieved by blending silk fibroin with pumpkin seed protein, which naturally possesses RGD and DGEA peptide binding motifs (Kong and Huan, 2023). Alternatively, chemical functionalisation strategies could be used to coat the electrospun scaffolds with recombinant capsular antigen fragment-1 (Caf1), a bacterial fimbrial protein that can be genetically engineered to mimic ECM cell adhesion motifs (Dura *et al*., 2022). Another option could involve degumming silk fibroin from wild *Antheraea mylitta* cocoons which naturally contains RGD peptide motifs (Boulet Audet *et al*., 2015; Naskar *et al*., 2021) however this would significantly reduce the scalability of silk fibroin regeneration due to its limited availability.

In addition, it would be worth measuring the antimicrobial effects of zein, in SFZ electrospun fibres, against common meat pathogens such as gram positive (*Staphylococcus aureus* or *Listeria monocytogenes*) and gram negative (*Escherichia coli* or *Salmonella enterica*) bacteria. To achieve this SFZ microcarriers could be first suspended in agar, after which the agar could be inoculated with bacteria. Subsequently, colony forming units would be counted using a plate counting method and compared with positive and negative controls.

6.2.3 Investigating differentiation

Due to the high stiffness of the electrospun randomly orientated silk fibroin nanofibres, it could be worth looking into possible spontaneous differentiation towards osteogenic lineages. This could be achieved by measuring osteogenic differentiation markers such as the expression of RUNX2, or accumulation of osteocalcin and alkaline phosphatase in cells (Nakamura *et al*., 2009; Sonomoto *et al*., 2016; Trivedi *et al*., 2020). Furthermore, it would be advantageous to measure the differentiation potential of bMSCs by swapping growth media with differentiation media after the exponential growth stage. This could be achieved by measuring the expression of early differentiation factors such as PAX7, MYOD1, and MYF5 using qPCR for myogenic lineages (Zhang *et al*., 2020) or measuring lipid accumulation using immunohistochemistry techniques (Yang *et al*., 2011) or histological stains such as Oil Red O for adipogenic lineages (Kraus *et al*., 2016). It would also be worth electrospinning silk scaffolds and microcarriers with aligned or woven nanofibers to promote myogenic differentiation and myoblast fusion (Kim *et al*., 2015) by using a fast-rotating collector drum (Kiselev and Rosell-Llompart, 2011).

6.2.4 Exploring bioprocess scalability

The efficiency of hsMCs and cryoMCs could be investigated in dynamic conditions starting with growth in spinner flasks. First, it would be necessary to observe the behaviour of the microcarriers in response to varying agitation speeds as it is important that they neither float nor stay at the bottom of the flask. Then studies could investigate optimal seeding concentration (in cells/mL) and the best cells to microcarrier ratio for maximal seeding efficiency. Finally, the nutrient and oxygen flow and distribution could be investigated to prepare for work in stir tank bioreactors.

REFERENCES

Abagnale, G., Steger, M., Nguyen, V. H., Hersch, N., Sechi, A., Joussen, S., Denecke, B., Merkel, R., Hoffmann, B., Dreser, A., Schnakenberg, U., Gillner, A., & Wagner, W. (2015). Surface topography enhances differentiation of mesenchymal stem cells towards osteogenic and adipogenic lineages. *Biomaterials*, *61*, 316–326. https://doi.org/10.1016/j.biomaterials.2015.05.030

Ahmad, M., Qureshi, S., Akbar, M. H., Siddiqui, S. A., Gani, A., Mushtaq, M., Hassan, I., & Dhull, S. B. (2022). Plant-based meat alternatives: Compositional analysis, current development and challenges. *Applied Food Research, 2*(2), 100154. https://doi.org/10.1016/j.afres.2022.100154

Ahn, H. H., Lee, I. W., Lee, H. B., & Kim, M. S. (2014). Cellular behavior of human adipose-derived stem cells on wettable gradient polyethylene surfaces. *International journal of molecular sciences*, *15*(2), 2075–2086. https://doi.org/10.3390/ijms15022075

Ajisawa, A. (1998). Dissolution aqueous of silk fibroin with calcium chloride/ethanol solution. *Journal of Sericultural Science in Japan 67*(2), 91–94. https://doi.org/10.11416/kontyushigen1930.67.91

Akdeniz, B., Calantone, R. J., & Voorhees, C. M. (2013). Effectiveness of marketing cues on consumer perceptions of quality: The moderating roles of brand reputation and third-party information. *Psychology & Marketing, 30*(1), 76–89. https://doi.org/10.1002/mar.20590

Alexander, M. R., & Williams, P. (2017). Water contact angle is not a good predictor of biological responses to materials. *Biointerphases, 12*(2), 02C201. https://doi.org/10.1116/1.4989843

Alexander, P., Brown, C., Arneth, A., Dias, C., Finnigan, J., Moran, D., & Rounsevell, M. (2017b). Could consumption of insects, cultured meat or imitation meat reduce global agricultural land use? *Global Food Security, 15*, 22-32. https://doi.org/10.1016/j.gfs.2017.04.001

Alkandari, S., Bhatti, M. E., Aldughpassi, A., Al-Hassawi, F., Al-Foudari, M., & Sidhu, J. S. (2021). Development of functional foods using psyllium husk and wheat bran fractions: Phytic acid contents. *Saudi journal of biological sciences, 28(*6), 3602–3606. https://doi.org/10.1016/j.sjbs.2021.03.037

Allan, S. J., De Bank, P. A., & Ellis, M. J. (2019). Bioprocess Design Considerations for Cultured Meat Production with a Focus on the Expansion Bioreactor. *Frontiers in Sustainable Food Systems, 3*(44). https://doi.org/10.3389/fsufs.2019.00044

Allardyce, B. J., Rajkhowa, R., Dilley, R. J., Atlas, M. D., Kaur, J., & Wang, X. (2016). The impact of degumming conditions on the properties of silk films for biomedical applications. *Textile Research Journal*, 86(3), 275–287. https://doi.org/10.1177/0040517515586166

Amiraliyan, N., Nouri, M., & Haghighat Kish, M. (2010). Structural characterization and mechanical properties of electrospun silk fibroin nanofibre mats. *Polym. Sci. Ser. A 52*(4), 407–412. https://doi.org/10.1134/S0965545X10040097

Andreassen, R. C., Rønning, S. B., Solberg, N. T., Grønlien, K. G., Kristoffersen, K. A., Høst, V., Kolset, S. O., & Pedersen, M. E. (2022). Production of food-grade microcarriers based on by-products from the food industry to facilitate the expansion of bovine skeletal muscle satellite cells for cultured meat production. *Biomaterials*, *286*, 121602. https://doi.org/10.1016/j.biomaterials.2022.121602

Anomaly J. (2015). What's Wrong With Factory Farming?. Public health ethics, 8(3), 246–254. https://doi.org/10.1093/phe/phu001

Asakura, T., Iwadate, M., Demura, M., & Williamson, M. P. (1999). Structural analysis of silk with 13C NMR chemical shift contour plots. *International journal of biological macromolecules*, *24*(2-3), 167–171. https://doi.org/10.1016/s0141-8130(98)00082-8

Asakura, T., Suita, K., Kameda, T., Afonin, S., & Ulrich, A.S. (2004). Structural role of tyrosine in Bombyx mori silk fibroin, studied by solid-state NMR and molecular mechanics on a model peptide prepared as silk I and II. *Magn. Reson. Chem. 42*(2), 258–266. https://doi.org/10.1002/mrc.1337

ASTM International. (2014). *D638-14 Standard Test Method for Tensile Properties of Plastics*. ASTM International.

Astudillo, M. F., Thalwitz, G., & Vollrath, F. (2014). Life cycle assessment of Indian silk. *Journal of Cleaner Production*, *81*, 158-167. https://doi.org/10.1016/j.jclepro.2014.06.007

Ba, Z., Chen, Z., Huang, Y., Feng, D., Zhao, Q., Zhu, J., & Wu, D. (2018). Nanoporous diopside modulates biocompatibility, degradability and osteogenesis of bioactive scaffolds of gliadin-based composites for new bone formation. *International journal of nanomedicine*, *13*, 3883–3896. https://doi.org/10.2147/IJN.S162262

Bacha, A. A., Din, Z. U., & Khan, I. (2022). Effect of Psyllium husk fiber and lifestyle modification on human body insulin resistance. *Nutrition and metabolic insights*, *15*, 11786388221107797. https://doi.org/10.1177/11786388221107797

Badoim, L. (2021, February 12). *World's First 3D Bioprinted And Cultivated Ribeye Steak Is Revealed.* Forbes. https://www.forbes.com/sites/lanabandoim/2021/02/12/worlds-first-3d-bioprinted-and-cultivated-ribeye-steak-is-revealed/

Balasubramanian, B., Liu, W., Pushparaj, K., & Park, S. (2021). The Epic of In Vitro Meat Production-A Fiction into Reality. *Foods (Basel, Switzerland)*, *10*(6), 1395. https://doi.org/10.3390/foods10061395

Balguid, A., Mol, A., van Marion, M. H., Bank, R. A., Bouten, C. V., & Baaijens, F. P. (2009). Tailoring fiber diameter in electrospun poly(epsilon-caprolactone) scaffolds for optimal cellular infiltration in cardiovascular tissue engineering. *Tissue engineering. Part A, 15*(2), 437–444. https://doi.org/10.1089/ten.tea.2007.0294

Bambridge-Sutton, A. (2024). *Finally, an approval application for cultivated meat submitted in the EU*. Food Navigator Europe. https://www.foodnavigator.com/Article/2024/08/01/Finally-an-approval-application-for-cultivated-meat-submitted-in-the-EU

Barjavel, R. (1943). *Ashes, Ashes (French: Ravage).* Doubleday.

Batka, O., Skrivanek, J., Holec, P., Beran, J., Valera, J., & Bilek, M. (2024). Methods for increasing productivity of AC-electrospinning using weir-electrode. *Scientific Reports, 14*, 24012. https://doi.org/10.1038/s41598-024-75946-5

Bauer, S., Park, J., von der Mark, K., & Schmuki, P. (2008). Improved attachment of mesenchymal stem cells on super-hydrophobic TiO2 nanotubes. *Acta Biomaterialia 4*(5), 1576-1582. https://doi.org/10.1016/j.actbio.2008.04.004

BBC. (2020, December 2). *Singapore approves lab-grown 'chicken' meat.* BBC News. https://www.bbc.co.uk/news/business-55155741

Beam Piper, H. (1961/2006). *The Four Day Planet*. The Project Gutenberg eBook. (Original work published 1961).

Beaudoin, É. J., Kubaski, M. M., Samara, M., Zednik, R. J., & Demarquette, N. R. (2022). Scaled-Up Multi-Needle Electrospinning Process Using Parallel Plate Auxiliary Electrodes. *Nanomaterials (Basel, Switzerland)*, *12*(8), 1356. https://doi.org/10.3390/nano12081356

Beena, M., Ameer, J. M., & Kasoju, N. (2022). Optically Clear Silk Fibroin Films with Tunable Properties for Potential Corneal Tissue Engineering Applications: A Process-Property-Function Relationship Study. *ACS omega, 7*(34), 29634–29646. https://doi.org/10.1021/acsomega.2c01579

Beijer, N. R. M., Nauryzgaliyeva, Z. M., Arteaga, E. M., Pieuchot, L., Anselme, K., van de Peppel, J., Vasilevich, A. S., Groen, N., Roumans, N., Hebels, D. G. A. J., & de Boer, J. (2019). Dynamic adaptation of mesenchymal stem cell physiology upon exposure to surface micropatterns. *Scientific Reports, 9*, 9099. https://doi.org/10.1038/s41598-019-45284-y

Bellani, C. F., Ajeian, J., Duffy, L., Miotto, M., Groenewegen, L., & Connon, C. J. (2020). Scale-Up Technologies for the Manufacture of Adherent Cells. *Frontiers in nutrition*, *7*, 575146. https://doi.org/10.3389/fnut.2020.575146

Belton, D. J., Plowright, R., Kaplan, D. L., & Perry, C. C. (2018). A robust spectroscopic method for the determination of protein conformational composition - Application to the annealing of silk. *Acta biomaterialia*, *73*, 355–364. https://doi.org/10.1016/j.actbio.2018.03.058

Ben Abla, A., Boeuf, G., Elmarjou, A., Dridi, C., Poirier, F., Changotade, S., Lutomski, D., & Elm'selmi, A. (2021). Engineering of Bio-Adhesive Ligand Containing Recombinant RGD and PHSRN Fibronectin Cell-Binding Domains in Fusion with a Colored Multi Affinity Tag: Simple Approach for Fragment Study from Expression to Adsorption. *International journal of molecular sciences, 22(*14), 7362. https://doi.org/10.3390/ijms22147362

Ben-Arye, T., & Levenberg, S. (2019). Tissue Engineering for Clean Meat Production. Frontiers in Sustainable *Food Systems, 3*. https://www.frontiersin.org/article/10.3389/fsufs.2019.00046

Ben-Arye, T., Shandalov, Y., Ben-Shaul, S., Landau, S., Zagury, Y., Ianovici, I., Lavon, N., & Levenberg, S. (2020). Textured soy protein scaffolds enable the generation of three-dimensional bovine skeletal muscle tissue for cell-based meat. *Nature Food, 1*, 210–220. https://doi.org/10.1038/s43016-020-0046-5

Bender A. (1992). Meat and meat products in human nutrition in developing countries. *FAO food and nutrition paper, 53*, 1–91. https://www.fao.org/4/t0562e/T0562E00.htm

Benjaminson, M. A., Gilchriest, J. A., & Lorenz, M. (2002). In vitro edible muscle protein production system (MPPS): stage 1, fish. *Acta astronautica, 51*(12), 879–889. https://doi.org/10.1016/s0094-5765(02)00033-4

Benković, M., Jurinjak Tušek, A., Sokač Cvetnić, T., Jurina, T., Valinger, D., & Gajdoš Kljusurić, J. (2023). An Overview of Ingredients Used for Plant-Based Meat Analogue Production and Their Influence on Structural and Textural Properties of the Final Product. *Gels (Basel, Switzerland)*, *9*(12), 921. https://doi.org/10.3390/gels9120921

Beyond Meat. (n.d.). Beyond Burger [Photograph]. Beyond Meat. https://beyond-meat-cms-production.s3.us-west-2.amazonaws.com/bf76ab69-3d8a-48a0-a850-7259e5b6f57d.jpeg

Bhat, Z. F., Kumar, S., & Fayaz, H. (2015). In vitro meat production: Challenges and benefits over conventional meat production. *Journal of Integrative Agriculture, 14*(2), 241-248. https://doi.org/10.1016/S2095-3119(14)60887-X

Biagiotti, M., Bassani, G. A., Chiarini, A., Vincoli, V. T., Dal Prà, I., Cosentino, C., Alessandrino, A., Taddei, P., & Freddi, G. (2022). Electrospun Silk Fibroin Scaffolds for Tissue Regeneration: Chemical,

Structural, and Toxicological Implications of the Formic Acid-Silk Fibroin Interaction. *Frontiers in bioengineering and biotechnology*, *10*, 833157. https://doi.org/10.3389/fbioe.2022.833157

Bitar, L., Isella, B., Bertella, F., Vasconcelos, C. B., Harings, J., Kopp, A., van der Meer, Y., Vaughan, T. J., & Bortesi, L. (2024). Sustainable *Bombyx mori* silk fibroin for biomedical applications as a molecular biotechnology challenge: A review. *International Journal of Biological Macromolecules, 264*(1), 130374. https://doi.org/10.1016/j.ijbiomac.2024.130374

Blossman-Myer, B., & Burggren, W. W. (2010). The silk cocoon of the silkworm, Bombyx mori: macro structure and its influence on transmural diffusion of oxygen and water vapor. *Comparative biochemistry and physiology. Part A, Molecular & integrative physiology*, *155*(2), 259–263. https://doi.org/10.1016/j.cbpa.2009.11.007

Bodiou, V., Moutsatsou, P., & Post, M. J. (2020). Microcarriers for Upscaling Cultured Meat Production. *Frontiers in nutrition*, *7*, 10. https://doi.org/10.3389/fnut.2020.00010

Bogliotti, Y. S., Wu, J., Vilarino, M., Okamura, D., Soto, D. A., Zhong, C., Sakurai, M., Sampaio, R. V., Suzuki, K., Izpisua Belmonte, J. C., & Ross, P. J. (2018). Efficient derivation of stable primed pluripotent embryonic stem cells from bovine blastocysts. *Proceedings of the National Academy of Sciences of the United States of America, 115(*9), 2090–2095. https://doi.org/10.1073/pnas.1716161115

Boles, J. A., & Shand, P. J. (1999). Effects of raw binder system, meat cut and prior freezing on restructured beef. *Meat science, 53*(4), 233–239. https://doi.org/10.1016/s0309-1740(99)00062-5

Bomkamp, C., Musgrove, L., Marques, D. M. C., Fernando, G. F., Ferreira, F. C., & Specht, E. A. (2023). Differentiation and Maturation of Muscle and Fat Cells in Cultivated Seafood: Lessons from Developmental Biology. *Marine Biotechnology 25*, 1–29. https://doi.org/10.1007/s10126-022-10174-4

Bomkamp, C., Skaalure, S. C., Fernando, G. F., Ben-Arye, T., Swartz, E. W., & Specht, E. A. (2022). Scaffolding Biomaterials for 3D Cultivated Meat: Prospects and Challenges. *Advanced science (Weinheim, Baden-Wurttemberg, Germany), 9*(3), e2102908. https://doi.org/10.1002/advs.202102908

Bomkamp, C., Skaalure, S. C., Fernando, G. F., Ben-Arye, T., Swartz, E. W., & Specht, E. A. (2022). Scaffolding Biomaterials for 3D Cultivated Meat: Prospects and Challenges. *Advanced science (Weinheim, Baden-Wurttemberg, Germany), 9*(3), e2102908. https://doi.org/10.1002/advs.202102908

Boulet-Audet, M., Vollrath, F., & Holland, C. (2015). Identification and classification of silks using infrared spectroscopy. *The Journal of experimental biology, 218*(Pt 19), 3138–3149. https://doi.org/10.1242/jeb.128306

Brienen, R., Phillips, O. L., Feldpausch, T. R. et al. (2015). Long-term decline of the Amazon carbon sink. *Nature, 519*, 344–348. https://doi.org/10.1038/nature14283

Brühl, C. A., Bakanov, N., Köthe, S., Eichler, L., Sorg, M., Hörren, T., Mühlethaler, R., Meinel, G., & Lehmann, G. U. C. (2021). Direct pesticide exposure of insects in nature conservation areas in Germany. *Scientific reports*, *11*(1), 24144. https://doi.org/10.1038/s41598-021-03366-w

Bryant C. J. (2020). Culture, meat, and cultured meat. *Journal of animal science*, *98*(8), skaa172. https://doi.org/10.1093/jas/skaa172

Bukowska, J., Szóstek-Mioduchowska, A.Z., Kopcewicz, M., Walendzik., K., Machcińska, S., & Gawrońska-Kozac, B. (2021). Adipose-Derived Stromal/Stem Cells from Large Animal Models: from Basic to Applied Science. *Stem Cell Reviews and Reports, 17*, 719–738. https://doi.org/10.1007/s12015-020-10049-y

Burkholder T. J. (2007). Mechanotransduction in skeletal muscle. *Frontiers in bioscience : a journal and virtual library, 12*, 174–191. https://doi.org/10.2741/2057

Business Analytiq. (2024, November) *Raw Silk Price Index*. Business Analytiq. https://businessanalytiq.com/procurementanalytics/index/raw-silk-price-index/

Cai, Z.X., Mo, X.M., Zhang, K.H., Fan, L.P., Yin, A.L., He, C.L., & Wang, H.S. (2010). Fabrication of chitosan/silk fibroin composite nanofibres for wound-dressing applications. *Int. J. Mol. Sci. 11*(9), 3529–3539. https://doi.org/10.3390/ijms11093529

Cao, L., Zhang, Z., Yuan, D., Yu, M., & Min, J. (2024). Tissue engineering applications of recombinant human collagen: a review of recent progress. *Frontiers in bioengineering and biotechnology, 12*, 1358246. https://doi.org/10.3389/fbioe.2024.1358246

Cao, S., Wang, F., Chen, Z., Liu, Z., Mei, C., Wu, H., Huang, J., Li, C., Zhou, L., & Liu, L. (2009). Isolation and culture of primary bovine embryonic stem cell colonies by a novel method. *Journal of experimental zoology. Part A, Ecological genetics and physiology*, *311*(5), 368–376. https://doi.org/10.1002/jez.535

Cardenas Turner, J., Collins, G., Blaber, E. A., Almeida, E. A. C., & Arinzeh, T. L. (2020). Evaluating the cytocompatibility and differentiation of bone progenitors on electrospun zein scaffolds. *Journal of Tissue Engineering and Regenerative Medicine*, *14*(1), 173–185. https://doi.org/10.1002/term.2984

Carissimi, G., Lozano-Pérez, A. A., Montalbán, M. G., Aznar-Cervantes, S. D., Cenis, J. L., & Víllora, G. (2019). Revealing the Influence of the Degumming Process in the Properties of Silk Fibroin Nanoparticles. *Polymers, 11*(12), 2045. https://doi.org/10.3390/polym11122045

Carrel A. (1912). On the permanent life of tissues outside the organism. *The Journal of experimental medicine, 15*(5), 516–528. https://doi.org/10.1084/jem.15.5.516

Carriles, J., Nguewa, P., & González-Gaitano, G. (2023). Advances in Biomedical Applications of Solution Blow Spinning. *International journal of molecular sciences*, *24*(19), 14757. https://doi.org/10.3390/ijms241914757

Carrington, D. (2018, December 14). *World's first lab-grown steak revealed – but the taste needs work*. The Guardian. https://www.theguardian.com/environment/2018/dec/14/worlds-first-lab-grown-beef-steak-revealed-but-the-taste-needs-work

Carrington, D. (2023, March 28). *Meatball from long-extinct mammoth created by Food Firm*. The Guardian. https://www.theguardian.com/environment/2023/mar/28/meatball-mammoth-created-cultivated-meat-firm

Castle, N. (2022). In Vitro Meat and Science Fiction: Contemporary Narratives of Cultured Flesh. *Extrapolation, 63*(2), 149-179. https://doi.org/10.3828/extr.2022.11

Castro, M., & Chambers, E., 4th (2019). Consumer Avoidance of Insect Containing Foods: Primary Emotions, Perceptions and Sensory Characteristics Driving Consumers Considerations. *Foods (Basel, Switzerland)*, *8*(8), 351. https://doi.org/10.3390/foods8080351

CD Projekt. (2022). Cyberpunk 2077 (Playstation 5) [Video Game]. CD Projekt Red,

Chachlioutaki, K., Karavasili, C., Adamoudi, E., Bouropoulos, N., Tzetzis, D., Bakopoulou, A., & Fatouros, D. G. (2022). Silk sericin/PLGA electrospun scaffolds with anti-inflammatory drug-eluting properties for periodontal tissue engineering. *Biomaterials advances*, *133*, 112723. https://doi.org/10.1016/j.msec.2022.112723

Chaturvedi, V., Naskar, D., Kinnear, B. F., Grenik, E., Dye, D. E., Grounds, M. D., Kundu, S. C., & Coombe, D. R. (2017). Silk fibroin scaffolds with muscle-like elasticity support in vitro differentiation of human skeletal muscle cells. *Journal of tissue engineering and regenerative medicine*, *11*(11), 3178–3192. https://doi.org/10.1002/term.2227

Chen, H. T., Lee, M. J., Chen, C. H., Chuang, S. C., Chang, L. F., Ho, M. L., Hung, S. H., Fu, Y. C., Wang, Y. H., Wang, H. I., Wang, G. J., Kang, L., & Chang, J. K. (2012). Proliferation and differentiation potential of human adipose-derived mesenchymal stem cells isolated from elderly patients with

osteoporotic fractures. *Journal of cellular and molecular medicine, 16*(3), 582–593. https://doi.org/10.1111/j.1582-4934.2011.01335.x

Chen, X., Li, L., Chen, L., Shao, W., Chen, Y., Fan, X., Liu, Y., Tang, C., Ding, S., Xu, X., Zhou, G., & Feng, X. (2023). Tea polyphenols coated sodium alginate-gelatin 3D edible scaffold for cultured meat. *Food research international (Ottawa, Ont.)*, *173*(Pt 1), 113267. https://doi.org/10.1016/j.foodres.2023.113267

Chen, Y., Zhang, W., Ding, X., Ding, S., Tang, C., Zeng, X., Wang, J., & Zhou, G. (2024). Programmable scaffolds with aligned porous structures for cell cultured meat. *Food chemistry*, *430*, 137098. https://doi.org/10.1016/j.foodchem.2023.137098

Cheng, G., Wang, X., Wu, M., Wu, S., Cheng, L., Zhang, X., & Dai, F. (2022). Insignificant Difference in Biocompatibility of Regenerated Silk Fibroin Prepared with Ternary Reagent Compared with Regenerated Silk Fibroin Prepared with Lithium Bromide. *Polymers, 14*(18), 3903. https://doi.org/10.3390/polym14183903

Cheng, Y., Koh, L.D., Li, D., Ji, B., Han, M.Y., & Zhang, Y.W. (2014). On the strength of β-sheet crystallites of Bombyx mori silk fibroin. *J. R. Soc. Interface 11*(96), 20140305. https://doi.org/10.1098/rsif.2014.0305

Cho, S. Y., & Ryu, G. H. (2022). Effects of oyster mushroom addition on quality characteristics of full fat soy-based analog burger patty by extrusion process. *Journal of Food Process Engineering, 46*(10), e14128. https://doi.org/10.1111/jfpe.14128

Choi, S., Son, T. J., & Lee, Y. K. (2023). Risk factors for COVID-19 outbreaks in livestock slaughtering and processing facilities in Republic of Korea. *Osong public health and research perspectives*, *14*(3), 207–218. https://doi.org/10.24171/j.phrp.2023.0035

Chow, C. Y., Bech, A.C., Sørensen, H., Olsen, A., & Bredie, W. L. P.(2024). Food texture preferences in early childhood: Insights from 3–6 years old children and parents. *Food Quality and Preference, 113*, 105063. https://doi.org/10.1016/j.foodqual.2023.105063

Chriki, S., & Hocquette, J. F. (2020). The Myth of Cultured Meat: A Review. *Frontiers in nutrition*, *7*, 7. https://doi.org/10.3389/fnut.2020.00007

Chriki, S., Picard, B., Faulconnier, Y., Micol, D., Brun, J.-P., Reichstadt, M., Jurie, C., Durand, D., Renand, G., Journaux, L., & Hocquette, J.-F. (2013). A Data Warehouse of Muscle Characteristics and Beef Quality in France and A Demonstration of Potential Applications. *Italian journal of animal science, 12*(2), e41. https://doi.org/10.4081/ijas.2013.e41

Churchill, W. (1931). Fifty Years Hence. *The Strand Magazine*.

COT. (2011). *COT Statement on the Effects of Chronic Dietary Exposure to Methanol*. Committee on Toxicity of Chemicals in Foods, Consumer Products and the Environment. https://cot.food.gov.uk/sites/default/files/cot/cotstatementmethanol201102revjuly.pdf

CSIRO. (2010). *An adult silkworm moth, Bombyx mori* [Photograph]. Science Image CSIRO. https://www.scienceimage.csiro.au/image/10746

Cui, H., Liu, G. L., & Padua, G. W. (2016). Cell spreading and viability on zein films may be facilitated by transglutaminase. *Colloids and Surfaces B: Biointerfaces*, *145*, 839–844. https://doi.org/10.1016/J.COLSURFB.2016.05.048

Dadras Chomachayi, M., Solouk, A., Akbari, S., Sadeghi, D., Mirahmadi, F., & Mirzadeh, H. (2018). Electrospun nanofibres comprising of silk fibroin/gelatin for drug delivery applications: Thyme essential oil and doxycycline monohydrate release study. *Journal of biomedical materials research. Part A*, *106*(4), 1092–1103. https://doi.org/10.1002/jbm.a.36303

Dagès, B. A. S**.**, Fabian, J., Polakova, D., Rysova, M., Topham, P. D., Souppez, J. -B., Hanga, M. P., & Theodosiou, E. (2025). Edible electrospun materials for scalable cultivated beef production. *Food and Bioproducts Processing*, 149, 118-129. https://doi.org/10.1016/j.fbp.2024.11.012

D'Angelo, F., Tiribuzi, R., Armentano, I., Kenny, J.M., Martino, S., & Orlacchio, A. (2011). Mechanotransduction: tuning stem cells fate. *J. Funct. Biomater. 2*(2), 67–87. https://doi.org/10.3390/jfb2020067

Daristotle, J. L., Behrens, A. M., Sandler, A. D., & Kofinas, P. (2016). A Review of the Fundamental Principles and Applications of Solution Blow Spinning. *ACS Applied Materials & Interfaces, 8*(51), 34951–34963. https://doi.org/10.1021/acsami.6b12994

Darling, N. J., Xi, W., Sideris, E., Anderson, A. R., Pong, C., Carmichael, S. T., & Segura, T. (2020). Click by Click Microporous Annealed Particle (MAP) Scaffolds. *Advanced healthcare materials*, *9*(10), e1901391. https://doi.org/10.1002/adhm.201901391

de Ávila, M. D. R, Cambero, M. I., Ordóñez, J. A., de la Hoz, L., & Herrero, A. M. (2024). Rheological behaviour of commercial cooked meat products evaluated by tensile test and texture profile analysis (TPA). *Meat Science, 98*(2), 310-315. https://doi.org/10.1016/j.meatsci.2014.05.003

de Bock, M., Derraik, J. G., Brennan, C. M., Biggs, J. B., Smith, G. C., Cameron-Smith, D., Wall, C. R., & Cutfield, W. S. (2012). Psyllium supplementation in adolescents improves fat distribution & lipid

profile: a randomized, participant-blinded, placebo-controlled, crossover trial. *PloS one, 7*(7), e41735. https://doi.org/10.1371/journal.pone.0041735

de Huidobro, F. R., Miguel, E., Blázquez, B., & Onega, E. (2005). A comparison between two methods (Warner-Bratzler and texture profile analysis) for testing either raw meat or cooked meat. *Meat science, 69*(3), 527–536. https://doi.org/10.1016/j.meatsci.2004.09.008

de Koning, W., Dean, D., Vriesekoop, F., Aguiar, L. K., Anderson, M., Mongondry, P., Oppong-Gyamfi, M., Urbano, B., Luciano, C. A. G., Jiang, B., Hao, W., Eastwick, E., Jiang, Z., & Boereboom, A. (2020). Drivers and Inhibitors in the Acceptance of Meat Alternatives: The Case of Plant and Insect-Based Proteins. *Foods, 9*(9):1292. https://doi.org/10.3390/foods9091292

De La Hamaide, S. (2023). *World food prices hit record high in 2022.* Reuters. https://www.reuters.com/markets/world-food-prices-hit-record-high-2022-despite-december-fall-2023-01-06/

De Luca, I., Di Salle, A., Alessio, N., Margarucci, S., Simeone, M., Galderisi, U., Calarco, A., & Peluso, G. (2016). Positively charged polymers modulate the fate of human mesenchymal stromal cells via ephrinB2/EphB4 signaling. *Stem cell research, 17*(2), 248–255. https://doi.org/10.1016/j.scr.2016.07.005

de Souza Paglarini, C., de Figueiredo Furtado, G., Honório, A. R., Mokarzel, L., da Silva Vidal, V. A., Ribeiro, A. P. B., Cunha, R. L., & Pollonio, M. A. R. (2019) Functional emulsion gels as pork back fat replacers in Bologna sausage. *Food Structure, 20*, 100105. https://doi.org/10.1016/j.foostr.2019.100105

Delgado, C. L. (2003). Rising Consumption of Meat and Milk in Developing Countries Has Created a New Food Revolution. *The Journal of Nutrition, 133*(11), 3907S-3910S. https://doi.org/10.1093/jn/133.11.3907S

Demiray, E. B., Sezgin Arslan, T., Derkus, B., & Arslan, Y. E. (2024). A Facile Strategy for Preparing Flexible and Porous Hydrogel-Based Scaffolds from Silk Sericin/Wool Keratin by In Situ Bubble-Forming for Muscle Tissue Engineering Applications. *Macromolecular bioscience*, e2400362. Advance online publication. https://doi.org/10.1002/mabi.202400362

Derakhti, S., Safiabadi-Tali, S. H., Amoabediny, G., & Sheikhpour, M. (2019). Attachment and detachment strategies in microcarrier-based cell culture technology: A comprehensive review. *Materials science & engineering. C, Materials for biological applications, 103*, 109782. https://doi.org/10.1016/j.msec.2019.109782

Derakhti, S., Safiabadi-Tali, S. H., Amoabediny, G., & Sheikhpour, M. (2019). Attachment and detachment strategies in microcarrier-based cell culture technology: A comprehensive review. *Materials science & engineering. C, Materials for biological applications*, *103*, 109782. https://doi.org/10.1016/j.msec.2019.109782

Devi, S. M., Balachandar, V., Lee, S. I., & Kim, I. H. (2014). An Outline of Meat Consumption in the Indian Population - A Pilot Review. *Korean journal for food science of animal resources, 34*(4), 507–515. https://doi.org/10.5851/kosfa.2014.34.4.507

Dierings de Souza, E. J., Kringel, D. H., Guerra Dias, A. R., & da Rosa Zavareze, E. (2021). Polysaccharides as wall material for the encapsulation of essential oils by electrospun technique. *Carbohydrate polymers*, *265*, 118068. https://doi.org/10.1016/j.carbpol.2021.118068

Djisalov, M., Knežić, T., Podunavac, I., Živojević, K., Radonic, V., Knežević, N. Ž., Bobrinetskiy, I., & Gadjanski, I. (2021). Cultivating Multidisciplinarity: Manufacturing and Sensing Challenges in Cultured Meat Production. *Biology*, *10*(3), 204. https://doi.org/10.3390/biology10030204

Dolgin, J., Hanumantharao, S. N., Farias, S., Simon, Jr. C. G., & Rao, S. (2023). Mechanical Properties and Morphological Alterations in Fiber-Based Scaffolds Affecting Tissue Engineering Outcomes. *Fibers, 11*(5), 39. https://doi.org/10.3390/fib11050039

Domingo, J. L., & Nadal, M. (2017). Carcinogenicity of consumption of red meat and processed meat: A review of scientific news since the IARC decision. *Food and chemical toxicology : an international journal published for the British Industrial Biological Research Association, 105*, 256–261. https://doi.org/10.1016/j.fct.2017.04.028

Dos Santos, A. E. A., Guadalupe, J. L., Albergaria, J. D. S., Almeida, I. A., Moreira, A. M. S., Copola, A. G. L., de Paula, A. M., Neves, B. R. A., Santos, J. P. F., da Silva, A. B., Jorge, E. C., Andrade, L. O., & de Araújo, I. P. (2024). Random cellulose acetate nanofibres: a breakthrough for cultivated meat production. *Frontiers in nutrition*, *10*, 1297926. https://doi.org/10.3389/fnut.2023.1297926

Dos Santos, F. V., Siqueira, R. L., de Morais Ramos, L., Yoshioka, S. A., Branciforti, M. C., & Correa, D. S. (2024b). Silk fibroin-derived electrospun materials for biomedical applications: A review. *International journal of biological macromolecules*, *254*(Pt 2), 127641. https://doi.org/10.1016/j.ijbiomac.2023.127641

dos Santos, F.V., Yoshioka, S.A., & Branciforti, M.C. (2021). Large-area thin films of silk fibroin prepared by two methods with formic acid as solvent and glycerol as plasticizer. *Journal of Applied Polymer Science, 138*, 50759. https://doi.org/10.1002/app.50759

Dou, H., & Zuo, B. (2015). Effect of sodium carbonate concentrations on the degumming and regeneration process of silk fibroin. *The Journal of The Textile Institute, 106*(3), 311-319. https://doi.org/10.1080/00405000.2014.919065

Du, H., Guo, Y., Bennett, D. A., Bragg, F., Bian, Z., Chadni, M., Yu, C., Chen, Y., Tan, Y., Millwood, I. Y., Gan, W., Yang, L., Yao, P., Luo, G., Li, J., Qin, Y., Lv, J., Lin, X., Key, T., Chen, J., Clarke, R., Li, L., & Chen, Z., (2020). Red meat, poultry and fish consumption and risk of diabetes: a 9 year prospective cohort study of the China Kadoorie Biobank. *Diabetologia, 63(*4), 767–779. https://doi.org/10.1007/s00125-020-05091-x

Duangpakdee, A., Laomeephol, C., Jindatip, D., Thongnuek, P., Ratanavaraporn, J., & Damrongsakkul, S. (2021). Crosslinked silk fibroin/gelatin/hyaluronan blends as scaffolds for cell-based tissue engineering. *Molecules, 26*(11), 3191. https://doi.org/10.3390/molecules26113191

Dupuis, J. H., Cheung, L. K. Y., Newman, L., Dee, D. R., & Yada, R. Y. (2023). Precision cellular agriculture: The future role of recombinantly expressed protein as food. *Comprehensive reviews in food science and food safety, 22(*2), 882–912. https://doi.org/10.1111/1541-4337.13094

Duque Sánchez, L., Brack, N., Postma, A., Pigram, P. J., & Meagher, L. (2016). Surface modification of electrospun fibres for biomedical applications: A focus on radical polymerization methods. *Biomaterials, 106*, 24–45. https://doi.org/10.1016/j.biomaterials.2016.08.011

Dura, G., Crespo-Cuadrado, M., Waller, H., Peters, D. T., Ferreira-Duarte, A., Lakey, J. H., & Fulton, D. A. (2022). Exploiting Meltable Protein Hydrogels to Encapsulate and Culture Cells in 3D. *Macromolecular bioscience*, *22*(9), e2200134. https://doi.org/10.1002/mabi.202200134

Ebeling A. H. (1922). A TEN YEAR OLD STRAIN OF FIBROBLASTS. *The Journal of experimental medicine, 35*(6), 755–759. https://doi.org/10.1084/jem.35.6.755

El Khoury, Y., Hielscher, R., Voicescu, M., Gross, J., & Hellwig, P. (2011). On the specificity of the amide VI band for the secondary structure of proteins. *Vibrational Spectroscopy, 55*(2), 258-266. https://doi.org/10.1016/j.vibspec.2010.12.001

Engler, A. J., Sen, S., Sweeney, H. L., & Discher, D. E. (2006). Matrix elasticity directs stem cell lineage specification. *Cell, 126*(4), 677–689. https://doi.org/10.1016/j.cell.2006.06.044

Engler, A. J., Sen, S., Sweeney, H. L., & Discher, D. E. (2006). Matrix elasticity directs stem cell lineage specification. *Cell, 126*(4), 677–689. https://doi.org/10.1016/j.cell.2006.06.044

Erben, J., Kalous, T., & Chvojka, J. (2020). AC Bubble Electrospinning Technology for Preparation of Nanofibrous Mats. *ACS Omega, 5*(14), 8268-8271. https://doi.org/10.1021/acsomega.0c00575

Erickson, D. P., Ozturk, O. K., Selling, G., Chen, F., Campanella, O. H., & Hamaker, B. R. (2020). Corn zein undergoes conformational changes to higher β-sheet content during self-assembly in an increasingly hydrophilic solvent. *International Journal of Biological Molecules, 157*, 232-239. https://doi.org/10.1016/j.ijbiomac.2020.04.169

Eslami, R., Azizi, A., & Najafi, M. (2021). Effects of different gums on tensile properties of cellulose nanofibrils (CNFs)-reinforced starch. *Polym. Polym. Compos. 29*(5), 436-443. https://doi.org/10.1177/0967391120923440

Estabridis, H. M., Jana, A., Nain, A., & Odde, D. J. (2018). Cell Migration in 1D and 2D Nanofibre Microenvironments. *Annals of biomedical engineering, 46*(3), 392–403. https://doi.org/10.1007/s10439-017-1958-6

European Comission. (1981). *Council Directive 81/602/EEC of 31 July 1981 concerning the prohibition of certain substances having a hormonal action and of any substances having a thyrostatic action.* European Commission Europa. https://eur-lex.europa.eu/eli/dir/1981/602/oj

Evans, M. J., & Kaufman, M. H. (1981). Establishment in culture of pluripotential cells from mouse embryos. *Nature*, *292*(5819), 154–156. https://doi.org/10.1038/292154a0

Falsafi, S. R., Topuz, F., Esfandiari, Z., Can Karaca, A., Jafari, S. M., & Rostamabadi, H. (2023). Recent trends in the application of protein electrospun fibers for loading food bioactive compounds. *Food chemistry: X, 20*, 100922. https://doi.org/10.1016/j.fochx.2023.100922

FAO. (2011). World Livestock 2011. *Livestock in Food Security*. https://www.fao.org/3/i3300e/i3300e00.htm

FAO. (2021). *A multi-billion-dollar opportunity – Repurposing agricultural support to transform food systems*. Food and Agriculture Organization. https://doi.org/10.4060/cb6683en

Farokhi, M., Mottaghitalab, F., Fatahi, Y., Khademhosseini, A., & Kaplan, D. L. (2018). Overview of Silk Fibroin Use in Wound Dressings. *Trends in biotechnology*, *36*(9), 907–922. https://doi.org/10.1016/j.tibtech.2018.04.004

Fasina, O. O., Craig-Schmidt, M., Colley, Z., & Hallman, H. (2008). Predicting melting characteristics of vegetable oils from fatty acid composition. *LWT - Food Science and Technology, 41*(8),1501-1505. https://doi.org/10.1016/j.lwt.2007.09.012

FAWC. (2012). Farm Animal Welfare: Health and Disease. *Farm Animal Welfare Committee*. https://assets.publishing.service.gov.uk/government/uploads/system/uploads/attachment_data/file/324616/FAWC_report_on_farm_animal_welfare_-_health_and_disease.pdf

Feng, L., Li, Y., Zeng, W., Xia, B., Zhou, D., & Zhou, J. (2017). Enhancing effects of basic fibroblast growth factor and fibronectin on osteoblast adhesion to bone scaffolds for bone tissue engineering through extracellular matrix-integrin pathway. *Experimental and therapeutic medicine, 14*(6), 6087–6092. https://doi.org/10.3892/etm.2017.5320

Feng, Y., Lin, J., Niu, L., Wang, Y., Cheng, Z., Sun, X., & Li, M. (2020). High Molecular Weight Silk Fibroin Prepared by Papain Degumming. *Polymers, 12*(9), 2105. https://doi.org/10.3390/polym12092105

Fernandes, A. M., de Souza Teixeira, O., Fantinel, A. L., Revillion, J. P. P., & de Souza, A. R. L. (2022). Technological prospecting: The case of cultured meat. *Future Foods, 6*, 100156. https://doi.org/10.1016/j.fufo.2022.100156

Fernandes, C., Acharya, P. C., & Bhatt, S. (2018). Preparation of Lauroyl Grafted Alginate-Psyllium Husk Gel Composite Film with Enhanced Physicochemical, Mechanical and Antimicrobial Properties. *Scientific reports*, *8*(1), 17213. https://doi.org/10.1038/s41598-018-35632-9

Fernandes, J. N., Hemsworth, P. H., Coleman, G. J., & Tillbrook, A. J. (2021). Costs and Benefits of Improving Farm Animal Welfare. *Agriculture, 11*(2), 104. https://doi.org/10.3390/agriculture11020104

Fernández-Muiños, T., Suárez-Muñoz, M., Sanmartí-Espinal, M., & Semino, C. E. (2014). Matrix dimensions, stiffness, and structural properties modulate spontaneous chondrogenic commitment of mouse embryonic fibroblasts. *Tissue engineering. Part A*, *20*(7-8), 1145–1155. https://doi.org/10.1089/ten.tea.2013.0369

Fernández-Pérez, J., & Ahearne, M. (2019). The impact of decellularization methods on extracellular matrix derived hydrogels. *Scientific reports, 9*(1), 14933. https://doi.org/10.1038/s41598-019-49575-2

Ferrari, M., Cirisano, F., & Morán, M. C. (2019). Mammalian Cell Behaviour on Hydrophobic Substrates: Influence of Surface Properties. *Colloids and Interfaces, 3*(2), 48. https://doi.org/10.3390/colloids3020048

Fiems, L. O., Campeneere, S. D., De Smet, S., Van de Voorde, G., Vanacker, J. M., & Boucqué, C. V. (2000). Relationship between fat depots in carcasses of beef bulls and effect on meat colour and tenderness. *Meat science, 56*(1), 41–47. https://doi.org/10.1016/s0309-1740(00)00017-6

Fish, K. D., Rubio, N. R., Stout, A. J., Yuen, J. S. K. & Kaplan, D. L. (2020).Prospects and challenges for cell-cultured fat as a novel food ingredient. *Trends in Food Science & Technology*, *98*, 53-67. https://doi.org/10.1016/j.tifs.2020.02.005

Flaibam, B., Alves, G. S., da Silva Vejnar, E. I., Nery, T. B. R., Damasio, A. & Goldbeck, R. (2025). Applications of recombinant proteins in cultured meat production. *Future Foods*, *11*, 100582. https://doi.org/10.1016/j.fufo.2025.100582

Fountain, H. (2013, August 5). A lab grown burger gets at taste test. The New York Times. https://www.nytimes.com/2013/08/06/science/a-lab-grown-burger-gets-a-taste-test.html

Freear, J. (2015). *Marks and Spencer and the social history of food c. 1950 - 1980, with particular reference to the relationship between consumer behaviour and retailing strategies* [Doctoral dissertation, University of Leeds]. White Rose eTheses Online. https://etheses.whiterose.ac.uk/10498/1/Josephine%20Freear%20thesis%20-%20final.pdf

Friedrich, B. (2019, September 29). *Why GFI uses the term "cultivated meat".* Good Food Institute. https://gfi.org/blog/cultivatedmeat/

Galen (150/2011) *Method of Medicine.* Loeb Classical Library. (Original work published in 150).

Gao, X., Gou, J., Zhang, L., Duan, S., & Li, C. (2018). A silk fibroin based green nano-filter for air filtration. *RSC advances*, *8*(15), 8181–8189. https://doi.org/10.1039/c7ra12879g

Gattazzo, F., Urciuolo, A., & Bonaldo, P. (2014). Extracellular matrix: a dynamic microenvironment for stem cell niche. *Biochimica et Biophysica Acta, 1840*(8), 2506–2519. https://doi.org/10.1016/j.bbagen.2014.01.010

Ge, J., Guo, L., Wang, S., Zhang, Y., Cai, T., Zhao, R. C. H., & Wu, Y. (2014). The Size of Mesenchymal Stem Cells is a Significant Cause of Vascular Obstructions and Stroke. *Stem Cell Reviews and Reports, 10*, 295–303. https://doi.org/10.1007/s12015-013-9492-x

Genovese, N. J., Domeier, T. L., Telugu, B. P., & Roberts, R. M. (2017). Enhanced Development of Skeletal Myotubes from Porcine Induced Pluripotent Stem Cells. *Scientific reports, 7*, 41833. https://doi.org/10.1038/srep41833

GFI. (2021). *2021 STATE OF THE INDUSTRY REPORT, Cultivated Meat and Seafood.* Good Food Institute. https://gfieurope.org/wp-content/uploads/2022/04/2021-Cultivated-Meat-State-of-the-Industry-Report.pdf

GFI. (2021b, February 2). *World's first cell-based steak from Aleph Farms, catalyzed by cross-sector collaboration*. The Good Food Institute. https://gfi.org/blog/worlds-first-cell-based-steak-from-aleph/

GFI. (2021c). *Reducing the price of alternative proteins.* Good Food Institute. https://gfi.org/wp-content/uploads/2021/12/Reducing-the-price-of-alternative-proteins_GFI_2022.pdf

GFI. (2023, July 26). *Aleph Farms make Europe's first cultivated meat approval submission to Swiss Regulators.* GFI Europe. https://gfieurope.org/blog/aleph-farms-make-europes-first-cultivated-meat-approval-submission-to-swiss-regulators/

GFI. (2024, July 11). *Alternative protein company database (2024): GFI*. The Good Food Institute. https://gfi.org/resource/alternative-protein-company-database/

Ghalei, S., Douglass, M., & Handa, H. (2022). Nitric Oxide-Releasing Nanofibrous Scaffolds Based on Silk Fibroin and Zein with Enhanced Biodegradability and Antibacterial Properties. *ACS Biomaterials Science & Engineering*, *8*(7), 3066–3077. https://doi.org/10.1021/acsbiomaterials.2c00103

Giannelli, M., Lacivita, V., Posati, T., Aluigi, A., Conte, A., Zamboni, R., & Del Nobile, M. A. (2021). Silk Fibroin and Pomegranate By-Products to Develop Sustainable Active Pad for Food Packaging Applications. *Foods (Basel, Switzerland)*, *10*(12), 2921. https://doi.org/10.3390/foods10122921

Gill, S. K., Rossi, M., Bajka, B., & Whelan, K. (2021). Dietary fibre in gastrointestinal health and disease. *Nature reviews. Gastroenterology & hepatology*, *18*(2), 101–116. https://doi.org/10.1038/s41575-020-00375-4

Gillies, A. R., & Lieber, R. L. (2011). Structure and function of the skeletal muscle extracellular matrix. *Muscle & Nerve, 44*(3), 318–331. https://doi.org/10.1002/mus.22094

Girão, A. F., Wieringa, P., Pinto, S. C., Marques, P. A. A. P., Micera, S., van Wezel, R., Ahmed, M., Truckenmueller, R., & Moroni, L. (2019). Ultraviolet Functionalization of Electrospun Scaffolds to Activate Fibrous Runways for Targeting Cell Adhesion. *Frontiers in bioengineering and biotechnology, 7*, 159. https://doi.org/10.3389/fbioe.2019.00159

Godschalk-Broers, L., Sala, G., & Scholten, E. (2022). Meat Analogues: Relating Structure to Texture and Sensory Perception. *Foods (Basel, Switzerland), 11*(15), 2227. https://doi.org/10.3390/foods11152227

Gómez-López, V. M., Jubinville, E., Rodríguez-López, M. I., Trudel-Ferland, M., Bouchard, S., & Jean, J. (2021). Inactivation of Foodborne Viruses by UV Light: A Review. *Foods (Basel, Switzerland), 10*(12), 3141. https://doi.org/10.3390/foods10123141

Gong, Y., Li, L., Gong, D., Yin, H., & Zhang, J. (2016). Biomolecular Evidence of Silk from 8,500 Years Ago. *PloS one*, *11*(12), e0168042. https://doi.org/10.1371/journal.pone.0168042

Gong, Y., Zhou, G., Qiao, C., & Pan, Y. (2024). Study on the photodegradation behaviors of thermal-aged silk. *Heritage Science, 12*, 151. https://doi.org/10.1186/s40494-024-01270-w

Grandin T. (2021). Methods to Prevent Future Severe Animal Welfare Problems Caused by COVID-19 in the Pork Industry. *Animals : an open access journal from MDPI*, *11*(3), 830. https://doi.org/10.3390/ani11030830

Grasso, S., & Goksen, G. (2023). The best of both worlds? Challenges and opportunities in the development of hybrid meat products from the last 3 years. *LWT, 173*, 114235. https://doi.org/10.1016/j.lwt.2022.114235

Griffin, M., Premakumar, Y., Seifalian, A., Butler, P. E., & Szarko, M. (2016). Biomechanical Characterization of Human Soft Tissues Using Indentation and Tensile Testing. *Journal of visualized experiments : JoVE*, (118), 54872. https://doi.org/10.3791/54872

Grossi, G., Goglio, P., Vitali, A., & Williams, A. G. (2019). Livestock and climate change: impact of livestock on climate and mitigation strategies, *Animal Frontiers, 9*(1), 69-76. https://doi.org/10.1093/af/vfy034

Gu, D., Andreev, K., & Dupre, M. E. (2021). Major Trends in Population Growth Around the World. *China CDC weekly, 3*(28), 604–613. https://doi.org/10.46234/ccdcw2021.160

Guo, B., & Ma, P. X. (2014). Synthetic biodegradable functional polymers for tissue engineering: a brief review. *Science China. Chemistry, 57*(4), 490–500. https://doi.org/10.1007/s11426-014-5086-y

Guo, Q., Cui, S. W., Wang, Q., & Christopher Young, J. (2008). Fractionation and physicochemical characterization of psyllium gum. *Carbohydrate Polymers*, *73*(1), 35–43. https://doi.org/10.1016/J.CARBPOL.2007.11.001

Guo, Y., Gilbert-Honick, J., Somers, S. M., Mao, H. Q., & Grayson, W. L. (2019). Modified cell-electrospinning for 3D myogenesis of C2C12s in aligned fibrin microfiber bundles. *Biochemical and biophysical research communications*, *516*(2), 558–564. https://doi.org/10.1016/j.bbrc.2019.06.082

Gurikar, A. M., Lakshmanan, V., Gadekar, Y. P., Sharma, B. D., & Anjaneyulu, A. S. (2014). Effect of meat chunk size, massaging time and cooking time on quality of restructured pork blocks. *Journal of food science and technology, 51*(7), 1363–1369. https://doi.org/10.1007/s13197-012-0644-9

Haider, A., Haider, S., & Kang, I.-K. (2018). A comprehensive review summarizing the effect of electrospinning parameters and potential applications of nanofibres in biomedical and biotechnology, *Arabian Journal of Chemistry, 11*(8), 1165-1188. https://doi.org/10.1016/j.arabjc.2015.11.015

Hamdan, M. N., Abdul Jalil, R., Ramli, M. A., Ramli, N., Ibrahim, M. N. A., Ab Rahman, M. F., Abdullah Thaidi, H., & Abd Rahman, N. N. H. (2024). A review of the discussions on cultivated meat from the Islamic perspective. *Heliyon, 10*(7), e28491. https://doi.org/10.1016/j.heliyon.2024.e28491

Hamlin, R. P., McNeill, L. S., & Sim, J. (2022). Food neophobia, food choice and the details of cultured meat acceptance. *Meat science*, *194*, 108964. https://doi.org/10.1016/j.meatsci.2022.108964

Hanga, M. P., Ali, J., Moutsatsou, P., de la Raga, F. A., Hewitt, C. J., Nienow, A., & Wall, I. (2020). Bioprocess development for scalable production of cultivated meat. *Biotechnology and bioengineering, 117*(10), 3029–3039. https://doi.org/10.1002/bit.27469

Hanga, M. P., de la Raga, F. A., Moutsatsou, P., Hewitt, C. J., Nienow, A. W., & Wall, I. (2021). Scale-up of an intensified bioprocess for the expansion of bovine adipose-derived stem cells (bASCs) in stirred tank bioreactors. *Biotechnology and bioengineering, 118(*8), 3175–3186. https://doi.org/10.1002/bit.27842

Hao, L., Fu, X., Li, T., Zhao, N., Shi, X., Cui, F., Du, C., & Wang, Y. (2016). Surface chemistry from wettability and charge for the control of mesenchymal stem cell fate through self-assembled monolayers. *Colloids and surfaces. B, Biointerfaces*, *148*, 549–556. https://doi.org/10.1016/j.colsurfb.2016.09.027

Hao, L., Yang, H., Du, C., Fu, X., Zhao, N., Xu, S., Cui, F., Mao, C., & Wang, Y. (2014). Directing the fate of human and mouse mesenchymal stem cells by hydroxyl-methyl mixed self-assembled monolayers with varying wettability. *Journal of materials chemistry. B*, *2*(30), 4794–4801. https://doi.org/10.1039/C4TB00597J

Hartrianti, P., Ling, L., Goh, L. M., Ow, K. S., Samsonraj, R. M., Sow, W. T., Wang, S., Nurcombe, V., Cool, S. M., & Ng, K. W. (2015). Modulating Mesenchymal Stem Cell Behavior Using Human Hair Keratin-Coated Surfaces. *Stem cells international*, *2015*, 752424. https://doi.org/10.1155/2015/752424

Hashimoto, T., Nakamura, Y., Tamada, Y., Kurosu, H., & Kameda, T. (2020). The influence of thermal treatments on the secondary structure of silk fibroin scaffolds and their interaction with fibroblasts. *Peer J Materials Science 2*, 8. https://doi.org/10.7717/peerj-matsci.8

He, J., Zhang, Q., Wu, Y., Ju, Y., Wang, Y., & Tang, S. (2023). Scalable nanofibrous silk fibroin textile with excellent Mie scattering and high sweat evaporation ability for highly efficient passive personal thermal management. *Chemical Engineering Journal*, *466*, 143127. https://doi.org/10.1016/j.cej.2023.143127

Heautrive, T. P., Piccolo, J., Rodrigues, A. S., Campagnol, P. C. B., Kubota, E. H. (2019). Effect of fat replacement by chitosan and golden flaxseed flour (wholemeal and defatted) on the quality of hamburgers. *LWT, 102*, 403-410. https://doi.org/10.1016/j.lwt.2018.12.025

Herrero, M., Havlík, P., Valin, H., Notenbaert, A., Rufino, M. C., Thornton, P. K., Blümmel, M., Weiss, F., Grace, D., & Obersteiner, M. (2013). Biomass use, production, feed efficiencies, and greenhouse gas emissions from global livestock systems. *Proceedings of the National Academy of Sciences of the United States of America*, *110*(52), 20888–20893. https://doi.org/10.1073/pnas.1308149110

Herrero, M., Havlíkb, P., Valinc, H., Notenbaert, A., Rufinob, M. C., Thorntond, P. K., Blümmelb, M., Weiss, F., Grace, D., & Obersteiner, M. (2013). Biomass use, production, feed efficiencies, and greenhouse gas emissions from global livestock systems. PNAS, 110(52), 20888-20893. https://doi.org/10.1073/pnas.1308149110

Higuita, N. I. A., LaRoque, R., & McGushin, A. (2023). Climate change, industrial animal agriculture, and the role of physicians – Time to act. *The Journal of Climate Change and Health, 13*, 100260. https://doi.org/10.1016/j.joclim.2023.100260

Hocquette, J. F., Chriki, S., Fournier, D., & Ellies-Oury, M. P. (2024). Review: Will "cultured meat" transform our food system towards more sustainability?. *Animal : an international journal of animal bioscience*, 101145. Advance online publication. https://doi.org/10.1016/j.animal.2024.101145

Holland, C., Numata, K., Rnjak-Kovacina, J., & Seib, F. P. (2019). The Biomedical Use of Silk: Past, Present, Future. *Advanced healthcare materials*, *8*(1), e1800465. https://doi.org/10.1002/adhm.201800465

Homer, W. J. A., Lisnenko, M., Gardner, A. C., Kostakova, E. K., Valtera, J., Wall, I. B., Jencova, V., Topham, P. D., & Theodosiou, E. (2023). Assessment of thermally stabilized electrospun poly(vinyl alcohol) materials as cell permeable membranes for a novel blood salvage device. *Biomaterials Advances, 144*, 213197. https://doi.org/10.1016/j.bioadv.2022.213197

Honderich, H. (2024a, May 2). *Ron DeSantis bans "global elite" lab-grown meat*. BBC News. https://www.bbc.co.uk/news/world-us-canada-68947766

Hong, T., Yin, J. Y., Nie, S. P., & Xie, M. Y. (2021). Applications of infrared spectroscopy in polysaccharide structural analysis: Progress, challenge and perspective. *Food Chemistry: X*, *12*, 100168. https://doi.org/10.1016/J.FOCHX.2021.100168

Hopkins, I., Farahnaky, A., Gill, H., Danaher, J., & Newman, L. P. (2023). Food neophobia and its association with dietary choices and willingness to eat insects. *Frontiers in nutrition*, *10*, 1150789. https://doi.org/10.3389/fnut.2023.1150789

Hosseini Ravandi, S. A., Sadrjahani, M., Valipouri, A., Dabirian, F., & Ko, F. K. (2022). Recently developed electrospinning methods: a review. *Textile Research Journal, 92*(23-24), 5130-5145. https://doi.org/10.1177/00405175211069880

Hu, F., Lin, N., & Liu, X. Y. (2020). Interplay between Light and Functionalized Silk Fibroin and Applications. *iScience, 23*(4), 101035. https://doi.org/10.1016/j.isci.2020.101035

Hu, P., Chiarini, A., Wu, J., Wei, Z., Armato, U., & Dal Prà, I. (2022). Adult Human Vascular Smooth Muscle Cells on 3D Silk Fibroin Nonwovens Release Exosomes Enriched in Angiogenic and Growth-Promoting Factors. *Polymers*, *14*(4), 697. https://doi.org/10.3390/polym14040697

Hu, X., Kaplan, D., & Cebe, P. (2006). Determining beta-sheet crystallinity in fibrous proteins by thermal analysis and infrared spectroscopy. *Macromolecules 39*(18), 6161-6170. https://doi.org/10.1021/ma0610109

Hu, X., Shmelev, K., Sun, L., Gil, E.S., Park, S.H., Cebe, P., & Kaplan, D.L. (2011). Regulation of silk material structure by temperature-controlled water vapor annealing. *Biomacromolecules 12*(5), 1686–1696. https://doi.org/10.1021/bm200062a

Hu, Y., Zhang, Q., You, R., Wang, L., & Li, M. (2012). The Relationship between Secondary Structure and Biodegradation Behavior of Silk Fibroin Scaffolds, *Advances in Materials Science and Engineering, 2012*(1), 185905. https://doi.org/10.1155/2012/185905

Huang, G. P., Shanmugasundaram, S., Masih, P., Pandya, D., Amara, S., Collins, G., & Arinzeh, T. L. (2015). An investigation of common crosslinking agents on the stability of electrospun collagen scaffolds. *Journal of Biomedical Materials Research. Part A, 103(*2), 762–771. https://doi.org/10.1002/jbm.a.35222

Huang, W., Liu, B., Chen, Z., Wang, H., Ren, L., Jiao, J., Zhuang, L., Luo, J., & Jiang, L. (2017). Fabrication of Magnetic Nanofibres by Needleless Electrospinning from a Self-Assembling Polymer

Ferrofluid Cone Array. *Nanomaterials (Basel, Switzerland)*, *7*(9), 277. https://doi.org/10.3390/nano7090277

Huang, X., Fan, S., Altayp, A. I. M., Zhang, Y., Shao, H., Hu, X., Xie, M., & Xu, Y. (2014) Tunable Structures and Properties of Electrospun Regenerated Silk Fibroin Mats Annealed in Water Vapor at Different Times and Temperatures. *Journal of Nanomaterials*, *2014*(1), 682563. https://doi.org/10.1155/2014/682563

Huang, Y., Li, Y., Zhang, Y., Yu, H., & Tan, Z. (2024). Near-field electrospinning for 2D and 3D structuring: Fundamentals, methods, and applications. *materialstoday ADVANCES, 21*, 100461. https://doi.org/10.1016/j.mtadv.2023.100461

Hwang, Y. H., & Joo, S. T. (2017). Fatty Acid Profiles, Meat Quality, and Sensory Palatability of Grain-fed and Grass-fed Beef from Hanwoo, American, and Australian Crossbred Cattle. *Korean journal for food science of animal resources, 37*(2), 153–161. https://doi.org/10.5851/kosfa.2017.37.2.153

Ianovici, I., Zagury, Y., Redenski, I., Lavon, N., & Levenberg, S. (2022). 3D-printable plant protein-enriched scaffolds for cultivated meat development. *Biomaterials*, *284*, 121487. https://doi.org/10.1016/j.biomaterials.2022.121487

Ibrahim, Y. S., Hussein, E. A., Zagho, M. M., Abdo, G. G., & Elzatahry, A. A. (2019). Melt Electrospinning Designs for Nanofibre Fabrication for Different Applications. *International journal of molecular sciences*, *20*(10), 2455. https://doi.org/10.3390/ijms20102455

Idaszek, J., Bruinink, A., & Święszkowski, W. (2015). Ternary composite scaffolds with tailorable degradation rate and highly improved colonization by human bone marrow stromal cells. *Journal of biomedical materials research. Part A*, *103*(7), 2394–2404. https://doi.org/10.1002/jbm.a.35377

Imtiyaz, H., Soni, P., & Yukongdi, V. (2021). Role of Sensory Appeal, Nutritional Quality, Safety, and Health Determinants on Convenience Food Choice in an Academic Environment. *Foods (Basel, Switzerland), 10*(2), 345. https://doi.org/10.3390/foods10020345

International Organization for Standardization. (2002). Plastics - Determination of compressive properties - Technical Report (ISO Standard No. 604:2002). https://www.iso.org/standard/31261.html

International Organization for Standardization. (2019a). Plastics - Determination of flexural properties - Technical Report (ISO Standard No. 178:2019). https://www.iso.org/standard/70513.html

International Organization for Standardization. (2019b). Plastics - Determination of tensile properties - Technical Report (ISO Standard No. 527:2019). https://www.iso.org/standard/75824.html

Izutsu, T., & Wani, K. (1985). Food texture and taste: A review. *Journal of Texture Studies, 16*(1), 1–28. https://doi.org/10.1111/j.1745-4603.1985.tb00677.x

Jahangirian, H., Azizi, S., Rafiee-Moghaddam, R., Baratvand, B., & Webster, T. J. (2019). Status of Plant Protein-Based Green Scaffolds for Regenerative Medicine Applications. *Biomolecules, 9*(10), 619. https://doi.org/10.3390/biom9100619

Jalaja, K., & James, N. R. (2015). Electrospun gelatin nanofibres: a facile cross-linking approach using oxidized sucrose. *International journal of biological macromolecules*, *73*, 270–278. https://doi.org/10.1016/j.ijbiomac.2014.11.018

Jalaja, K., Naskar, D., Kundu, S. C., & James, N. R. (2016). Potential of electrospun core-shell structured gelatin-chitosan nanofibres for biomedical applications. *Carbohydrate polymers*, *136*, 1098–1107. https://doi.org/10.1016/j.carbpol.2015.10.014

James, B., & Yang, S. W. (2011). Testing meat tenderness using an in situ straining stage with variable pressure scanning electron microscopy. *Procedia Food Science, 1*, 258–266. https://doi.org/10.1016/j.profoo.2011.09.041

Jaramillo-Quiceno, N., & Restrepo-Osorio, A. (2020), Water-annealing treatment for edible silk fibroin coatings from fibrous waste. *Journal of Applied Polymer Sciences, 137*, 48505. https://doi.org/10.1002/app.48505

Jedrzejczak-Silicka, M. (2017). History of Cell Culture. *InTechOpen*. https://doi.org/10.5772/66905

Jenkins, T.L., & Little, D. (2019). Synthetic scaffolds for musculoskeletal tissue engineering: cellular responses to fiber parameters. *npj Regenerative Medicine 4*, 15 https://doi.org/10.1038/s41536-019-0076-5

Jeong, D., Jang, G., Jung, W. K., Park, Y. H., & Bae, H. (2024). Stretchable zein-coated alginate fiber for aligning muscle cells to artificially produce cultivated meat. *NPJ science of food, 8*(1), 13. https://doi.org/10.1038/s41538-024-00257-y

Jirsak, O., Sanetrnik, F., Lukas, D., Kotek, V., Martinova, L., & Chaloupek, J. (2009). *Method of Nanofibres Production from a Polymer Solution Using Electrostatic Spinning and a Device for Carrying out the Method* (European Patent No. EP1673493B1). https://data.epo.org/publication-server/rest/v1.0/publication-dates/20090708/patents/EP1673493NWB1/document.pdf

Jo, Y.-Y., Kweon, H., & Oh, J.-H. (2020). Sericin for Tissue Engineering. *Applied Sciences, 10*(23), 8457.

Johari, N., Moroni, L., & Samadikuchaksaraei, A. (2020). Tuning the conformation and mechanical properties of silk fibroin hydrogels. *Eur. Polym. J. 134*, 109842. https://doi.org/10.1016/j.eurpolymj.2020.109842

Jones, H. (2024, July 17). *Lab-grown meat in pet food: UK to allow sales of meatly product.* BBC News. https://www.bbc.co.uk/news/articles/c19k0ky9v4yo

Jonnalagadda, J. B., & Rivero, I. V. (2014). Effect of cryomilling times on the resultant properties of porous biodegradable poly(e-caprolactone)/poly(glycolic acid) scaffolds for articular cartilage tissue engineering. *Journal of the mechanical behavior of biomedical materials, 40*, 33–41. https://doi.org/10.1016/j.jmbbm.2014.08.009

Kaewpirom, S., & Boonsang, S. (2020). Influence of alcohol treatments on properties of silk-fibroin-based films for highly optically transparent coating applications. *RSC advances, 10*(27), 15913–15923. https://doi.org/10.1039/d0ra02634d

Kamei, M., Nishibe, M., Araki, R., Kohyama, K., Kusakabe, Y. (2024). Effect of texture preference on food texture perception: Exploring the role of matching food texture and preference. *Appetite, 192*, 107078. https://doi.org/10.1016/j.appet.2023.107078

Kang, D. H., Louis, F., Liu, H., Shimoda, H., Nishiyama, Y., Nozawa, H., Kakitani, M., Takagi, D., Kasa, D., Nagamori, E., Irie, S., Kitano, S., & Matsusaki, M. (2021). Engineered whole cut meat-like tissue by the assembly of cell fibers using tendon-gel integrated bioprinting. *Nature communications*, *12*(1), 5059. https://doi.org/10.1038/s41467-021-25236-9

Kang, Z., Wang, Y., Xu, J., Song, G., Ding, M., Zhao, H., & Wang, J. (2018). An RGD-Containing Peptide Derived from Wild Silkworm Silk Fibroin Promotes Cell Adhesion and Spreading. *Polymers, 10*(11), 1193. https://doi.org/10.3390/polym10111193

Kapałczyńska, M., Kolenda, T., Przybyła, W., Zajączkowska, M., Teresiak, A., Filas, V., Ibbs, M., Bliźniak, R., Łuczewski, Ł., & Lamperska, K. (2018). 2D and 3D cell cultures - a comparison of different types of cancer cell cultures. *Archives of medical science : AMS*, *14*(4), 910–919. https://doi.org/10.5114/aoms.2016.63743

Katiyar, N. K., Biswas, K., & Tiwary, C. S. (2020). Cryomilling as environmentally friendly synthesis route to prepare nanomaterials. *International Materials Reviews, 66*(7), 493–532. https://doi.org/10.1080/09506608.2020.1825175

Kaur, A., Midha, S., Giri, S., & Mohanty, S. (2019). Functional skin grafts: where biomaterials meet stem cells. *Stem Cells Int. 2019*, 1286054. https://doi.org/10.1155/2019/1286054

Kawecki, N. S., Norris, S. C. P., Xu, Y., Davis, A. R., Fridman, E., Chen, K. K., Crosbie, R. H., Garmyn, A. J., Li, S., Mason, T. G., & Rowat, A. C. (2023). Engineering multicomponent tissue by spontaneous adhesion of myogenic and adipogenic microtissues cultured with customized scaffolds. *Food Research International, 172*, 113080. https://doi.org/10.1016/j.foodres.2023.113080

Keshanidokht, S., Via, M. A., Falco, C. Y., Clausen, M. P., & Risbo, J. (2022). Zein-stabilized emulsions by ethanol addition; stability and microstructure. *Food Hydrocolloids, 133*, 107973. https://doi.org/10.1016/J.FOODHYD.2022.107973

Kessick, R., Fenn, J., & Tepper, G. (2004). The use of AC potentials in electrospraying and electrospinning processes, *Polymer, 45*(9), 2981-2984. https://doi.org/10.1016/j.polymer.2004.02.056

Khakshoor, O., & Nowick, J. S. (2008). Artificial beta-sheets: chemical models of beta-sheets. *Current opinion in chemical biology*, *12*(6), 722–729. https://doi.org/10.1016/j.cbpa.2008.08.009

Kim, J. H., Jin, P., Duan, R., & Chen, E. H. (2015). Mechanisms of myoblast fusion during muscle development. *Current opinion in genetics & development*, *32*, 162-170. https://doi.org/10.1016/j.gde.2015

Kim, S. -H., Kim, C. -J., Lee, E. -Y., Hwang, Y. -H., & Joo, S. -T. (2024). Chicken Embryo Fibroblast Viability and Trans-Differentiation Potential for Cultured Meat Production Across Passages. *Cells, 13*, 1734. https://doi.org/10.3390/cells13201734

Kim, S., Nam, Y., Lee, T., & Park, W. H. (2003). Silk Fibroin Nanofibre. Electrospinning, Properties, and Structure. *Polym J 35*, 185–190. https://doi.org/10.1295/polymj.35.185

Kim, S., Uroz, M., Bays, J.L., & Chen, C.S. (2021). Harnessing mechanobiology for tissue engineering. *Dev. Cell 56*(2), 180–191. https://doi.org/10.1016/j.devcel.2020.12.017

Kirsch, M., Morales-Dalmau, J., & Lavrentieva, A. (2023). Cultivated meat manufacturing: Technology, trends, and challenges. *Engineering in life sciences, 23*(12), e2300227. https://doi.org/10.1002/elsc.202300227

Kiselev, P., & Rosell-Llompart, J. (2012), Highly aligned electrospun nanofibres by elimination of the whipping motion. *Journal of Applied Polymer Science, 125*, 2433-2441. https://doi.org/10.1002/app.36519

Klein, Z. (2023, January 19). *Chief Rabbi: Cultured meat is considered a vegetable but can't be consumed with dairy.* The Jerusalem Post. https://www.jpost.com/judaism/article-728978

Ko, C., Davies, A., & Auty, M. (2023). Putting Meat to the Test: Imaging and Mechanical Testing Used to Understand the Properties of Meat Alternatives and How They Mimic Our Typical Meat Sensory Experience. *Microscopy Today, 31*(2), 21–25. https://doi.org/10.1093/mictod/qaad011

Kocis, L., Pokorny, P., Lukas, D., Mikes, P., Chvojka, J., Kostakova, E., Beran, J., Bilek, M., Valtera, J., Amler, E., Buzgo, M., & Mickova, A. (2018). Method for production of polymeric nanofibres by spinning of solution or melt of polymer in electric field, and a linear formation from polymeric nanofibres prepared by this method (European Patent WO2014094694A1). European Patent Office. https://worldwide.espacenet.com/patent/search/family/049551971/publication/EP2931951A1?q=pn%3DEP2931951A1%3F

Kolkmann, A. M., Post, M. J., Rutjens, M. A. M., van Essen, A. L. M., & Moutsatsou, P. (2020). Serum-free media for the growth of primary bovine myoblasts. *Cytotechnology*, *72*(1), 111–120. https://doi.org/10.1007/s10616-019-00361-y

Konda, A., Prakash, A., Moss, G.A., Schmoldt, M., Grant, G.D., & Guha, S. (2020). Aerosol filtration efficiency of common fabrics used in respiratory cloth masks. *ACS Nano 14*(5), 6339-6347. https://doi.org/10.1021/acsnano.0c03252

Kong, J., & Yu, S. (2007). Fourier transform infrared spectroscopic analysis of protein secondary structures, *Acta Biochimica et Biophysica Sinica, 39*(8), 549–559. https://doi.org/10.1111/j.1745-7270.2007.00320.x

Kong, Y., & Huang, D. (2023). Pumpkin seed proteins rival animal gelatin in increasing the cytoaffinity of edible microbeads for cell-based meat culture. *Food research international (Ottawa, Ont.)*, *168*, 112750. https://doi.org/10.1016/j.foodres.2023.112750

Kong, Y., Toh, N. P., Wu, Y., & Huang, D. (2023). Trypsin-treated chickpea protein hydrolysate enhances the cytoaffinity of microbeads for cultured meat application. *Food research international (Ottawa, Ont.)*, *173*(Pt 2), 113299. https://doi.org/10.1016/j.foodres.2023.113299

Koperska, M. A., Pawcenis, D., Bagniuk, J., Zaitz, M. M., Missori, M., Lojewski, T., & Lojewska, J. (2014). Degradation markers of fibroin in silk through infrared spectroscopy. *Polymer Degradation and Stability, 105*, 185-196. https://doi.org/10.1016/j.polymdegradstab.2014.04.008

Kopittke, P. E., Menzies, N. W., Wang, P., McKenna, B. A., & Lombi, E. (2019). Soil and the intensification of agriculture for global food security. *Environment International, 132*, 105078, https://doi.org/10.1016/j.envint.2019.105078

Kraus, N. A., Ehebauer, F., Zapp, B., Rudolphi, B., Kraus, B. J., & Kraus, D. (2016). Quantitative assessment of adipocyte differentiation in cell culture. *Adipocyte*, *5*(4), 351–358. https://doi.org/10.1080/21623945.2016.1240137

Kruid, S., Macedo, M. N., Gorelik, S. R., Walker, W., Paulo, M., Brando P. M., Castanho, A., Alencar, A., Baccini, A., & Coe, M. T. (2021). Beyond Deforestation: Carbon Emissions from Land Grabbing and Forest Degradation in the Brazilian Amazon. *Frontiers in Forests and Global Change, 4*. https://doi.org/10.3389/ffgc.2021.645282

Krutty, J. D., Schmitt, S. K., Gopalan, P., & Murphy, W. L. (2016). Surface functionalization and dynamics of polymeric cell culture substrates. *Current opinion in biotechnology, 40*, 164–169. https://doi.org/10.1016/j.copbio.2016.05.006

Ku, S. H., & Park, C. B. (2010). Human endothelial cell growth on mussel-inspired nanofibre scaffold for vascular tissue engineering. *Biomaterials, 31*(36), 9431–9437. https://doi.org/10.1016/j.biomaterials.2010.08.071

Kurz, J., Efendic, E., & Goukens, C. (2023). Pricey therefore good? price affects expectations, but not quality perceptions and liking. *Psychology & Marketing, 40*(6), 1115-1129. https://doi.org/10.1002/mar.21799

Kyriakopoulou, K., Keppler, J. K., & van der Goot, A. J. (2021). Functionality of Ingredients and Additives in Plant-Based Meat Analogues. *Foods (Basel, Switzerland), 10(*3), 600. https://doi.org/10.3390/foods10030600

Laber, M., Klimek, P., Bruckner, M., Yang, L., & Thurner, S. (2023). Shock propagation from the Russia-Ukraine conflict on international multilayer food production network determines global food availability. *Nature food, 4*(6), 508–517. https://doi.org/10.1038/s43016-023-00771-4

Lamb, W.F., Wiedmann, T., Pongratz, J., Andrew, R., Crippa, M., Olivier, J.G., et al. (2021). A review of trends and drivers of greenhouse gas emissions by sector from 1990 to 2018. *Environmental research letters, 16*, 073005. https://doi.org/10.1088/1748-9326/abee4e

Lanzoni, D., Rebucci, R., Formici, G., Cheli, F., Ragone, G., Baldi, A., Violini, L., Sundaram, T. S., & Giromini, C. (2024). Cultured meat in the European Union: Legislative context and food safety issues. *Current research in food science*, *8*, 100722. https://doi.org/10.1016/j.crfs.2024.100722

Latorre, M. E., & Velazquez, D. E. (2021). Effects of thermal treatment on collagen present in bovine M. Semitendinosus intramuscular connective tissue. Analysis of the chemical, thermal and mechanical properties. *Food Structure, 27*, 100165. https://doi.org/10.1016/j.foostr.2020.100165

Lawton, J. W. (2006) Isolation of Zein using 100% Ethanol. *Cereal Chemistry, 83*(5), 565-568. https://doi.org/10.1094/CC-83-0565

Leal Filho, W., Fedoruk, M., Paulino Pires Eustachio, J. H., Barbir, J., Lisovska, T., Lingos, A., & Baars, C. (2023). How the War in Ukraine Affects Food Security. *Foods (Basel, Switzerland), 12*(21), 3996. https://doi.org/10.3390/foods12213996

Lee, D. K., Kim, M., Jeong, J., Lee, Y. S., Yoon, J. W., An, M. J., Jung, H. Y., Kim, C. H., Ahn, Y., Choi, K. H., Jo, C., & Lee, C. K. (2023). Unlocking the potential of stem cells: Their crucial role in the production of cultivated meat. *Current research in food science, 7,* 100551. https://doi.org/10.1016/j.crfs.2023.100551

Lee, H. G., Jang, M. J., Park, B. D., & Um, I. C. (2023c). Structural Characteristics and Properties of Redissolved Silk Sericin. Polymers, 15(16), 3405. https://doi.org/10.3390/polym15163405

Lee, J. K., Link, J. M., Hu, J. C. Y., & Athanasiou, K. A. (2017). The Self-Assembling Process and Applications in Tissue Engineering. *Cold Spring Harbor perspectives in medicine*, *7*(11), a025668. https://doi.org/10.1101/cshperspect.a025668

Lee, J., Song, H., Seo, K. -H., Lee, H. -G., Kim, H., Choi, M. -J. (2023b). Physicochemical and sensory properties of plant-based meat patties using oil-in-water emulsion. *Food Bioscience, 56*, 103084. https://doi.org/10.1016/j.fbio.2023.103084

Lee, K. Y., Jeong, L., Kang, Y. O., Lee, S. J., & Park, W. H. (2009). Electrospinning of polysaccharides for regenerative medicine. *Advanced drug delivery reviews, 61*(12), 1020–1032. https://doi.org/10.1016/j.addr.2009.07.006

Lee, K. Y., Loh, H. X., & Wan, A. C. A. (2022). Systems for Muscle Cell Differentiation: From Bioengineering to Future Food. *Micromachines, 13*(1), 71. https://doi.org/10.3390/mi13010071

Lee, M., Choi, W., Lee, J. M., Lee, S. T., Koh, W. G., & Hong, J. (2024). Flavor-switchable scaffold for cultured meat with enhanced aromatic properties. *Nature communications*, *15*(1), 5450. https://doi.org/10.1038/s41467-024-49521-5

Lee, M., Park, S., Choi, B., Choi, W., Lee, H., Lee, J. M., Lee, S. T., Yoo, K. H., Han, D., Bang, G., Hwang, H., Koh, W. G., Lee, S., & Hong, J. (2024b). Cultured meat with enriched organoleptic properties by

regulating cell differentiation. *Nature communications, 15*(1), 77. https://doi.org/10.1038/s41467-023-44359-9

Lee, N. M., Erisken, C., Iskratsch, T., Sheetz, M., Levine, W. N., & Lu, H. H. (2017b). Polymer fiber-based models of connective tissue repair and healing. *Biomaterials, 112*, 303–312. https://doi.org/10.1016/j.biomaterials.2016.10.013

Lee, S. -H., & Choi, J. (2024). Three-dimensional scaffolds, materials, and fabrication for cultured meat applications: A scoping review and future direction. *Food Hydrocolloids, 152*, 109881. https://doi.org/10.1016/j.foodhyd.2024.109881

Lee, S., Kim, S. H., Jo, Y. Y., Ju, W. T., Kim, H. B., & Kweon, H. (2021). Effects of Ultraviolet Light Irradiation on Silk Fibroin Films Prepared under Different Conditions. *Biomolecules, 11*(1), 70. https://doi.org/10.3390/biom11010070

Lefèvre, T., Rousseau, M. E., & Pézolet, M. (2007). Protein secondary structure and orientation in silk as revealed by Raman spectromicroscopy. *Biophysical journal*, *92*(8), 2885–2895. https://doi.org/10.1529/biophysj.106.100339

Lenzuni, M., Fiorentini, F., Summa, M., Bertorelli, R., Suarato, G., Perotto, G., & Athanassiou, A. (2024). Electrosprayed zein nanoparticles as antibacterial and anti-thrombotic coatings for ureteral stents. *International Journal of Biological Macromolecules*, *257*, 128560. https://doi.org/10.1016/J.IJBIOMAC.2023.128560

Levi, S., Yen, F. -C., Baruch, L., & Machluf, M. (2022). Scaffolding technologies for the engineering of cultivated meats: towards a safe, sustainable, and scalable production. *Trends in Food Science and Technology, 126*, 13-25. https://doi.org/10.1016/j.tifs.2022.05.011

Li, B., Ma, Y., Wang, S., & Moran, P. M. (2005). Influence of carboxyl group density on neuron cell attachment and differentiation behavior: gradient-guided neurite outgrowth. *Biomaterials*, *26*(24), 4956–4963. https://doi.org/10.1016/j.biomaterials.2005.01.018

Li, C., Teng, X., Peng, H., Yi, X., Zhuang, Y., Zhang, S., & Xia, J. (2020). Novel scale-up strategy based on three-dimensional shear space for animal cell culture. *Chemical Engineering Science, 212*, 115329. https://doi.org/10.1016/j.ces.2019.115329

Li, G., Liu, H., Li, T. D., & Wang, J. (2012a). Surface modification and functionalization of silk fibroin fibers/fabric toward high performance applications. *Material Science and Engineering: C, 32*(4), 627-636. https://doi.org/10.1016/j.msec.2011.12.013

Li, L., Chen, L., Chen, X., Chen, Y., Ding, S., Fan, X., Liu, Y., Xu, X., Zhou, G., Zhu, B., Ullah, N., & Feng, X. (2022). Chitosan-sodium alginate-collagen/gelatin three-dimensional edible scaffolds for building a structured model for cell cultured meat. *International journal of biological macromolecules*, *209*(Pt A), 668–679. https://doi.org/10.1016/j.ijbiomac.2022.04.052

Li, M., Tian, W., Yu, Y., Zhang, Y., Zhang, B., Xu, & Wang, J. (2023). Effect of degumming degree on the structure and tensile properties of RSF/RSS composite films prepared by one-step extraction. *Scientific Reports*, *13*, 6689. https://doi.org/10.1038/s41598-023-33844-2

Li, M., Zhang, D., Hou, Y., Jiao, L., Zheng, X., & Wang, W. H. (2003). Isolation and culture of embryonic stem cells from porcine blastocysts. *Molecular reproduction and development, 65*(4), 429–434. https://doi.org/10.1002/mrd.10301

Li, W., Han, Y., Yang, H., Wang, G., Lan, R., & Wang, J. Y. (2016). Preparation of microcarriers based on zein and their application in cell culture. *Materials science & engineering. C, Materials for biological applications*, *58*, 863–869. https://doi.org/10.1016/j.msec.2015.09.045

Li, Y., Li, J., Xia, Q., Zhang, B., Wang, Q., & Huang, Q. (2012b). Understanding the dissolution of α-zein in aqueous ethanol and acetic acid solutions. The journal of physical chemistry. B, 116(39), 12057–12064. https://doi.org/10.1021/jp305709y

Linnes, M. P., Ratner, B. D., & Giachelli, C. M. (2007). A fibrinogen-based precision microporous scaffold for tissue engineering. *Biomaterials*, *28*(35), 5298–5306. https://doi.org/10.1016/j.biomaterials.2007.08.020

Listrat, A., Lebret, B., Louveau, I., Astruc, T., Bonnet, M., Lefaucheur, L., Picard, B., & Bugeon, J. (2016). How Muscle Structure and Composition Influence Meat and Flesh Quality. *The Scientific World Journal, 2016*(1), 3182746. https://doi.org/10.1155/2016/3182746

Liu, J., Shim, Y. Y., Tse, T. J., Wang, Y., & Reaney, M. J. T. (2018). Flaxseed gum a versatile natural hydrocolloid for food and non-food applications, *Trends in Food Science & Technology, 75*, 146-157. https://doi.org/10.1016/j.tifs.2018.01.011

Liu, L., Xu, W., Ding, Y., Agarwal, S., Greiner, A., Duan, G. (2020). A review of smart electrospun fibers toward textiles. *Composites Communications, 22*, 100506. https://doi.org/10.1016/j.coco.2020.100506

Liu, S. L., Huang, Y. Y., Zhang, H. D., Sun, B., Zhang, J. C., & Long, Y. Z. (2014). Needleless electrospinning for large scale production of ultrathin polymer fibres. *Materials Research Innovations, 18(*sup4), S4-833-S4-837. https://doi.org/10.1179/1432891714Z.000000000802

Liu, S., Liu, H., Meng, Y., Li, Q., & Wang, L. (2022). Review of carbon emission and carbon neutrality in the life cycle of silk products. *Fibres and Textiles in Eastern Europe*, *151*(2), 1-7. https://doi.org/10.2478/ftee-2022-0001

Liu, X., Huang, Q., Pan, P., Fang, M., Zhang, Y., Yang, S., Li, M., & Liu, Y. (2023). Comparative Study of the Preparation of High-Molecular-Weight Fibroin by Degumming Silk with Several Neutral Proteases. *Polymers, 15*(16), 3383. https://doi.org/10.3390/polym15163383

Liu, X., Xia, Q., Zhou, J., Zhang, Y., Ju, H., & Deng, Z. (2022). Chemical Modification of Silk Fibroin through Serine Amino Acid Residues. *Materials (Basel, Switzerland), 15*(13), 4399. https://doi.org/10.3390/ma15134399

Liu, Y., He, J. -H., & Yu, J. -Y. (2008) Bubble-electrospinning: a novel method for making nanofibres. *Journal of Physics: Conference Series, 96*, 012001. https://doi.org/10.1088/1742-6596/96/1/012001

Lloyd, S. S., Dawkins, S. T., & Dawkins, R. L. (2014). A novel method of measuring the melting point of animal fats. *Journal of animal science, 92*(10), 4775–4778. https://doi.org/10.2527/jas.2014-7981

Lob, J., & Rochette, J. -M. (1982). *Le Transperceneige*. Casterman.

Low, J. T., Yusoff, N. I. S. M., Othman, N., Wong, T. W., & Wahit, M. U. (2022). Silk fibroin-based films in food packaging applications: A review. *Comprehensive reviews in food science and food safety*, *21*(3), 2253–2273. https://doi.org/10.1111/1541-4337.12939

Loyon L. (2017). Overview of manure treatment in France. *Waste management (New York, N.Y.)*, *61*, 516–520. https://doi.org/10.1016/j.wasman.2016.11.040

Lu, H., Liu, Y., Guo, J., Wu, H., Wang, J., & Wu, G. (2016). Biomaterials with Antibacterial and Osteoinductive Properties to Repair Infected Bone Defects. *International Journal of Molecular Sciences, 17*(3), 334. https://doi.org/10.3390/ijms17030334

Lu, Q., Hu, X., Wang, X., Kluge, J. A., Lu, S., Cebe, P., & Kaplan, D. L. (2010). Water-insoluble silk films with silk I structure. *Acta biomaterialia, 6*(4), 1380–1387. https://doi.org/10.1016/j.actbio.2009.10.041

Luo, C. J., Stoyanov, S. D., Stride, E., Pelan, E., & Edirisinghe, M. (2012). Electrospinning versus fibre production methods: from specifics to technological convergence. *Chemical Society reviews*, *41*(13), 4708–4735. https://doi.org/10.1039/c2cs35083a

Luu, T., Gristwood, K., Knight, J. C., & Jörg, M. (2024). Click Chemistry: Reaction Rates and Their Suitability for Biomedical Applications. Bioconjugate chemistry, 35(6), 715–731. https://doi.org/10.1021/acs.bioconjchem.4c00084

Luzak, B., Siarkiewicz, P., & Boncler, M. (2022). An evaluation of a new high-sensitivity PrestoBlue assay for measuring cell viability and drug cytotoxicity using EA.hy926 endothelial cells. Toxicology in vitro : an international journal published in association with BIBRA, 83, 105407. https://doi.org/10.1016/j.tiv.2022.105407

Lv, H., Li, L., Sun, M., Zhang, Y., Chen, L., Rong, Y., & Li, Y. (2015). Mechanism of regulation of stem cell differentiation by matrix stiffness. *Stem cell research & therapy, 6*(1), 103. https://doi.org/10.1186/s13287-015-0083-4

Lynch, J., & Pierrehumbert, R. (2019) Climate Impacts of Cultured Meat and Beef Cattle. *Frontiers in Sustainable Food Systems, 3*(5), 1-11. https://doi.org/10.3389/fsufs.2019.00005

Lynch, J., & Pierrehumbert, R. (2019). Climate impacts of cultured meat and beef cattle. *Frontiers in sustainable food systems*, *3*, 5. https://doi.org/10.3389/fsufs.2019.00005

Lyu, S., Huang, C., Yang, H., & Zhang, X. (2013). Electrospun fibers as a scaffolding platform for bone tissue repair. *Journal of orthopaedic research : official publication of the Orthopaedic Research Society*, *31*(9), 1382–1389. https://doi.org/10.1002/jor.22367

Ma, L., Dong, W., Lai, E., & Wang, J. (2024). Silk fibroin-based scaffolds for tissue engineering. *Frontiers in bioengineering and biotechnology*, *12*, 1381838. https://doi.org/10.3389/fbioe.2024.1381838

Ma, T., Ren, R., Lv, J., Yang, R., Zheng, X., Hu, Y., Zhu, G., & Wang, H. (2024). Transdifferentiation of fibroblasts into muscle cells to constitute cultured meat with tunable intramuscular fat deposition. *eLife, 13*, RP93220. https://doi.org/10.7554/eLife.93220

MacQueen, L.A., Alver, C.G., Chantre, C.O. Ahn, S., Cera, L., Gonzalez, G. M., O'Connor, B. B., Drennan, D. J., Peters, M. M., Motta, S. E., Zimmerman, J. F., & Parker, K. K. (2019). Muscle tissue engineering in fibrous gelatin: implications for meat analogs. *npj Science of Food 3*, 20. https://doi.org/10.1038/s41538-019-0054-8

Majumder, R., Miatur, S., Saha, A., & Hossain, S. (2024). Mycoprotein: production and nutritional aspects: a review. *Sustainable Food Technology, 2*, 81-89. https://doi.org/10.1039/d3fb00169e

Maki, K. C., Dicklin, M. R., & Kirkpatrick, C. F. (2021). Saturated fats and cardiovascular health: Current evidence and controversies. *Journal of clinical lipidology, 15*(6), 765–772. https://doi.org/10.1016/j.jacl.2021.09.049

Malerich, M., & Bryant, C. (2022). Nomenclature of cell-cultivated meat & seafood products. *NPJ science of food*, *6*(1), 56. https://doi.org/10.1038/s41538-022-00172-0

Manek, R. V., Builders, P. F., Kolling, W. M., Emeje, M., & Kunle, O. O. (2012). Physicochemical and binder properties of starch obtained from Cyperus esculentus. *AAPS PharmSciTech, 13*(2), 379–388. https://doi.org/10.1208/s12249-012-9761-z

Maran, B. A. V., Jeyachandran, S., & Kimura, M. (2024). A Review on the Electrospinning of Polymer Nanofibres and Its Biomedical Applications. *Journal of Composite Science, 8*(1), 32. https://doi.org/10.3390/jcs8010032

Marelli, B., Brenckle, M. A., Kaplan, D. L., & Omenetto, F. G. (2016). Silk Fibroin as Edible Coating for Perishable Food Preservation. *Scientific reports, 6*, 25263. https://doi.org/10.1038/srep25263

Marga, F., Forgacs, G., Purcell, B. P., & Forgacs, A. (2015). *Edible and animal-product free microcarriers for engineered meat* (Patent No. WO2015038988). World Intellectual Property Organisation. https://patentscope.wipo.int/search/en/detail.jsf?docId=WO2015038988

Marris, C. (2001). Public views on GMOs: deconstructing the myths. Stakeholders in the GMO debate often describe public opinion as irrational. But do they really understand the public?. *EMBO reports, 2*(7), 545–548. https://doi.org/10.1093/embo-reports/kve142

Martin, M. J., Thottathil, S. E., & Newman, T. B. (2015). Antibiotics Overuse in Animal Agriculture: A Call to Action for Health Care Providers. *American Journal of Public Health, 105*(12), 2409–2410. https://doi.org/10.2105/AJPH.2015.302870

Maryskova, M., Rysova, M., Novotny, V., & Sevcu, A. (2019). Polyamide-Laccase Nanofibre Membrane for Degradation of Endocrine-Disrupting Bisphenol A, 17α-ethinylestradiol, and Triclosan. *Polymers*, *11*(10), 1560. https://doi.org/10.3390/polym11101560

Masri, F., Hoeve, M., de Sousa, P., & Willoughby, N. (2017). Challenges and advances in scale-up of label-free downstream processing for allogeneic cell therapies. *Cell Gene Therapy Insight, 3*(6), 447-467. https://doi.org/10.18609/cgti.2017.041

Mattick, C. S., Landis, A. E., Allenby, B. R., & Genovese, N. J. (2015). Anticipatory Life Cycle Analysis of In Vitro Biomass Cultivation for Cultured Meat Production in the United States. *Environmental science & technology*, *49*(19), 11941–11949. https://doi.org/10.1021/acs.est.5b01614

McBeath, R., Pirone, D. M., Nelson, C. M., Bhadriraju, K., & Chen, C. S. (2004). Cell Shape, Cytoskeletal Tension, and RhoA Regulate Stem Cell Lineage Commitment. *Developmental Cell, 6*(4), 483-495. https://doi.org/10.1016/S1534-5807(04)00075-9

McManus, M. C., Boland, E. D., Koo, H. P., Barnes, C. P., Pawlowski, K. J., Wnek, G. E., Simpson, D. G. & Bowlin, G. L. (2006). Mechanical properties of electrospun fibrinogen structures. *Acta biomaterialia, 2*(1), 19–28. https://doi.org/10.1016/j.actbio.2005.09.008

McNamara, E., & Bomkamp, C. (2022). Cultivated meat as a tool for fighting antimicrobial resistance. *Nature food*, *3*(10), 791–794. https://doi.org/10.1038/s43016-022-00602-y

Melzener, L., Spaans, S., Hauck, N., Pötgens, A. J. G., Flack, J. E., Post, M. J., & Doğan, A. (2023). Short-Stranded Zein Fibers for Muscle Tissue Engineering in Alginate-Based Composite Hydrogels. *Gels (Basel, Switzerland)*, *9*(11), 914. https://doi.org/10.3390/gels9110914

Melzener, L., Spaans, S., Hauck, N., Pötgens, A. J. G., Flack, J. E., Post, M. J., & Doğan, A. (2023). Short-Stranded Zein Fibers for Muscle Tissue Engineering in Alginate-Based Composite Hydrogels. *Gels (Basel, Switzerland)*, *9*(11), 914. https://doi.org/10.3390/gels9110914

Mensah, D. O., Mintah, F. O., Oteng, S. A., Lillywhite, R., & Oyebode, O. (2022). 'We're meat, so we need to eat meat to be who we are': Understanding motivations that increase or reduce meat consumption among emerging adults in the University of Ghana food environment. *Meat Science, 193*, 108927. https://doi.org/10.1016/j.meatsci.2022.108927

Metreveli, N. O., Jariashvili, K. K., Namicheishvili, L. O., Svintradze, D. V., Chikvaidze, E. N., Sionkowska, A., & Skopinska, J. (2010). UV-vis and FT-IR spectra of ultraviolet irradiated collagen in the presence of antioxidant ascorbic acid. *Ecotoxicology and environmental safety*, *73*(3), 448–455. https://doi.org/10.1016/j.ecoenv.2009.12.005

Miguel, E., Grosbois, V., Caron, A., Pople, D., Roche, B., & Donnelly, C. A. (2020). A systemic approach to assess the potential and risks of wildlife culling for infectious disease control. *Communications biology, 3*(1), 353. https://doi.org/10.1038/s42003-020-1032-z

Milleret, V., Hefti, T., Hall, H., Vogel, V., & Eberli, D. (2012). Influence of the fiber diameter and surface roughness of electrospun vascular grafts on blood activation. *Acta biomaterialia*, *8*(12), 4349–4356. https://doi.org/10.1016/j.actbio.2012.07.032

Milman, O. (2023, June 21). *USDA allows lab-grown meat to be sold to US consumers*. The Guardian. https://www.theguardian.com/us-news/2023/jun/21/us-lab-grown-meat-sold-public

Min, S., Byeon, Y., Kim, M., Lee, Y., Lee, S.-H., Lee, Y., Farooqi, H.M.U., Lee, H.-K., & Paeng, D.-G. (2022). Production enhancement of human adipose-derived mesenchymal stem cells by low-intensity ultrasound stimulation. *Sci Rep 12*, 22041. https://doi.org/10.1038/s41598-022-24742-0

Mitić, R., Cantoni, F., Börlin, C. S., Post, M. J., & Jackisch, L. (2022). A simplified and defined serum-free medium for cultivating fat across species. *iScience*, *26*(1), 105822. https://doi.org/10.1016/j.isci.2022.105822

Mohammadinejad, R., Kumar, A., Ranjbar-Mohammadi, M., Ashrafizadeh, M., Han, S. S., Khang, G., & Roveimiab, Z. (2020). Recent Advances in Natural Gum-Based Biomaterials for Tissue Engineering and Regenerative Medicine: A Review. *Polymers, 12*(1), 176. https://doi.org/10.3390/polym12010176

Mohammadzadehmoghadam, S., & Dong, Y. (2019). Fabrication and characterization of electrospun silk fibroin/gelatin scaffolds crosslinked with glutaraldehyde vapor. *Frontier Materials. 6*, 91. https://doi.org/10.3389/fmats.2019.00091

Moiraghi, M., Sciarini, L. S., Paesani, C., León, A. E., & Pérez, G. T. (2019). Flour and starch characteristics of soft wheat cultivars and their effect on cookie quality. *Journal of food science and technology, 56*(10), 4474–4481. https://doi.org/10.1007/s13197-019-03954-9

Molina, E. M. I., Malollari, K. G., & Komvopoulos, K. (2021). Design Challenges in Polymeric Scaffolds for Tissue Engineering. *Frontiers in Bioengineering and Biotechnology, 9*, 617141. https://doi.org/10.3389/fbioe.2021.617141

Moon, S., Gil, M., & Lee, K. (2017). Syringeless Electrospinning toward Versatile Fabrication of Nanofibre Web. *Scientific Reports, 7*, 41424. https://doi.org/10.1038/srep41424

Morwood, A. J., El-Karim, I. A., Clarke, S. A., & Lundy, F. T. (2023). The Role of Extracellular Matrix (ECM) Adhesion Motifs in Functionalised Hydrogels. *Molecules (Basel, Switzerland)*, *28*(12), 4616. https://doi.org/10.3390/molecules28124616

Mosa Meat. (2019, November 15). *Growth Medium without Fetal Bovine Serum (FBS).* Mosa Meat. https://mosameat.com/blog/growth-medium-without-fetal-bovine-serum-fbs

Mottaghitalab, F., Farokhi, M., Shokrgozar, M.A., Atyabi, F., & Hosseinkhani, H. (2015). Silk fibroin nanoparticle as a novel drug delivery system. *J. Control. Release 206*, 161–176. https://doi.org/10.1016/j.jconrel.2015.03.020

Moutsatsou, P., Cameron, P., Dagès, B., Nienow, A. W., Lye, G., Theodosiou, E., & Hanga, M. P. (2023). Scaling cell production sustainably in cultured meat product development. In M. Post, C. Connon & C. Bryant (Eds.), *Advances in cultured meat technology* (1st ed., pp261-296). Burleigh Dodds Science Publishing. https://doi.org/10.19103/AS.2023.0130.11

Mridul, A. (2024, September 17). *Aleph farms to launch cultivated beef with Miznon chef Eyal Shani*. Green Queen. https://www.greenqueen.com.hk/aleph-farms-miznon-chef-eyal-shani-lab-grown-meat-cultivated-cuts/

Murphy, C. M., Haugh, M. G., & O'Brien, F. J. (2010). The effect of mean pore size on cell attachment, proliferation and migration in collagen-glycosaminoglycan scaffolds for bone tissue engineering. *Biomaterials*, *31*(3), 461–466. https://doi.org/10.1016/j.biomaterials.2009.09.063

Murray, J. M., Delahunty, C. M., Baxter, I. A. (2001). Descriptive sensory analysis: past, present and future. *Food Research International, 34(*6), 461-471. https://doi.org/10.1016/S0963-9969(01)00070-9

Murugan, P., Yap, W. S., Ezhilarasu, H., Suntornnond, R., Le, Q. B., Singh, S., Seah, J. S. H., Tan, P. L., Zhou, W., Tan, L. P., & Choudhury, D. (2024). Decellularised plant scaffolds facilitate porcine skeletal muscle tissue engineering for cultivated meat biomanufacturing. *NPJ science of food*, *8*(1), 25. https://doi.org/10.1038/s41538-024-00262-1

Nakamura, A., Dohi, Y., Akahane, M., Ohgushi, H., Nakajima, H., Funaoka, H., & Takakura, Y. (2009). Osteocalcin secretion as an early marker of in vitro osteogenic differentiation of rat mesenchymal stem cells. *Tissue engineering. Part C, Methods*, *15*(2), 169–180. https://doi.org/10.1089/ten.tec.2007.0334

Narayanan, N., Jiang, C., Wang, C., Uzunalli, G., Whittern, N., Chen, D., Jones, O. G., Kuang, S., & Deng, M. (2020). Harnessing Fiber Diameter-Dependent Effects of Myoblasts Toward Biomimetic Scaffold-Based Skeletal Muscle Regeneration. *Frontiers in bioengineering and biotechnology, 8*, 203. https://doi.org/10.3389/fbioe.2020.00203

Narita, C., Okahisa, Y., Wataoka, I., & Yamada, K. (2020). Characterization of Ground Silk Fibroin through Comparison of Nanofibroin and Higher Order Structures. *ACS omega*, *5*(36), 22786–22792. https://doi.org/10.1021/acsomega.0c01750

Naskar, D., Nayak, S., Dey, T., & Kundu, S. C. (2014). Non-mulberry silk fibroin influence osteogenesis and osteoblast-macrophage cross talk on titanium based surface. *Scientific reports, 4*, 4745. https://doi.org/10.1038/srep04745

Nasrollahzadeh, F., Alexi, N., Skov, K. B., Roman, L., Sfyra, K., & Martinez, M. M. (2024). Texture profiling of muscle meat benchmarks and plant-based analogues: An instrumental and sensory design approach with focus on correlations, *Food Hydrocolloids, 151*, 109829. https://doi.org/10.1016/j.foodhyd.2024.109829

Nekoukar, Z., Zakariaei, Z., Taghizadeh, F., Musavi, F., Banimostafavi, E. S., Sharifpour, A., Ebrahim Ghuchi, N., Fakhar, M., Tabaripour, R., & Safanavaei, S. (2021). Methanol poisoning as a new world challenge: A review. *Annals of medicine and surgery (2012)*, *66*, 102445. https://doi.org/10.1016/j.amsu.2021.102445

Nezarati, R. M., Eifert, M. B., & Cosgriff-Hernandez, E. (2013). Effects of humidity and solution viscosity on electrospun fiber morphology. Tissue engineering. Part C, *Methods, 19*(10), 810–819. https://doi.org/10.1089/ten.TEC.2012.0671

Nguyen, T. P., Nguyen, Q. V., Nguyen, V. H., Le, T. H., Huynh, V., Vo, D. N., Trinh, Q. T., Kim, S. Y., & Le, Q. V. (2019). Silk Fibroin-Based Biomaterials for Biomedical Applications: A Review. *Polymers, 11*(12), 1933. https://doi.org/10.3390/polym11121933

Nieminen, H. J., Laidmäe, I., Salmi, A., Rauhala, T., Paulin, T., Heinämäki, J., & Hæggström, E. (2018). Ultrasound-enhanced electrospinning. *Scientific reports, 8*(1), 4437. https://doi.org/10.1038/s41598-018-22124-z

Nokes, C. (2017). *UK: National Risk Register Of Civil Emergencies, 2017 Edition.* Cabinet Office. https://assets.publishing.service.gov.uk/government/uploads/system/uploads/attachment_data/file/644968/UK_National_Risk_Register_2017.pdf

Nolan, J., & Joy, L. (Executive Producers). (2016-2022). *Westworld* [TV series]. HBO entertainment; Kilter Films; Bad Robot; Warner Bros. Television.

Nollkaemper, A. (2023). International Law and the Agony of Animals in Industrial Meat Production. *European Journal of International Law, 34*(4), 939-972. https://doi.org/10.1093/ejil/chad049

Nonthanum, P., Lee, Y., & Padua, G. W. (2013). Effect of pH and ethanol content of solvent rheology of zein solutions. *Journal of Cereal Science*, *58*(1), 76-81. https://doi.org/10.1016/j.jcs.2013.04.001

Norris, S. C. P., Kawecki, N. S., Davis, A. R., Chen, K. K., & Rowat, A. C. (2022). Emulsion-templated microparticles with tunable stiffness and topology: Applications as edible microcarriers for cultured meat. *Biomaterials*, *287*, 121669. https://doi.org/10.1016/j.biomaterials.2022.121669

Nowell, C. (2024, April 9). *'Political efforts': the Republican states trying to ban lab-grown meat*. The Guardian. https://www.theguardian.com/environment/2024/apr/09/us-states-republicans-banning-lab-grown-meat

Nunes-Pereira, J., Ribeiro, S., Ribeiro, C., Gombek, C. J., Gama, F. M., Gomes, A. C., Patterson, D., & Lanceros-Méndez, S. (2015). Poly(vinylidene fluoride) and copolymers as porous membranes for

tissue engineering applications. *Polymer Testing, 44*, 234-241. https://doi.org/10.1016/j.polymertesting.2015.05.001

Nurul Alam, A. M. M., Kim, C. J., Kim, S. H., Kumari, S., Lee, E. Y., Hwang, Y. H., & Joo, S. T. (2024b). Scaffolding fundamentals and recent advances in sustainable scaffolding techniques for cultured meat development. *Food research international (Ottawa, Ont.)*, *189*, 114549. https://doi.org/10.1016/j.foodres.2024.114549

Nurul Alam, A. N., Kim, C. J., Kim, S. H., Kumari, S., Lee, S. Y., Hwang, Y. H., & Joo, S. T. (2024). Trends in Hybrid Cultured Meat Manufacturing Technology to Improve Sensory Characteristics. *Food science of animal resources*, *44*(1), 39–50. https://doi.org/10.5851/kosfa.2023.e76

OECD., & FAO. (2024). *OECD-FAO Agricultural Outlook 2024-2033.* Organisation for Economic Co-operation and Development and Food and Agriculture Organization of the United Nations. https://doi.org/10.1787/4c5d2cfb-en

Ogawa, M., Kermani, A. S., Huynh, M. J., Baar, K., Leach, J. K., & Block, D. E. (2024). Edible mycelium as proliferation and differentiation support for anchorage-dependent animal cells in cultivated meat production. *NPJ science of food*, *8*(1), 23. https://doi.org/10.1038/s41538-024-00263-0

Okeudo, N. J., & Moss, B. W. (2005). Interrelationships amongst carcass and meat quality characteristics of sheep. *Meat science, 69*(1), 1–8. https://doi.org/10.1016/j.meatsci.2004.04.011

Oliveira, S. M., Alves, N. M., & Mano, J. F. (2012). Cell interactions with superhydrophilic and superhydrophobic surfaces. *Journal of Adhesion Science and Technology*, *28*(8–9), 843–863. https://doi.org/10.1080/01694243.2012.697776

Omer, S., Forgách, L., Zelkó, R., & Sebe, I. (2021). Scale-up of Electrospinning: Market Overview of Products and Devices for Pharmaceutical and Biomedical Purposes. *Pharmaceutics*, *13*(2), 286. https://doi.org/10.3390/pharmaceutics13020286

O'Neill, E. N., Cosenza, Z. A., Baar, K., & Block, D. E. (2021). Considerations for the development of cost-effective cell culture media for cultivated meat production. *Comprehensive reviews in food science and food safety, 20*(1), 686–709. https://doi.org/10.1111/1541-4337.12678

O'Neill, J. (2014). Antimicrobial Resistance: Tackling a crisis for the health and wealth of nations. https://amr-review.org/sites/default/files/AMR%20Review%20Paper%20-%20Tackling%20a%20crisis%20for%20the%20health%20and%20wealth%20of%20nations_1.pdf

Owusu-Ansah, P., Besiwah, E. K., Bonah, E., & Amagloh, F. K. (2022). Non-meat ingredients in meat products: A scoping review. *Applied Food Research, 2*(1), 100044. https://doi.org/10.1016/j.afres.2022.100044

Oxoby, R.J., & Finnigan, H. (2007). Developing heuristic-based quality judgments: Blocking in consumer choice. *Psychology & Marketing, 24*, 295-313. https://doi.org/10.1002/mar.20162

Pakseresht, A., Ahmadi Kaliji, S., & Canavari, M. (2022). Review of factors affecting consumer acceptance of cultured meat. *Appetite, 170*, 105829. https://doi.org/10.1016/j.appet.2021.105829

Pan, C. T., Chien, S. T., Chiang, T. C., Yen, C. K., Wang, S. Y., Wen, Z. H., Yu, C. Y., & Shiue, Y. L. (2020). Optimization of the spherical integrity for sustained-release alginate microcarriers-encapsulated doxorubicin by the Taguchi method. *Scientific reports*, *10*(1), 21758. https://doi.org/10.1038/s41598-020-78813-1

Paredes, J., Cortizo-Lacalle, D., Imaz, A. M., Aldazabal, J., & Vila, M. (2022). Application of texture analysis methods for the characterization of cultured meat. *Scientific Reports, 12*, 3898. https://doi.org/10.1038/s41598-022-07785-1

Park, J.S., Chu, J.S., Tsou, A.D., Diop, R., Tang, Z., Wang, A., & Li, S. (2011). The effect of matrix stiffness on the differentiation of mesenchymal stem cells in response to TGF-β. *Biomaterials 32*(16), 3921–3930. https://doi.org/10.1016/j.biomaterials.2011.02.019

Parry, D. (2013). [Photograph]. David Parry Photography. https://www.davidparryphotography.com/blog/2013/8/6/look-moos-on-the-front-page.html

Partheniadis, I., Nikolakakis, I., Laidmäe, I., & Heinämäki, J. (2020). A Mini-Review: Needleless Electrospinning of Nanofibres for Pharmaceutical and Biomedical Applications. *Processes, 8*(6), 673. https://doi.org/10.3390/pr8060673

Pasitka, L., Cohen, M., Ehrlich, A., Gildor, B., Reuveni, E., Ayyash, M., Wissotsky, G., Herscovici, A., Kaminker, R., Niv, A., Bitcover, R., Dadia, O., Rudik, A., Voloschin, A., Shimoni, M., Cinnamon, Y., & Nahmias, Y. (2023). Spontaneous immortalization of chicken fibroblasts generates stable, high-yield cell lines for serum-free production of cultured meat. *Nature food, 4*(1), 35–50. https://doi.org/10.1038/s43016-022-00658-w

Penna Franca, P. A., Duque-Esrada, P., da Fonseca e Sá, B. F., van der Groot, A. J., & Trindale Rocha Pieruchi, A. P. (2022). Meat substitutes - past, present, and future of products available in Brazil: changes in the nutritional profile. *Future Foods, 5*, 100133. https://doi.org/10.1016/j.fufo.2022.100133

Pérez-Guzmán, C. J., & Castro-Muñoz, R. (2020). A Review of Zein as a Potential Biopolymer for Tissue Engineering and Nanotechnological Applications. *Processes, 8*(11), 1376.

Perez-Puyana, V. M., Romero, A., Guerrero, A., Moroni, L., & Wieringa, P. A. (2025). Enabling low molecular weight electrospinning through binary solutions of polymer blends. *Next Materials, 6,* 100306. https://doi.org/10.1016/j.nxmate.2024.100306

Perez-Puyana, V., Wieringa, P., Yuste, Y., de la Portilla, F., Guererro, A., Romero, A., & Moroni, L. (2021). Fabrication of hybrid scaffolds obtained from combinations of PCL with gelatin or collagen via electrospinning for skeletal muscle tissue engineering. *Journal of biomedical materials research. Part A*, *109*(9), 1600–1612. https://doi.org/10.1002/jbm.a.37156

Petersen, B. (2018). Transgenic pigs to the rescue. *eLife, 7*, e37641. https://doi.org/10.7554/eLife.37641

Pharmco. (2018). *Food Grade Statement*. Pharmco by GreenField Global. https://greenfield.com/wp-content/uploads/2018/11/Food-Grade-Statement-Methanol.pdf

Phelan, M. A., Kruczek, K., Wilson, J. H., Brooks, M. J., Drinnan, C. T., Regent, F., Gerstenhaber, J. A., Swaroop, A., Lelkes, P. I., & Li, T. (2020). Soy Protein Nanofibre Scaffolds for Uniform Maturation of Human Induced Pluripotent Stem Cell-Derived Retinal Pigment Epithelium. *Tissue engineering. Part C, Methods*, *26*(8), 433–446. https://doi.org/10.1089/ten.TEC.2020.0072

Plath, A. M. S., Facchi, S. P., Souza, R. M., Sabino, R. M., Corradini, E., Muniz, E. C., Popat, K. C., Filho, L. C., Kipper, M. J., & Martins, A. F. (2021). Zein supports scaffolding capacity toward mammalian cells and bactericidal and antiadhesive properties on poly(ε-caprolactone)/zein electrospun fibers. *Materialstoday CHEMISTRY, 20*, 100465. https://doi.org/10.1016/j.mtchem.2021.100465

Podgórski, R., Wojasiński, M. & Ciach, T. (2022). Nanofibrous materials affect the reaction of cytotoxicity assays. *Scientific Reports, 12*, 9047. https://doi.org/10.1038/s41598-022-13002-w

Pohl, F., & Kornbluth, C. M. (1952). *Space Merchants.* Ballantyne Books.

Pokorny, P., Kostakova, E., Sanetrnik, F., Mikes, P., Chvojka, J., Kalous, T., Bilek, M., Pejchar, K., Valtera, J., & Lukas, D. (2014). Effective AC needleless and collectorless electrospinning for yarn production. *Physical Chemistry Chemical Physics, 16,* 26816-26822. https://doi.org/10.1039/c4cp04346d

Polachini, T.C., Morales, S. A. V., Filho, L. R. P., Ribeiro, E. F., Saraiva, L. S., & Basso, R. C. (2023). Physical Properties and Molecular Interactions Applied to Food Processing and Formulation. *Processes, 11*(7), 2181. https://doi.org/10.3390/pr11072181

Polakova, D., Capek, L., Bartos, M., Kejzlar, P., Rysova, M., Martinova, L., & Sevcu, A. (2022). The stiffness variability of a silk fibroin scaffold during bone cell proliferation. *Proceedings of the Institution of Mechanical Engineers. Part H, Journal of engineering in medicine*, 9544119211070345. Advance online publication. https://doi.org/10.1177/09544119211070345

Politi, S., Carotenuto, F., Rinaldi, A., Di Nardo, P., Manzari, V., Albertini, M. C., Araneo, R., Ramakrishna, S., & Teodori, L. (2020). Smart ECM-Based Electrospun Biomaterials for Skeletal Muscle Regeneration. *Nanomaterials (Basel, Switzerland)*, *10*(9), 1781. https://doi.org/10.3390/nano10091781

Porras Hernández, A. M., Pohlit, H., Sjögren, F., Shi, L., Ossipov, D., Antfolk, M., & Tenje, M. (2020). A simplified approach to control cell adherence on biologically derived in vitro cell culture scaffolds by direct UV-mediated RGD linkage. *Journal of Material Science: Materials in Medicine, 31,* 89. https://doi.org/10.1007/s10856-020-06446-x

Post M. J. (2014). An alternative animal protein source: cultured beef. *Annals of the New York Academy of Sciences*, *1328*, 29–33. https://doi.org/10.1111/nyas.12569

Post, M.J., Levenberg, S., Kaplan, D.L., Genovese, N., Fu, J., Bryant, C. J., Negoweti, N., Verzijden, K., & Moutsatsou, P. (2020). Scientific, sustainability and regulatory challenges of cultured meat. *Nature Food, 1*, 403–415. https://doi.org/10.1038/s43016-020-0112-z

Puerta, M., Arango, M. C., Jaramillo-Quiceno, N., Alvarez-Lopez, C., & Restrepo-Osorio, A. (2019). Influence of ethanol post-treatments on the properties of silk protein materials. *SN Appl. Sci. 1*, 1443 https://doi.org/10.1007/s42452-019-1486-0

Puerta, M., Peresin, M. S., & Restrepo-Osorio, A. (2020). Effects of Chemical Post-treatments on Structural and Physicochemical Properties of Silk Fibroin Films Obtained From Silk Fibrous Waste. *Frontiers in bioengineering and biotechnology, 8*, 523949. https://doi.org/10.3389/fbioe.2020.523949

Qu, J., Wang, L., Niu, L., Lin, J., Huang, Q., Jiang, X., & Li, M. (2018). Porous Silk Fibroin Microspheres Sustainably Releasing Bioactive Basic Fibroblast Growth Factor. *Materials (Basel, Switzerland), 11*(8), 1280. https://doi.org/10.3390/ma11081280

Quorn. (n.d.). Quorn Meat-Free Quarter Pounder Burger [Photograph]. Quorn. https://www.quorn.co.uk/recipes/vegetarian-quarter-pounder

Rafiq, Q. A., Ruck, S., Hanga, M. P., Heathman, T. R. J., Coopman, K., Nienow, A. W., Williams, D. J., Hewitt, C. J. (2018). Qualitative and quantitative demonstration of bead-to-bead transfer with bone

marrow-derived human mesenchymal stem cells on microcarriers: Utilising the phenomenon to improve culture performance. *Biochemical Engineering Journal, 135*, 11-21. https://doi.org/10.1016/j.bej.2017.11.005

Rahman, M., Dip, T. M., Haase, T., Truong, Y. B., Le, T. C., & Houshyar, S. (2023). Fabrication of Zein-Based Fibrous Scaffolds for Biomedical Applications—A Review. *Macromolecular Materials and Engineering, 308*(*12*), 2300175. https://doi.org/10.1002/mame.202300175

Rahmati, M., Mills, D. K., Urbanska, A. M., Saeb, M. R., Venugopal, J. R., Ramakrishna, S., & Mozafari, M. (2021). Electrospinning for tissue engineering applications. *Progress in Materials Science, 117*, 100721. https://doi.org/10.1016/j.pmatsci.2020.100721

Raman, N., Imran, S. A. M., Ahmad Amin Noordin, K. B., Zaman, W. S. W. K., & Nordin, F. (2022). Mechanotransduction in Mesenchymal Stem Cells (MSCs) Differentiation: A Review. *International journal of molecular sciences*, *23*(9), 4580. https://doi.org/10.3390/ijms23094580

Rao, K. M., Kim, H. J., Won, S., Choi, S. M., & Han, S. S. (2023). Effect of Grape Seed Extract on Gelatin-Based Edible 3D-Hydrogels for Cultured Meat Application. *Gels (Basel, Switzerland)*, *9*(1), 65. https://doi.org/10.3390/gels9010065

Rastogi, S., & Kandasubramanian, B. (2020). Processing trends of silk fibers: Silk degumming, regeneration and physical functionalization. *The Journal of The Textile Institute, 111*(12), 1794–1810. https://doi.org/10.1080/00405000.2020.1727269

Reiss, J., Robertson, S., & Suzuki, M. (2021). Cell Sources for Cultivated Meat: Applications and Considerations throughout the Production Workflow. *International journal of molecular sciences, 22*(14), 7513. https://doi.org/10.3390/ijms22147513

Ren, Y. E., Yin, J. Y., & Wang, X. P. (2016). Assessment of silk textiles. *Consume Guide*, *66*(10), 33-35.

Ren, Y., Yakubov, G. E., Linter, B. R., MacNaughtan, W., & Foster, T. J. (2020). Temperature fractionation, physicochemical and rheological analysis of psyllium seed husk heteroxylan. *Food Hydrocolloids*, *104*, 105737. https://doi.org/10.1016/J.FOODHYD.2020.105737

Reynolds, M. (2024, February 2). *You can't buy lab-grown meat even if you wanted to*. Wired. https://www.wired.com/story/upside-foods-good-meat-cultivated-lab-grown-sale-stopped-singapore-california-crenn/

Ritchie, H., Rosado, P., & Roser, M. (2023) *Meat and Dairy Production.* Our World in Data. https://ourworldindata.org/meat-production

Rivaroli, S., Baldi, B., & Spadoni, R. (2020). Consumers' perception of food product craftsmanship: A review of evidence. *Food Quality and Preferenc*e, *79*,103796. https://doi.org/10.1016/j.foodqual.2019.103796

Robinson, A. J., Pérez-Nava, A., Ali, S. C., González-Campos, J. B., Holloway, J. L., & Cosgriff-Hernandez, E. M. (2021). Comparative Analysis of Fiber Alignment Methods in Electrospinning. *Matter*, *4*(3), 821–844. https://doi.org/10.1016/j.matt.2020.12.022

Rogalski, J. J., Bastiaansen, C. W. M., & Peijs, T. (2017). Rotary jet spinning review – a potential high yield future for polymer nanofibres. *Nanocomposites, 3*(4), 97–121. https://doi.org/10.1080/20550324.2017.1393919

Römer, L., & Scheibel, T. (2008). The elaborate structure of spider silk: structure and function of a natural high performance fiber. *Prion*, *2*(4), 154–161. https://doi.org/10.4161/pri.2.4.7490

Roser, M. (2023, September 26). *How many animals get slaughtered every day?*. Our World in Data. https://ourworldindata.org/how-many-animals-get-slaughtered-every-day

Rubio, N. R., Xiang, N., & Kaplan, D. L. (2020). Plant-based and cell-based approaches to meat production. *Nature Communications, 11*(1), 6276. https://doi.org/10.1038/s41467-020-20061-y

Ruggeri, E., Kim, D., Cao, Y., Farè, S., De Nardo, L., & Marelli, B. (2020). A multilayered edible coating to extend product shelf life. *ACS Sustain. Chem. Eng. 8*(38), 14312-14321. https://doi.org/10.1021/acssuschemeng.0c03365

Rzymski, P., Kulus, M., Jankowski, M., Dompe, C., Bryl, R., Petitte, J. N., Kempisty, B., & Mozdziak, P. (2021). COVID-19 Pandemic Is a Call to Search for Alternative Protein Sources as Food and Feed: A Review of Possibilities. *Nutrients*, *13*(1), 150. https://doi.org/10.3390/nu13010150

Sabelli, C. (2023, April 5). *Scientists protest Italy's ban on cultivated meat*. Nature News. https://www.nature.com/articles/d43978-023-00050-7

Sadat, A., Corradini, M. G., & Joye, I. J. (2022). Vibrational and fluorescence spectroscopy to study gluten and zein interactions in complex dough systems. *Current research in food science*, *5*, 479–490. https://doi.org/10.1016/j.crfs.2022.02.009

Safonova, L., Bobrova, M., Efimov, A., Davydova, L., Tenchurin, T., Bogush, V., Agapova, O., & Agapov, I. (2021). Silk Fibroin/Spidroin Electrospun Scaffolds for Full-Thickness Skin Wound Healing in Rats. *Pharmaceutics*, *13*(10), 1704. https://doi.org/10.3390/pharmaceutics13101704

Salehi, G., Díaz, E., & Redondo, R. (2023). Forty-five years of research on vegetarianism and veganism: A systematic and comprehensive literature review of quantitative studies. *Heliyon, 9*(5), e16091. https://doi.org/10.1016/j.heliyon.2023.e16091

Saltik Çirkin, D., & Yüksek, M. (2021). Fibroin nanofibres production by electrospinning method. *Turkish journal of chemistry, 45*(4), 1279–1298. https://doi.org/10.3906/kim-2011-36

Sameen, D. E., Ahmed, S., Lu, R., Li, R., Dai, J., Qin, W., Zhang, Q., Li, S., & Liu, Y. (2022). Electrospun nanofibres food packaging: trends and applications in food systems. *Critical reviews in food science and nutrition*, *62*(22), 6238–6251. https://doi.org/10.1080/10408398.2021.1899128

Sasithorn, N., & Martinová, L. (2014). Fabrication of Silk Nanofibres with Needle and Roller Electrospinning Methods. Journal of Nanomaterials, 1, 947315. https://doi.org/10.1155/2014/947315

Schlangen, M., Schlangen, E., & van der Goot, A. J. (2023). Advanced tensile testing as a new tool to quantify properties of food. *Current research in food science, 7*, 100577. https://doi.org/10.1016/j.crfs.2023.100577

Schmidt C. W. (2009). Swine CAFOs & novel H1N1 flu: separating facts from fears. *Environmental Health Perspectives, 117*(9), A394–A401. https://doi.org/10.1289/ehp.117-a394

Schmidt, T., Puchalla, N., Schedzielorz, M., & Kramell, A. E. (2023). Degumming and characterization of Bombyx mori and non-mulberry silks from Saturniidae silkworms. *Scientific Reports, 13,* 19504. https://doi.org/10.1038/s41598-023-46474-5

Scholze, M., Safavi, S., Li, K. C., Ondruschka, B., Werner, M., Zwirner, J., & Hammer, N. (2020). Standardized tensile testing of soft tissue using a 3D printed clamping system. *HardwareX, 8*, e00159. https://doi.org/10.1016/j.ohx.2020.e00159

Schreuders, F. K., Schlangen, M., Kyriakopoulou, K., Boom, R. M., & van der Goot, A. J. (2021). Texture methods for evaluating meat and meat analogue structures: A review. *Food Control 127*, 108103. https://doi.org/10.1016/j.foodcont.2021.108103

Sehnal, F., & Sutherland, T. (2008). Silks produced by insect labial glands. *Prion*, *2*(4), 145–153. https://doi.org/10.4161/pri.2.4.7489

Sencadas, V., Garvey, C., Mudie, S., Kirkensgaard, J. J. K.,Gouadec, G., & Hauser, S. (2019). Electroactive properties of electrospun silk fibroin for energy harvesting applications. *Nano Energy*, *66*, 104106. https://doi.org/10.1016/j.nanoen.2019.104106

Senchou, V., Weide, R., Carrasco, A., Bouyssou, H., Pont-Lezica, R., Govers, F., & Canut, H. (2004). High affinity recognition of a Phytophthora protein by Arabidopsis via an RGD motif. *Cellular and molecular life sciences : CMLS*, *61*(4), 502–509. https://doi.org/10.1007/s00018-003-3394-z

Seo H. S. (2020). Sensory Nudges: The Influences of Environmental Contexts on Consumers' Sensory Perception, Emotional Responses, and Behaviors toward Foods and Beverages. *Foods (Basel, Switzerland),* 9(4), 509. https://doi.org/10.3390/foods9040509

Shamshina, J. L., Acharya, S., Rumi, S. S., Liyanage, S., Parajuli, P., & Abidi, N. (2021). Choosing the right strategy: cryogrinding vs. ball milling – comparing apples to apples. *Carbohydrate Polymers, 289*, 119408.

Sharma, H., Sharma, B. D., Mendiratta, S. K., Talukder, S., & Ramasamy, G. (2014). Efficacy of flaxseed flour as bind enhancing agent on the quality of extended restructured mutton chops. *Asian-Australasian journal of animal sciences, 27*(2), 247–255. https://doi.org/10.5713/ajas.2013.13319

Sharma, V., Singh, B., & Thakur, R. K. (2024). Functionalization of psyllium to develop bioactive network hydrogels for sustained drug delivery. *Bioactive Carbohydrates and Dietary Fibre, 32*, 100427. https://doi.org/10.1016/j.bcdf.2024.100427

Shenoy, S. L., Bates, W. D., Frisch, H. L., Wnek, G. E. (2005). Role of chain entanglements on fiber formation during electrospinning of polymer solutions: good solvent, non-specific polymer–polymer interaction limit, *Polymer, 46*(10), 3372-3384. https://doi.org/10.1016/j.polymer.2005.03.011

Shepherd, J. H., Howard, D., Waller, A. K., Foster, H. R., Mueller, A., Moreau, T., Evans, A. L., Arumugam, M., Bouët Chalon, G., Vriend, E., Davidenko, N., Ghevaert, C., Best, S. M., & Cameron, R. E. (2018). Structurally graduated collagen scaffolds applied to the ex vivo generation of platelets from human pluripotent stem cell-derived megakaryocytes: Enhancing production and purity. *Biomaterials*, *182*, 135–144. https://doi.org/10.1016/j.biomaterials.2018.08.019

Shin, H., Jo, S., & Mikos, A. G. (2003). Biomimetic materials for tissue engineering. *Biomaterials, 24*(24), 4353–4364. https://doi.org/10.1016/s0142-9612(03)00339-9

Shirvan, A. R., Nouri, A., & Sutti, A. (2022). A perspective on the wet spinning process and its advancements in biomedical sciences. *European Polymer Journal*, *181*, 111681. https://doi.org/10.1016/j.eurpolymj.2022.111681

Shit, S. C., & Shah, P. M. (2014). Edible Polymers: Challenges and Opportunities. *Journal of Polymers, 2014*(1), 427259. https://doi.org/10.1155/2014/427259

Siddalingaswamy, N., Basavaiah, U. D., Dandin, S. B., Narayanagowda, S. N., & Shivaprakash, R. M. (2007). A study on the efficiency of micro-irrigation systems on growth yield and quality of mulberry. *Indian Journal of Sericulture*, *46*, 76-79.

Siegrist M., & Sütterlin, B. (2017). Importance of perceived naturalness for acceptance of food additives and cultured meat. *Appetite, 113*, 320-326. https://doi.org/10.1016/j.appet.2017.03.019.

Siegrist, M., & Hartmann, C. (2020). Consumer acceptance of novel food technologies. *Nature Food, 1*, 343–350. https://doi.org/10.1038/s43016-020-0094-x

Singh, A., Benjakul, S., Prodpran, T., & Nuthong, P. (2021). Effect of Psyllium (Plantago ovata Forks) Husk on Characteristics, Rheological and Textural Properties of Threadfin Bream Surimi Gel. *Foods (Basel, Switzerland)*, *10*(6), 1181. https://doi.org/10.3390/foods10061181

Singh, A., Kumar, V., Singh, S. K., Gupta, J., Kumar, M., Sarma, D. K., & Verma, V. (2023). Recent advances in bioengineered scaffold for in vitro meat production. *Cell and tissue research*, *391*(2), 235–247. https://doi.org/10.1007/s00441-022-03718-6

Sionkowska, A. (2011). Current research on the blends of natural and synthetic polymers as new biomaterials: Review. *Progress in Polymer Science, 36*(9), 1254-1276. https://doi.org/10.1016/j.progpolymsci.2011.05.003

Sionkowska, A., & Planeka, A. (2011). The influence of UV radiation of silk fibroin. *Polymer Degradation and Stability, 96*(4), 523-528. https://doi.org/10.1016/j.polymdegradstab.2011.01.001

Sionkowska, A., Płanecka, A., Lewandowska, K., & Michalska, M. (2014). The influence of UV-irradiation on thermal and mechanical properties of chitosan and silk fibroin mixtures. *Journal of photochemistry and photobiology. B, Biology, 140*, 301–305. https://doi.org/10.1016/j.jphotobiol.2014.08.017

Sivan, M., Madheswaran, D., Hauzerova, S., Novotny, V., Hedvicakova, V., Jencova, V., Kostakova, E. K., Schindler, M., & Lukas, D. (2022). AC electrospinning: impact of high voltage and solvent on the electrospinnability and productivity of polycaprolactone electrospun nanofibrous scaffolds. *Materialstoday CHEMISTRY, 26*, 101025. https://doi.org/10.1016/j.mtchem.2022.101025

Sivan, M., Madheswaran, D., Valtera, J., Kostakova, E. K., & Lukas, D. (2022). Alternating current electrospinning: The impacts of various high-voltage signal shapes and frequencies on the spinnability and productivity of polycaprolactone nanofibres. *Materials & Design, 213*, 110308. https://doi.org/10.1016/j.matdes.2021.110308

Skrivergaard, S., Krøyer Rasmussen, M., Sahebekhtiari, N., Feveile Young, J., & Therkildsen, M. (2023). Satellite cells sourced from bull calves and dairy cows differs in proliferative and myogenic capacity - Implications for cultivated meat. *Food research international (Ottawa, Ont.), 173*(Pt 1), 113217. https://doi.org/10.1016/j.foodres.2023.113217

Smetana, S., Mathys, A., Knoch, A., & Heinz, V. (2015). Meat alternatives: life cycle assessment of most known meat substitutes. *The International Journal of Life Cycle Assessment, 20*, 1254-1267. https://doi.org/10.1007/s11367-015-0931-6

Smith, F. E. (1930). *The World in 2030*. Hodder & Stoughton.

Sonnaert, M., Papantoniou, I., Luyten, F. P., & Schrooten, J. I. (2015). Quantitative Validation of the Presto Blue Metabolic Assay for Online Monitoring of Cell Proliferation in a 3D Perfusion Bioreactor System. *Tissue engineering. Part C, Methods*, *21*(6), 519–529. https://doi.org/10.1089/ten.TEC.2014.0255

Sonomoto, K., Yamaoka, K., Kaneko, H., Yamagata, K., Sakata, K., Zhang, X., Kondo, M., Zenke, Y., Sabanai, K., Nakayamada, S., Sakai, A., & Tanaka, Y. (2016). Spontaneous Differentiation of Human Mesenchymal Stem Cells on Poly-Lactic-Co-Glycolic Acid Nano-Fiber Scaffold. *PloS one*, *11*(4), e0153231. https://doi.org/10.1371/journal.pone.0153231

Sood, A., Singhmar, R., Son, Y., Jo, C. H., Choi, S., Kumar, A., & Soo Han, S. (2024). Tuning the efficacy of decellularized apple by coating with alginate/gelatin to behave as a bioscaffold for cultured meat production. *Food research international (Ottawa, Ont.)*, *177*, 113907. https://doi.org/10.1016/j.foodres.2023.113907

Souppez, J. -B. R. G., Dagès, B. A. S., Pavar, G. S., Fabian, J., Thomas, J. M., & Theodosiou, E. (2025). Mechanical properties and texture profile analysis of beef burgers and plant-based analogues. *Journal of Food Engineering*, *385*, 112259. https://doi.org/10.1016/j.jfoodeng.2024.112259

Southney, F. (2024, January 26). *Regulatory greenlight for cultivated beef leaves EU sector "hopeful*". Food Navigator Europe. https://www.foodnavigator.com/Article/2024/01/26/aleph-farms-cultivated-beef-approved-in-israel

Souza Filho, P. F., Andersson, D., Ferreira, J. A., & Taherzadeh, M. J. (2019). Mycoprotein: environmental impact and health aspects. *World journal of microbiology & biotechnology*, *35*(10), 147. https://doi.org/10.1007/s11274-019-2723-9

Space10. (2019). The Bug Burger [Photograph]. Space10. https://space10.com/the-fast-food-of-thefuture/

Srivastava, Y., Semwal, A. D., Sajeevkumar, V. A., & Sharma, G. K. (2017). Melting, crystallization and storage stability of virgin coconut oil and its blends by differential scanning calorimetry (DSC) and Fourier transform infrared spectroscopy (FTIR). *Journal of food science and technology, 54*(1), 45–54. https://doi.org/10.1007/s13197-016-2427-1

Starkey, C. P., Geesink, G. H., Collins, D., Oddy, V. H., & Hopkins, D. L. (2016). Do sarcomere length, collagen content, pH, intramuscular fat and desmin degradation explain variation in the tenderness of three ovine muscles?. *Meat Science, 113*, 51-58. https://doi.org/10.1016/j.meatsci.2015.11.013

Stephens, N., Di Silvio, L., Dunsford, I., Ellis, M., Glencross, A., & Sexton, A. (2018). Bringing cultured meat to market: Technical, socio-political, and regulatory challenges in cellular agriculture. *Trends in food science & technology, 78*, 155–166. https://doi.org/10.1016/j.tifs.2018.04.010

Stephens, N., Sexton, A. E., & Driessen, C. (2019). Making Sence of Making Meat: Key Moments in the First 20 Years of Tissue Engineering Muscle to Make Food. *Frontiers in Sustainable Food Systems, 3*, 45. https://doi.org/10.3389/fsufs.2019.00045

Stijnman, A. C., Bodnar, I., & Tromp, R. H. (2011). Electrospinning of food-grade polysaccharides. *Food Hydrocolloids, 25*(5), 1393-1398. https://doi.org/10.1016/j.foodhyd.2011.01.005

Stijnman, A. C., Bodnar, I., & Tromp, R. H. (2011). Electrospinning of food-grade polysaccharides. *Food Hydrocolloids, 25*(5), 1393-1398. https://doi.org/10.1016/j.foodhyd.2011.01.005

Stout, A. J., Arnett, M. J., Chai, K., Guo, T., Liao, L., Mirliani, A. B., Rittenberg, M. L., Shub, M., White, E. C., Yuen, J. S. K., Jr, Zhang, X., & Kaplan, D. L. (2023). Immortalized Bovine Satellite Cells for Cultured Meat Applications. *ACS synthetic biology, 12*(5), 1567–1573. https://doi.org/10.1021/acssynbio.3c00216

Stout, A. J., Mirliani, A. B., Rittenberg, M. L., Shub, M., White, E. C., Yuen, J. S. K., Jr, & Kaplan, D. L. (2022). Simple and effective serum-free medium for sustained expansion of bovine satellite cells for cell cultured meat. *Communications biology, 5*(1), 466. https://doi.org/10.1038/s42003-022-03423-8

Stout, A. J., Mirliani, A. B., Rittenberg, M. L., Shub, M., White, E. C., Yuen, J. S. K., Jr, & Kaplan, D. L. (2022). Simple and effective serum-free medium for sustained expansion of bovine satellite cells for cell cultured meat. *Communications Biology, 5*(1), 466. https://doi.org/10.1038/s42003-022-03423-8

Stout, A.J., Mirliani, A.B., Rittenberg, M.L., Shub, M., White, E. C., Yuen Jr., J. S. K., & Kaplan, D. L. (2022). Simple and effective serum-free medium for sustained expansion of bovine satellite cells for cell cultured meat. *Communications Biology, 5*, 466. https://doi.org/10.1038/s42003-022-03423-8

Strassner, A. -M., & Wirth, W. (2024). Shades and shifts in flexitarian and meat-orientated consumer profiles in a German panel study. *Appetite, 197*, 107298. https://doi.org/10.1016/j.appet.2024.107298

Su, L., Jing, L., Zeng, S., Fu, C., & Huang, D. (2024). 3D Porous Edible Scaffolds from Rye Secalin for Cell-Based Pork Fat Tissue Culturing. *Journal of agricultural and food chemistry*, *72*(20), 11587–11596. https://doi.org/10.1021/acs.jafc.3c09713

Su, L., Jing, L., Zeng, X., Chen, T., Liu, H., Kong, Y., Wang, X., Yang, X., Fu, C., Sun, J., & Huang, D. (2023). 3D-Printed prolamin scaffolds for cell-based meat culture. *Advanced Materials*, *35*(2), 2207397. https://doi.org/10.1002/adma.202207397

Su, Y., Wang, L., Fan, Z., Liu, Y., Zhu, J., Kaback, D., Oudiz, J., Patrick, T., Yee, S. P., Tian, X. C., Polejaeva, I., & Tang, Y. (2021). Establishment of Bovine-Induced Pluripotent Stem Cells. *International journal of molecular sciences, 22*(19), 10489. https://doi.org/10.3390/ijms221910489

Subbiahanadar Chelladurai, K., Selvan Christyraj, J. D., Rajagopalan, K., Yesudhason, B. V., Venkatachalam, S., Mohan, M., Chellathurai Vasantha, N., & Selvan Christyraj, J. R. S. (2021). Alternative to FBS in animal cell culture - An overview and future perspective. *Heliyon*, *7*(8), e07686. https://doi.org/10.1016/j.heliyon.2021.e07686

Sun, M., Cao, Y., Sun, Q., Ren, X., Hu, J., Sun, Z., & Duan, J. (2021). Exposure to polydopamine nanoparticles induces neurotoxicity in the developing zebrafish. *NanoImpact*, *24*, 100353. https://doi.org/10.1016/j.impact.2021.100353

Sun, W., Gregory, D. A., Tomeh, M. A., & Zhao, X. (2021b). Silk Fibroin as a Functional Biomaterial for Tissue Engineering. *International journal of molecular sciences, 22*(3), 1499. https://doi.org/10.3390/ijms22031499

Sun, Z., Guo, S. S., & Fässler, R. (2016). Integrin-mediated mechanotransduction. *The Journal of cell biology, 215*(4), 445–456. https://doi.org/10.1083/jcb.201609037

Talluri, T. R., Kumar, D., Glage, S., Garrels, W., Ivics, Z., Debowski, K., Behr, R., Niemann, H., & Kues, W. A. (2015). Derivation and characterization of bovine induced pluripotent stem cells by transposon-mediated reprogramming. *Cellular reprogramming*, *17*(2), 131–140. https://doi.org/10.1089/cell.2014.0080

Tanaka, R. I., Sakaguchi, K., Yoshida, A., Takahashi, H., Haraguchi, Y., & Shimizu, T. (2022). Production of scaffold-free cell-based meat using cell sheet technology. *NPJ science of food*, *6*(1), 41. https://doi.org/10.1038/s41538-022-00155-1

Tang, Y., Shi, C., Zhu, Y., Yang, M., Sheng, K., & Zhang, X. (2024). Cellulose as a sustainable scaffold material in cultivated meat production. *Current research in food science*, *9*, 100846. https://doi.org/10.1016/j.crfs.2024.100846

Tang, Y., Shi, C., Zhu, Y., Yang, M., Sheng, K., & Zhang, X. (2024). Cellulose as a sustainable scaffold material in cultivated meat production. *Current research in food science*, *9*, 100846. https://doi.org/10.1016/j.crfs.2024.100846

Teague, W. R., Apfelbaum, S., Lal, R., Kreuter, U., Rountree, J., Davies, C., Conser, R., DeLonge, M., Rasmussen, M., Hatfield, J., Wang, T., & Byck, P. (2016). The role of ruminants in reducing agricultrure's carbon footprint in North America. *The Journal of Soil and Water Conservation, 71*(2), 156-164. https://doi.org/10.2489/jswc.71.2.156

Teo, W.-E., Inai, R., & Ramakrishna, S. (2011). Technological advances in electrospinning of nanofibres. *Science and Technology of Advanced Materials, 12*(1). https://doi.org/10.1088/1468-6996/12/1/013002

Terada, D., Yokoyama, Y., Hattori, S., Kobayashi, H., & Tamada, Y. (2016). The outermost surface properties of silk fibroin films reflect ethanol-treatment conditions used in biomaterial preparation. *Materials science & engineering. C, Materials for biological applications*, *58*, 119–126. https://doi.org/10.1016/j.msec.2015.07.041

Thakar, R. G., Cheng, Q., Patel, S., Chu, J., Nasir, M., Liepmann, D., Komvopoulos, K., & Li, S. (2009). Cell-shape regulation of smooth muscle cell proliferation. *Biophysical journal*, *96*(8), 3423–3432. https://doi.org/10.1016/j.bpj.2008.11.074

Theron, S. A., Yarin, A. L., Zussman, E., & Kroll, E. (2005). Multiple jets in electrospinning: experiment and modeling. *Polymer, 46*(9), 2889-2899. https://doi.org/10.1016/j.polymer.2005.01.054

Thyden, R., Perreault, L. R., Jones, J. D., Notman, H., Varieur, B. M., Patmanidis, A. A., Dominko, T., Gaudette, G. R. (2022). An Edible, Decellularized Plant Derived Cell Carrier for Lab Grown Meat. *Applied Sciences, 12*(10), 5155. https://doi.org/10.3390/app12105155

Tian, H., Xu, R., Canadell, J. G., Thompson, R. L., Winiwarter, W., Suntharalingam, P., Davidson, E. A., Ciais, P., Jackson, R. B., Janssens-Maenhout, G., Prather, M. J., Regnier, P., Pan, N., Pan, S., Peters, G. P., Shi, H., Tubiello, F. N., Zaehle, S., Zhou, F., Arneth, A., et al. (2020). A comprehensive quantification of global nitrous oxide sources and sinks. *Nature, 586*, 248–256. https://doi.org/10.1038/s41586-020-2780-0

Tilman D. (1999). Global environmental impacts of agricultural expansion: the need for sustainable and efficient practices. *Proceedings of the National Academy of Sciences of the United States of America*, *96*(11), 5995–6000. https://doi.org/10.1073/pnas.96.11.5995

Tornberg E. (1996). Biophysical aspects of meat tenderness. *Meat science, 43S1*, 175–191. https://doi.org/10.1016/0309-1740(96)00064-2

Treich N. (2021). Cultured Meat: Promises and Challenges. *Environmental & resource economics*, *79*(1), 33–61. https://doi.org/10.1007/s10640-021-00551-3

Treich, N. (2021). Cultured Meat: Promises and Challenges. *Environmental & Resource Economics, 79*, 33-61. https://doi.org/10.1007/s10640-021-00551-3

Tretinnikov, O. N., & Tamada, Y. (2001). Influence of Casting Temperature on the Near-Surface Structure and Wettability of Cast Silk Fibroin Films. *Langmuir, 17*(23), 7406-7413. https://doi.org/10.1021/la010791y

Trivedi, S., Srivastava, K., Gupta, A., Saluja, T. S., Kumar, S., Mehrotra, D., & Singh, S. K. (2020). A quantitative method to determine osteogenic differentiation aptness of scaffold. *Journal of oral biology and craniofacial research*, *10*(2), 158–160. https://doi.org/10.1016/j.jobcr.2020.04.006

Tuomisto, H. L., & de Mattos, M. J. (2011). Environmental impacts of cultured meat production. *Environmental science & technology*, *45*(14), 6117–6123. https://doi.org/10.1021/es200130u

Tuomisto, H. L., Allan, S. J., & Ellis, M. J. (2022). Prospective life cycle assessment of a bioprocess design for cultured meat production in hollow fiber bioreactors. *The Science of the total environment*, *851*(Pt 1), 158051. https://doi.org/10.1016/j.scitotenv.2022.158051

Uchiyama, H., Yamada, M., Ishizaki, K., & Sakurai, K. (2014). Specific ultraviolet-C irradiation energy for functionalization of titanium surface to increase osteoblastic cellular attachment. *Journal of Biomaterials Applications, 28*(9), 1419-1429. https://doi.org/10.1177/0885328213511678

Ulagesan, S., Krishnan, S., Nam, T. -J., & Choi, Y -H. (2024). Production of fish fillet analogues using novel fish muscle cell powder and sodium alginate-κ-carrageenan based bio-ink. *Food Hydrocolloids, 157*, 110446. https://doi.org/10.1016/j.foodhyd.2024.110446

UN. (2024). *World Population Prospects 2019: Highlights*. United Nations. https://population.un.org/wpp/

UPSIDE Foods. (2021, December 9). *UPSIDE Foods Develops Breakthrough Cell Feed that is Free of Animal Components.* CISION PR Newswire. https://www.prnewswire.com/news-releases/upside-foods-develops-breakthrough-cell-feed-that-is-free-of-animal-components-301441242.html

Vale, P., Gibbs, M., Vale, R., Christie, M., Florence, E., Munger, J., & Sabaini, D. (2019). The Expansion of Intensive Beef Farming to the Brazilian Amazon. *Global Environmental Change, 57*, 101922. https://doi.org/10.1016/j.gloenvcha.2019.05.006

Valtera, J., Kalous, T., Pokorny, P., Batka, O., Bilek, M., Chvojka, J., Mikes, P., Kostakova, E. K., Zabka, P., Ornstova, J., Beran, J., Stanishevsky, A., & Lukas, D. (2019). Fabrication of dual-functional composite yarns with a nanofibrous envelope using high throughput AC needleless and collectorless electrospinning. Scientific reports, 9(1), 1801. https://doi.org/10.1038/s41598-019-38557-z

Valtera, J., Vysloužilová, L., Komárek, J., Skřivánek, J., Žabka, P., Beran, J., Lukáš, D. (2015). Protusion of the Rod Electrode in the Electrospinning Process. *Journal of Nanotechnology, 2015*(1), 301636. https://doi.org/10.1155/2015/301636

van der Vossen-Wijmenga, W. P., Zwietering, M. H., Boer, E. P. J., Velema, E., & den Besten, H. M. W. (2022). Perception of food-related risks: Difference between consumers and experts and changes over time. *Food Control, 141*, 109142. https://doi.org/10.1016/j.foodcont.2022.109142

Van Eelen, W. F., van Kooten, W. J., & Westerhof, W. (1999). *Industrial production of meat from in vitro cell cultures* (Patent No. WO1999031222). World Intellectual Property Organisation. http://www.wipo.int/pctdb/en/wo.jsp?wo=1999031223

Van Eelen, W. F., van Kooten, W. J., & Westerhof, W. (1999). *Industrial production of meat from in vitro cell cultures* (Patent No. WO1999031222). World Intellectual Property Organisation. http://www.wipo.int/pctdb/en/wo.jsp?wo=1999031223

van Huis, A., & Oonincx, D. G. A. B. (2017). The environmental sustainability of insects as food and feed. A review. *Agronomy for Sustainable Development, 37*, 43. https://doi.org/10.1007/s13593-017-0452-8

Venkatesan, M., Semper, C., Skrivergaard, S., Di Leo, R., Mesa, N., Rasmussen, M.K., Young, J.F., Therkildsen, M., Stogios, P.J., & Savchenko, A. (2022). Recombinant production of growth factors for application in cell culture. *iScience, 25*(10), 105054. https://doi.org/10.1016/j.isci.2022.105054

Verbeke, W., Marcu, A., Rutsaert, P., Gaspar, R., Seibt, B., Fletcher, D., & Barnett, J. (2015). 'Would you eat cultured meat?': Consumers' reactions and attitude formation in Belgium, Portugal and the United Kingdom. *Meat science*, *102*, 49–58. https://doi.org/10.1016/j.meatsci.2014.11.013

Verbruggen, S., Luining, D., van Essen, A., & Post, M. J. (2018). Bovine myoblast cell production in a microcarriers-based system. *Cytotechnology*, *70*(2), 503–512. https://doi.org/10.1007/s10616-017-0101-8

Wale, M. E., Nesbitt, D. Q., Henderson, B. S., Fitzpatrick, C. K., Creechley, J. J., & Lujan, T. J. (2021). Applying ASTM Standards to Tensile Tests of Musculoskeletal Soft Tissue: Methods to Reduce Grip Failures and Promote Reproducibility. *Journal of biomechanical engineering, 143*(1), 011011. https://doi.org/10.1115/1.4048646

Walsh, H & Simmonds, E. (2024, February 26) *Supermarkets reviewed: compare the best and worst*. Which?. https://www.which.co.uk/reviews/supermarkets/article/best-supermarkets-aOJjN2J0A10N

Wang, H., Duan, Z., Feng, X., Mao, Z. -S., & Yang, C. (2022). Effect of impeller type and scale-up on spatial distribution of shear rate in a stirred tank. *Chinese Journal of Chemical Engineering, 42*, 351-363. https://doi.org/10.1016/j.cjche.2021.03.004

Wang, H., Zhang, Y., Shao, S., & Hu, X. (2005). A study on the flow stability of regenerated silk fibroin aqueous solution, *International Journal of Biological Macromolecules, 36*(1–2), 66-70. https://doi.org/10.1016/j.ijbiomac.2005.03.011

Wang, K., Ma, Q., Zhou, H., Zhao, J., Cao, M. & Wang, S. (2023). Review on Fabrication and Application of Regenerated Bombyx mori Silk Fibroin Materials. *AUTEX Research Journal, 23*(2), 164-183. https://doi.org/10.2478/aut-2021-0059

Wang, L., Wu, Y., Guo, B., & Ma, P. X. (2015). Nanofibre Yarn/Hydrogel Core-Shell Scaffolds Mimicking Native Skeletal Muscle Tissue for Guiding 3D Myoblast Alignment, Elongation, and Differentiation. *ACS nano, 9*(9), 9167–9179. https://doi.org/10.1021/acsnano.5b03644

Wang, Y., Fang, Y., Witting, P. K., Charchar, F. J., Sobey, C. G., Drummond, G. R., Golledge, J. (2023). Dietary fatty acids and mortality risk from heart disease in US adults: an analysis based on NHANES. *Scientific Reports, 13*, 1614. https://doi.org/10.1038/s41598-023-28738-2

Wang, Y., Zhong, Z., Munawar, N., Wang, R., Zan, L., & Zhu, J. (2024). Production of green-natural and "authentic" cultured meat based on proanthocyanidins-dialdehyde chitosan-collagen ternary hybrid edible scaffolds. *Food research international (Ottawa, Ont.)*, *175*, 113757. https://doi.org/10.1016/j.foodres.2023.113757

Wang, Z., Cui, Y., Feng, Y., Guan, Li., Dong, M., Liu, Z., & Liu, L. (2021). A versatile Silk Fibroin based filtration membrane with enhanced mechanical property, disinfection, and biodegradability. *Chemical Engineering Journal, 426*, 131947. https://doi.org/10.1016/j.cej.2021.131947

Warwicker, J. O. (1954). The crystal structure of silk fibroin. *Acta Crystallographica, 7*, 565-573. https://doi.org/10.1107/S0365110X54001867

Watson, E. (2022, May 10). *From mush to meat? Talking edible scaffolding for cultivated meat with Gelatex and Matrix F.T.* Food Navigator USA. https://www.foodnavigator-usa.com/Article/2022/05/10/From-mush-to-meat-Talking-edible-scaffolding-for-cultivated-meat-with-Gelatex-and-Matrix-F.T#

Wei, W., Zhang, Y., Shao, H., & Hu, X. (2011). Posttreatment of the dry-spun fibers obtained from regenerated silk fibroin aqueous solution in ethanol aqueous solution. *Journal of Materials Research, 26*(9), 1100–1106. https://doi.org/10.1557/jmr.2011.47

Wei, Z., Dai, S., Huang, J., Hu, X., Ge, C., Zhang, X., Yang, K., Shao, P., Sun, P., & Xiang, N. (2023). Soy Protein Amyloid Fibril Scaffold for Cultivated Meat Application. *ACS applied materials & interfaces*, *15*(12), 15108–15119. https://doi.org/10.1021/acsami.2c21702

Weiss, L., & Zeigel, R. (1971). Cell surface negativity and the binding of positively charged particles. *Journal of cellular physiology*, *77*(2), 179–186. https://doi.org/10.1002/jcp.1040770208

Weng, Z., Wang, Y., Ouchi, T., Liu, H., Qiao, X., Wu, C., Zhao, Z., Li, L., & Li, B. (2022). Mesenchymal Stem/Stromal Cell Senescence: Hallmarks, Mechanisms, and Combating Strategies. *Stem cells translational medicine*, *11*(4), 356–371. https://doi.org/10.1093/stcltm/szac004

Whitton, C., Bogueva, D., Marinova, D., & Phillips, C. J. C. (2021). Are We Approaching Peak Meat Consumption? Analysis of Meat Consumption from 2000 to 2019 in 35 Countries and Its Relationship to Gross Domestic Product. *Animals : an open access journal from MDPI, 11*(12), 3466. https://doi.org/10.3390/ani11123466

WHO. (2012). *The Evolving Threat of Antimicrobial Resistance: Options for Action*. World Health Organization. https://apps.who.int/iris/handle/10665/44812

WHO. (2014). *Antimicrobial resistance: global report on surveillance*. World Health Organization. https://apps.who.int/iris/handle/10665/112642

Wibawa, H., Henning, J., Wong, F., Selleck, P., Junaidi, A., Bingham, J., Daniels, P., & Meers, J. (2011). A molecular and antigenic survey of H5N1 highly pathogenic avian influenza virus isolates from smallholder duck farms in Central Java, Indonesia during 2007-2008. *Virology Journal, 8*, 425. https://doi.org/10.1186/1743-422X-8-425

Wiercigroch, E., Szafraniec, E., Czamara, K., Pacia, M. Z., Majzner, K., Kochan, K., Kaczor, A., Baranska, M., & Malek, K. (2017). Raman and infrared spectroscopy of carbohydrates: A review.

Spectrochimica Acta. Part A, Molecular and Biomolecular Spectroscopy, 185, 317–335. https://doi.org/10.1016/j.saa.2017.05.045

Witkowski J. A. (1980). Dr. Carrel's immortal cells. *Medical history, 24*(2), 129–142. https://doi.org/10.1017/s0025727300040126

Witte, F., Sawas, E., Berger, L.M., Gibis, M., Weiss, J., Röser, A., Upmann, M., Joeres, E., Juadjur, A., Bindrich, U., Heinz, V., & Terjung, N. (2022). Influence of Finely Chopped Meat Addition on Quality Parameters of Minced Meat. *Applied Sciences, 12*(20),10590. https://doi.org/10.3390/app122010590

Wolfson, W. (2002). Lab-Grown Steaks Nearing the Menu. New Scientist. Available online at: https://www.newscientist.com/article/dn3208-lab-grown-steaks-nearing-the-menu (accessed October 22, 2024).

Wolk, A. (2017). Potential health hazards of eating red meat. *Journal of Internal Medicine, 281*(2), 106–122. https://doi.org/10.1111/joim.12543

Wollschlaeger, J. O., Maatz, R., Albrecht, F. B., Klatt, A., Heine, S., Blaeser, A., & Kluger, P. J. (2022). Scaffolds for Cultured Meat on the Basis of Polysaccharide Hydrogels Enriched with Plant-Based Proteins. *Gels (Basel, Switzerland)*, *8*(2), 94. https://doi.org/10.3390/gels8020094

Wu, J., & Hong, Y. (2016). Enhancing cell infiltration of electrospun fibrous scaffolds in tissue regeneration. *Bioactive materials, 1*(1), 56–64. https://doi.org/10.1016/j.bioactmat.2016.07.001

Wu, X. M., Han, W. M., Hou, L. Y., Lin, D. D., Li, J. Y., Lin, S. T., Yang, J. P., Liao, L., & Zeng, X. A. (2024). Glutenin-chitosan 3D porous scaffolds with tunable stiffness and systematized microstructure for cultured meat model. *International journal of biological macromolecules*, *267*(Pt 1), 131438. https://doi.org/10.1016/j.ijbiomac.2024.131438

Wu, Z., Xu, W., Wu, X., & Ding, X. (2025). Life cycle environmental and economic assessment of raw silk production in China. *Sustainable Production and Consumption*, *55*, 11-23. https://doi.org/10.1016/j.spc.2025.02.002

Wurgaft, B. A. (2015, April 8). *"Godfather of Cultured Meat" Willem Van Eelen Passes Away at 91*. New Harvest. https://new-harvest.org/willem-van-eelen-passes-away/

Xia, L., Robock, A., Scherrer, K., Harrison, C. S., Bodirsky, B. L., Weindl, I., Jägermeyr, J., Bardeen, C. G., Toon, O. B., & Heneghan, R. (2022). Global food insecurity and famine from reduced crop, marine fishery and livestock production due to climate disruption from nuclear war soot injection. *Nature food*, *3*(8), 586–596. https://doi.org/10.1038/s43016-022-00573-0

Xiang, N., Yuen, J. S. K., Jr, Stout, A. J., Rubio, N. R., Chen, Y., & Kaplan, D. L. (2022). 3D porous scaffolds from wheat glutenin for cultured meat applications. *Biomaterials*, *285*, 121543. https://doi.org/10.1016/j.biomaterials.2022.121543

Xiao, Z., Connor, A. J., Worland, A. M., Tang, Y. J., Zha, R. H., & Koffas, M. (2023). Silk fibroin production in Escherichia coli is limited by a positive feedback loop between metabolic burden and toxicity stress. *Metabolic engineering*, *77*, 231–241. https://doi.org/10.1016/j.ymben.2023.03.011

Xie, J., Shen, H., Yuan, G., Lin, K., & Su, J. (2021). The effects of alignment and diameter of electrospun fibers on the cellular behaviors and osteogenesis of BMSCs. *Materials science & engineering. C, Materials for biological applications*, *120*, 111787. https://doi.org/10.1016/j.msec.2020.111787

Xiong, J., Liu, Y., Li, A., Wei, L., Wang, L., Qin, X., & Yu, J. (2021) Mass production of high-quality nanofibres via constructing pre-Taylor cones with high curvature on needleless electrospinning, Materials & Design, 197, 109247. https://doi.org/10.1016/j.matdes.2020.109247

Xu, M., McCanna, D. J., & Sivak, J. G. (2015). Use of the viability reagent PrestoBlue in comparison with alamarBlue and MTT to assess the viability of human corneal epithelial cells. *Journal of pharmacological and toxicological methods, 71*, 1–7. https://doi.org/10.1016/j.vascn.2014.11.003

Xue, Y., Lofland, S., & Hu, X. (2020). Comparative study of silk-based magnetic materials: effect of magnetic particle types on the protein structure and biomaterial properties. *Internation Journal of Molecular Sciences, 21*(20), 7583. https://doi.org/10.3390/ijms21207583

Yadav, P., Beniwal, G., & Saxena, K.K. (2021). A review on pore and porosity in tissue engineering, *Materials Today Proceedings, 44*(1), 2623-2628. https://doi.org/10.1016/j.matpr.2020.12.661

Yamanaka, K., Haraguchi, Y., Takahashi, H., Kawashima, I., & Shimizu, T. (2023). Development of serum-free and grain-derived-nutrient-free medium using microalga-derived nutrients and mammalian cell-secreted growth factors for sustainable cultured meat production. *Scientific Reports, 13*, 498. https://doi.org/10.1038/s41598-023-27629-w

Yamazaki, M., Kojima, H., & Myoshi, H. (2020). Morphology and differentiation of human mesenchymal stem cells cultured on a nanoscale structured substrate. *Electronics and Communications in Japan, 103*(9), 23-28. https://doi.org/10.1002/ecj.12260

Yang, P., Chen, Y., Jiang, S., Shen, P., Lu, X., & Xiao, Y. (2018). Association between antibiotic consumption and the rate of carbapenem-resistant Gram-negative bacteria from China based on 153 tertiary hospitals data in 2014. *Antimicrobial Resistance and Infection Control, 7*, 137. https://doi.org/10.1186/s13756-018-0430-1

Yang, Z., Schmitt, J. F., & Lee, E. H. (2011). Immunohistochemical analysis of human mesenchymal stem cells differentiating into chondrogenic, osteogenic, and adipogenic lineages. *Methods in molecular biology (Clifton, N.J.)*, *698*, 353–366. https://doi.org/10.1007/978-1-60761-999-4_26

Yao, C., Li, X., Song, T., Li, Y. & Pu, Y. (2009). Biodegradable nanofibrous membrane of zein/silk fibroin by electrospinning. *Polymer International*, *58*(4), 396-402. https://doi.org/10.1002/pi.2544

Yao, Y., Yuen, J. S. K., Jr, Sylvia, R., Fennelly, C., Cera, L., Zhang, K. L., Li, C., & Kaplan, D. L. (2024). Cultivated Meat from Aligned Muscle Layers and Adipose Layers Formed from Glutenin Films. *ACS biomaterials science & engineering*, *10*(2), 814–824. https://doi.org/10.1021/acsbiomaterials.3c01500

Yen, F. C., Glusac, J., Levi, S., Zernov, A., Baruch, L., Davidovich-Pinhas, M., Fishman, A., & Machluf, M. (2023). Cultured meat platform developed through the structuring of edible microcarrier-derived microtissues with oleogel-based fat substitute. *Nature communications*, *14*(1), 2942. https://doi.org/10.1038/s41467-023-38593-4

Yi, B., Xu, Q., & Liu, W. (2021). An overview of substrate stiffness guided cellular response and its applications in tissue regeneration. *Bioactive materials, 15*, 82–102. https://doi.org/10.1016/j.bioactmat.2021.12.005

Yigit, S., Hallaj, N. S., Sugarman, J. L., Chong, L. C., Roman, S. E., Abu-Taleb, L. M., Goodman, R. E., Johnson, P. E., & Behrens, A. M. (2021). Toxicological assessment and food allergy of silk fibroin derived from Bombyx mori cocoons. *Food and chemical toxicology : an international journal published for the British Industrial Biological Research Association*, *151*, 112117. https://doi.org/10.1016/j.fct.2021.112117

Yin, Y., & Xiong, J. (2017). Effect of the distribution of fiber orientation on the mechanical properties of silk fibroin/polycaprolactone nanofibre mats. *Journal of Engineered Fibers and Fabrics, 12*(3). https://doi.org/10.1177/155892501701200303

Yonesi, M., Garcia-Nieto, M., Guinea, G. V., Panetsos, F., Pérez-Rigueiro, J., & González-Nieto, D. (2021). Silk Fibroin: An Ancient Material for Repairing the Injured Nervous System. *Pharmaceutics*, *13*(3), 429. https://doi.org/10.3390/pharmaceutics13030429

Yuan, S., Xiong, G., He, F., Jiang, W., Liang, B., Pehkonen, S., & Choong, C. (2015). PCL microspheres tailored with carboxylated poly(glycidyl methacrylate)–REDV conjugates as conducive microcarriers for endothelial cell expansion. *Journal of Materials Chemistry B, 3*(44), 8670-8683. https://doi.org/10.1039/C5TB01836F

Zagury, Y., Ianovici, I., Landau, S., Lavon, N., & Levenberg, S. (2022). Engineered marble-like bovine fat tissue for cultured meat. *Communications Biology 5*, 927. https://doi.org/10.1038/s42003-022-03852-5

Zehorai. E., Maor-Shoshani, A., Molotski, N., Dorojkin, A., Marelly, N., Dvash, T., Lavon, N. (2024). From fertilised oocyte to cultivated meat – harnessing bovine embryonic stem cells in the cultivated meat industry. *Reproduction, Fertility and Development 36*, 124-132. https://doi.org/10.1071/RD23169

Zernov, A., Baruch, L., & Machluf, M. (2022). Chitosan-collagen hydrogel microparticles as edible cell microcarriers for cultured meat. *Food Hydrocolloids, 129*, 107632. https://doi.org/10.1016/j.foodhyd.2022.107632

Zhan, X.-S.; El-Ashram, S.; Luo, D.-Z.; Luo, H.-N.; Wang, B.-Y.; Chen, S.-F.; Bai, Y.-S.; Chen, Z.-S.; Liu, C.-Y.; Ji, H.-Q. (2019). A Comparative Study of Biological Characteristics and Transcriptome Profiles of Mesenchymal Stem Cells from Different Canine Tissues. *International Journal of Molecular Sciences, 20*(6), 1485. https://doi.org/10.3390/ijms20061485

Zhang, H., Deng, L., Yang, M., Min, S., Yang, L., & Zhu, L. (2011). Enhancing Effect of Glycerol on the Tensile Properties of Bombyx mori Cocoon Sericin Films. *International Journal of Molecular Sciences, 12*(5), 3170-1818. https://doi.org/10.3390/ijms12053170

Zhang, N., Mendieta-Esteban, J., Magli, A., Lilja, K. C., Perlingeiro, R. C. R., Marti-Renom, M. A., Tsirigos, A., & Dynlacht, B. D. (2020). Muscle progenitor specification and myogenic differentiation are associated with changes in chromatin topology. *Nature communications*, *11*(1), 6222. https://doi.org/10.1038/s41467-020-19999-w

Zhang, W., Liu, Y. & Zhang, H. (2021). Extracellular matrix: an important regulator of cell functions and skeletal muscle development. *Cell & Bioscience, 11*, 65. https://doi.org/10.1186/s13578-021-00579-4

Zhang, X., & Pan, Z. (2019). Microstructure Transitions and Dry-Wet Spinnability of Silk Fibroin Protein from Waste Silk Quilt. *Polymers*, *11*(10), 1622. https://doi.org/10.3390/polym11101622

Zhang, X., & Wyeth, P. (2010). Using FTIR spectroscopy to detect sericin on historic silk. *Science China Chemistry, 53*, 626–631. https://doi.org/10.1007/s11426-010-0050-y

Zhang, X., Liu, C., Kong, Y., Li, F., & Yue, X. (2022). Effects of intramuscular fat on meat quality and its regulation mechanism in Tan sheep. *Frontiers in nutrition, 9*, 908355. https://doi.org/10.3389/fnut.2022.908355

Zhang, X., Owens, C. M., & Schilling, M. W. (2017). Meat: the edible flesh from mammals only or does it include poultry, fish, and seafood?. *Animal Frontiers*, *7*(4), 12-18. https://doi.org/10.2527/af.2017.0437

Zhang, Y., Brouwer, R., Sala, G., Scholten, E., & Stieger, M. (2024). Exploring relationships between juiciness perception, food and bolus properties of plant-based meat analogue and beef patties. *Food Hydrocolloids, 147B*, 109443. https://doi.org/10.1016/j.foodhyd.2023.109443

Zhao, H., & Chi, H. (2017). *Electrospun Bead-on-String Fibers: Useless or Something of Value?* In T. Lin (Eds.) *Novel Aspects of Nanofibres*. IntechOpen. https://doi.org/10.5772/intechopen.74661

Zhao, M., Qi, Z., Tao, X., Newkirk, C., Hu, X., & Lu, S. (2021). Chemical, thermal, time, and enzymatic stability of silk materials with silk I structure. *International Journal of Molecular Sciences, 22*(8), 4136. https://doi.org/10.3390/ijms22084136

Zhao, P., Jiang, H., Pan, H., Zhu, K., & Chen, W. (2007). Biodegradable fibrous scaffolds composed of gelatin coated poly(epsilon-caprolactone) prepared by coaxial electrospinning. *Journal of biomedical materials research. Part A*, *83*(2), 372–382. https://doi.org/10.1002/jbm.a.31242

Zhao, Z-L., Li, W-W., Wang, F., & Zhang, Y-Q. (2018). Using hydrated lime water as a novel degumming agent of silk and sericin recycling from wastewater. *Journal of Cleaner Production, 172*, 2090-2096. https://doi.org/10.1016/j.jclepro.2017.11.213

Zheng, G., Jiang, J., Wang, X., Li, W., Liu, J., Fu, G., & Lin, L. (2020). Nanofibre membranes by multi-jet electrospinning arranged as arc-array with sheath gas for electrodialysis applications. *Materials & Design, 189*, 108504. https://doi.org/10.1016/j.matdes.2020.108504

Zhou, P., Xia, Y., Cheng, X., Wang, P., Xie, Y., & Xu, S. (2014). Enhanced bone tissue regeneration by antibacterial and osteoinductive silica-HACC-zein composite scaffolds loaded with rhBMP-2. *Biomaterials, 35*(38), 10033–10045. https://doi.org/10.1016/j.biomaterials.2014.09.009

Zhou, Y., Liu, Y., Zhang, M., Feng, Z., Yu, D. G., & Wang, K. (2022). Electrospun Nanofibre Membranes for Air Filtration: A Review. *Nanomaterials (Basel, Switzerland)*, *12*(7), 1077. https://doi.org/10.3390/nano12071077

Zhu, Z., Xu, G., Chen, R., Wang, Z., Huang, J., Chen, X., Zeng, J., Liang, F., Fang, F., Wang, H., Wu, P., He, Y., Zhao, Y., & Li, Y. (2018). Uniform electric field enabled multi-needles electrospinning head based on trapezoid arrangement. *AIP Advances, 8* (8), 085126. https://doi.org/10.1063/1.5026908

Zidi, C. (Director). (1976). *L'Aile ou la Cuisse* [Film]. Les Films Christian Fechner.

Zinck, M., & Vaszily, H. (2021, August 20). *Matrix Meats and the world of 3D Scaffolding.* Lab Grown Meat. https://labgrownmeat.com/matrix-meats/

Appendix A

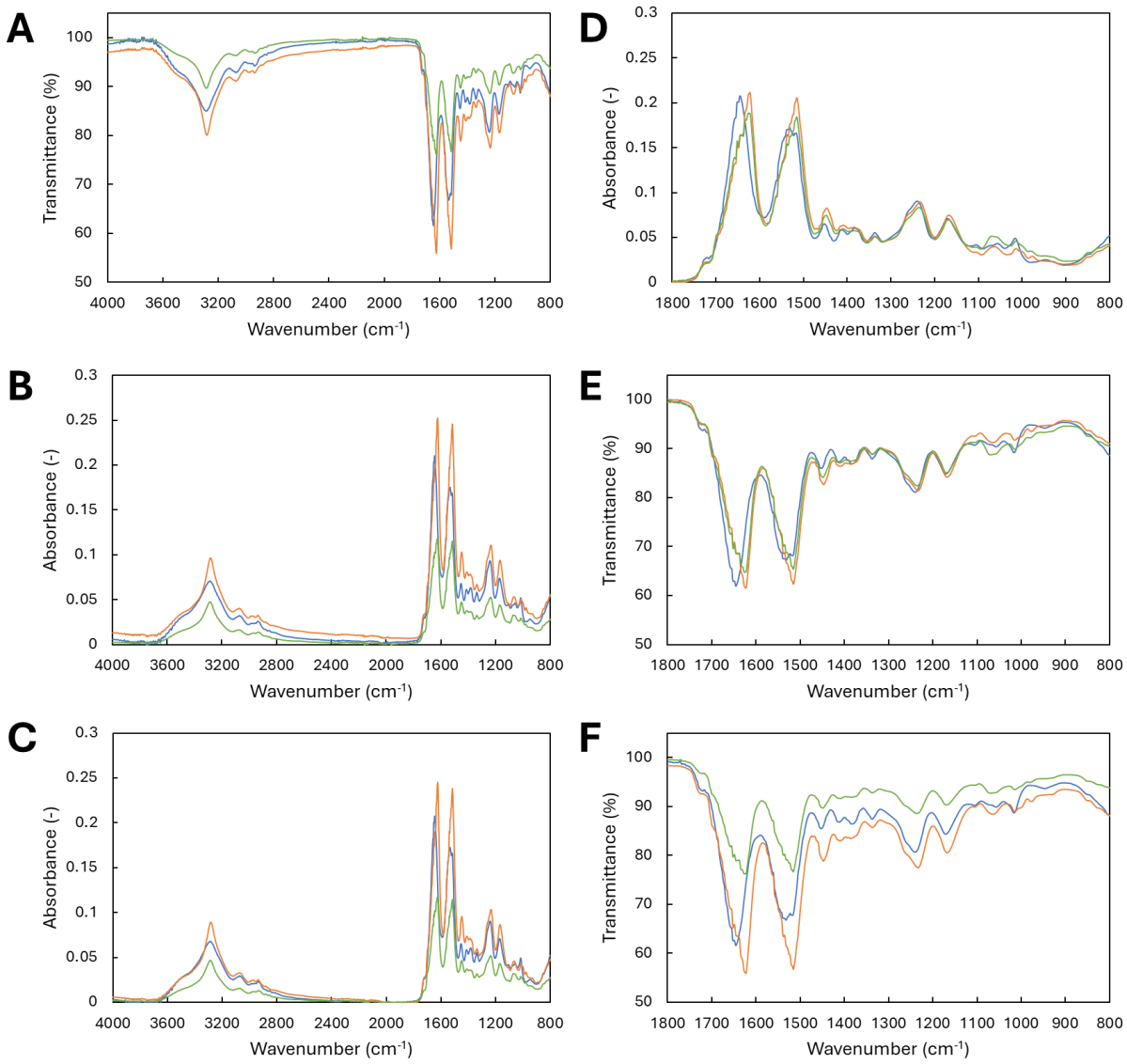

Figure S1: FTIR normalisation steps. (A) Raw FTIR data, the blue line will be used as the control. (B) Transmittance spectra are converted to absorbance for data manipulation $A = 2 - log(\%T)$. (C) Noise is reduced by subtracting the average absorbance of the region spanning 1950 – 1900 cm^{-1} from the entire spectra. (D) Normalisation is achieved by matching the integrated absorbance of each spectrum from 1800 – 800 cm^{-1} against the integrated absorbance of the control. (E) The absorbance spectra are converted back into transmittance spectra for presentation purposes. As a comparison, (F) shows FTIR of the same region (1800 – 800 cm^{-1}) without normalisation.

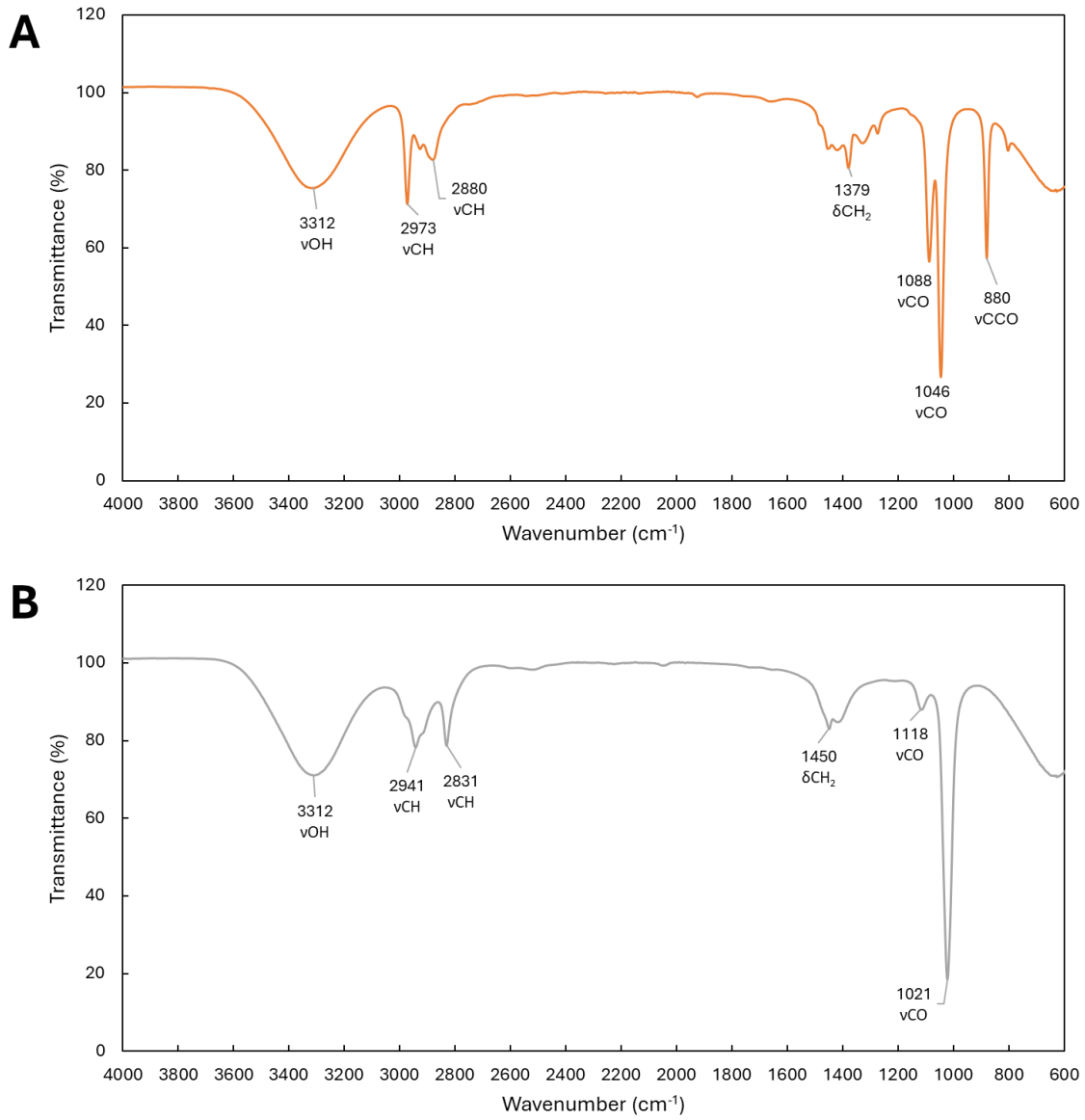

Figure S2: FTIR spectra of 99.8% (A) Ethanol and (B) Methanol (v – stretching vibration; δ – bending deformation).

The FTIR characteristic absorbance bands of EtOH are the C-O stretching vibrations in 1088 cm^{-1} and 1046 cm^{-1} and C-O-C stretching vibration at 880 cm^{-1} while those of MeOH are the C-O stretching vibrations at 1118 cm^{-1} and 1021 cm^{-1}. These characteristic bands are used to determine the presence of EtOH or MeOH in a compound (Garrigues *et al*., 1997).

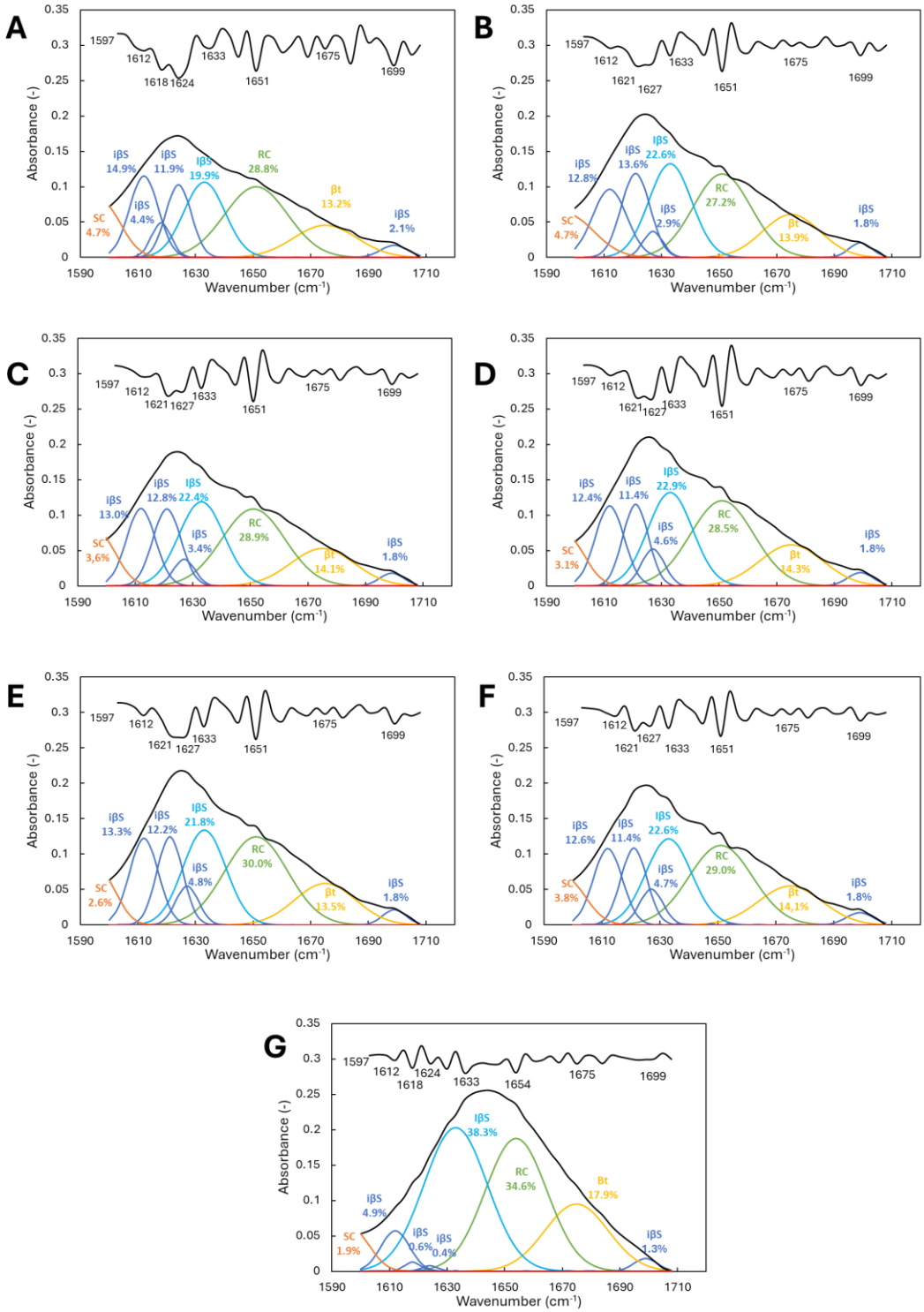

Figure S3: Effect of 99.8% (v/v) EtOH-treatment time on the secondary structure of silk fibroin. (A) 0 min, (B) 10 min, (C) 20 min, (D) 30 min, (E) 45 min and (F) 60 min and (G) untreated. (SC: Tyrosine side chains, iβS: intermolecular β-sheets, Iβ S: intramolecular β-sheets, RC: random coils, βt: β-turns).

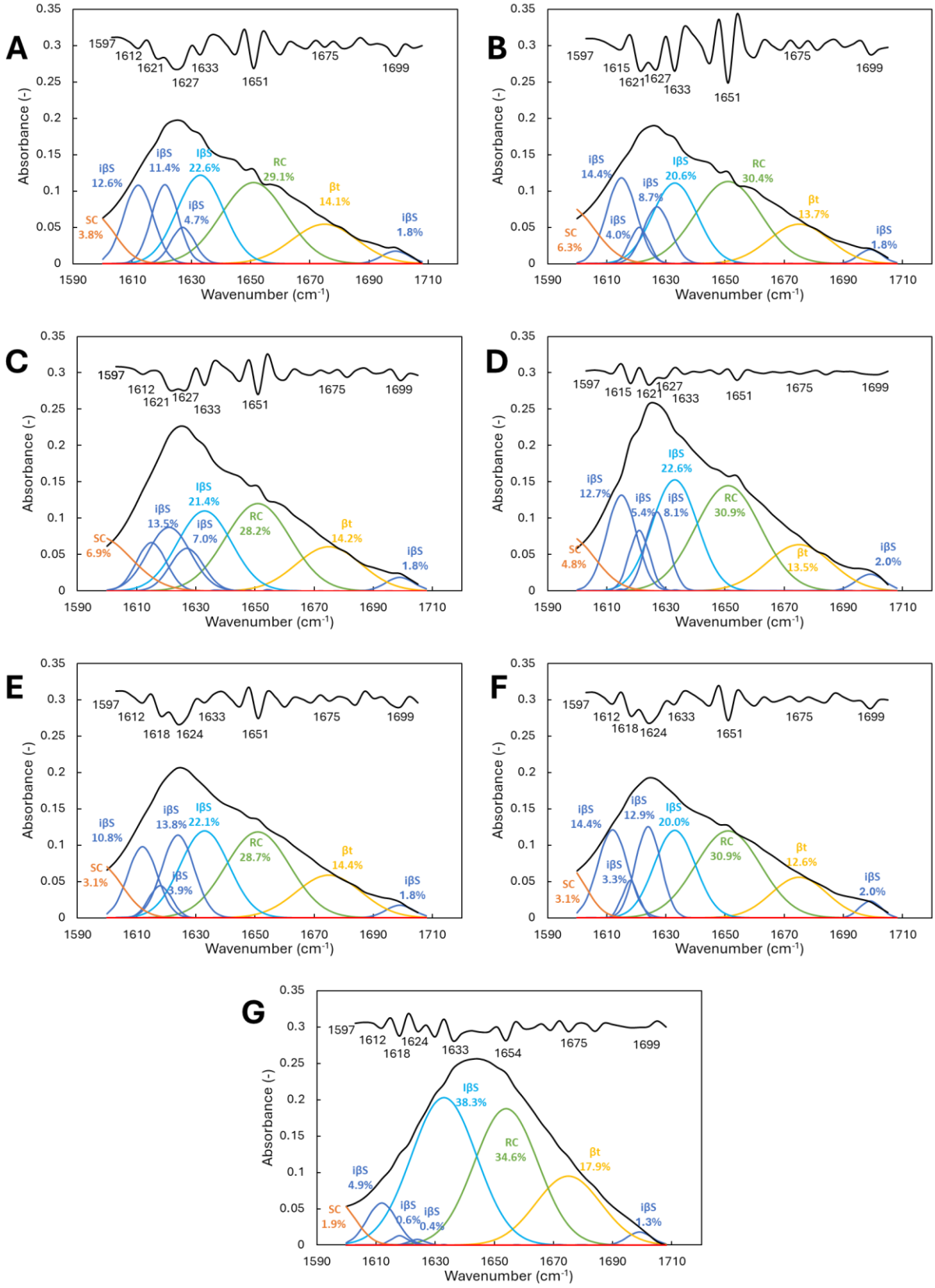

Figure S4: Effect of 99.8% (v/v) MeOH-treatment time on the secondary structure of silk fibroin. (A) 0 min, (B) 10 min, (C) 20 min, (D) 30 min, (E) 45 min and (F) 60 min and (G) untreated. (SC: Tyrosine side chains, iβS: intermolecular β-sheets, Iβ S: intramolecular β-sheets, RC: random coils, βt: β-turns).

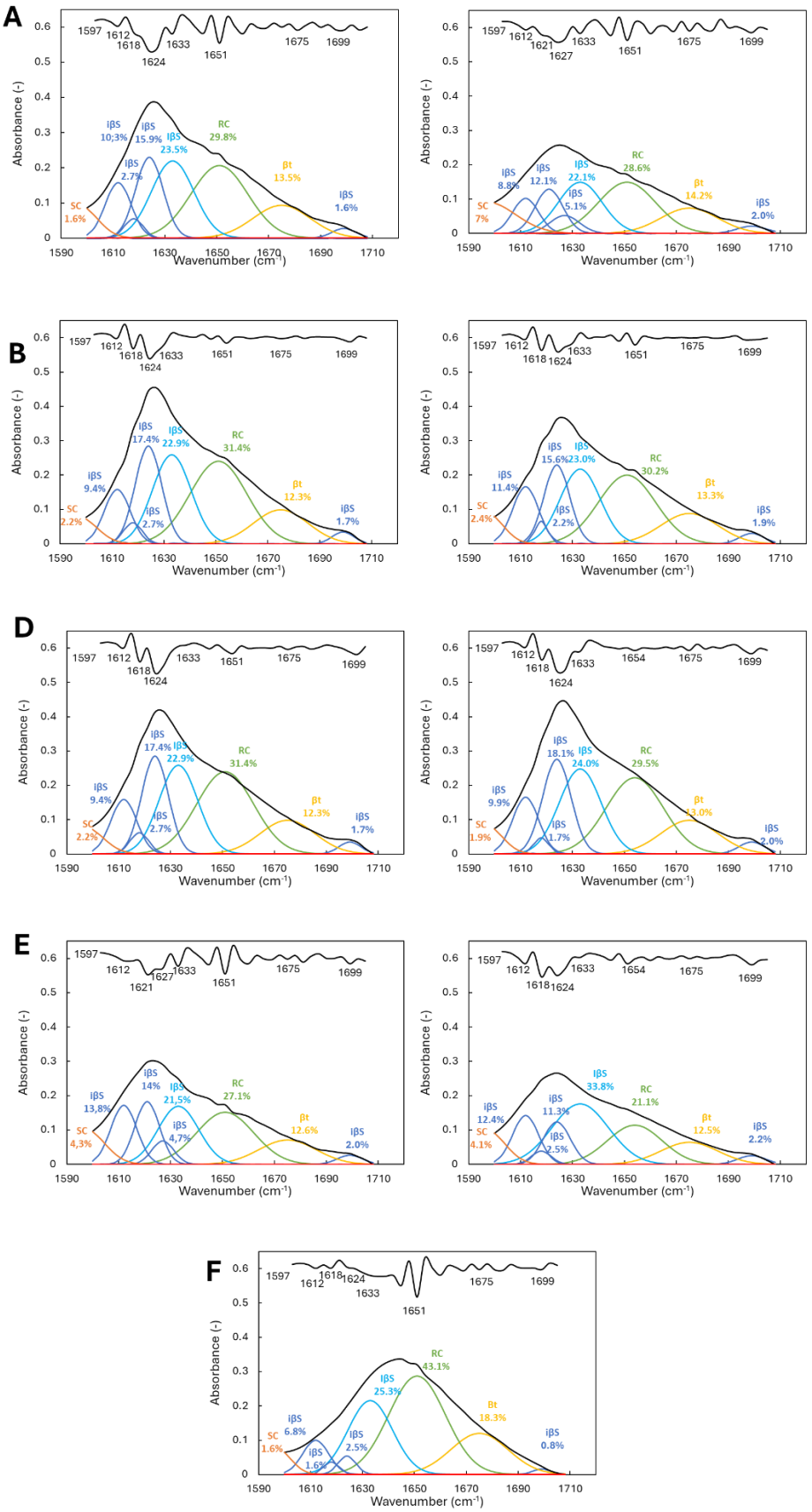

Figure S5: Effects of EtOH (left) and MeOH (right) concentration on electrospun silk fibroin during a 20 min stabilisation. (A) 100% (v/v), (B) 90% (v/v), (C) 80% (v/v), (D) 70% (v/v) and (E) untreated. (SC: Tyrosine side chains, iβS: intermolecular β-sheets, Iβ5: intramolecular β-sheets, RC: random coils, βt: β-turns).

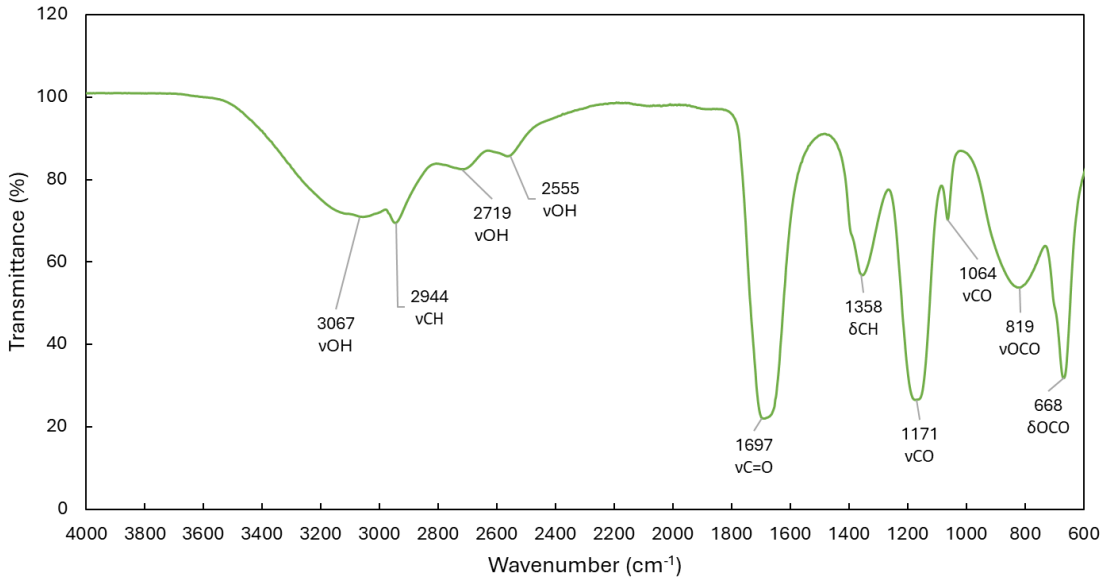

Figure S6: FTIR spectrum of 98%+ formic acid (ν – stretching vibration; δ – bending deformation).

The FTIR characteristic absorbance bands of formic acid are C=O stretching vibrations at 1697 cm^{-1} and C-O stretching vibrations at 1171 cm^{-1}.

Appendix B

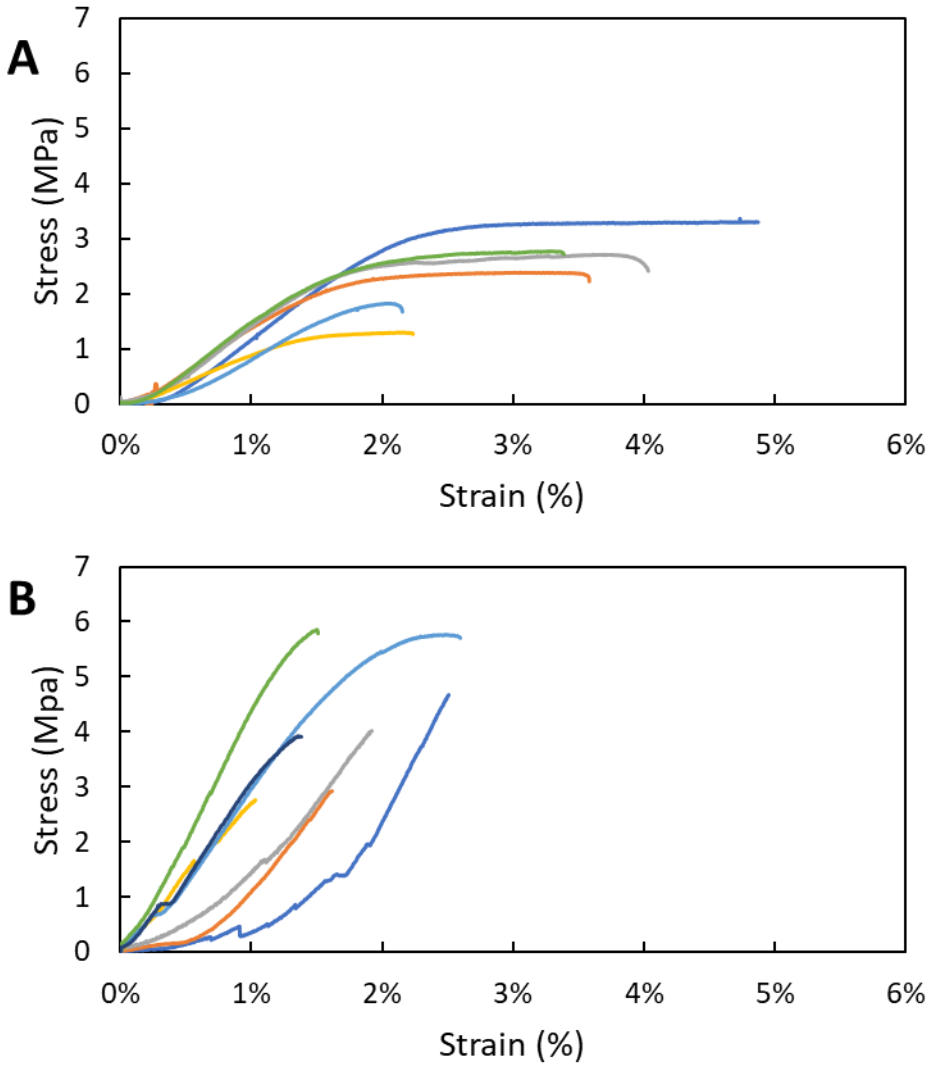

Figure S7: Stress:strain curve of needle-electrospun regenerated silk fibroin (A) before (SF_{12}-U) and (B) after EtOH treatment (SF_{12}-E).

EtOH-treatment increased the Young's modulus from 154.3 ± 33.1 MPa to 356.9 ± 84.0 MPa, the ultimate tensile strength from 2.4 ± 0.7 MPa to 4.3 ± 1.1 MPa, and reduced yield strain from 3.3 ± 0.9% to 1.8 ± 0.5% in NSF_{12}-U and NSF_{12}-E, respectively. As such, no differences were observed between the tensile properties of needle electrospun commercial silk fibroin and regenerated silk fibroin.

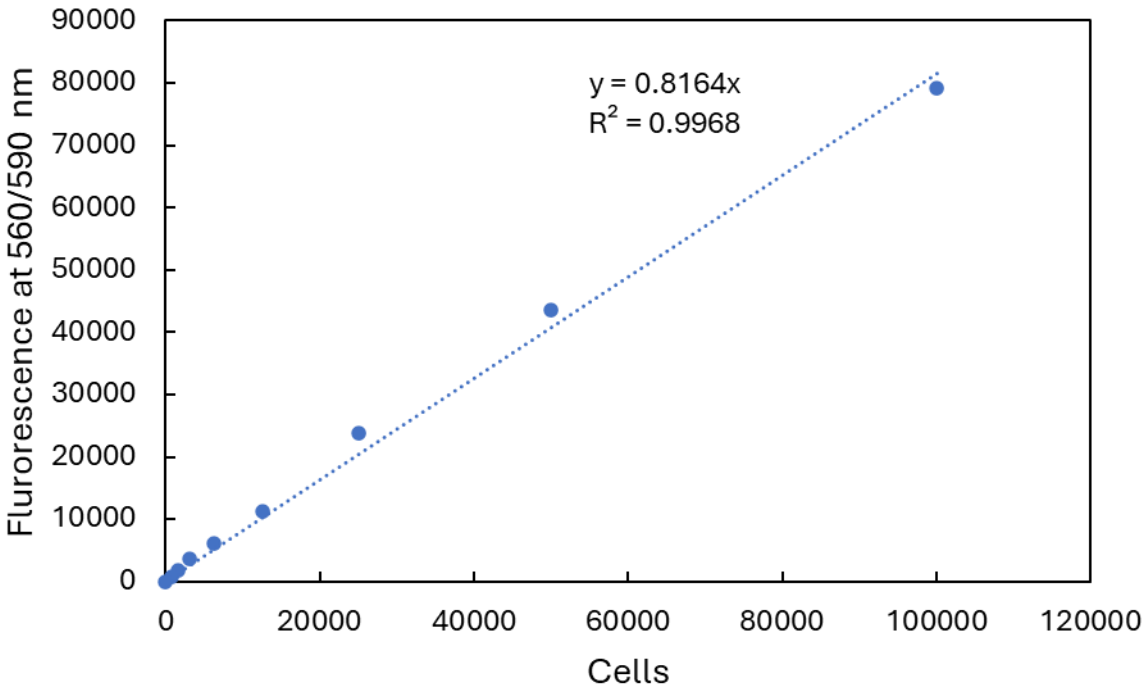

Figure S8: PrestoBlue assay calibration curve in for experiments in 24-well plates. This calibration curve was used to quantify cell density and growth kinetics for all scaffold experiments.

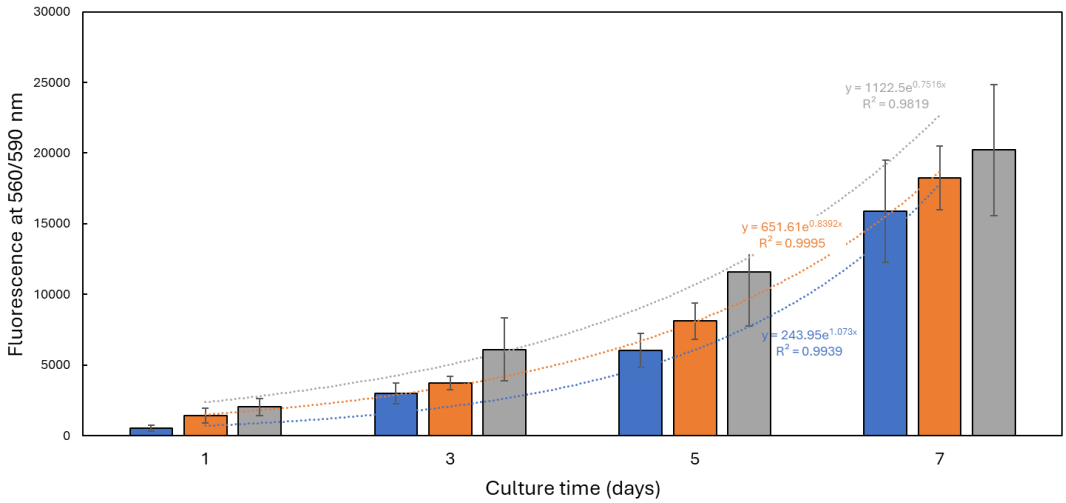

Figure S9: Exponential growth phase on electrospun silk fibroin seeded at 3000 (grey), 6000 (orange), 10000 (grey) cells/cm². Results displayed as mean ± SD.

The trendlines for cells grown on 3000, 6000 and 10000 cells/cm^2 demonstrated an exponential growth between day 1 and day 7, as shown by high R^2 values. Beyond day 7 the R^2 of the exponential trendlines reduced considerably indicating slowing down of the proliferation rate.

Appendix C

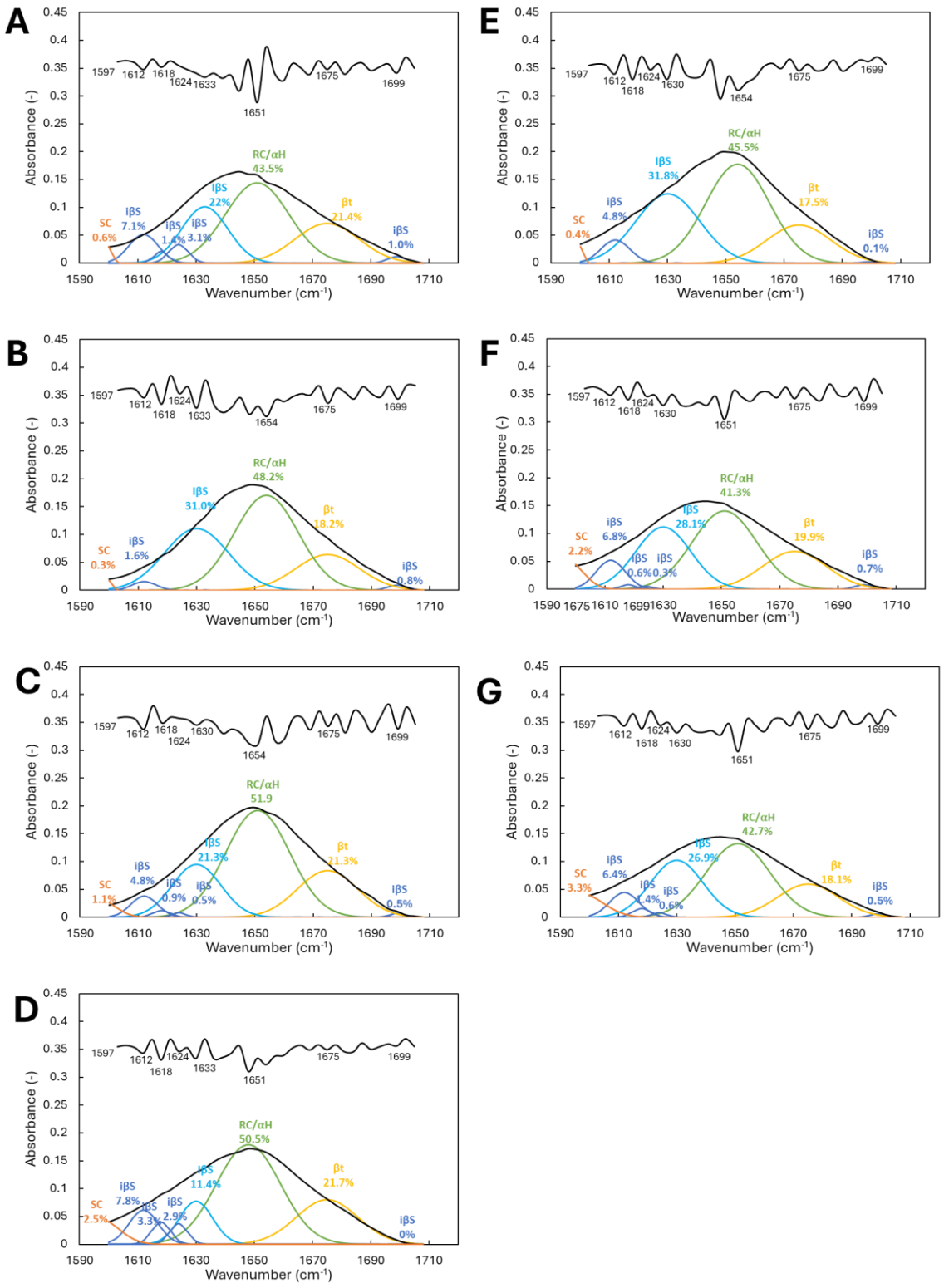

Figure S10: Spectral decomposition of the amide I of SFZ untreated electrospun blends. (A) SF_{12}-U, (B) $SF_9Z_{6.25}$-U, (C) $SF_6Z_{12.5}$-U, (D) $SF_3Z_{18.75}$-U, (E) Z_{25}-U, (F) $SF_{12}Z_{6.25}$-U and (G) $SF_{12}Z_{12.5}$-U.

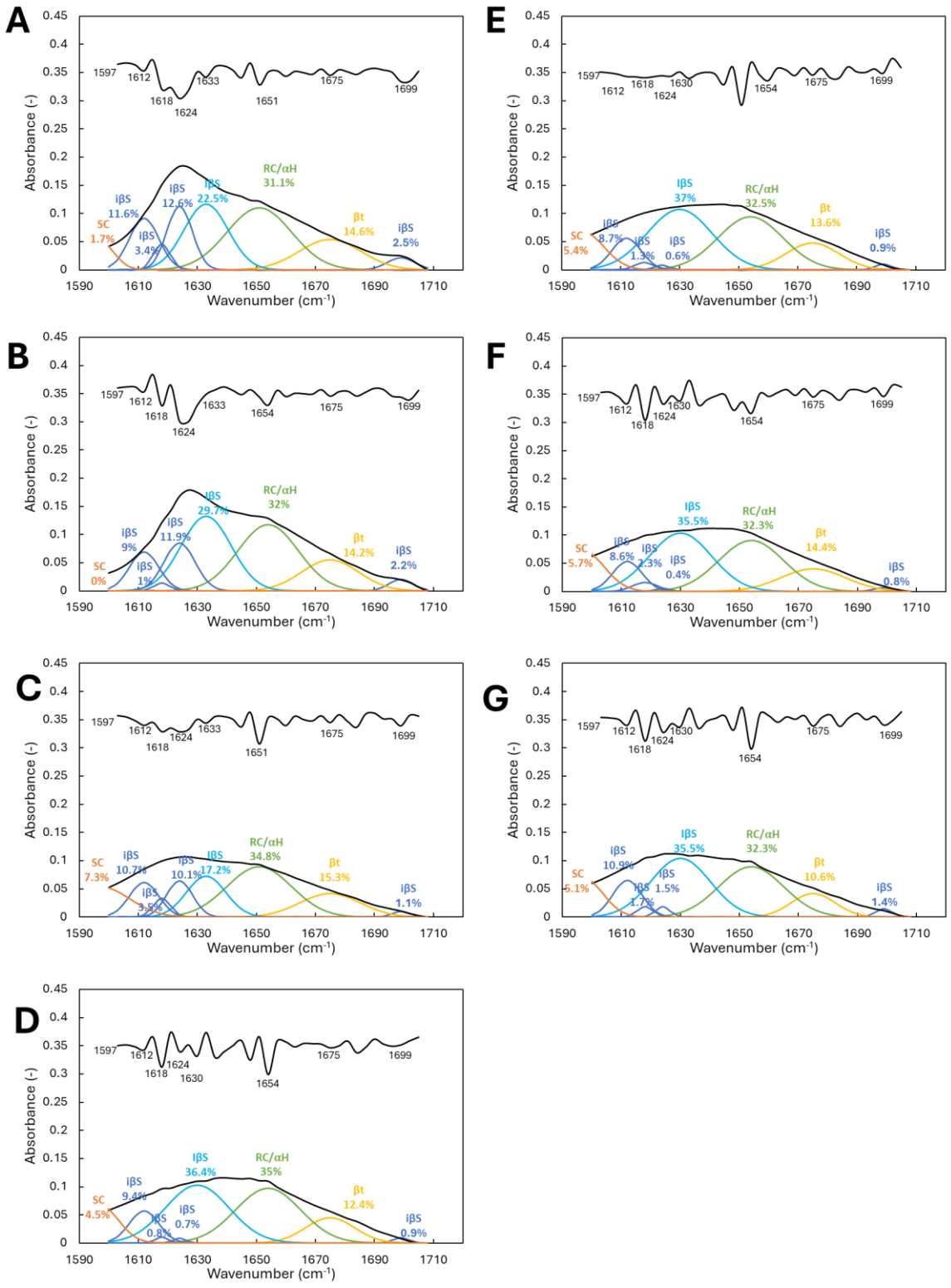

Figure S11: Spectral decomposition of the amide I of SFZ EtOH-treated electrospun blends. (A) SF_{12}-E, (B) $SF_9Z_{6.25}$-E, (C) $SF_6Z_{12.5}$-E, (D) $SF_3Z_{18.75}$-E, (E) Z_{25}-E, (F) $SF_{12}Z_{6.25}$-E and (G) $SF_{12}Z_{12.5}$-E.

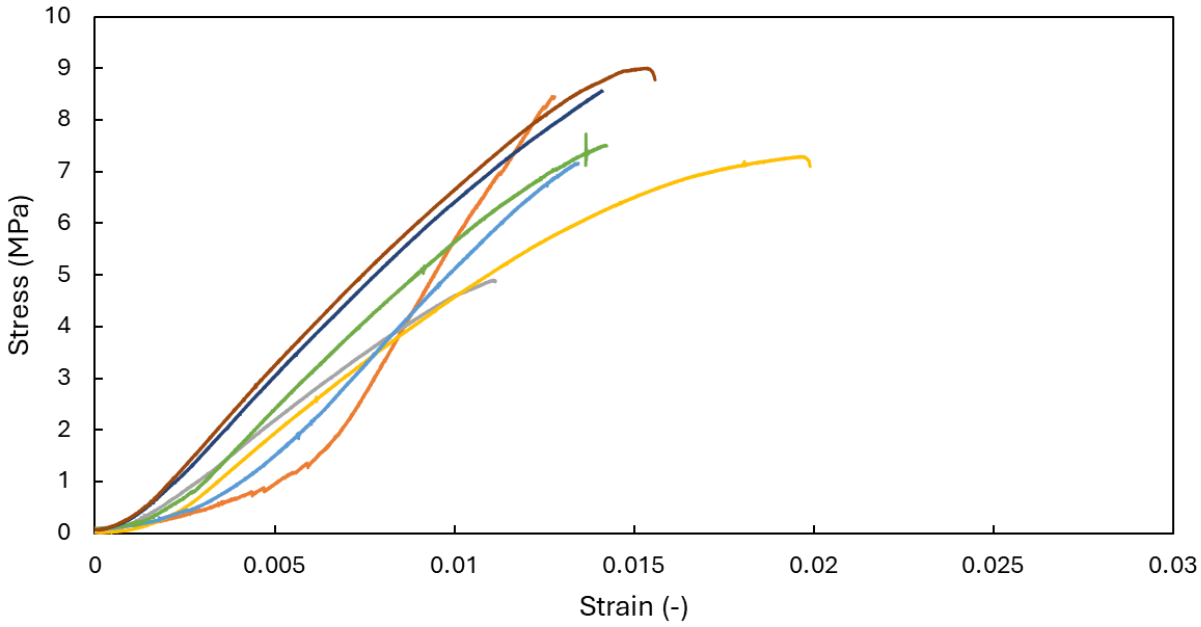

Figure S12: Stress:strain curve of EtOH-treated needle-electrospun silk fibroin $SF_{12}Z_{6.25}$-E.

EtOH-treated $SF_{12}Z_{6.25}$-E electrospun mats had a Young's modulus of 671.1 ± 83.4 MPa, an ultimate tensile strength of 7.6 ± 1.3 MPa, and a yield strain of 1.4 ± 0.3%. Therefore, blending silk fibroin with zein increased the brittleness of the electrospun scaffolds.

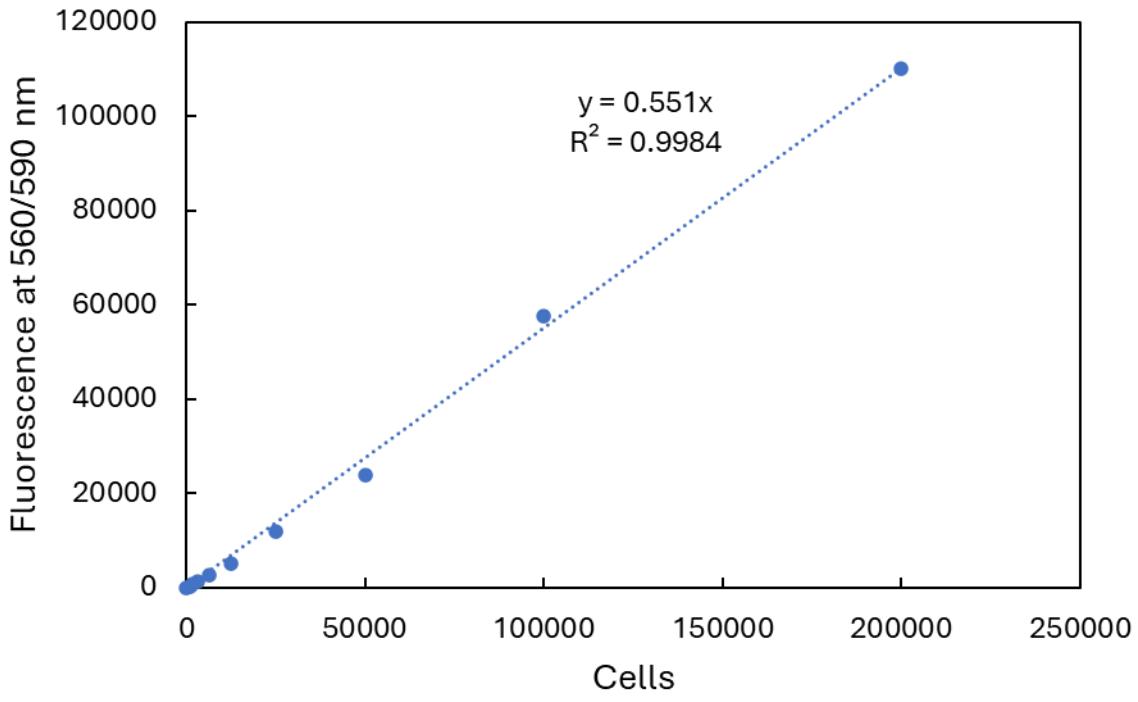

Figure S13: PrestoBlue assay calibration curve in for experiments in 6-well plates. This calibration curve was used to quantify cell density and growth kinetics for all microcarrier experiments.